

SMALL- AND HALF-SCALE EXPERIMENTAL STUDIES OF ROCKFALL IMPACTS ON SANDY SLOPES

THÈSE N° 3059 (2004)

PRÉSENTÉE À LA FACULTÉ ENVIRONNEMENT NATUREL, ARCHITECTURAL ET CONSTRUIT

Institut des infrastructures, des ressources et de l'environnement

SECTION DE GÉNIE CIVIL

ÉCOLE POLYTECHNIQUE FÉDÉRALE DE LAUSANNE

POUR L'OBTENTION DU GRADE DE DOCTEUR ÈS SCIENCES TECHNIQUES

PAR

Barbara HEIDENREICH

Diplom-Ingenieur, Technische Universität Darmstadt, Allemagne
et de nationalité allemande

acceptée sur proposition du jury:

Dr V. Labiouse, directeur de thèse
Prof. G. Giani, rapporteur
Dr R. Mayoraz, rapporteur
Prof. A. Muttoni, rapporteur

Lausanne, EPFL
2004

Acknowledgements

This research was realized at the Rock Mechanics Laboratory (LMR) of the Swiss Federal Institute of Technology of Lausanne (EPFL) between May 2000 and June 2004. Even if a doctoral thesis is mainly a personal work, the present thesis could not have been performed without the help of many hands and heads. I am deeply grateful and would like to express my thanks to:

Dr. V. Labiouse for his great supervision of the research, for many hours of inspiring and very helpful discussions and for never losing patience and the sense of humour throughout the period of my research.

Prof. G.-P. Giani, Prof. M. Hirt, Dr. R. Mayoraz and Prof. A. Muttoni for accepting being member of the examination committee.

Prof. P. Egger for his continuous scientific and moral support during my stay at the EPFL.

J.-P. Dudt for his very useful suggestions and criticism during our discussions.

P. Dubey, L. Gastaldo, B. Marguerat, J.-F. Mathier, F. Mottier and G. Steinmann for their excellent technical assistance and plenty of resourceful propositions to solve technical problems occurring during the experimental phases of the research.

H. Bernau, L. Gastaldo, R. Gärber, G. Joliat and I. Manzella for their amicable acceptance, their enthusiastic support especially during my first months at the EPFL and the highly enjoyable ambiance in our office, as well as my colleagues of the Rock and Soil Mechanics Laboratory of the EPFL for the wonderful working atmosphere and the continuous fruitful collaboration.

B. Schneider-Muntau, J. Bisshot and I. Grillon for performing a good part of the small-scale impact tests and their contribution to the development of the adopted interpretation method.

J.-Y. Burguet for the fantastic online support and his help in solving several problems related to the optical distortion of the films, as well as M. Frischholz for providing an efficient support for the software WINalyze.

O. Jaques (Alder & Eisenhut) for sponsoring some of their old gym mats used as shock absorber for the half-scale tests.

The Swiss National Science Foundation for founding the research.

And last but not least my family and friends for their love and friendship, and for always supporting and encouraging me during all these years.

Summary

In the framework of rockfall trajectory modelling, the bouncing phenomenon occurring when a rock block impacts with the slope surface is the most difficult to predict, owing to its complexity and its very limited understanding. Up to now, the rebound is commonly quantified by means of (one or) two coefficients of restitution expressing the amount of energy dissipated during impact. These restitution coefficients generally are evaluated from a rough description of the ground material, whereas other parameters likely to influence the rebound phenomenon as the characteristics of the block itself and the kinematics are often neglected.

In the framework of this thesis, two experimental campaigns have been performed in laboratory to acquire a better knowledge of the impact mechanisms governing the rebound phenomenon of rock blocks on granular (sandy) slopes and to quantify the discovered dependencies. About 200 impact tests on a small scale have helped to identify first the most significant impact parameters and to qualify their influence. Further, a half-scale testing campaign has been performed to quantify these influences. The impact of a rock block on a granular material is modelled for varying impact parameters, concerning:

- the ground material (internal friction angle, compaction)
- the block (weight, radius, shape) and
- the kinematics (slope angle, impact direction (vertical or inclined), impact velocity).

The impact process has been filmed by a high-speed camera. The analysis of the block movement before, during and after the shock allowed to gather information concerning the impact process itself (velocity and acceleration of the block, penetration into the ground material, duration of impact etc.) and to determine a criterion for which the impact process is completed. By means of this criterion, the normal (R_n), tangential (R_t) and energetic (R_{TE}) coefficients of restitution have been evaluated for the mass centre of the block according to the most common formulations (ratio of the normal or tangential velocities respectively the total energies before and after impact).

The qualitative analysis of the small and half-scale tests proves that the rebound of rock blocks as well as the coefficients of restitution commonly used to characterise the rebound depend not only on the ground characteristics (material, slope inclination), but also on parameters related to the block (weight, geometry) and the kinematics (impact velocity and angle). A thorough observation of the impacts has shown that the block motion during impact is governed by three mechanisms (penetration, sliding, rotation), acting partly antagonistically. For

different impact conditions, one or another of these mechanisms is privileged, governing on his part the block motion after impact.

The quantitative interpretation of the half-scale tests leads first to a proposition of formulations expressing the maximal penetration of the block into the ground material, the maximal contact force and the rotation of the block acquired during impact. Parting from these formulations and inspired by the principle of the conservation of linear momentum, expressions for the normal and tangential component of the coefficients of restitution are developed.

The implementation of coefficients of restitution defined by similar formulations as the proposed ones in rockfall trajectory codes should lead to a better prediction capacity of the latter and finally to a better delineation of areas at risk by hazard maps.

Résumé

Lorsqu'on analyse la propagation de blocs rocheux dans des versants montagneux, on constate que le phénomène de rebond qui se produit lorsqu'un bloc percute la surface du versant est très complexe et mal connu. Bon nombre de logiciels de trajectographie quantifient le rebond à l'aide d'un ou deux coefficient(s) de restitution fonction uniquement de la couverture du terrain, négligeant de la sorte l'influence de caractéristiques du bloc et de la cinématique.

Dans le cadre de la thèse, deux campagnes expérimentales ont été réalisées en laboratoire afin de mieux comprendre et quantifier le phénomène d'impact et de rebond de blocs rocheux sur des pentes sableuses. Quelque 200 essais à petite échelle ont d'abord permis d'identifier les paramètres d'impact les plus significatifs et d'analyser qualitativement leur influence. Une campagne d'essais en semi-grandeur a ensuite été menée pour quantifier ces influences. L'impact d'un bloc rocheux sur une pente granulaire est modélisé en variant les conditions d'impact suivantes:

- le matériau de la pente (angle de frottement interne, compacité)
- le bloc (poids, radius, géométrie) et
- la cinématique (angle de la pente, direction d'impact (verticale ou inclinée), vitesse d'impact).

L'impact est filmé par une caméra digitale d'acquisition rapide. L'analyse du mouvement du bloc avant, pendant et après le choc a apporté des informations sur le processus d'impact (vitesse et accélération du bloc, pénétration dans le terrain, durée de l'impact etc.). Un critère de fin de choc a été déterminé à l'aide duquel les coefficients de restitution normale, tangentielle et énergétique ont été évalués pour le centre de masse du bloc selon les définitions utilisées habituellement (rapport entre les vitesses normales ou tangentielles, voir les énergies totales avant et après l'impact).

L'interprétation qualitative des essais à petite échelle et en semi-grandeur confirme que le rebond de blocs rocheux et les coefficients de restitution, qui traditionnellement le caractérisent, dépendent non seulement de caractéristiques du terrain (compacité), mais aussi de paramètres relatifs au bloc (poids et géométrie) et à la cinématique (vitesse et angle d'impact). Une observation attentive des impacts a mis en évidence que le mouvement des blocs est fonction de trois mécanismes (pénétration, glissement, rotation) partiellement antagonistes. Les conditions d'impact privilégient l'un ou l'autre de ces mécanismes qui à son tour conditionne le mouvement du bloc après impact.

L'interprétation quantitative des essais en semi-grandeur conduit d'abord à la proposition de formules pour évaluer l'enfoncement maximum du bloc dans le versant, la force de contact maximale ainsi que la rotation acquise par le bloc au cours de l'impact. Ensuite, s'inspirant du principe de conservation de quantité de mouvement, elle aboutit à des expressions pour les composantes normale et tangentielle des coefficients de restitution.

A terme, l'implémentation de telles formules dans des logiciels de trajectographie devrait se traduire par un accroissement de la capacité de prédiction des trajectoires de blocs rocheux et dès lors par une meilleure délimitation des zones à risques.

Zusammenfassung

Bei der Modellierung von Steinschlagsturzbahnen stellt der Abprall eines Gesteinblockes von der Geländeoberfläche den am schwierigsten vorherzusagenden Teil der Sturzbahn dar. Gründe hierfür sind sowohl die Komplexität des Abprallvorgangs als auch dessen bisher sehr begrenztes Verständnis. Die meisten Programme zur Berechnung von Sturzbahnen (Trajektorien) modellieren den Abprall mittels (ein oder) zwei Restitutionskoeffizienten, die den Betrag der während des Stoßes absorbierten Energie ausdrücken. Diese Restitutionskoeffizienten werden generell anhand einer groben Beschreibung des Hangmaterials abgeschätzt. Andere den Abprall beeinflussende Parameter, wie die Eigenschaften des stürzenden Blocks und die kinematischen Randbedingungen, werden dabei im allgemeinen außer Acht gelassen.

Im Rahmen der vorliegenden Arbeit wurden zwei Versuchskampagnen unter Laborbedingungen durchgeführt, um den Stossvorgang und den Abprall von Gesteinsblöcken von granulären (sandigen) Hängen besser verstehen und mathematisch erfassen zu können. Mit Hilfe von mehr als 200 kleinmaßstäblichen Versuchen konnten die wichtigsten Stossparameter identifiziert und deren Einfluss qualitativ ermittelt werden. Für die quantitative Auswertung der Einflüsse wurde des weiteren eine Kampagne mit halbmaßstäblichen Versuchen durchgeführt. Der Zusammenprall zwischen Felsblock und granulärem Bodenmaterial wurde dabei für folgende variable Stossparameter modelliert:

- Bodenmaterial (innerer Reibungswinkel, Lagerungsdichte)
- Block (Gewicht, Radius, Form) und
- Kinematik (Hangneigung, Stossrichtung (vertikal oder schräg), Stossgeschwindigkeit)

Der Stossvorgang wurde mittels einer digitalen Hochgeschwindigkeitskamera gefilmt. Die Untersuchung der Blockbewegung vor, während und nach dem Stoss ermöglichte es, Informationen über den Stossvorgang zu gewinnen (Geschwindigkeit und Beschleunigung des Blocks, Eindringtiefe in das Bodenmaterial, Dauer des Stoßes usw.) und ein Kriterium zu bestimmen, für das der Stoss als beendet erklärt werden kann. Mittels dieses Kriteriums wurden die normale (R_n) und tangentielle (R_t) sowie die energetische (R_{TE}) Komponente des Restitutionskoeffizienten für den Schwerpunkt des Blocks nach den gängigen Formulierungen ermittelt. Dafür werden die normalen oder tangentiellen Geschwindigkeitskomponenten bzw. die Gesamtenergie vor und nach dem Stoss ins Verhältnis gesetzt.

Die qualitative Analyse der kleinmaßstäblichen Versuche beweist, dass der Abprall sowie die Restitutionskoeffizienten keineswegs ausschließlich von der

Bodenbeschaffenheit (Material, Hangneigung), sondern auch von Blockeigenschaft (Gewicht, Geometrie) und Kinematik (Stossgeschwindigkeit und -richtung) abhängen. Eine eingehende Untersuchung der Daten hat gezeigt, dass die Blockbewegung während des Zusammenpralls von drei teils antagonistisch wirkenden Mechanismen (Eindringen, Rutschen, Rollen) gesteuert wird. Je nach Stossbedingung überwiegt einer der Mechanismen und bestimmt so die Art der Blockbewegung nach dem Stoss.

Bei der quantitativen Interpretation der halbmaßstäblichen Versuche wurden zunächst Formelvorschläge zur Berechnung der maximalen Eindringtiefe des Blocks in den Boden, der maximal wirkenden Kontaktkraft und der durch den Stoss erzeugten Rotation entwickelt. Darauf aufbauend und inspiriert vom Prinzip der Impulserhaltung wurden mathematische Formulierungen für die normale und tangentielle Komponente des Restitutionskoeffizienten entwickelt.

Die Implementierung von ähnlichen Formulierungen in Steinschlag-Simulationsprogramme kann in Zukunft zu einer besseren Vorhersage der Sturzbahnen führen und in der Folge zu einer besseren Demarkation von Gefahrenzonen mittels Gefahrenkarten.

1	INTRODUCTION.....	1
2	STATE OF THE ART	3
2.1	General framework	3
2.2	Trajectory studies.....	6
2.2.1	Back analysis of rockfall events	7
2.2.2	<i>In situ</i> tests.....	7
2.2.3	Laboratory tests	8
2.2.4	Programs.....	9
2.3	Mathematical models of the bouncing phenomenon	11
2.3.1	Velocity models.....	12
2.3.2	Energy models	14
2.3.3	Impulse models.....	15
2.3.4	Model proposed by Azimi & Desvarreux [1977]	17
2.3.5	Model proposed by Pfeiffer & Bowen [1989].....	18
2.3.6	Model proposed by Ushiro & al. [2000].....	19
2.3.7	Values of coefficient(s) of restitution stated in literature	21
2.4	Models for rolling and sliding.....	25
2.5	Former experiments for a better characterisation of the parameters influencing the rebound.....	27
2.5.1	General statements.....	28
2.5.2	Insight gained by <i>in situ</i> tests and trajectory back analysis	29
2.5.3	Trends investigated by physical modelling	31
2.6	Rotational motion of blocks down slopes.....	41
2.7	Miscellaneous references not directly related to the bouncing of rock blocks	43
2.7.1	Impact theory.....	44
2.7.2	Impact tests on rock sheds	44
2.7.3	Foundations under static and dynamic loading.....	45
2.8	Summary and contribution of the thesis.....	46
3	PRELIMINARY SMALL-SCALE EXPERIMENTAL CAMPAIGN	49
3.1	Physical modelling	49
3.1.1	Motivation	49
3.1.2	Experimental set-up.....	50
3.1.2.1	Testing device	51
3.1.2.2	Materials	52
3.1.2.3	Procedure for an impact test.....	54
3.1.3	Measuring devices	54
3.1.3.1	Capturing of the block motion	54
3.1.3.2	Measurement of traces	56
3.1.4	Data acquisition and data processing.....	57
3.1.4.1	Motion analysis by WINalyze.....	57
3.1.4.2	Further data processing	62
3.1.5	Small-scale test program	70
3.2	Qualitative interpretation of the small-scale tests.....	73
3.2.1	Observations during small-scale tests.....	73
3.2.2	Sensibility of the coefficients of restitution to the tested parameters	80
3.2.3	Summary	88
3.3	Scale effects	90

4	HALF-SCALE EXPERIMENTAL CAMPAIGN	97
4.1	Physical modelling.....	97
4.1.1	Motivation.....	97
4.1.2	Experimental set-up.....	98
4.1.2.1	Testing device.....	99
4.1.2.2	Materials	101
4.1.2.3	Procedure for the impact tests.....	102
4.1.3	Measuring devices.....	103
4.1.3.1	Capturing of the block motion.....	103
4.1.3.2	Ground compaction.....	105
4.1.3.3	Measurement of traces.....	108
4.1.4	Data acquisition and data processing	108
4.1.4.1	Correction of distorted films.....	108
4.1.4.2	Data acquisition and processing.....	112
4.1.5	Half-scale test programme.....	113
4.2	Qualitative interpretation of the half-scale tests.....	115
4.2.1	Observations during half-scale tests	115
4.2.2	Closer investigation of several important characteristics	116
4.2.2.1	Maximum penetration depth d_{\max}	116
4.2.2.2	Block acceleration during impact	119
4.2.2.3	Impact time	122
4.2.2.4	Impulse or linear momentum p	123
4.2.3	Sensibility of the coefficients of restitution to the tested parameters	125
4.2.3.1	Slope inclination β (respectively impact angle θ).....	125
4.2.3.2	Block weight W	129
4.2.3.3	Block shape.....	136
4.2.3.4	Falling height H	138
4.2.3.5	Impact energy E	140
4.2.3.6	Impulse p	143
4.2.4	Synopsis: parameters found to influence the coefficients of restitution.....	144
4.3	Quantitative interpretation of the half-scale tests	147
4.3.1	Impact mechanisms.....	147
4.3.1.1	Ground failure during impact.....	148
4.3.1.2	Conditions for which global shear failure occurs	156
4.3.2	Quantification of some impact characteristics.....	159
4.3.2.1	Evaluation of d_{\max} through energy consideration.....	159
4.3.2.2	Evaluation of the acceleration force $F_{y,\max}$ and the acceleration $a_{y,\max}$	169
4.3.2.3	Relation between acceleration force $F_{y,\max}$ and block penetration d_{\max}	172
4.3.2.4	Relation between rotational and translational energy at the end of impact.....	175
4.3.3	Quantification of the coefficients of restitution.....	182
4.3.3.1	Normal component of the coefficient of restitution R_n	182
4.3.3.2	Tangential component of the coefficient of restitution R_t	190
4.3.3.3	Coefficient of restitution R_{TE} defined by means of the ratio $E_{r,tot}/E_{i,tot}$	196
4.3.4	Synopsis and domain of validity	197
5	APPLICATION AND COMPARISON WITH EXISTING MODELS	201
6	CONCLUSIONS AND PROSPECTS	211
	REFERENCES.....	219
	APPENDIX.....	227
	CURRICULUM VITAE	231

1 Introduction

Within the context of slope instability phenomena, the detachment of blocks from steep rock faces and their subsequent fall along slopes are particularly significant and involve high risks in densely populated mountain areas, such as the Alps. It is particularly important in these areas to have the widest possible knowledge of rockfall trajectories (in particular maximum path length, height and velocity) and energies in order to evaluate hazard maps and construct adequate defence systems.

The trajectory of a falling block can be described with the aid of four main types of movement: free fall, rolling, sliding and bouncing. The latter occurs when the falling block impacts with the slope surface. Up to now, the bouncing phenomenon is governed mathematically by one or two coefficients, called the coefficients of restitution. This expression is based on the theory of perfectly elastic impacts. For impacts of hard rock blocks on hard rock slopes, this approach may be vindicated (disregarding the frangibility of the block). For impacts on granular material, characterising most talus slopes and thus rockfall prone areas, this approach is highly suspicious to match reality. The variety of definitions and interpretations quoted in literature to define the coefficients of restitution illustrate the complexity and the general lack of proper understanding of the impact mechanism(s) guiding the movement of the block at impact end (its “rebound”).

The present thesis aims firstly at investigating which of the parameters supposed to govern the block movement during and after impact (related to the impacting block, the ground material as well as the kinematics) have a relevant influence and, secondly, at quantifying the determined influences. Following a qualitative analysis of the tests results, the thesis attempts to develop a new method of mathematically expressing the coefficients of restitution as a function of the parameters found to govern the impact process.

By means of two comprehensive experimental campaigns on a small- and half-scale, the impact of a rock block on a granular material is modelled. The small-scale tests aim at qualifying the influence of several parameters related to ground material, slope inclination, unit weight of the block and impact direction relative to the ground surface. The impact tests performed on a half-scale are performed in order to qualify as well as quantify the influence of parameters related to the kinematics (dropping height, slope angle), the block itself (shape, weight and size) on the rebound of the block. In order to analyse the movement of the block during impact, the impact is filmed at high speed (250 frames per second). As all impact tests are performed without initial rotation of the block and - in case of the half-

scale tests - at vertical impact directions, the modelled impact represents more or less the first impact of a rock block detached from a steep rock wall on the talus slope below.

The thesis is set out as follows:

Firstly, a bibliographic study sets out the state of the art and illustrates the lack of knowledge of the bouncing phenomenon (Chapter 2).

The next section (Chapter 3) presents the experimental campaign of small-scale impact tests. This chapter also includes a description of the original methodology developed and applied to perform and analyse the impact tests and determine the coefficients of restitution according to the most common formulations. The qualitative interpretation of the small-scale test results concludes the third chapter. The most important part of the thesis as regards its extent as well as substance is the next chapter (Chapter 4) concerning the half-scale tests performed within the framework of this thesis. Chapter 4 is divided into three parts: The first describes the half-scale test campaign and the methods used for data processing and interpretation. The second section contains the qualitative interpretation of the half-scale tests and a comparison of the thus obtained results with the small-scale test results. The third section quantifies the most important characteristics found to govern the impact of the block and its subsequent movement. Furthermore, a new and original mathematical formulation for the coefficients of restitution is proposed based on the knowledge gained from the detailed analysis of the impact tests.

In Chapter 5, the developed formulations are applied to several half-scale impact tests to investigate if the influence of varying impact velocities, slope angles and block masses are adequately reproduced. The resulting rebound velocities as well as the coefficients of restitution are compared to both the measured data and the results of two other mathematical models.

Chapter 6 sums up all conclusions arrived at by the present thesis and also suggests ideas for further research into the impact phenomenon during rockfalls.

2 State of the art

2.1 General framework

In the context of slope instability phenomena, the detachment of blocks from steep rock walls and their subsequent falls along slopes are particularly significant and involve high risk in densely populated mountain areas, such as the Alps. Only in 2003, several large boulder falls occurred in the Swiss Alps, destroying buildings (houses, roads) and causing fatal casualties. In January, the highway connecting Interlaken and Brienz had to be closed for several weeks due to a rockfall, which breached the roof of the Chüebalm tunnel. Few time after that incident, in February, a rock block of 3 m³ burst the gallery roof covering the road between Brunnen (SZ) and Sisikon (UR) on a surface of 2.5 to 5 m. In April, a rock block of 50 tons broke through the gallery roof of the highway at Gurtnellen (UR). In September, a chalet situated in Evolène (VS) and constructed in 1971 was partially destroyed by a rockfall. A block of about 3 m³, detached from the pendently rock face towering the village, broke into the house by the roof, passed through the entire first floor, erupted on the other side of the chalet destroying the front wall and terminating its trajectory some 20 m underneath the building. Finally in November, an avalanche gallery was destroyed by a rockfall of 600 m³ burying a car and causing one death on the highly frequented connection road between Martigny and Grand St.-Bernard. Such events illustrate that galleries, constructed to protect roads from avalanches and small rockfall impacts, can not stand events which are too important.

Accidents as these are not uncommon and regularly reported from mountainous parts all over the world. To reduce rockfall hazard, different techniques are used. Currently a differentiation is made between prevention and mitigation (or protective) measures. The first method tries to prevent the detachment of a rock block and its subsequent fall by nailing or anchoring it to a stable part of the cliff. The latter is applied to mitigate the danger either by limiting the natural travelling distance and catching the block (static or dynamic barriers as embankments, rock fences or cable nets) or by deviating its trajectory (galleries). Concerning mitigation structures, quite comprehensive lists are given for example by Heierli & al. [1985], Richards [1988] or Spang & Sönser [1995]. In general, the mitigation or prevention technique, which is adopted for a particular site, depends on the site characteristics and the desired result (deviation or catching of the blocks). The location and design of a rockfall mitigation structure is chosen based on an estimation of the trajectory and the kinetic energy of the probable rockfall events. Therefore, it is particularly important to have the best possible knowledge of the parameters influencing these initial design values.

Before computer simulations were adopted to investigate rockfall problems, this phenomenon and specifically remedial activities were mostly managed on an empirical basis. First field tests were made mainly to gain insight into the phenomenology of a rockfall and treat the dynamic process of the whole trajectory. Since the 1980, the development of computer programs, together with valuable experience gathered through a more rational observation of the phenomenon (in particular with laboratory and special *in situ* tests), has increased rockfall knowledge significantly. Today, computer based trajectory simulation represents one of the most popular approaches to gather the information needed for the mitigation structure design and even the determination of areas at risk. It should be mentioned that trajectory models are appropriated to simulate events of single boulder falls and to cover small survey areas. For the investigation of large survey areas, other approaches as cone models can be used.

The trajectory of a falling block may be modelled as a combination of four types of movement: free flight, rolling, sliding and bouncing (Figure 2.1). Bouncing occurs when the falling block impacts with the slope surface, with trees or other obstacles. Due to its complexity it is considered as the part within a trajectory, which is the less understood and the most difficult to predict. Most of the rockfall models used today represent the bouncing phenomenon in a simplified way by one or two overall coefficients, called the coefficients of restitution, which are sometimes combined with a coefficient of frictional resistance. As we will see further on (Chapter 2.3), the mathematical expressions defining the bouncing phenomenon are not at all standardised, showing the still poor understanding of the impact mechanism. However, the coefficients of restitution constitute the most crucial input parameters for the trajectory simulation, controlling the loss of velocity and energy during impact. The reliability of any trajectory analysis therefore depends highly on a thorough calibration of the model, including an adequate estimation of the coefficients of restitution. The user of any rockfall simulation program therefore necessarily has to be familiar with the program he operates, to be able to produce reasonable and significant results.

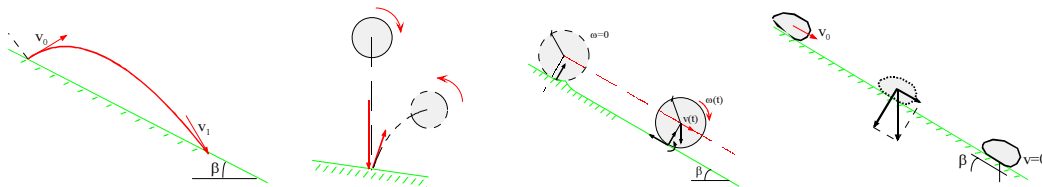


Figure 2.1: Basic types of block movement: free fall, bouncing, rolling and sliding [Descoedres, 1997]

In order to perform more rational analyses and gain more accurate predictions, it is thus crucial to improve the trajectory models by acquiring the best possible

knowledge of the bouncing phenomenon and the energy loss during impact. A precise observation and analysis of the phenomenon is essential for the calibration of the parameters used in rockfall models. Several approaches can be used to gather this information:

- back analysis of natural rockfall events
- special *in situ* tests
- laboratory scale tests

In the following, a literature review lists the main results of former research carried out in the scientific context of rockfall analysis. First, a synopsis is given on the methods used to analyse the complete dynamic process of a rockfall (back analysis of natural rockfalls, *in situ* tests, laboratory scale models and trajectory simulation programs). Then the review focuses on the information gained to date on the rebound of a rock block during its trajectory. The common mathematical definitions of the bouncing phenomenon are introduced and several values of the coefficients of restitution stated in literature are exemplified. The parameters found to influence the rebound of a block and their effects are pointed out. Finally, the contribution of the thesis to the state of the art is pointed out. In the last part of this section, miscellaneous literature used in the context of the thesis but not directly related to rockfall problems is stated.

It should be pointed out that this thesis covers only the dynamic part of a single boulder fall - the trajectory, with special emphasis on the rebound of the rock block - and not the likewise very interesting question if and when a rock will detach from a cliff. Further, it is supposed that no interaction occurs between single falling blocks, as the trajectories of the blocks normally are observed to be independent of each other. In case of events involving larger rock masses as e.g. rock avalanches, this supposition clearly does not apply. The interaction of blocks and its influence on the propagation is subject of a newly initiated research project at the Laboratory of Rock Mechanics, EPFL.

2.2 Trajectory studies

One of the first authors who described a large rockfall event (the bergsturz of Elm) from a geological point of view was Heim [1882]. Yet, the first practical approach to the design of rockfall protection structures and towards an analytical solution of single boulder falls was not published until 1963 by Ritchie. As illustrated in Figure 2.2, a rockfall usually takes place in the following manner [Lied, 1977]:

1. free, nearly vertical fall of a single boulder or rock mass,
2. impact at top of a talus slope,
3. jumping, rolling and / or sliding downwards along talus,
4. deceleration and arrest on a gently inclined valley bottom or by protecting structures (fences, nets, galleries, embankments).

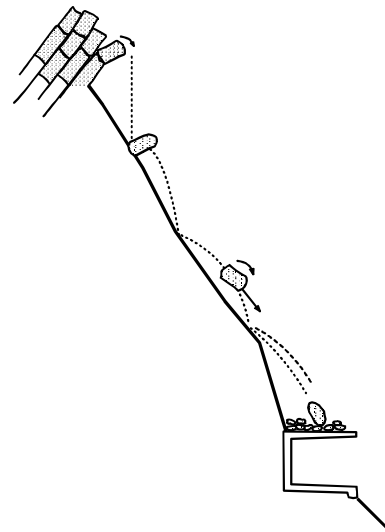


Figure 2.2: Trajectory of a rockfall
[Descoedres, 1997]

The free fall of the block can be described by a parabolic trajectory [Ritchie, 1963]. From a series of artificially triggered *in situ* rockfalls, Ritchie [1963] experienced, that the main type of block motion is rolling on slopes with an inclination β up to 45° (β being the angle between horizontal and slope), bouncing for a β between 46° and 63° and free fall for slopes steeper than 63° . In general, large boulders tend to roll and slide down a slope, staying near the slope surface rather than bouncing [Richtie, 1963; Bozzolo & Pamini, 1986]. They often travel long runout distances, whereas deposits of small rocks are found more often in the upper part of a cone, near the base of the origin rock face [Evans & Hungr, 1993]. This depositional pattern is due to the relative roughness between block and slope surface: while small irregularities of the slope surface cause small particles to retard in the depressions, loosing much energy during the impacts, large blocks are able to bridge the roughness elements of the surface and are less affected and deflected by them [Statham, 1979]. Rolling being a much more energy efficient motion type than bouncing, the size sorting of a talus slope is considered as “natural record” of the energy loss of the blocks during impact.

Several approaches are used to gather information and analyse the rockfall phenomenon. The back analysis of natural rockfall events was probably one of the first methods. Later, the rational observation and analysis of the phenomenon (in particular with special *in situ* and laboratory tests), has increased rockfall knowledge significantly. Based on this information, numerical models represent a

valuable tool for the quantitative evaluation of potential trajectories – provided that they are accurately calibrated.

2.2.1 Back analysis of rockfall events

After the occurrence of natural rockfall events, the analysis of the tracks left in the field or on trees and the observation of block deposits can help to understand the phenomenon and to gather valuable information (as e.g. range of block size, horizontal and lateral runout distance, bouncing height and length, ...). By back analysis of such events, the velocities and energies of the falling blocks as well as the percentage of velocity or energy lost during impact can be evaluated [e.g. for natural events: Lied, 1977; Evans & Hungr, 1993]. Such observations should be used to calibrate computer programs for trajectory analyses on the site of interest or other slopes with similar characteristics [Labieuse & al., 2001].

Although the observation and back analysis of natural events is indispensable for the correct calibration of trajectory programs, this kind of rockfall investigation is not appropriate for parametrical studies or - in the case of few observations - statistically significant conclusions. This is due to the natural inhomogeneity of the tested materials (surface roughness, shape and strength of blocks and slope, etc...).

2.2.2 *In situ* tests

Beside the observation of natural events, *in situ* experiments are important for the study of the phenomenology and the assessment of the relevant physical parameters as well as for the correct calibration of numerical models. For *in situ* tests, blocks are released at the top of a slope with well-known geological and geomorphological features. Their trajectories down the slope are recorded by cameras and analysed to determine block velocities, heights of bounce and runout distances. For each relevant impact of the block, the translational and rotational velocities before and after impact and, consequently, the coefficients of restitution are evaluated. Many field experiments have already been performed and analysed world-wide [e.g. Ritchie, 1963; Japanese highway public corporation, 1973; Broili, 1977; Lied, 1977; Statham, 1979; Wu, 1985; Bozzolo & al., 1988; Pfeiffer & Bowen, 1989; Fornaro & al., 1990; Kobayashi & al., 1990; Azzoni & al., 1992; Giani, 1992; Evans & Hungr, 1993; Azzoni & De Freitas, 1995; Urciuoli, 1996; Yoshida, 1998; Teraoka & al., 2000].

Among those *in situ* tests, the most complete series was carried out by ISMES in Italy between 1989 and 1995 on natural rock slopes of different geological and geomorphological features (Chapter 2.5.2). Those tests allowed to analyse the influence of parameters related to both the block (as block size, shape and

mechanical features) and the ground (nature, geometry) on the trajectory [Azzoni & al, 1992; Azzoni & De Freitas, 1995]. A special attention has been paid to evaluate the coefficients of restitution and of rolling friction [Giani, 1992; Azzoni, 1993]. These coefficients, together with the geometry of the slope and the falling blocks, are identified to be the most relevant parameters for defining the characteristics of rockfall motion. Some values of the coefficients of restitution cited in literature are given exemplarily in Chapter 2.3.7.

In situ tests are extremely important for the study of rockfalls because they alone allow the visualisation of many different and complicated aspects of this highly random phenomenon. These tests permit both the study of the phenomenology and the assessment of relevant physical parameters, not to mention the correct calibration of mathematical models [Azzoni & De Freitas, 1995]. Yet, *in situ* tests are expensive and (as natural events) not very suitable for statistical and parametric analysis. Therefore, laboratory scale tests represent an important supplement for accurate experimental investigation.

2.2.3 Laboratory tests

The experimental studies carried out in laboratories mainly consist in performing tests on small- or sometimes large-scale models. In some cases, a whole trajectory is simulated [Camponuovo, 1977; Azimi & Desvarreux, 1977 and Azimi & al., 1982; Statham, 1979; Ujihira & al., 1993; Murata & Shibuya, 1997], while other experiments concentrate on a single impact [Kawahara & Muro, 1999; Kamijo & al., 2000; Wong & al., 1999 and 2000; Ushiro & al., 2000; Chau & al. 1998, 1999a, b, 2002].

These experiments are very helpful to understand the mechanism of a rockfall and to gain insight into the most important parameters. However, the quantitative interpretation of the results is not straightforward, owing to the difficulty in matching the similitude requirements for all the parameters involved in the dynamic process (see Chapter 3.3). Based on small-scale experiments, Camponuovo [1977] stressed that while it is reasonably possible to determine and match the static characteristics of materials (deformability, strength, density, static friction angle) on the model, irrespective of its small size, it is not as simple to determine or match the characteristics involved in dynamic fall occurrences (coefficient of restitution, impact strength, dynamic friction angle). For instance, according to Camponuovo, a scale model rock verifying the mechanical similitude requirements and impacting a rock surface provides a far lower energy of restitution than the one observed on full-scale rebound tests.

If it is possible to perform large-scale experimental campaigns in laboratory, the advantages of laboratory and *in situ* tests can be combined:

- the test conditions and the parameters are easy to control, and
- the energies and materials used for large-scale tests can be chosen to match the parameters found in nature for small rockfall events.

Some results of small- and large-scale tests relevant for the thesis are given in the Chapters 2.3.7 and 2.5.

2.2.4 Programs

Since the late seventies, the rapid development of computer programs, together with valuable experience gathered through a more rational observation of the phenomenon (in particular with special *in situ* and laboratory tests), has increased rockfall knowledge significantly. To date, a huge number of rockfall simulation programs allow to perform more rational trajectory analyses. The main objectives of these rockfall models are the assessment of

- potential trajectories,
- heights of bounces, velocities and energies achieved during the fall, and of
- maximum runout distances in order to determine the areas at risk.

Provided that programs are well calibrated, the simulation results are very helpful to gain accurate information on design values for protective structures and identify rockfall prone areas.

The existing models can be distinguished in two main categories, the rigorous and the lumped-mass methods [Hungr & Evans, 1988; Giani, 1992]:

- Rigorous methods consider the block as a body with its own shape and volume and account for all types of block movement, including rotation. Examples of programs from this category are: the Distinct Element Method by Cundall [1971], Falcetta [1985], the three-dimensional program EBOULEMENT by Descoedres & Zimmermann [1987] and Dudt & Heidenreich [2001], Cadma by Azzoni & al. [1995], Rockfall 6.0 by Spang & Krauter [2001] etc.
- Lumped-mass methods consider the block to have either no mass or a mass concentrated in one point. They do not take into account the shape of the blocks nor the rotational movement. Numerical models based on these hypotheses are more frequent, e.g. Ritchie [1963], the Computer Rockfall Model by Piteau [1977], Hungr & Evans [1988], RocFall by Hoek [1986] and Stevens [1998] or Stone by Guzzetti & al. [2002].

Some programs take advantage of the fast and easy simulation of the free flight for lumped masses but consider some geometrical and mechanical characteristics of the slope and the block for the modelling of the impact. Examples of such methods, qualified as hybrid, are the program developed at the ADRGT based on Azimi & Desvarreux [1977], the program SASS by Bozzolo & Pamini [1986], PROPAG developed by Rochet [1987] or CRSP by Pfeiffer & Bowen [1989] and Jones et al. [2000] as well as Kobayashi & al. [1990].

Rigorous and hybrid methods are generally better than lumped-mass methods, as they are more capable of accurately reproducing the different phases of the fall phenomena: free fall, bouncing, rolling and sliding.

Most programs analyse the trajectory in a two-dimensional space, since three-dimensional analysis is theoretically more demanding and therefore more expensive. However, on complicated slope geometries, a three-dimensional program can be very helpful in determining the main rockfall paths [Descœudres & Zimmermann, 1987].

Further, the trajectory programs are differentiated according to the description and analysis of the phenomenon being either statistical or deterministic. “Deterministic” programs use either mean input values or a “worst case” assumption for the calculation of the rockfall trajectory. For a single trajectory simulation, the input parameters therefore are fixed on a certain value and stay constant for whole of the simulation process. The result of the simulation is a single mean or worst-case trajectory with the associated characteristics (such as height of bounce, energy, runout distance...). However, most of the important parameters (such as the shape of the block, the mechanical characteristics of the slope, local slope angle at impact, detachment area, etc.) show a natural variability. The programs classified as “statistical” (such as Wu [1985], Azzoni & al. [1995] or Dudt & Heidenreich [2001]) account for this variability by the adoption of random values chosen within a previously determined range. As result, not only one but a large number of potential trajectories are modelled. A statistical distribution of the trajectory characteristics (such as height of bounce, energy, runout distance...) is the result.

A detailed list of rockfall programs and their main characteristics can be found in Labiouse & al. [2001] or in Guzzetti & al. [2002].

To simulate the rebound of the blocks during their trajectory, most rockfall models represent the bouncing phenomenon in a simplified way by one or two overall coefficients, called coefficients of restitution. In some cases, the frictional loss is modelled by means of an additional friction coefficient. Controlling the

loss of energy or velocity during impact, these coefficients constitute the most crucial input parameters. The reliability of any trajectory simulation therefore depends highly on a thorough calibration of the model on the studied site, including an adequate estimation of the coefficients of restitution and friction.

2.3 Mathematical models of the bouncing phenomenon

When the trajectory of a block intercepts the slope surface, the boulder induces an impulse to the ground and bounces back. The height of bounce, the rebound direction and the rotational rate induced to the block during impact depend on the impact conditions which can be specified by a large number of parameters.

During impact, a certain amount of energy is dissipated. The energy dissipation is due to the elasto-plastic behaviour of the ground on which the block impacts, to the elastic wave generation, to the block and / or ground grain destruction and to the rolling and sliding resistance [Giani, 1992].

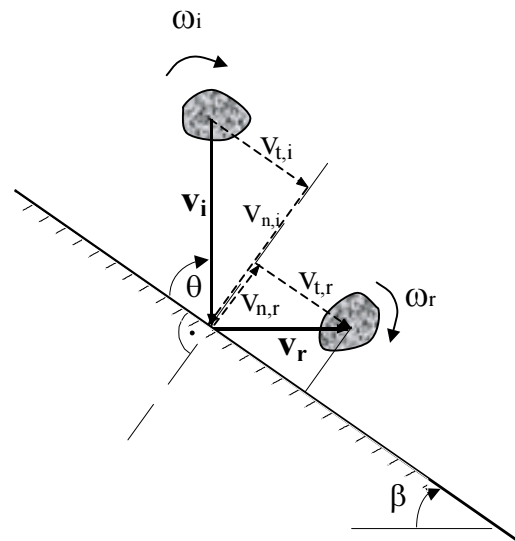


Figure 2.3: Scheme of the translational and rotational velocities and their components before and after impact

In general, two main energy dissipation modes are differentiated. While the plasticity of the ground material determines the kinetic energy dissipation **normal** to the slope surface, the mechanism in resisting motion **parallel** to the slope is sliding or rolling friction. Due to the different mechanisms involved in resisting motion normal and tangential to the slope, different definitions to measure the resistance are used. The measure of the resistance normal to the slope therefore is called **normal coefficient of restitution**, while the measure of the resistance to movement parallel to the slope is called **tangential coefficient of restitution**.

Depending on the impact conditions, the impact is further differentiated according to the contact between block and ground. If the tangential velocity of the part of the block being in contact with the ground is zero, the impact is called “sticking” impact. The process can be described as pure instantaneous rolling. In case of a non-zero tangential velocity component at the contact point, the impact is called

“sliding” or “slipping” impact. In this case, the block motion is a combination of sliding and rolling.

From a mathematical point of view, various models have been proposed to describe the mechanisms occurring during impact. Thus, there seems to be no consensus on which model is more appropriate for rockfall prediction. The most common models are written in terms of velocities or energies, while other, less common models use e.g. the ratio of impulse (as Descoeurdes & Zimmermann [1987] and Bozzolo & al. [1988]). These ratios, each expressing the amount of velocity and/or energy dissipated during impact, are commonly called “coefficient of restitution”, even if this terminology is not quite correct in the sense proposed by Newton, who defined the coefficient of restitution only by the ratio of velocities (equation (2-1)). In the following, the models most commonly used in the context of rockfall analysis are stated.

2.3.1 Velocity models

According to Newton’s theory of centric particle collision, the coefficient of restitution R is defined for rigid and smooth particles as:

$$R = \frac{v_{r,2} - v_{r,1}}{v_{i,2} - v_{i,1}} \quad (2-1)$$

where v_i represents the initial particle velocity and v_r the velocity after the collision of two particles 1 and 2 (the subscripts “i” and “r” stand for “incident” and “rebound” respectively). The coefficient of restitution R can take values between 0 and 1, where $R = 0$ is termed perfectly inelastic collision and $R = 1$ corresponds to perfectly elastic collisions. In case of a block impacting the ground (which has no impact or rebound velocity), the coefficient of restitution is simplified to:

$$R_v = \frac{v_r}{v_i} \quad (2-2)$$

where v_i and v_r are the magnitudes of the incoming and rebounding block velocities (Figure 2.3). This definition is used by several authors [e.g. Habib, 1977; Spang & Rautenstrauch, 1988; Paronuzzi, 1989; Spang & Sönsler, 1995; Kamijo, 2000].

For tests with initial free fall, equation (2-2) can also be written as:

$$R_H = \sqrt{\frac{H_r}{H_i}} \quad (2-3)$$

where H_i and H_r are the incident drop and the rebound height respectively.

Experimental evidence shows that a better definition is obtained by a differentiation into normal and tangential components of the incoming and rebounding velocity. The coefficients of restitution R_n and R_t then are defined as:

$$R_n = -\frac{v_{n,r}}{v_{n,i}} \quad (2-4)$$

$$R_t = \frac{v_{t,r}}{v_{t,i}} \quad (2-5)$$

where v_n and v_t are the normal and tangential components of the block velocities with respect to the slope surface (Figure 2.3). During impact, the normal component of velocity is changed in sign. To get nevertheless a positive definition of the normal component of the coefficient of restitution and according to Newton's law of impact, the expression includes the factor (-1) . Both the normal and tangential coefficients are defined only for incident velocity components greater than zero. This definition is used by many authors such as Piteau & Clayton [1976], Wu [1985], Urciuoli [1988], Pfeiffer & Bowen [1989], Fornaro & al. [1990], Hoek [1987], Kobayashi & al. [1990], Giani [1992], Evans & Hungry [1993], Budetta & Santo [1994], Ushiro & al. [2000].

According to the fact that many computer programs consider the block as a mass concentrated in one point, the velocities used to define the coefficients of restitution correspond to the mass centre velocities, and not – as in the theory of shocks – to the velocity relative to the contact point.

It should be noted that the definition given in equation (2-4) sometimes is used without mentioning that the equation applies only for the normal components of the block velocity. Due to the mix-up with the notion stated in (2-2), some misinterpretations are found in literature. To avoid this mistake, the notation of the coefficients of restitution should be used according to the above listed (and most common) notations.

The coefficients of restitution R_n and R_t , defined by the ratio of the normal and tangential components of the incident and the rebound velocity of the mass centre of the block, indicate the amount of translational velocity dissipated during impact. In practice, several values are proposed to be associated with a certain

ground material (refer Table 2.1). However, such definition implies that the coefficients of restitution are independent of other factors as the block characteristics (mass, shape...) or the kinematics (incident velocity...). Even if stated to have an important influence on the trajectory and the total energy of the block (e.g. Japan Road Association [1983], Yoshida [1998], Kawahara & Muro [1999], Chau & al. [2002]), the impact velocity or the rotation at impact end are completely neglected. To take into account the rotation of the block, a further definition by means of the block energy is proposed and introduced hereafter.

2.3.2 Energy models

The model presented in the following expresses the restitution by means of the ratio between the block energies before and after impact. Several slightly different definitions are cited in literature. Most authors (e.g. Bozzolo & Pamini [1986], Azzoni & al. [1995], Chau & al. [1999 b]) express the coefficient of restitution by means of the translational energy of the boulder before and after impact:

$$R_E = \frac{E_{\text{trans},r}}{E_{\text{trans},i}} = \frac{0.5 \cdot m \cdot v_r^2}{0.5 \cdot m \cdot v_i^2} = \frac{v_r^2}{v_i^2} \quad (2-6)$$

where m is the mass of the boulder and v_i and v_r are the impact and rebound velocity of the mass centre of the block, respectively. The last equation is not valid in case of a change in mass, e.g. by fragmentation of the block.

Urciuoli [1988] proposes a slight variation of this formulation, differentiating a normal and tangential component of the energy restitution:

$$R_{E,n} = \frac{v_{n,r}^2}{v_{n,i}^2 + v_{t,i}^2} = \frac{v_{n,r}^2}{v_i^2} \quad (2-7)$$

$$R_{E,t} = \frac{v_{t,r}^2}{v_{n,i}^2 + v_{t,i}^2} = \frac{v_{t,r}^2}{v_i^2} \quad (2-8)$$

As long as friction exists between boulder and slope surface, partial locking is likely to occur. Consequently, rotation is induced to the boulder during an inclined impact, which should not be neglected. Thus, a further mathematical definition of the coefficient of restitution is proposed, accounting for the total energy of the boulder:

$$R_{TE} = \frac{E_{\text{tot},r}}{E_{\text{tot},i}} = \frac{0.5 \left(m(v_{n,r}^2 + v_{t,r}^2) + I\omega_r^2 \right)}{0.5 \left(m(v_{n,i}^2 + v_{t,i}^2) + I\omega_i^2 \right)} \quad (2-9)$$

where v and ω are the translational and rotational velocity of the mass centre respectively, m is the mass and I the moment of inertia relative to the block centre. To date, only few authors [Japan Road Association, 1983; Azzoni & De Freitas, 1995; Yoshida, 1998; Chau & al., 2002] have investigated the rotational energy induced during each boulder impact. To be able to calculate the rotational part ω_r of the block movement after impact, a relationship between translation and rotation has to be established. The observation of block trajectories showed that blocks leave the ground in general in a rolling mode. Therefore, the relation between translational and rotational velocity is commonly assumed to be $\omega_r \cdot r = v_r$. However, this relation implies block rolling without sliding, which – in the opinion of the author and based on the experience made during the impact tests performed during the present thesis – can perhaps be assumed in case of impacts on rock slopes, but does not represent reality for impacts on granular slopes (as rolling *and* sliding occurs).

By means of the presented formulations, the rebound direction can not be determined. Other assumptions, as a relation between the incident and the rebound angle or the coefficients R_n and R_t have to be used additionally.

Even if the rotation of the block is taken into account, the coefficients of restitution R_E and R_{TE} still are constant values assigned to a certain ground material and independent of other parameters as e.g. the incident velocity of the block or its impact configuration.

A further possible mathematical model to express the coefficient of restitution is proposed by Stronge [1990]. He suggests that the ratio of work of the normal force during compression to that during restitution is a better candidate for a “material constant” than the coefficients of restitution defined by the ratio of energy or velocity [Smith & Liu, 1992]. However, this definition is not yet used in the context of rockfall studies.

2.3.3 Impulse models

An alternative definition has been proposed and implemented by Descoedres & Zimmermann [1987] and Bozzolo & al. [1988]. Based on the hypothesis of a plastic shock, the approach consists in defining a single coefficient of restitution R_I being the ratio between the normal component of impulse during the compression and the restitution phase (equation (2-10)). In case equation (2-11) is fulfilled, no instantaneous sliding occurs (“sticking” impact), else sliding is supposed to occur in the contact point (“sliding” impact). The formulation proposed by Descoedres & Zimmermann [1987] is written as follows:

$$R_I = \frac{I_{n,r}}{I_{n,i}} = \frac{\int_{t_2}^{t_3} F_n(t) dt}{\int_{t_1}^{t_2} F_n(t) dt} \leq \frac{C}{\sqrt{m \cdot v_{n,i}}} \quad (2-10)$$

$$I_{t,r} = \int_{t_2}^{t_3} F_t(t) dt \leq \int_{t_2}^{t_3} \mu \cdot F_n(t) dt = \mu \cdot I_{n,r} \quad (2-11)$$

where I_n and I_t are the normal and tangential component of impulse, F_n and F_t are the normal and tangential components of the contact force acting during impact between block and ground (Figure 2.4), μ is the coefficient of friction and C is a plasticity factor, limiting R_I for large block masses and/or normal velocities. Thus, the normal coefficient of restitution R_I depends not only on the ground characteristics but also on the mass m of the block and the normal component of its initial velocity $v_{n,i}$. The friction coefficient μ however is assumed to depend just on the slope material. The impulse is defined as the integration over time of the impact force in the contact point, t_1 being the begin, t_2 the paroxysm and t_3 the end of the shock (Figure 2.4).

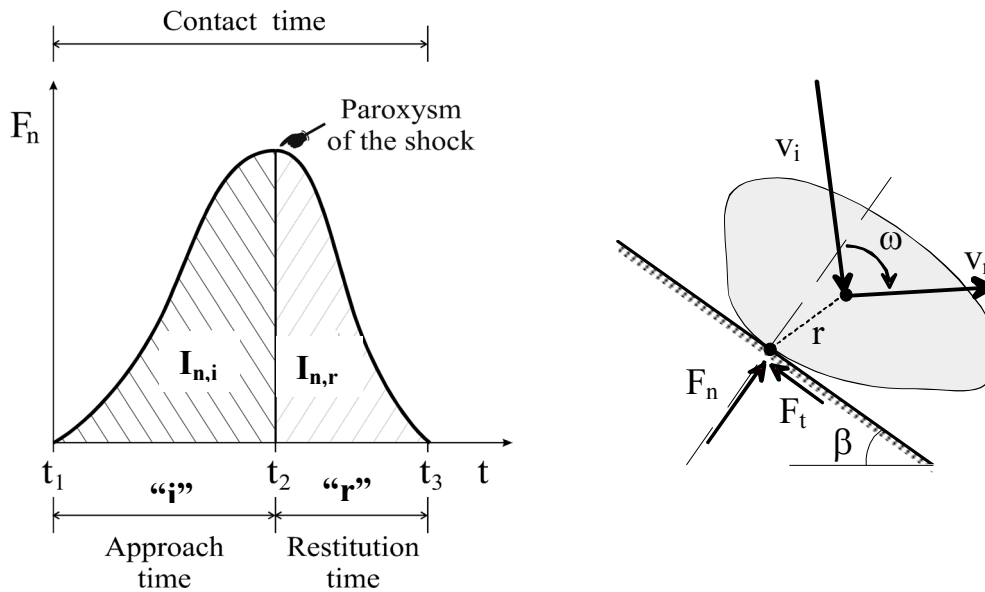


Figure 2.4: Time dependence of the impact force $F_n = m \cdot a_n$ acting on the block [talk given by Labiouse, 1999, inspired by Bozzolo & al, 1988]. A scheme of the forces acting on the block at impact is given on the right hand side [Labiouse & al., 2001].

Apart the method proposed by Descoedres & Zimmermann [1987], Azimi & Desvarreux [1977] and Pfeiffer & Bowen [1989] have developed further methods to account for the influence of other parameters than the ground characteristics. Both models are stated in the following.

2.3.4 Model proposed by Azimi & Desvarreux [1977]

Azimi & Desvarreux [1977] developed a rockfall simulation program which differentiates between impacts on soft and on hard ground material, considering the block penetration into the ground during impact. The block is simulated as mass point.

For impacts on **hard ground** (Figure 2.5), the ground is considered as perfectly elastic whereas the block is modelled as elastic perfectly-plastic. In this case, the coefficients of restitution R_n and R_t are used to model the loss of velocity during impact. The normal component R_n depends not only on the ground material, but also on the block mass and shape and its incident velocity. The tangential component R_t is function of the incident velocity, the slope angle, the impact time and a global friction coefficient η accounting for rolling and sliding friction. Further, the block resistance is considered to account for a possible fragmentation of the block.

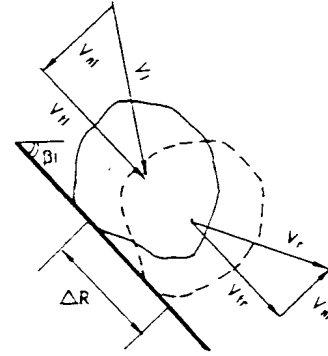


Figure 2.5: Impact on hard ground material [Azimi & Desvarreux, 1977]

For impacts on **soft ground** (Figure 2.6), the block, considered as rigid, is supposed to penetrate into the ground material which behaves perfectly plastic. The rebound velocity is evaluated considering the following parameters by incrementing the penetration depth h of the block into the ground:

$$m \cdot v_n \frac{dv_n}{dn} = f(\eta, \theta, K, p, h, S(h), m) \quad (2-12)$$

$$m \cdot \frac{dv_t}{dt} = f_1(\eta, \theta, K, p, h, S(h), m) \quad (2-13)$$

$$dt = \frac{dh}{v_n} \quad (2-14)$$

The normal and tangential component of the rebounding velocity are proposed to depend on the block mass m , the incident velocity, the global friction coefficient η , the stress normal to the slope surface (which is evaluated by means of two coefficients K and p , and the penetration depth h), the contact surface between block and crater $S(h)$ and the angle θ between the actual moving direction and the slope surface.

These formulations account for:

- the penetration of the block into the ground normal to the slope. During penetration, the contact surface $S(h)$ and the normal contact force tend to grow till the kinetic energy in normal direction ($E_{kin,n} = 0.5 \cdot m \cdot v_{n,i}^2$) is completely dissipated by the plastic ground deformation;
- the creation of a crater, its form depending on the characteristics of the ground material and the incident velocity;
- the sliding and rolling of the block on the crater base during its creation, diminishing the blocks tangential velocity.

The full mathematical expressions are unfortunately not available.

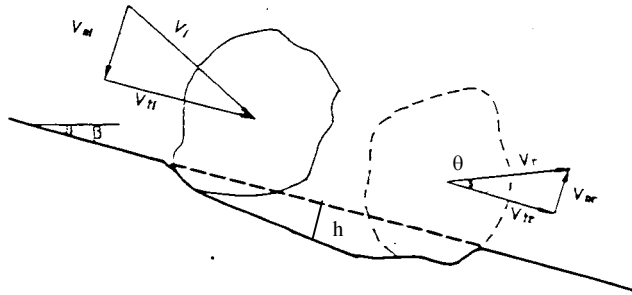


Figure 2.6: Impact on soft ground material [Azimi & Desvarreux, 1977]

2.3.5 Model proposed by Pfeiffer & Bowen [1989]

Also Pfeiffer & Bowen [1989] propose a very interesting rebound model, which is implemented in their rockfall simulation program CRSP. The energy dissipation provoked by rolling or sliding during impact is taken into account by reducing the incident energy component tangential to the slope by a friction function $f(F)$ and a scaling factor SF:

$$\left(\frac{1}{2} I \omega_i^2 + \frac{1}{2} m v_{t,i}^2 \right) \cdot f(F) \cdot SF = \frac{1}{2} I \omega_r^2 + \frac{1}{2} m v_{t,r}^2 \quad (2-15)$$

with I being the moment of inertia relative to the block centre, ω and v being the rotational and translational velocities of the block ($i = \text{incident}$, $r = \text{rebound}$), and m being the block mass. The friction function $f(F)$ is defined to depend on R_t as follows:

$$f(F) = R_t + \frac{1 - R_t}{\left(\frac{v_{t,i} - \omega_i r}{20} \right)^2 + 1.2} \quad (2-16)$$

where r is the block radius. The friction function $f(F)$ adjusts the tangential coefficient R_t according to the velocity at the surface of the rock relative to the ground at the beginning of the impact.

The scaling factor SF is defined as:

$$SF = \frac{R_t}{\left(\frac{v_{n,i}}{250 \cdot R_n}\right)^2 + 1} \quad (2-17)$$

The constants used in the equations for $f(F)$ and SF were determined by fitting several *in situ* experimental series performed in the US and in Switzerland. It is very important to note that the constant factors (20, 250 and 30) given in the formulations (2-16) to (2-19) are relative to US-American units for length [ft] and weight [lb] and have to be adapted if used with European units.

Solving equation (2-15) for the tangential component of the rebound velocity and supposing pure rolling at impact end ($v_{t,r} = \omega_r \cdot r$) yields:

$$v_{t,r} = \sqrt{\frac{r^2 (I\omega_i^2 + mv_{t,i}^2) \cdot f(F) \cdot SF}{(I + mr^2)}} \quad (2-18)$$

The normal component of the rebound velocity is evaluated by:

$$v_{n,r} = \frac{v_{n,i} \cdot R_n}{1 + \left(\frac{v_{n,i}}{30}\right)^2} = v_{n,i} \cdot R_n \cdot B \quad (2-19)$$

where the velocity-dependent normal scaling factor $B = 1/(1 + (v_{n,i}/30)^2)$ adjusts for the decrease in normal coefficient of restitution R_n as the impact velocity increases. This factor represents a transition from nearly elastic conditions at low velocities to highly inelastic conditions caused by increased fracturing of the rock and cratering of the slope surface at higher impact velocities [Habib, 1977].

2.3.6 Model proposed by Ushiro & al. [2000]

As Azimi & Desvarreux [1977], Ushiro & al. [2000] propose a differentiation between impacts on hard and soft ground material. On **hard ground material**, the contact between block and ground surface is defined to be pure instantaneous rolling for a contact friction greater or equal to a certain limit depending on R_n

and to be a combination of rolling and sliding for a contact friction smaller than the limit. The normal rebound velocity is computed by means of the coefficient of restitution defined in equation (2-4). The tangential and rotational rebound velocities depend on the contact friction and are reduced by a predefined factor (for rolling) or by means of R_n combined with the friction coefficient μ (for rolling and sliding) as follows:

for $\mu \geq \frac{2(v_{t,i} + r\omega_i)}{7v_{n,i}(1 + R_n)}$ (pure instantaneous rolling):

$$v_{t,r} = \frac{5v_{t,i} + 2r\omega_i}{7} \Rightarrow R_t = \frac{5v_{t,i} + 2r\omega_i}{7v_{t,i}} \quad (2-20)$$

$$\omega_r = \frac{v_{t,r}}{r} = \frac{5v_{t,i} + 2r\omega_i}{7r} \quad (2-21)$$

for $\mu < \frac{2(v_{t,i} + r\omega_i)}{7v_{n,i}(1 + R_n)}$ (combined rolling and sliding):

$$v_{t,r} = v_{t,i} + \mu(1 + R_n)v_{n,i} \Rightarrow R_t = 1 + \mu(1 + R_n) \cdot \tan \theta \quad (2-22)$$

$$\omega_r = \omega_i - \frac{5\mu(1 + R_n)v_{n,i}}{2r} \quad (2-23)$$

with θ being the angle between the slope inclination and the horizontal.

For **soft ground material**, the block is supposed to penetrate into the ground material during impact (Figure 2.7). The penetration depth is guided by the normal force acting between block and ground and depends on both the contact surface as well as the ground stiffness. The normal velocity component after impact therefore depends on the normal contact force N , the block mass m (corresponding to M in Figure 2.7), the contact surface A , the ground stiffness k , the slope angle β and the penetration depth δ . It is determined by:

$$v_{n,r} = \sqrt{\frac{\varepsilon \cdot N^2}{m \cdot k \cdot A} - 2g \cdot \cos \beta \cdot \delta} \quad (2-24)$$

where g the gravity. The normal component of the coefficient of restitution can therefore be written in dependency of the ground elasticity as:

$$R_{n,Ushiro} = \frac{v_{n,r}}{v_{n,i}} = \frac{1}{v_{n,i}} \sqrt{\frac{\varepsilon \cdot N^2}{m \cdot k \cdot A} - 2g \cdot \cos \beta \cdot \delta} \quad (2-25)$$

In case of $\frac{\varepsilon \cdot N^2}{m \cdot k \cdot A} \leq 2g \cdot \cos \beta \cdot \delta$, $R_{n,Ushiro}$ is equal to 0.

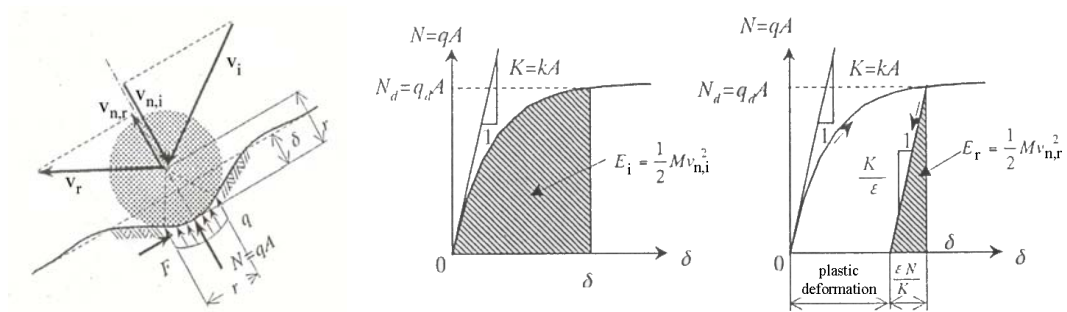


Figure 2.7: Block impacting a soft ground material: strength-deformation diagram for the compaction (middle) and restitution (right) phase of the impact; after Ushiro [2000]

2.3.7 Values of coefficient(s) of restitution stated in literature

As mentioned above, the most reliable way to determine the coefficients of restitution is through experimental observations (*in situ* tests or back analysis of natural rockfalls). In case the trajectory is filmed, the translational and rotational approach and separation velocities can be evaluated for each relevant impact of the block. Consequently the coefficients of restitution are assessed. In case of back analysis, the coefficients are achieved by trial and error checking whether the numerical predictions are comparable to field observations, like velocity, height and length of bounce and runout distance.

For lack of precedent *in situ* tests or natural events, the coefficients required as input parameters for rockfall programs are to date determined by experience based on the geological conditions of the slope or by a calibration of the program on precedent natural events or tests on similar slopes. In the following, a summary of coefficients of restitution evaluated by several researchers by means of back analysis of natural events, *in situ* or special large-scale tests, is presented (Table 2.1). In literature, the values are commonly associated to certain ground characteristics. Independent of the definition forming the basis of the coefficient of restitution, its value ranges between 0 and 1, where $R = 0$ stands for a purely plastic shock (impulse completely dissipated) while $R = 1$ defines a purely elastic shock (full restitution of the impulse to the block). As various as the definitions of the coefficient of restitution stated in literature, are the values reported for it. Their variability even for comparable ground materials reveals the problematic related to their definition as material constants.

!!! It has to be pointed out that any coefficient of restitution taken from literature or obtained through in situ tests and/or back analysis are likely to provide incorrect results when used on other sites. Therefore these values are not to be used for trajectory simulations without a thorough calibration of the model.

!!! Furthermore, one has to keep in mind that the coefficients of restitution summarised in Table 2.1 are related to different bouncing models (see subheadings 2.3.1 to 2.3.6).

This list (Table 2.1) states an example for the difficulty to describe a rockfall event by means of the currently used definitions of the coefficient of restitution. Due to the fact, that the coefficients of restitution defined above are mostly considered as material constants, it would not be possible even with an endless number of impact tests to find the right coefficient for each possible impact configuration (velocity, impact angle, block shape and mass, slope angle, material etc...). As long as the common definition of the coefficients of restitution cited above are used in computer simulation programs, one can understand that the user of any rockfall simulation program has to be downright familiar with the program and the definitions forming its mathematical basis to be able to produce reasonable results. In most cases, the program has to be calibrated especially on each site to find by trial and error the appropriated coefficients.

In general it can be stated that compact rock slopes have higher coefficients of restitution than debris or earth slopes. A vegetation cover seems to reduce the coefficient of restitution. An interesting summary of values given in literature for three slope materials (rock, debris or detrital slope) is provided by Fornaro & al. [1990]. The authors graphically present the range of values for the coefficients of restitution R_n and R_t (defined after equations (2-4) and (2-5)) according to different slope characteristics (Figure 2.8). The values for R_n and R_t are plotted against each other, revealing a high variability. Nevertheless, a domain for values can be assigned to each of the rough slope material descriptions.

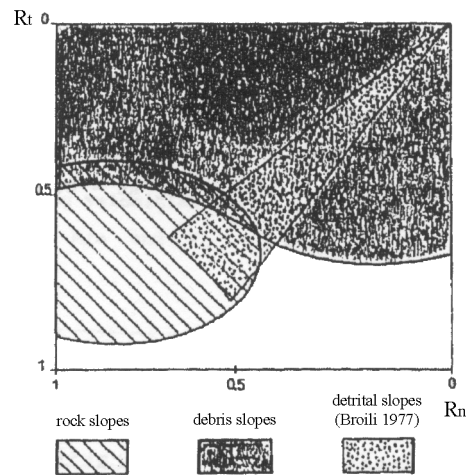


Figure 2.8: Variability ranges of the coefficients of restitution R_n and R_t according to the ground material [Fornaro & al., 1990].

The high variability of values given in Table 2.1 and represented in Figure 2.8 for similar ground materials reveals that there must be other parameters influencing the rebound phenomenon than the ground characteristics. To date, several parameters are identified to influence the rebound mechanism and thus the coefficients of restitution. These parameters and their effects on the rebound of a block are discussed in Chapter 2.5.

Reference	Value for R_n	Value for R_t	Value for R_E	Value for R_{TE}	Value for R_I	Remarks
Habib 1977	0.75-0.80					Based on experience in Italy
	0.5-0.6					Based on experience in Norway
Piteau & Clayton 1977	0.8-0.9	0.65-0.75				Solid rock
	0.5-0.8	0.45-0.65				Detrital material mixed with large rock boulders
	0.4-0.5	0.35-0.45				Compact detrital material mixed with small boulders
	0.2-0.4	0.2-0.3				Grass covered slopes
Wu 1985	0.2-0.8	0.5-0.75				Rock on rock or wood platform
Heierli 1985	0.95		0.9			Rock
	0.55		0.3			Gravel layer (35 cm)
	0.45		0.2			Gravel layer (70 cm)
	0.45		0.2			debris
Bozzolo & Pamini, 1986				0.7		Rock at a slope angle of 44°
				0.55		Debris at a slope angle of 57°
Descoedres & Zimmermann 1987					0.4	Vineyard slopes
					0.85	Rock slopes
Hoek 1987	0.53	0.99				Clean hard bedrock
	0.4	0.9				Asphalt roadway
	0.35	0.85				Bedrock outcrops with hard surface, large boulders
	0.32	0.82				Talus cover
	0.32	0.8				Talus cover with vegetation
	0.3	0.8				Soft soil, some vegetation
Urciuoli 1988**	0.05-0.35	0.5-1	0.02-1			Rock block impacting limestone
	~0	0.24				Debris fan

Reference	Value for R_n	Value for R_t	Value for R_E	Value for R_{TE}	Value for R_I	Remarks
Pfeiffer & Bowen 1989*** (older versions of program CRSP)	0.37-0.42	0.87-0.92				Smooth, hard surface as paving, rock
	0.33-0.37	0.83-0.87				Bedrock or boulders with little soil or vegetation
	0.30-0.33	0.83-0.87				Talus with little vegetation
	0.30-0.33	0.80-0.83				Talus with some vegetation
	0.28-0.32	0.80-0.83				Soft soil slope with little vegetation
	0.28-0.32	0.78-0.82				Vegetated soil slope
Giani 1992, Barbieri & al. 1988	0.5	0.95				Bedrock
	0.35	0.85				Bedrock covered by large blocks
	0.3	0.7				Debris formed by uniform distributed elements
	0.25	0.55				Soil covered by vegetation
Evans & Hungr 1993	0.9	0.9				Small blocks on clean rock
	0.7	20.8*				Large blocks on talus
Azzoni & al. 1995				0.75-0.90		Rock (limestone)
				0.55-0.6		Fine angular debris and earth (compacted)
				0.35-0.45		Fine angular debris and earth (soft)
				0.45-0.50		Medium angular debris with angular rock fragments
				0.4-0.5		Medium angular debris with scattered trees
				0.55-0.70		coarse angular debris with angular rock fragments
				0.5-0.6		Earth with grass and some vegetation
				<0.20		Ditch with mud
				0.5-0.65		Flat surface of artificially compacted ground
Gerber 1995	0.17-0.43	0.45-0.88				Rock (limestone)
Kamijo 2000	0.1-0.35					Vertical impact of a 220kg rock on hard surface
	0.1					Vertical impact of a 800kg rock on hard surface
Ushiro & al. 2000	0.1-0.4	0.71				?
Jones & al. 2000*** (Values gathered by program calibration for CRSP 4.0)	0.6-1.0	0.9-1.0				Smooth hard surface and paving
	0.15-0.30	0.75-0.95				Bedrock and boulder fields
	0.12-0.2	0.65-0.95				Talus and firm soil slopes
	0.1-0.2	0.5-0.8				Soft soil slopes
Budetta & Santo 1994 evaluated by program calibration	0.2	0.53				Rock

* values larger than 1 can be evaluated by back analysis if the initial velocity component is very small or 0. The ratio defining R therefore yields large values not really expressing the restitution but rather an abrupt change of direction.

** Urciuoli [1988] states that R_n , R_t and R_E depend on the impact velocity.

*** Pfeiffer & Bowen [1989] and Jones & al. [2000] use R_n and R_t as material constants but account for several other parameters by means of scaling factors.

Table 2.1: Values of the coefficient of restitution stated in literature.

2.4 Models for rolling and sliding

Some authors use a tangential damping coefficient related to the rolling and / or sliding friction between block and slope. Different coefficients for the rolling and sliding phase of a block are proposed (e.g. Statham [1979], Bozzolo & Pamini [1986], Azzoni & De Freitas, [1995]). The sliding friction is defined by means of the normal component of the block weight according to Coulomb's law of dry friction:

$$F_f = \mu_f \cdot N = \mu_f \cdot m \cdot g \cdot \cos \beta \quad (2-26)$$

where μ_f is the friction coefficient, m the block mass, g the gravity constant and β the slope angle. The direction of the force F_f is opposite to the velocity of the rock at the point of contact. The authors state the range of $0.6 \leq \mu_f \leq 1$ as typical values.

For the rolling phase, a differentiation is made between pure rolling and a combination of rolling and slipping in the point of contact. According to Statham [1979], a fairly accurate description of this complex phase can again be given by using Coulomb's law of friction with a friction coefficient that depends on the properties of block and slope. The following formula is stated:

$$F_r = \mu_r \cdot m \cdot g \cdot \cos \beta \quad (2-27)$$

where μ_r is the "dynamic friction coefficient" typical for rolling. It is expressed as the tangent of the angle at which a block can be considered to move with a steady velocity on a slope. It includes all processes of retardation included within the motion. On a slope steeper than this angle, the block accelerates, while on flatter slopes it decelerates and finally stops. This angle depends both on the type and shape of the materials and the ratio between the size of the block and the size of the debris. Statham proposed the following formula to assess the dynamic friction coefficient:

$$\mu_r = \mu_0 + k \cdot (d/D) \quad (2-28)$$

where μ_0 is the tangent of the angle of dynamic friction ϕ_0 when the block is by far bigger than those constituting the scree, k is an empirical derived parameter, while d and D are characteristic diameters of the rocks of the bed and the rolling block, respectively. According to Statham [1979] and Bozzolo & Pamini [1986], the values of μ_0 range between 0.37 and 0.67 (corresponding to $\phi_0 = 20^\circ$ to 33°), k between 0.17 and 0.26 and μ_r between 0.4 and 1.5 [Azzoni & De Freitas, 1995].

Average decrease of velocity along a slope

Parting from the principle of frictional loss, a definition for the average decrease of velocity along a slope is proposed by some authors (as e.g. Statham [1979], Japan Road Association [1983]). As this definition does not apply for a particular impact but for the whole trajectory, it is quite different from all other models cited above. Without considering every particular impact, rockfall is simulated as a movement of particles over a simple frictional surface. The Japan Road Association [1983] defined the coefficient α expressing the average decrease of velocity along a slope versus the velocity of pure gravitational fall of a boulder:

$$v = \alpha \cdot \sqrt{2gH} \quad (2-29)$$

where v is the velocity of the block, g the gravity and H the difference of level passed through by the block. If the boulder does not hit the slope surface, α equals to 1 (free fall). In case the boulder hits the slope surface during its downslope trajectory, the velocity v decreases with each impact and yields $\alpha < 1$. The Japan Road Association [1983] approximates the coefficient α by:

$$\alpha = \sqrt{1 - \frac{\mu}{\tan \beta}} \quad (2-30)$$

where β is the slope angle and μ is the equivalent coefficient of dynamic frictional loss, proposed to range between $0 \leq \mu \leq 0.35$ depending on the block and slope characteristics [Masuya, 1993]. The coefficient α does not fit in the classic definition of the coefficient of restitution. It should rather be titled as phenomenological parameter and has to be determined by means of field tests or back analysis.

Rockfall shadow angles

The considerations stated above can be compared to the definition of the “rockfall shadow angle” proposed by several authors (e.g. Lied [1977], Hungr & Evans [1988] and Evans & Hungr [1993]). The rockfall shadow is determined as the angle between the limit of the block deposit zone and the top of the talus slope (Figure 2.9). Lied [1977] stated shadow angles of about 28-30° for natural rockfalls observed and analysed in Norway. These observations are confirmed by Evans & Hungr [1993] who experienced minimal shadow angles of 27,5°.

The empirically determined shadow limits can be a useful device to get a preliminary estimation of maximum rockfall runout at the base of talus slopes. The method has been enhanced and extended to three dimensions (cone method) by Jaboyedoff & Labiouse [2003].

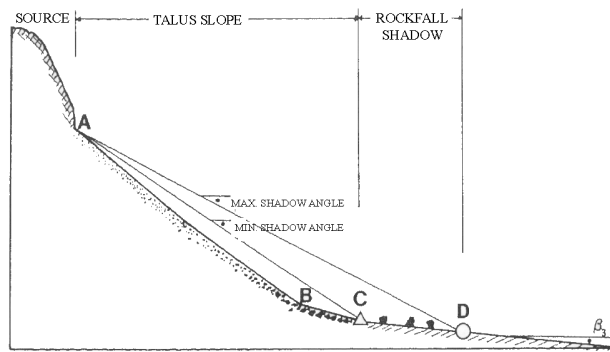


Figure 2.9: Definition of the shadow angle after Hungr & Evans [1988]

2.5 Former experiments for a better characterisation of the parameters influencing the rebound

Based on Newton's theory of rigid particle collision, Szabo [1966] mentioned that the restitution between the particles is by no means a material constant but depends also on particle velocities, material and geometry. As stated above, in the context of rockfall studies the coefficients of restitution often are considered as "material constants" only function of the slope material. This implies their independence of e.g. configuration, direction of approach velocity and friction. Consequently, the coefficients of restitution used for trajectory calculation are estimated based on a rough description of the slope material (as shown in Table 2.1: rock, scree, loose soil, etc.) sometimes completed by information regarding its roughness, its compaction degree, the vegetation cover (including trees) and other obstacles.

However, as mentioned by several authors who have experienced natural and / or artificial *in situ* rockfalls (Chapter 2.2), the analysis of impacts shows that the movement of the block at impact end is affected not only by the slope characteristics, but also by several parameters related to the block as well as to the kinematics during impact.

Table 2.2 recapitulates the parameters listed in literature assumed to influence the bouncing phenomenon of a rock block.

Slope characteristics	Block characteristics	Kinematics
<ul style="list-style-type: none"> • strength • stiffness • roughness compared to block size • inclination 	<ul style="list-style-type: none"> • strength • stiffness • weight • size • shape 	<ul style="list-style-type: none"> • velocity (translational and rotational) • collision angle • configuration of the block at impact

Table 2.2: Parameters assumed to influence the bouncing phenomenon [Labiouse & Descoedres, 1999]

To date several authors have analysed the impact phenomenon and the influence of several parameters on the rebound of a rock block. Most of these parameter studies are performed in laboratory at small scale. That way the impact conditions are easy to control and repeatable, requirements which are quite difficult to fulfil in a natural environment (uneven ground surface, variability of the ground material, dependency on meteorological conditions, etc...). In the following, the most important research results concerning the mechanism of the bouncing phenomenon and the parameters influencing it are specified succinctly.

2.5.1 General statements

Ritchie [1963] stated during *in situ* test series, that the slope inclination and its irregularities mainly determine the kinematics of the blocks. Without giving coefficients of restitution, he observed that the loss of energy becomes bigger with

- i) the increase of the roughness of slope surface versus block diameter (smaller blocks having a lower momentum and more likely to lodge among irregularities, they will travel less far than larger rocks),
- ii) the increase of plastic behaviour of the slope surface (especially for loose soil) and
- iii) increasing impact angle (between slope and the impact direction of the block).

The worst condition possible (greatest horizontal impulse) is given when the impact velocity vector makes an angle of about 45° with the plane of the slope. The shape and size of rock are mentioned to have little influence (not confirmed by other authors), if not related to the roughness of the slope surface. Rocks falling in (free) trajectory seldom give a high bounce after impact but rather change their linear momentum into angular momentum.

Broili [1974] observed during *in situ* tests among other things the influence of the ratio between the normal and tangential component of the incident velocity: in case of a tangential velocity four times greater than the normal velocity, the rotational moments generated by the impacts provoke a relative increase of the post-impact normal velocity and a decrease of the post-impact tangential velocity. In other words: for an impact angle θ of about 14° (corresponding to a four times

greater tangential than normal incident velocity), the rebound of the block is more normal than for blocks with lower tangential incident velocity.

Habib [1977] stressed that the coefficient of restitution R_v is not a constant only dependent of the ground material, but changes probably with the incident velocity and rotation of the block, the mass and shape of the block and the impact angle.

Statham [1979] simulated the trajectory of a block in laboratory and field tests at small scale. He noticed a linear relation between the initial free falling height H of the blocks and their downslope travel distance x parallel to the slope (Figure 2.10). This relation is affected by the relative particle size between block and scree (evidently blocks with a diameter larger than the scree travel further than blocks with a diameter smaller than the scree) and the slope angle (the steeper the slope, the further travel the blocks). He therefore proposed to simulate rockfall as a movement of particles over simple frictional surface.

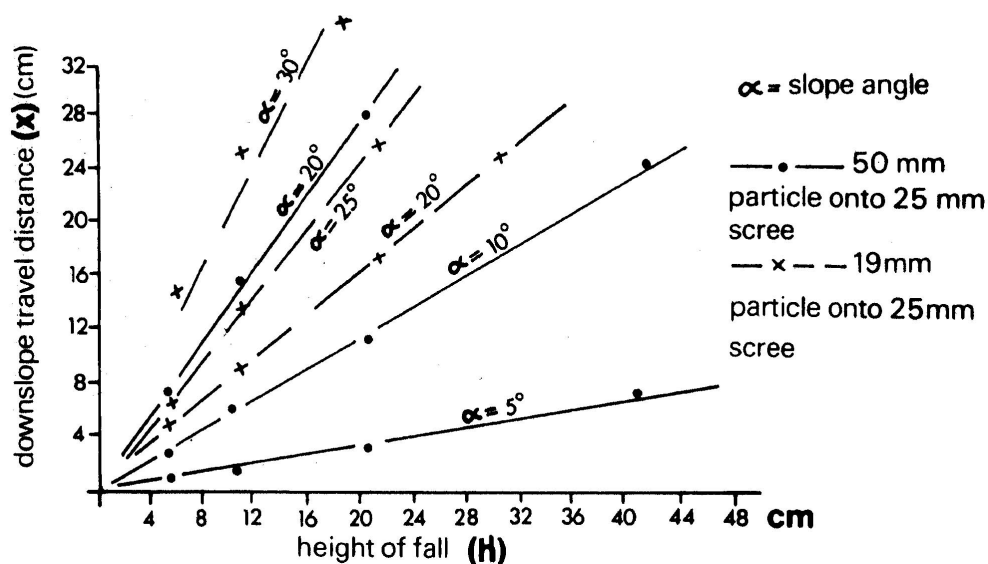


Figure 2.10: Linear relation between drop height H and travel distance x parallel to the slope [Statham, 1979].

Falcetta [1985a and b] stresses that the configuration of the block at impact as well as its shape has an important influence on its rebound.

2.5.2 Insight gained by *in situ* tests and trajectory back analysis

Bozzolo & Pamini [1986] noticed by back analysis of filmed *in situ* experiments, that the velocity of the block at the contact point tangential to the slope is almost always equal to zero for “rock on rock” impacts. The impact process can hence be

described as pure instantaneous rolling. During impacts on fine gravel however, the tangential velocity at the contact point is not zero and slipping of the block occurs. In this case the contact point does not necessarily form an instantaneous centre of rotation. As slipping of the block consumes more energy than instantaneous rolling, the energy restitution is larger for rolling impacts than for sliding impacts. Thus, the loss of energy during impact is stated to be lower on rock than on fine soil.

Further, the runout distance is governed by the ratio between the block and scree diameters.

Moreover, the coefficient of restitution R_{TE} is found to depend on the impact angle θ (angle between the vector of the initial velocity of the block and the ground surface, refer to Figure 2.3). The more normal the impact is to the slope surface, the more energy is dissipated which is expressed by a smaller coefficient of restitution R_{TE} . The configuration of the block at impact has a certain influence on R_{TE} for an ellipsoidal block, however no clear trend can be noted.

Gerber [1995] also performed *in situ* tests and evaluated the normal and tangential coefficients of restitution. He stated that the impact angle has an important influence on the rebound velocity of the block. The more tangential the impact is to the slope surface, the higher are the reported rebound velocities. In other words: for increasing impact angles θ , the rebound velocity of the block decreases.

Barbieri & al [1988] and Azzoni & al, [1992, 1995b] have gathered different coefficients of restitution by means of a comprehensive experimental *in situ* testing campaign carried out by ISMES. On different sites, rock blocks of different sizes and shapes were dropped and their trajectory down the slopes were filmed by video cameras. By means of the films, the movement type (free fall, rolling, sliding, bouncing and their combinations) of the blocks during their trajectory was analysed and the coefficients of restitution for the normal and tangential velocity (R_n and R_t), the coefficient of total kinetic energy (R_{TE}) as well as a rolling friction coefficient were determined.

The different sites allowed to perform tests on different slope angles (up to 80°) and ground materials (rock, different sorts of debris). The influence of these parameters on the trajectory of the blocks and on the coefficients of restitution was investigated. It was stated that the rotational velocity as well as the bouncing motion of the blocks (and thus their total kinetic energy) is less distinct for soft debris slopes than for rock slopes. Further, the smoother a slope is, the less energy is stated to be dissipated during the trajectory, resulting in high values for the restitution and rotation of the blocks. The coefficients of restitution thus are stated

to decrease with decreasing hardness of the slope material (bare rock to fine debris).

Further, the mass loss of the block during impact (fracture of the block) is stated to be a very important parameter for the assessment of the block's kinetic energy after impact.

2.5.3 Trends investigated by physical modelling

Wu [1985] determined the coefficient of restitution from laboratory and *in situ* tests. He investigated the influence of different slope angles on the rebound of rock blocks on a wooden platform or a rock slope. He found that, even if the coefficients of restitution show large scatter, the mean values of R_n and R_t for each of the impact series with similar impact parameters are linearly related to the impact angle θ (definition given in Figure 2.3; the block being dropped freely, the impact angle θ and slope angle β complete each other to 90°). For increasing impact angles θ (respectively decreasing slope angles β ; impact becoming more normal to the slope), the normal component R_n diminishes whereas the tangential component R_t stays quite constant with a slight increasing trend. The following relations are given:

$$R_n = 0.995 - 0.013 \cdot \theta \quad (2-31)$$

$$R_t = 0.535 + 0.0028 \cdot \theta \quad (2-32)$$

where θ is the impact angle in degrees. Both relations are valid for rock-on-rock and rock-on-wood impacts. (Attention: if the trends stated by Wu and illustrated in Figure 2.11 are right, the formulations are misstated in his article, as R_n is stated to equal $0.995 + 0.013 \cdot \theta$, whereas R_t is stated to equal $0.535 + 0.028 \cdot \theta$!).

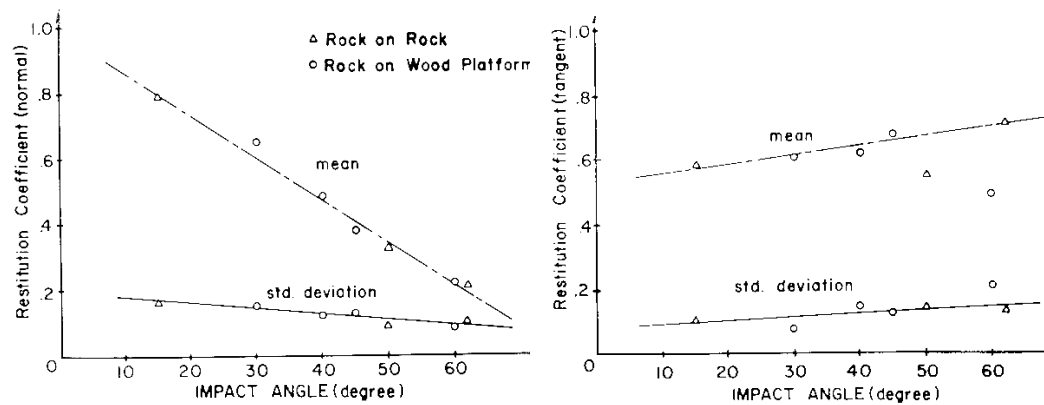


Figure 2.11: Linear dependency of R_n and R_t on the impact angle θ proposed by Wu [1985].

Further, Wu found that the scattering of the rebound velocities, which is due to the local surface irregularities of both the block and the impact surface, can be assumed to be distributed normally. This also applies for the coefficients of restitution. The proposed model for rockfall simulation included already a probabilistic approach to simulate the random nature of the rock bounce characteristics by means of the Monte Carlo technique.

Urciuoli [1988] evaluated by back analysis and single impact tests the coefficients of restitution R_n , R_t and the normal and tangential component of R_E (equations (2-7) and (2-8)) for *in situ* impact tests on limestone. He found that all coefficients are function of the slope angle, the height of free fall and the related impact velocity, the block shape and its impact configuration (both of the latter are casual in his tests). R_n , R_t , $R_{E,n}$ and $R_{E,t}$ are found to decrease with increasing impact velocities resp. drop heights. R_t and $R_{E,t}$ seem to be more sensible to the impact velocity increase than R_n . During impact tests with blocks of irregular shape dropped vertically on horizontal ground, Urciuoli observed a redistribution of normal incident energy to tangential rebound energy due to the irregular block shape (lateral rebound). The trends are given in Figure 2.12.

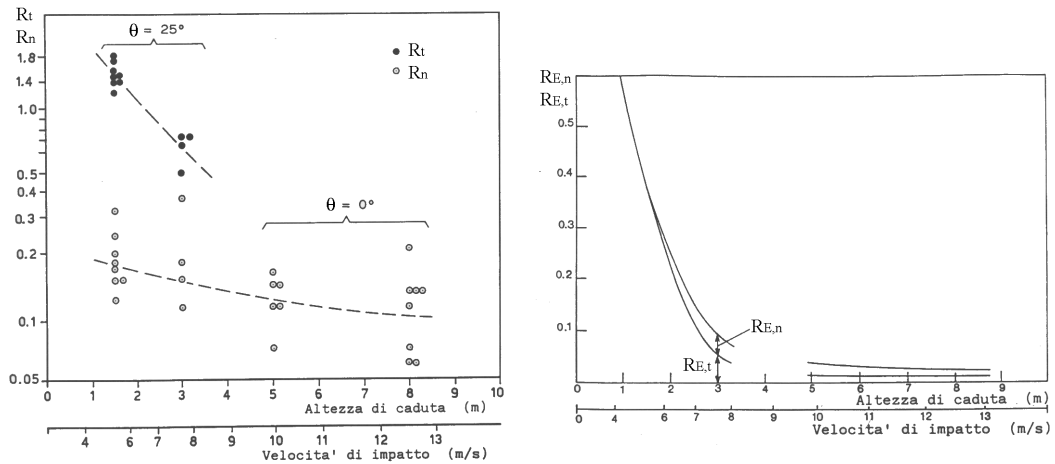


Figure 2.12: Normal and tangential component of the coefficients of restitution R_n , R_t , RE_n and RE_t versus falling height resp. impact velocity [Urciuoli, 1988].

Pfeiffer & Bowen [1989] propose a combination of the tangential component of the coefficient of restitution with a friction function $f(F)$ and a scaling factor SF (equations (2-16) and (2-17)) to express the energy dissipation during impact. The friction function $f(F)$ adjusts the tangential coefficient R_t according to the velocity at the surface of the rock relative to the ground at the beginning of the impact. Figure 2.13 (left) illustrates the dependency of $f(F)$ on the tangential coefficient of restitution R_t and the incident purely translational velocity $v_{t,i-\omega_i r}$ of the block. It can be stated that for low translational impact velocities, the energy loss due to friction is less important than for high velocities. The scaling factor SF accounts for the increased frictional resistance due to an increase in the normal force by increasing normal incident velocity.

To calculate the normal component of the rebound velocity, the normal scaling factor B (equation (2-19)) is used. B reduces the normal coefficient of restitution R_n for increasing incident normal velocity (Figure 2.13, right).

Both the friction function $f(F)$ and the normal scaling factor B account for the fact that slower blocks dissipate less energy during impact than blocks with higher velocity. These formulations are used in the rockfall simulation program CRSP. The latest version CRSP 4.0 of the program, developed by **Jones & al. [2000]**, has been calibrated on several *in situ* test series performed on slopes ranging from talus and firm soil slopes to smooth hard surfaces, to find the appropriate coefficients of restitution R_n and R_t . The coefficients proposed for the different slope materials are given in Table 2.1 (values for soft soils are extrapolated). As the coefficients R_n and R_t are used together with the factors $f(F)$, SF and B (see

equations (2-16) to (2-19)), a coefficient of 1.0 for CRSP does not represent complete energy conservation, but rather produces output consistent with the field observations [Jones & al., 2000].

During the *in situ* tests performed to calibrate the model, the authors observed that the normal coefficient is much more sensitive than the tangential coefficient to changes of the impact conditions. R_t is large especially for hard slopes, presumably because the rock does not embed into hard slopes, and for slopes covered with vegetation, which can impede the falling rock.

Further, the field observations appear to point out a maximum velocity for each given slope for increasing block diameters. The influence of the rock size on the travelling velocities along smooth hard surfaces is proposed to be minimal, whereas it has a certain influence on soft slopes. It is observed that with increasing block diameter, the influence of the rock size on the velocity diminishes. Based on this observation it is supposed that on hard slopes the influence becomes least. That effect is stated to probably be due to a condition of rock embedment into an underlying slope, having a smaller effect on the velocity of large rocks than small ones and no effect where embedment does not occur.

The observation that both coefficients R_n and R_t are higher for hard than for soft ground material is proposed to depend on the difference in rock-slope interaction. Falling rocks that embed into their underlying slope are proposed to possess less rotational energy than blocks impacting hard surfaces. Also, a shearing of soft slope material seems likely to occur during impact (as we will see later on, this assumption is verified by the tests performed in the framework of this thesis!), resulting in a lesser amount of rotational energy gained from an impact on a soft slope compared to a relatively harder slope. In addition, on harder slopes the block conserves more energy resulting in longer bounces and higher travelling energies. Consequently, due to their lower velocities and shorter bounces, the rocks falling on softer slopes probably impact the slope more often, compounding the effects of embedment and shearing. Therefore, the gradual increase in suggested normal and tangential coefficient values from soft to hard slopes is possibly accounted for by decreasing degrees of rockfall embedment and shearing of slope materials and increasing conservation of energy as slope hardness increases [Jones & al., 2000].

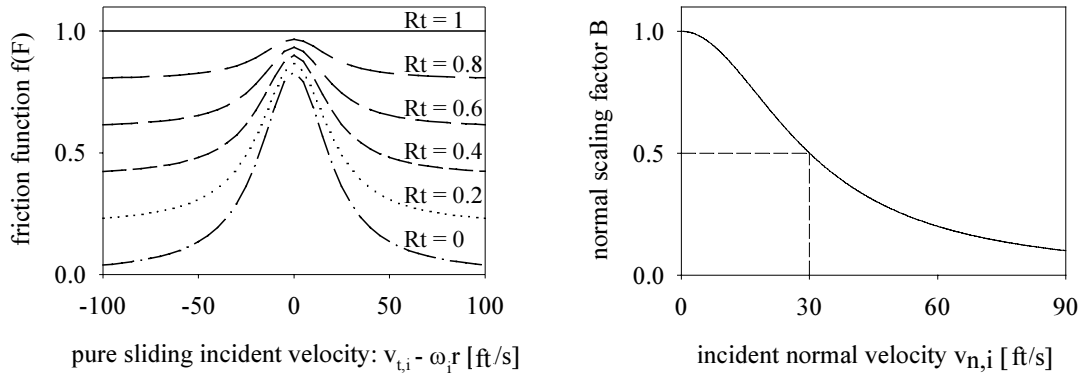


Figure 2.13: Friction function $f(F)$ (left) and normal scaling factor B (right) defined by Pfeiffer & Bowen [1989] to adjust the tangential and normal coefficients R_t and R_n for higher incident velocities of the block.

Kamijo [2000] investigated the rebound of naturally shaped blocks of 220 and 800 kg respectively, dropped vertically from different height (max. 3 m) on a concrete slab. The measured coefficient of restitution R_v proves to decrease with increasing impact velocity resp. drop height and increasing block mass.

Ushiro & al. [2000] investigated by small-scale tests on rock and concrete slopes the influence of the impact velocity on the coefficients of restitution R_n and R_t . They stated that while R_t is relatively insensitive to the impact velocity (constant values for increasing incident tangential velocity), R_n slightly decreases with increasing incident normal velocity. An exponential relationship between R_n and the normal incident velocity is proposed in dependency of the ground material (Figure 2.14):

$$R_n = 0.8478 \cdot e^{-0.0842 \cdot (-v_n)} \quad \text{for concrete slopes} \quad (2-33)$$

$$R_n = 2.506 \cdot e^{-0.1053 \cdot (-v_n)} \quad \text{for rock slopes} \quad (2-34)$$

Further, R_n is found to decrease with increasing block mass, independently on the incident velocity of the blocks.

In Figure 2.14 measured values larger than 1 are stated. The formulations given above seem to fit well the test results. However, whereas for concrete slopes the formulation seems to produce reasonable results, in case of rock slopes, the proposed formulation produces values larger than 1 for R_n , which should not be possible “per definitionem”.

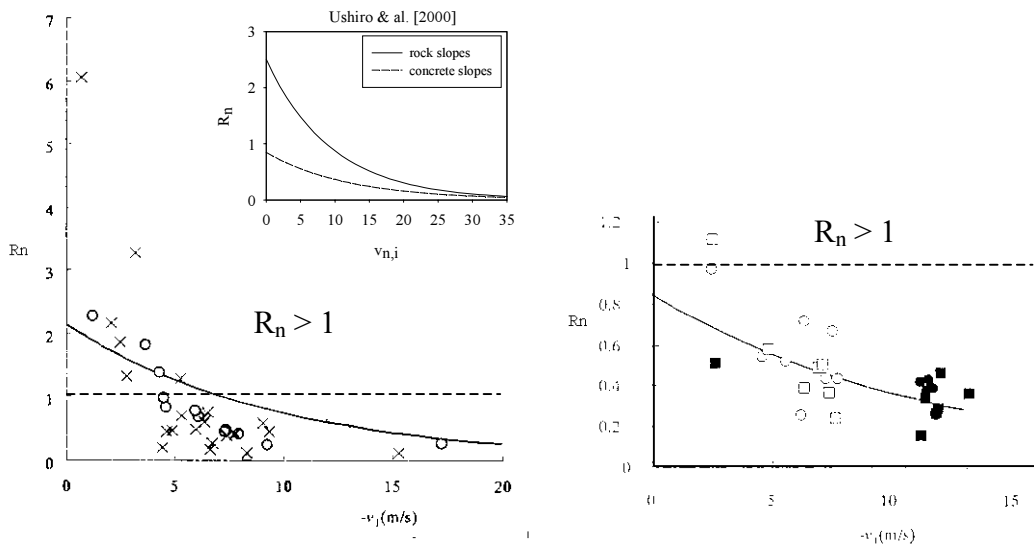


Figure 2.14: Exponential decrease of R_n with increasing impact velocity $v_{n,i}$ for impacts on hard ground after the equations (2-33) and (2-34) proposed by Ushiro & al. [2000].

Chau & al.: The probably most complete series of small-scale impact tests with regard on the influence of several parameters on the coefficient of restitution is

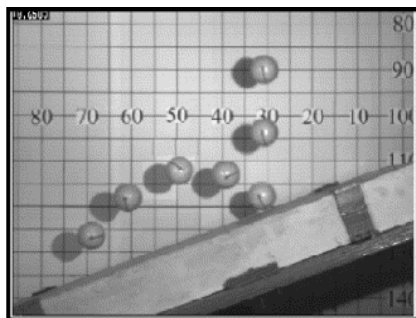
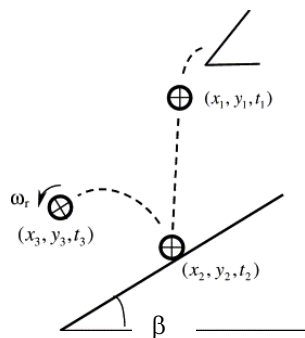


Figure 2.15: Scheme of the experimental set-up (above) and a sequence of positions of a falling sphere (below); from Chau & al. [2002].

performed by the research group of Prof. K.T. Chau in Hong Kong. **Chau & al. [1998a and b, 1999a and b, 2002] and Wong & al. [1999, 2000]** carried out a number of small-scale tests on different ground materials (plaster, compacted soil, shotcrete and granite) to investigate the effect of the shape of the boulder, the impact angle, the impact velocity and energy and the mechanical properties of the slope material (Young's modulus, water content) on the coefficients of restitution R_n , R_t , R_v and R_E . Further, the rotational motion induced to the blocks during the impact is investigated. The blocks are dropped from a releasing tube on a horizontal or inclined platform supporting the ground material. The free fall, the impact and the following trajectory are filmed by means of a high-speed video camera and analyzed by superimposing the pictures and

determining the position of the block for each photo (Figure 2.15). The similarity requirements of the scaling laws are not satisfied exactly. The following observations are reported:

Shape of the boulder:

Chau & al. [1999b] performed small-scale vertical impact tests on a slope made of **plaster material** to find the influence of the block shape on its rebound. They found that R_n can be very sensitive to the shape of the boulder, depending on the impact angle θ (as defined in Figure 2.3) respectively on the slope angle β ($\theta + \beta = 90^\circ$). For slope angles between 30° and 50° , R_n roughly is independent of the block shape. For steeper slopes ($60^\circ < \beta < 75^\circ$), however, R_n increases with β for cubic and hexagonal blocks, whereas it stays constant for spherical and cylindrical blocks.

R_t is found to be relatively independent of the block shape for any slope inclination. A trend can be noted for spherical blocks having the largest tangential restitution, whereas cubes have the lowest tangential restitution.

Also the coefficient of restitution R_E is judged quite independent of the block shape, whereas in the narrow range of values again R_E is largest for spheres and smallest for cubes. For all block shapes, R_E clearly increases with increasing slope angles β .

Wong & al. [2000] have studied the influence of the boulder's shape for impacts on a **granite ground**. A shape factor is defined as follows:

$$S = A_s / A_b \quad (2-35)$$

where A_b is the boulders total surface area and A_s is the surface area of a sphere including the same volume as the real block.

On granite ground material, R_n is found to decrease with increasing angularity of the boulder. Thus, unlike Chau & al. [1999b] stated for plaster ground material, R_n averages greater values for spherical boulders (0.85-1) than for other shapes (cube, cylinder, hexagonal prism). To describe the reduction R of R_n with increasing angular shape of the boulder, expressed by the shape factor S defined in Eq. (2-35), the following empirical formulas are developed:

$$R = R_n \cdot 0.038e^{3.2S} \quad \text{for blocks with smooth or round edges, and} \quad (2-36)$$

$$R = R_n \cdot 0.0001e^{9.1S} \quad \text{for angular shapes with sharp edges,} \quad (2-37)$$

where R_n is the normal coefficient of restitution measured for a spherical block.

As by Chau & al. [1999b], it was found that the tangential coefficient of restitution R_t is relatively insensitive to the shape of angular boulders. Unlike stated by Chau & al. [1999b] on plaster ground material, however, R_t is observed to average lower values for spherical boulders than for angular boulders.

On granite ground material, the energy dissipation is lower for spheres and blocks with smooth edges than for angular blocks. That means R_E is highest for spheres

among other shapes. The same trend is observed by Chau & al. [1999b] on softer ground material (plaster). Probably local crushing at the block corners is the reason for the higher energy dissipation of angular shapes.

Impact angle θ resp. slope angle β :

For the impact tests performed by Wong & al. [2000], the block is released over an inclined or horizontal platform supporting the ground material. The block impacts the ground with a purely vertical velocity after a vertical free fall. Therefore, the impact angle θ (defined in Figure 2.3) and the slope inclination β are directly related and complete each other to 90° .

For normal impacts on the ground, no rebound value is recorded.

In general, R_n decreases slightly with the increase of the impact angle θ respectively with the decrease of the slope angle β (Figure 2.16). For hard ground material (granite, shotcrete) the influence is less pronounced than for softer ground material (plaster) [Wong & al., 2000]. This trend corresponds to the one reported by Chau & al. [2002] for small-scale tests on granite and Wu [1985] for *in situ* tests (Figure 2.16).

As reported in Figure 2.16, the trend of R_t with the slope angle β is less obvious. For decreasing slope angles β (resp. increasing impact angles θ), Wu [1985] suggested a slight increasing trend for R_t , whereas Chau & al. [2002] give no trend at all. The data are rather scattered for both Chau & al. [2002] and Wu [1985]. In general, it can be stated that R_t seems not sensitive to the impact respectively the slope angle.

For the coefficients of restitution defined in terms of resultant velocity $R_v = v_r/v_i$ and energy R_E (equation (2-6)), a very clear increasing trend with increasing slope angles β is stated (Figure 2.17).

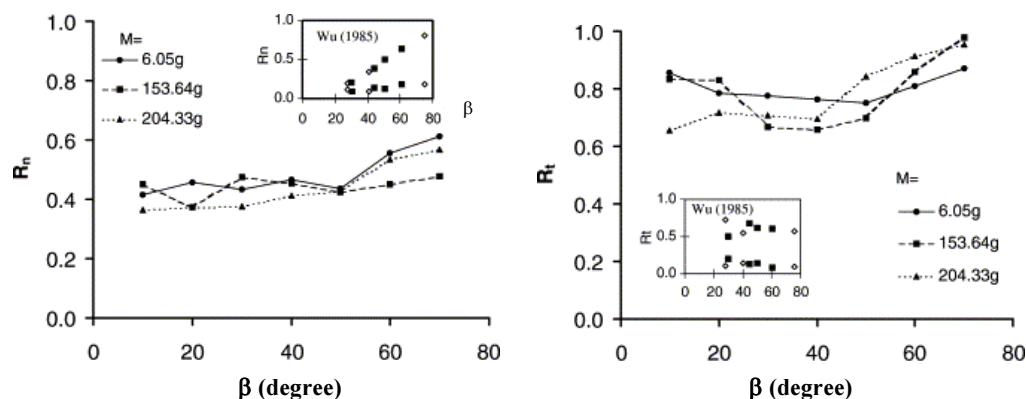


Figure 2.16: Normal and tangential component of the coefficient of restitution R_n and R_t versus slope angle β for various sphere masses (M). Both blocks and slope are made of plaster. [Chau & al. 2002]

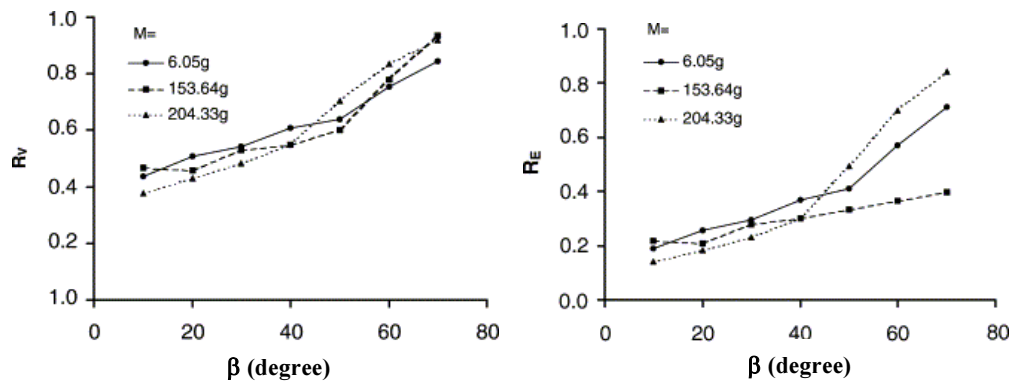


Figure 2.17: Coefficients of restitution R_v and R_E versus slope angle β for various sphere masses (M). Both blocks and slope are made of plaster. [Chau & al. 2002]

Ground material:

Inspired by the representation of R_n versus R_t for different ground materials, first presented by Fornaro & al. [1990], Chau & al. [2002] plot their values of R_n and R_t gathered from small-scale laboratory tests and some values gathered from literature in the same manner to investigate their range for certain ground characteristics (Figure 2.18). The values found for different ground materials (compacted soil, plaster and rock) by small-scale tests provide in general similar values for R_t but smaller values for R_n than the regime proposed by Fornaro & al. [1990] shown in the right lower corner. The regime boundary for rock slopes proposed by Fornaro & al. [1990] is also shown by the dotted line in the diagram.

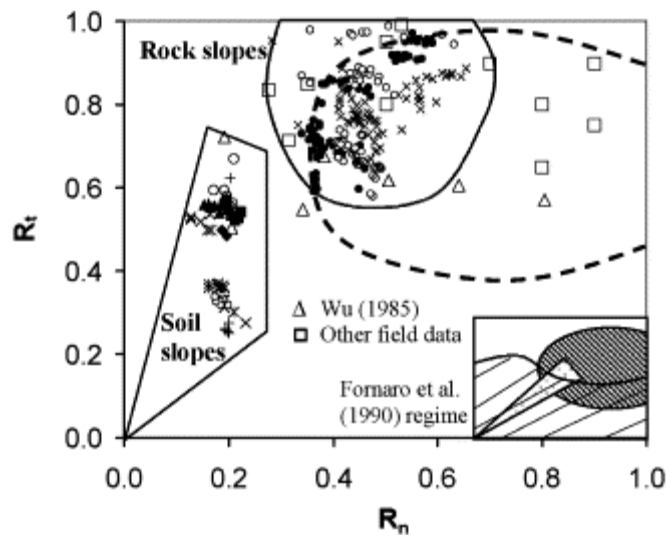


Figure 2.18: Variability ranges of the coefficients of restitution R_n and R_t according to small-scale test results by Wu [1985] and Chau & al. [2002], after Chau & al. [2002].

Young's modulus of the ground material:

R_n increases with the Young's modulus of the slope material, due to the decreasing energy loss during impact. The energy loss can be caused by friction work, plastic deformation, impulse contact time and vibration of the platform supporting the ground material. An empirical formula for R_n of granite rock impacting a slope of various moduli is established, being valid for impact energies between 0.1-3 J:

$$R_n = 0.2 + 0.9 E_p / E_b \quad (2-38)$$

where E_p and E_b are the Young's modulus of the ground material and the boulder respectively. For this evaluation, the R_n value is the mean value taken from different impact angles, even if R_n varies with the latter.

R_t is not as sensitive as R_n to the change of the Young's modulus.

Water content and dry density of the ground material:

Chau & al. [1999a] found that for a water content w of the soil lower than the optimal water content w_{opt} , R_n , R_t and R_E are relatively insensitive to the change of w . For a water content w exceeding w_{opt} , however, the soil is fully saturated and incompressible (as water is incompressible). Thus for $w > w_{opt}$, R_n increases while R_t and R_E decrease linearly with increasing w .

Further, it is stated that R_n , R_t and R_E increase with the dry density of the soil if the water content is less than w_{opt} . When the optimum water content is exceeded, however, R_n , R_t and R_E remain roughly constant regardless to the values of the dry density of the soil.

It should be stated that the dry density of the soil material is related to its compaction and its Young's modulus. The influence found for the dry density of the ground could also be due to change of the ground compaction or the Young's modulus of the material.

Impact energy:

Chau & al. [1998b] investigated the influence of the impact energy of the falling block on the coefficients of restitution. Therefore, a normalized impact energy value I_e is defined as the ratio between the incident impact kinetic energy $E_{kin,i}$ of the block and the impact kinetic energy $E_{kin,f}$ required to fracture the latter:

$$I_e = \frac{E_{kin,i}}{E_{kin,f}} \quad (2-39).$$

$E_{kin,f}$ is determined by means of a standard testing procedure, which investigates the dynamic tensile strength of the block.

The results show that for low impact energy levels (less than 20% of the dynamic tensile strength of the block), R_n is slightly sensitive to the impact angle θ (respectively the slope angle β). In this case, R_n increases with increasing slope angles resp. decreasing impact angles (as stated also by Wu [1985], Wong & al. [2000] or Chau & al. [2002]). However, for higher impact energy levels, R_n seems less sensitive to a change of the slope or impact angle, the values being quite close to each other.

R_t decreases slightly with increasing impact energy level, independent of the slope or impact angle, as stated also by Wong & al. [2000] for slopes made of granite, shotcrete, plaster and soil.

R_E also decreases slightly with increasing impact energy level. This trend is independently stated for several slope resp. impact angles.

2.6 Rotational motion of blocks down slopes

The rotation of a rock block and its effect on the rebound is not taken into account by the coefficients of restitution. Except R_{TE} no coefficient of restitution accounts for the rotational velocity or energy of a block and its restitution after impact. Even though considered as important factor for the post-impact block movement, most authors ignore the rotational velocity or energy of the block before and after impact. The knowledge concerning the rotational energy of a falling block gained by means of impact tests is cited in the following.

The **Japan Road Association [1983]** performed 60 *in situ* rockfall tests with round to angular boulders traveling down slopes with an inclination between 32° to 55° . The investigation of the trajectories showed that the rotational energy of the blocks was always smaller than 40% of the translational kinetic energy. For more than half of the data, the rotational energy amounts only to 10% of the translational energy.

These results [JRA, 1983] are supported by **Yoshida [1998]**, who evaluated the ratio between the rotational and the translational component of the block energy during its trajectory down a slope. He discovered a linear relation, the rotational energy being 2 to 20% of the translational energy.

Kawahara & Muro [1999] have developed a formulation to express the rotational energy induced to a block during its combined rolling-sliding motion down an artificial compacted sand slope. The used blocks have a cylindrical shape and therefore a moment of inertia I equal to $0.5mr^2$ (m being the mass and r the radius

of the cylinder). For a cylindrical block, the kinetic energy ratio of rotational (E_r) to translational (E_v) energy is calculated as follows:

$$\frac{E_r}{E_v} = \frac{\left(1 + \left(\frac{r\omega - v}{v}\right)^2\right)}{2} \quad (\text{valid for cylindrical blocks only}). \quad (2-40)$$

r being the block radius, ω and v its rotational and translational velocity respectively. By several small-scale tests, the authors found that the ratio E_r/E_v decreases with increasing block mass m and increasing slope angle β .

Ushiro & al. [2000] takes into account the incident block rotation for the computation of the translational and rotational rebound velocities. For sticking impacts (pure instantaneous rolling, no slip in the contact point), the incident tangential and rotational velocity components are included in the definition of the tangential rebound velocity. The rebound velocities $v_{t,r}$ and ω_r are calculated as given in equations (2-20) and (2-21):

$$v_{t,r} = \frac{5v_{t,i} + 2r\omega_i}{7} \quad \text{and} \quad \omega_r = \frac{v_{t,r}}{r} .$$

For a combination of rolling and sliding, the incident rotation of the block has no influence on the tangential rebound velocity (equation (2-22)). The rotation after impact is calculated as defined in equation (2-23) by means of the initial rotation and the normal velocity component before and after impact:

$$\omega_r = \omega_i - \frac{5\mu(1+R_n)v_{n,i}}{2r} .$$

With regard to the results of the Japan Road Association [1983], **Chau & al. [2002]** evaluate the rotational energy induced to a block during impact on rock slopes. As reported in Figure 2.19 (right), it can be stated that the rotational rate acquired after each boulder impact depends strongly on the angle of impact itself. The values given by the Japan Road Association [1983] are stated to be valid only for slope angles at about 20° or 50° (Figure 2.19).

For sticking impact (no slip at the contact point), the following equation is developed theoretically. Therefore, the rebound velocity v_r in the equation for the translational energy $E_v = \frac{1}{2} \cdot m \cdot v_r^2$ by substituted by its normal and tangential components ($v_r^2 = v_{n,r}^2 + v_{t,r}^2$). Subsequently, the normal and tangential components of the rebound velocity are expressed by means of the coefficients of restitution R_n and R_t . Further, the rotational velocity after impact ω_r is supposed to equal $v_{t,i}/r$

($v_{t,i}$ being the tangential component of the impact velocity and r the block radius). The ratio between rotational and translational energy after impact can thus be written as:

$$\frac{E_r}{E_v} = \frac{2 \cdot \tan^2 \beta}{5 \cdot (R_t^2 \cdot \tan^2 \beta + R_n^2)} \approx \frac{1.6 \cdot \tan^2 \beta}{1 + 2.56 \cdot \tan^2 \beta} \quad (2-41).$$

In obtaining the last equation of equation (2-41), it is assumed that $R_t \approx 0.8$ and $R_n \approx 0.5$, which are extracted from Figure 2.16 and for which the assumption of sticking impact applies (at least for $\beta \leq 40^\circ$). For partial sticking with slipping at the contact point, the energy ratio gradually drops to zero, however no exact trend is proposed. For pure slipping at the contact point, no angular velocity is developed during impact, the post-impact rotational energy then equals to zero.

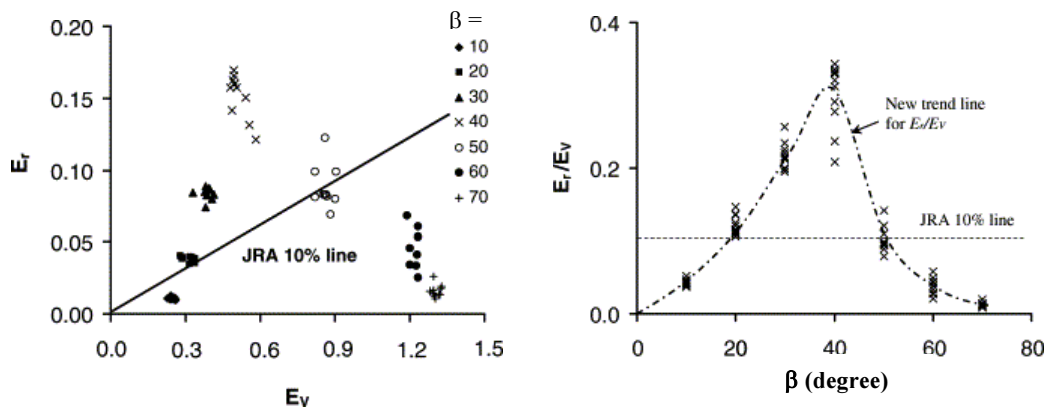


Figure 2.19: Left - The rotational kinetic energy E_r versus the translational kinetic energy E_v after each impact for various slope angles β (from 10° to 70°). The JRA 10% line is also plotted for comparison.

Right - The energy ratio E_r/E_v versus the slope angle β . The JRA 10% line becomes a horizontal line. A new trend line for E_r/E_v is also proposed. [Chau & al. 2002]

2.7 Miscellaneous references not directly related to the bouncing of rock blocks

Several research topics not directly related to the bouncing of rock blocks can yield important information concerning the coefficients of restitution and the parameters influencing it. Most of these topics concern impact engineering and military research projects. Theoretical considerations as well as experimentally gained observations used in the further context of the research for the interpretation of the test results are summarized very succinctly in this section.

2.7.1 Impact theory

As very good introduction to impact theory and the considerations for elastic, plastic and elastic-perfectly plastic materials relative to rockfall problems is given by Montani-Stoffel [1998].

In this place therefore only a very succinct overview is given on the authors who have investigated impact problems related to rockfalls:

- elastic impact: Hertz [1881] (impact of two elastic spheres), Goldsmith [1960] (impacts of a spherical block on a horizontal ground), Tonello [1988] (impacts on gallery), Lang [1974] (impacts on ground material)
- plastic impact: Habib [1979], Heierli [1984]
- elastic-perfectly plastic: Tonello [1988], Lang [1974], Azimi & Desvarreux [1988]
- empiric formulations: Poncelet [Lang, 1974], Masuya [1992]

The formulations used in context of the present thesis are presented in the corresponding chapter.

2.7.2 Impact tests on rock sheds

In the framework of the doctoral thesis of **Montani-Stoffel [1998]**, a comprehensive experimental campaign of laboratory half-scale impact tests on a rock shed model was performed at the Rock Mechanics Laboratory (LMR), EPFL in the same testing shaft used for the present half-scale tests (Chapter 4). By means of vertical impact tests on a horizontal rock shed model (concrete slab) covered with granular damping material, the most important parameters influencing the impulsive force on the slab were determined. The parameters investigated in this study were related to the impacting block (weight), the damping material (thickness and material properties as granulometry, compaction degree, internal friction angle), the structural characteristics of the rock shed and the kinematics (falling height). To investigate the influence of the slab (vibration, natural frequencies, stiffness, etc.), several impacts were performed on damping material resting directly on the foundation of the test shaft. The main result of the thesis was the quantification of the maximum forces due to acceleration acting between block and damping material, the integrated pressure (force acting on the slab) and the support reaction.

In context with the present thesis, the following results are of further interest:

- A linear relation was observed between the impact energy (corresponding to the potential energy E_{pot} as no rotation of the blocks occurs) and the product of the maximum acceleration force (F_{acc} , acting between block and damping material) and the maximum penetration depth d . For impacts on

damping material resting on the slab and on the shaft foundation, different relating factors (gradients) are stated:

$$F_{\text{acc}} \cdot d = 1.6 \cdot E_{\text{pot}} \quad (\text{impact on slab}) \quad (2-42)$$

$$F_{\text{acc}} \cdot d = 1.5 \cdot \exp\left(\frac{r}{1.5 \cdot e}\right) \cdot E_{\text{pot}} \quad (\text{impact on shaft foundation}) \quad (2-43)$$

- The maximum force due to acceleration F_{acc} acting between damping material and block can be expressed depending on the maximum penetration depth d . Slightly different formulations are proposed for impacts on damping material resting on the slab and on the foundation:

$$F_{\text{acc}} = 1.05 \cdot r^{0.5} \cdot \exp\left(\frac{r}{1.2 \cdot e}\right) \cdot M_E \cdot (\tan \varphi)^{0.5} \cdot d^{1.5} \quad (\text{slab}) \quad (2-44)$$

$$F_{\text{acc}} = 1.05 \cdot \exp\left(\frac{r}{1.5 \cdot e}\right) \cdot M_E \cdot (\tan \varphi)^{0.6} \cdot d^2 \quad (\text{foundation}) \quad (2-45)$$

- F_{acc} also can be expressed as function of the impact energy (in the present case equal to the potential energy E_{pot}):

$$F_{\text{acc}} = 1.35 \cdot r^{0.2} \cdot \exp\left(\frac{r}{3 \cdot e}\right) \cdot M_E^{0.4} \cdot (\tan \varphi)^{0.2} \cdot E_{\text{pot}}^{0.6} \quad (\text{slab}) \quad (2-46)$$

$$F_{\text{acc}} = 1.33 \cdot \exp\left(\frac{r}{1.5 \cdot e}\right) \cdot M_E^{1/3} \cdot (\tan \varphi)^{0.2} \cdot E_{\text{pot}}^{2/3} \quad (\text{foundation}) \quad (2-47)$$

In all formulations, r corresponds to the radius of the block in the contact point, e is the thickness of the damping layer, M_E is the plate bearing modulus and φ the internal friction angle of the damping material. These formulations are valid for vertical impacts on horizontal ground and for impact energies up to 100 kJ (as the maximum block weight is 1000 kg and the maximum falling height is 10 m). These formulations will be used as basis in the present thesis to quantify the maximum force acting between block and damping material and the maximum acceleration of the block during impact.

2.7.3 Foundations under static and dynamic loading

Selig & McKee [1961] experienced the dynamic (impulsive) loading phenomenon on dry, sandy ground materials at small scale for small footings. They stated that the ground reaction and failing mode differs for static and dynamic loading as well as for the shape of the footing: Whereas for static loading the ground material generally fails along clearly defined shear surfaces, Selig & McKee [1961] observed no clearly defined shear surfaces for dynamic loading tests. The failure pattern corresponds more to the ground distortion occurring during static loading of loose sand. Only after repeated impulsive loading of the footing, a clear shear failure pattern is observed.

The total settlement for dynamic tests is reported to increase linearly with impact energy for the individual footing. For same impact energies but decreasing footing size, the settlement becomes larger at increasingly greater rate as the size of the footing decreases.

Wang [1971] investigated the penetration of projectiles in dense sand at low impact velocities ($v_i < 7.6$ m/s). He analysed the energy dissipation due to the inertial resistance, the bearing capacity and the pulverisation of the sand. The penetration is found to increase as the weight of the projectile increases, but it does not increase linearly as other authors propose. The deceleration of the projectile increases slightly during penetration. As the dynamic effects on shear strength and friction angle are found to be minimal for cohesionless material ($c=0$), the static resistance of dense sand is proposed to apply for projectile penetration problems at low impact velocity.

2.8 Summary and contribution of the thesis

In the framework of rockfall trajectory modelling, the bouncing phenomenon occurring when a rock block impacts with the slope surface is undoubtedly the most difficult to predict, owing to its complexity and its very limited understanding. To date, the rebound is commonly quantified by means of (one or) two coefficients of restitution estimated from a rough description of the ground material, sometimes completed by a friction coefficient to account for the rolling and sliding loss. As stated by different authors and proved by several *in situ* or laboratory tests, the bouncing phenomenon yet is guided by many other factors characterizing not only the ground material but also the block and the kinematics. The parameters found to influence the rebound usually are not represented in the numerical models. It is therefore obvious that a rebound model, which is based on coefficients of restitution depending only on the slope material is quite restricted.

A comprehensive bibliographic study showed the investigations performed to date by means of back analysis, *in situ* and laboratory tests. The knowledge gathered to date is based mainly on impact tests on hard ground materials (as rock or concrete for real-scale tests or plaster for small-scale tests). Surprisingly few investigations deal with soft ground material. The parameters stated in literature to influence the coefficients of restitution are recapitulated in Table 2.3, indicating the trends mentioned by the corresponding authors. The trends are illustrated by arrows (arrows pointing up denote increasing values, pointing down decreasing values). As it can be seen, in several cases no clear or even contradictory trends are stated. Some of the contradictions are due to varying impact conditions, whereas others cannot be allocated.

Nevertheless, these former investigations emphasise thoroughly that the coefficients of restitution defined to date can by no means be stated as ground material constants, not depending on other factors as the block characteristics and the kinematics.

It is therefore crucial to acquire a better knowledge of the bouncing phenomenon of rock blocks on soft ground materials and to investigate the influence of the various impact parameters. The present thesis aims at:

- clarifying the bouncing mechanism for impacts on granular material,
- analysing qualitatively the influence of several impact parameters concerning the block (block weight, radius), the slope (internal friction angle, compaction degree, slope inclination) and the kinematics (impact direction, impact velocity respectively falling height),
- quantifying the influence of the most important parameters governing the block movement during impact and its rebound, and finally
- putting forward mathematical formulations quantifying the rebound.

The implementation of these formulations in numerical models should lead to a better prediction capacity of the trajectories of rock blocks and subsequently to a better delineation of areas at risk (hazard maps).

Parameter		R_v	R_n	R_t	R_E	ground material	reference
BLOCK	block mass ↗		↘			concrete, rock	Ushiro & al., 2000
		↘				concrete	Kamijo, 2000
	(shape changing from sphere to angular block as e.g. cube)		↘	↗ (slightly)	↘	granite	Wong & al., 2000
			30°<β<60°: - 60°<β<75°: ↗	↘ (slightly)	↘ (slightly)	plaster	Chau & al, 1999b
GROUND MATERIAL	Young's modulus ↗		↗	↗		natural slopes	Pfeiffer & Bowen, 1989
			↗	↗		natural slopes	Fornaro & al., 1990
			↗	↗		soil, plaster, rock	Chau & al, 2002; Wu, 1985
	dry density ↗		w < w _{opt} : ↗ w > w _{opt} : -	w < w _{opt} : ↗ w > w _{opt} : -	w < w _{opt} : ↗ w > w _{opt} : -	soil, plaster	Chau & al, 1999a
			w < w _{opt} : - w > w _{opt} : ↗	w < w _{opt} : - w > w _{opt} : ↘	w < w _{opt} : - w > w _{opt} : ↘	soil, plaster	Chau & al, 1999a
KINEMATICS	impact angle θ ↗ resp.		↘	↗ (slightly)		wood, rock	Wu, 1985
			↘ (slightly)			granite, shotcrete	Wong & al., 2000
			↘			plaster, soil	
	slope angle β ↘	↘	↘ (slightly)	-	↘	granite, shotcrete	Chau & al. 2002
		↘	↘	-	↘	plaster, soil	
	drop height H ↗ resp.		↘ (less than R _t , R _{E,t})	↘	↘ (R _{E,n} , R _{E,t})	limestone	Urciuoli, 1988
		↘				concrete	Kamijo, 2000
impact velocity ↗			↘ (slightly)	-		concrete, rock	Ushiro & al., 2000

Table 2.3: Summary of the parameters influencing the coefficients of restitution and the corresponding trends stated in literature.

3 Preliminary small-scale experimental campaign

The present chapter focuses on a comprehensive small-scale experimental campaign of spherical blocks impacting granular slopes under various conditions. In the first part, the testing device and the data processing methods are presented. Then, data from different testing series are compared, allowing to determine the significant impact parameters and to qualify their influence on the block rebound and the coefficients of restitution commonly used in trajectory programs to compute the rebound velocity (R_n , R_t) and energy (R_{TE}). The third part illustrates the problem arising with downscaling dynamic impact tests and points out the particular importance of large-scale or *in situ* tests to allow a correct quantification of the coefficients of restitution.

3.1 Physical modelling

3.1.1 Motivation

The experimental campaign started with impact tests at small scale. The small-scale experiments are carried out in laboratory. The preliminary small-scale campaign was motivated by numerous reasons:

- The influence on the bouncing phenomenon of several parameters is determined qualitatively to restrict the number of half scale experiments,
- Easy handling of the experimental set-up: the ground inclination and the impact direction can be changed independently and quickly,
- Test series can be realised in relatively short time (about 20 minutes for the preparation and realisation of each impact test),
- Check the functioning of the measuring device (digital high speed camera),
- Development of an interpretation method which can be used for both small- and half scale tests.

The experimental small-scale test series have mainly been carried out in the framework of two student works (study thesis by Schneider-Muntau [2002], diploma thesis by Bisschot [2002]) and a practical course [Grillon, 2003]. During the altering phases between tests and analysis of the test results and due to the experiences gained with time, the methods of result interpretation have evolved. For the first test series, only the coefficient of restitution for the total energy was calculated, and the determination method for the end of impact was significantly different and less exact. The gain of knowledge finally required a reanalysis and reinterpretation of all tests by the author of this thesis.

Though it is possible to scale down quite exactly the static properties of a material to perform significant small-scale tests, things are much more complex for the dynamic properties. Therefore, the small-scale tests performed in the framework of this thesis do not claim to reproduce exactly the properties of certain ground or block materials. They shall simply clarify the role of several parameters on the bouncing phenomenon of a block on a granular, cohesionless ground material. The results gained out of the small-scale test series are therefore interpreted only in a qualitative way. A correct quantification of the influence of some parameters can only be achieved by real- or half-scale tests, presented in Chapter 4.

3.1.2 Experimental set-up

The experimental set-up (Figure 3.1) consists of an inclinable box containing the soil, two different block-releasing devices (a vertical tube and an inclined ramp with a sled) and a numerical high-speed camera installed perpendicularly to the block motion plane. Spherical blocks with a diameter of 7.5 cm and different weights are dropped on different granular materials at a speed of about 4.4 m/s (corresponding to one meter of free fall). The trajectory of the boulders during the impact is captured at a camera operating speed of 250 frames per second. All in all, approximately 210 impacts have been carried out. They are organised in series to systematically isolate and investigate the influence of the impact parameters. In the following, the testing device and the used materials are described in detail. Chapter 3.1.3 gives details on the measuring devices for the motion analysis.

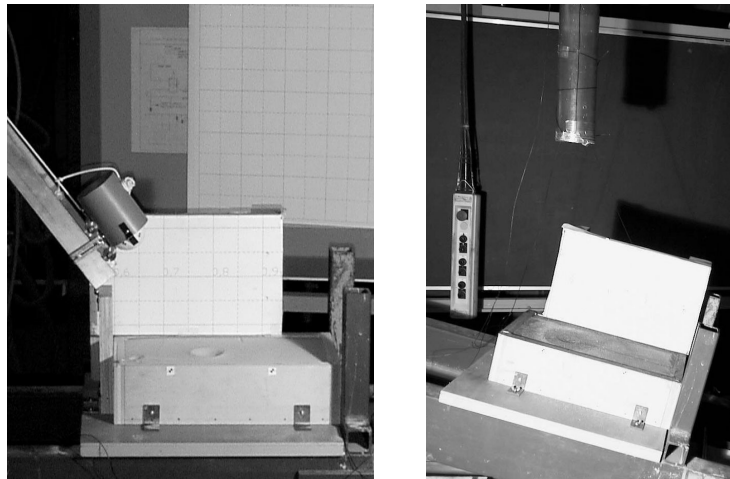


Figure 3.1: Experimental set-up for small-scale tests. Left hand side: inclined impact (ramp) on horizontal ground. Right hand side: vertical impact (tube) on inclined ground.

3.1.2.1 Testing device

The ground material is retained in an inclinable wooden box measuring 40 x 20 x 10 cm, which is fixed on a stable sub-construction. Optionally the box can be replaced by a hard surface.

A vertical tube or an inclined ramp with a sled (Figure 3.2) is used to launch the block either on a vertical or inclined trajectory. The inclination of the ramp and the position of the vertical tube can be chosen independently of the inclination of the box containing the ground material.

The translational velocity before impact is maintained constant for all test series. Due to the friction between ramp and sled, the releasing height for the inclined impact tests is calibrated for each test configuration to obtain an impact velocity closed to 4.4 m/s.

The rotational velocity before impact is zero for all test configurations. To prevent the block from rolling on the inclined ramp, it is released from the sled only about 20 cm before touching the ground.

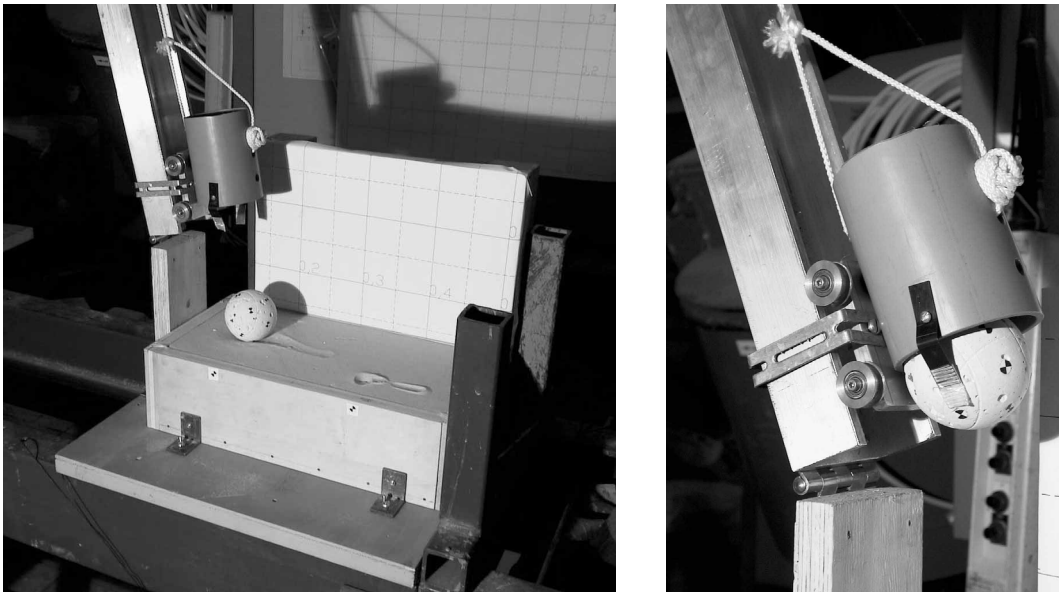


Figure 3.2: Photograph of the experimental set-up for inclined impact tests: releasing of the block from the sled about 20 cm above ground (left). Right: the releasing sled.

3.1.2.2 Materials

Blocks

Spheres (diameter of 7.5 cm) are used as impact blocks. By the perfect symmetry of the spherical blocks, the influence of different impact configurations is eliminated. They are made of expanded gypsum (130 g), concrete (380 g) and metal (750 g). Their unit weight corresponds to 5.9, 17.2 and 34 kN/m³, respectively. The surface of the blocks is smooth and covered by a layer of white colour. Consequently it can be assumed that the different materials do not influence the surface characteristics of the blocks.

Ground materials

As ground, four granular, dry and cohesionless materials with different characteristics are used for the small-scale tests. Two of them are uniformly graded **foundry sands** called “**SF I**” and “**SF II**”. Except for the friction angle φ (35° for SF I, 43° for SF II), the characteristics of both foundry sands are quite comparable (see Table 3.1).

Further, a cohesionless granular material with a lower friction angle is created. Therefore, the foundry sand **SF I** is **mixed with graphite** at a weight proportion of 5:1. The resulting mixture is called “**SF I+G**” and its friction angle φ amounts to 32°.

Some tests are performed on the material used for the half scale tests. The **natural sand**, coming from the deposits of the Lake Geneva, has a maximum grain size of 4 mm and is called “**S0-4**”. Its friction angle amounts to 33°.

As the internal friction angle depends on the compaction of the ground material, the friction angles stated above correspond to the “critical state” friction angles. The grading of all used granular materials is illustrated in Figure 3.3. As the ratio between grain and block diameter is very small ($k = D_{50(\text{sand})}/D_{(\text{boulder})} \ll 1$), all soils can be seen as a continuum.

Except for two test series carried out on bulked SF I, the impact tests are performed on compacted ground material. All the ground materials are compacted by the same procedure in tow layers: first, the box is filled up to the half and the first layer is compacted. Then, the box is completely filled and the material is compacted once more. Finally the surface of the granular material is smoothed. The resulting compaction degree is controlled by means of the weight of the filled box (see description hereafter). For the tests on non-compacted soil, the sand is passed through a sieve to get the least possible density. Also here, the density of

the ground material is controlled before each impact test by means of the box weight.

Table 3.1 resumes the characteristics and the compaction degree, defined as the ratio between the compacted to the bulked unit weight of the material, of all four ground materials.

material	unit weight γ bulked	unit weight γ compacted	compaction degree	“critical state” friction angle ϕ
SF I+G	10.6 kN/m ³	13.6 kN/m ³	1.28	32°
SF I	13.6 kN/m ³	15.6 kN/m ³	1.15	35°
SF II	14.7 kN/m ³	16.6 kN/m ³	1.13	43°
S0-4	12.0 kN/m ³	15.0 kN/m ³	1.25	33°

Table 3.1 : Characteristics of the soil materials used for the small-scale tests

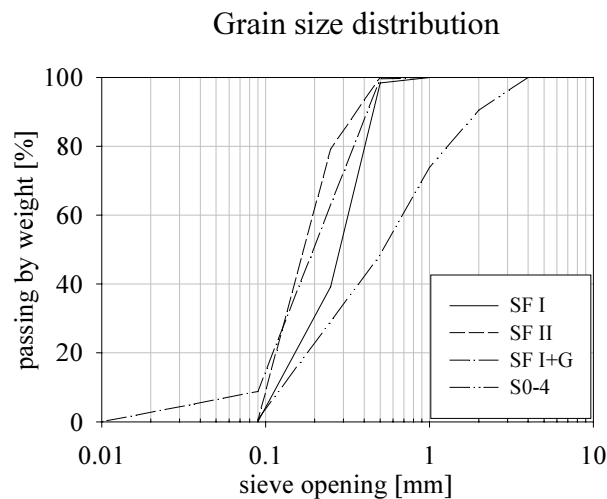


Figure 3.3: Grain size distribution of the granular materials used for the small-scale tests

Being an important parameter (whose influence on the bouncing behaviour is investigated in the following), the ground compaction has to be controlled. For the small-scale tests, the ground compaction is maintained constant by emptying entirely the box containing the ground material after each impact test and refilling it anew for the next test after the methods described above.

The compaction degree of the bulked and compacted ground materials is controlled by its weight. Knowing the volume (0.008m³) and the net weight (3.56kg) of the wooden box, the unit weight of the bulked or compacted ground material is determined by weighing the completely filled and levelled box, calculating the net weight of the ground and dividing the net weight by the

volume. Even if the ground material is filled in and compacted by hand, the weight control reveals a very constant unit weight ($\pm 2\%$) of the bulked and compacted ground materials.

3.1.2.3 Procedure for an impact test

To assure the repeatability of the series, each impact test is carried out under the same conditions and therefore takes place in the same way. The box containing the ground material is fixed to the horizontal or inclined substructure and the releasing tube or the ramp for respectively the vertical or inclined impact is brought into position. Then, the camera is prepared (choice of the appropriate lens aperture, exposure time, number of frames per second (250 f/s), trigger etc.) and the recording is activated. The trigger is set on 100% so that it can be operated right after the impact stopping the recording and saving all frames of the preceding four seconds. Then the block is brought into position and is released. As soon as the impact is over, the trigger is operated manually stopping the recording. The filmed scene is controlled to contain the entire impact process and the impact-relevant part of the film (in general about 100 frames) is saved under the individual series' name and ready for further data processing.

After each impact test, the box containing the ground material is entirely emptied and refilled anew. To check the repeatability of the tests and to estimate the variability of the results, three blocks are released for each parameter combination.

3.1.3 Measuring devices

3.1.3.1 Capturing of the block motion

Camera

The trajectory of the blocks during the impact is filmed by a digital high-speed video camera. The operating speed of the camera ranges from 60 to 8000 frames per second. For higher recording speeds the resolution of the frames and the maximum recording time decrease. Therefore, a compromise had to be found between optimal operating speed, frame resolution and a sufficient recording time. Preliminary tests have shown that an operating speed of 250 frames/sec is sufficient to follow the block motion with accuracy. At this operating speed, the frame resolution is still maximal (480 x 420 pixel) and the maximum recording time is four seconds.

The camera is installed perpendicularly to the block motion plane (image plan parallel to motion plan) in a distance of about 1.5 m.

Lens

For the recording of the small-scale tests, a 16 mm C-mount lens (corresponding to a normal photo lens without zoom or wide angle) is used.

Targets

To follow the motion of the blocks during impact and to control, if the block moves during impact (what clearly is to avoid!), photographic targets (black and white reference points) are fixed on the surface of both the block and the box containing the ground material.

The area displayed in one pixel on a small-scale is about 0.8 x 0.8 mm. Adapted to this pixel size, circular black and white reference points comparable to the ones used in crash tests are used as targets (Figure 3.4). As a result of some preliminary tests, their size is chosen to a diameter of about 8 mm. Thus their centre is clearly visible on the films and the program used to track the targets automatically can detect them commonly without any problems.

Due to the fact that only one camera is used (and not two needed for a three-dimensional analysis of the problem), the block and its motion are projected onto the image plane. As long as the motion plane and the block surface are parallel to the image plane, this projection does not falsify the information resulting from the two-dimensional analysis of the film. In case of the spherical blocks used for the small-scale experiments, however, the block surface is curved and the targets fixed on it are therefore not on the same plane but dispersed in space. The resulting error in radial direction starting from the centre of the block can be calculated according to the theorem of intersecting lines as follows:

$$\Delta x = X - \frac{X \cdot (Z - r)}{Z} \quad (3-1)$$

with Δx being the error due to the assumption that the targets are on the same plane as the block centre, Z being the distance between the centre of the block (motion plane) and the camera (image plane), X being the real position of the target on the motion plane and r being the radius of the block.

In the case of the small-scale tests, the distance Z between camera and motion plane is at least about 1.40 m and the block radius is 0.0375 m. By means of these values it can easily be evaluated that even for a maximal X equal to the block radius r the maximum error Δx is about 1 mm. Taking into account the inaccuracy for the determination of the target centre being in the order of one pixel (Figure 3.4, right), the error due to the assumption of a planar block surface (max. 1 mm = 1.25 pixel) can be neglected.

Further, only the rotation of the block is sensible to this error, being determined by means of the targets. The translational movement of the block, determined by means of the circumference of the spherical block and not by means of the targets (see following section), is not concerned by the discussed error.

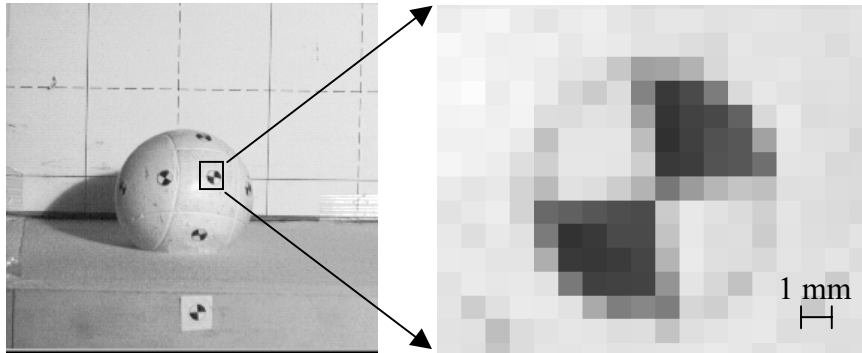


Figure 3.4: Black and white targets on block and box used for small-scale tests (left) and zoom on a single target (right).

3.1.3.2 Measurement of traces

The impact of a block as well as its further motion leaves clearly visible traces on the ground. The shape, diameter and depth of an impact crater gives information about the size and even the energy of the originating block. To be able to correlate the size and shape of a crater with the kinematical and geometrical parameters of the initiating block, all concerning data are measured manually and recorded in the experimental report. After each impact test, the diameter of the resulting crater and of the crater rim is measured lengthwise and in transverse direction (Figure 3.5). If rolling or sliding of the block occurs (in general for slopes steeper than 10°), the width and every eventual deflection of the rolling trace (as illustrated in Figure 3.6) are recorded. The maximum depth is measured at the middle of the crater in vertical direction beginning at surface level.

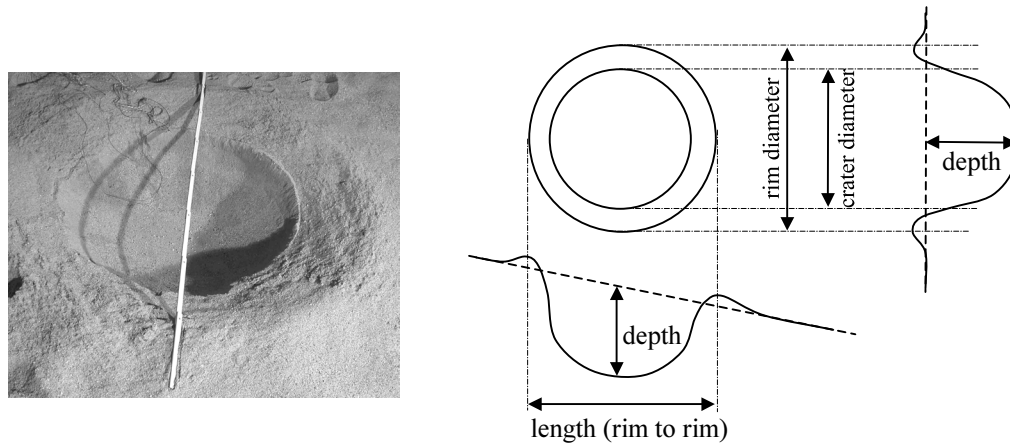


Figure 3.5: Photograph of an impact crater on a half-scale (left) and scheme of the manually measured dimensions of a crater (right).



Figure 3.6: Example for a deflection of the rolling trace left by a block.

3.1.4 Data acquisition and data processing

3.1.4.1 Motion analysis by WINalyze

The motion of the block is analysed by means of a specialised image analysing software (WINalyze 1.4). This software automatically tracks one or several objects in a film sequence. The object can be either a small target or a larger item as for example one of the blocks used for the experiences. In the present case, both the targets and the block centre, detected as the centre of its circumference, are tracked (Figure 3.7). For each frame of the film, the x and y coordinates of all tracked objects are saved automatically. By means of these coordinates the

translational and rotational velocities respectively energies of the tracked block are computed for any time of the impact (see Chapter 3.1.4.2).

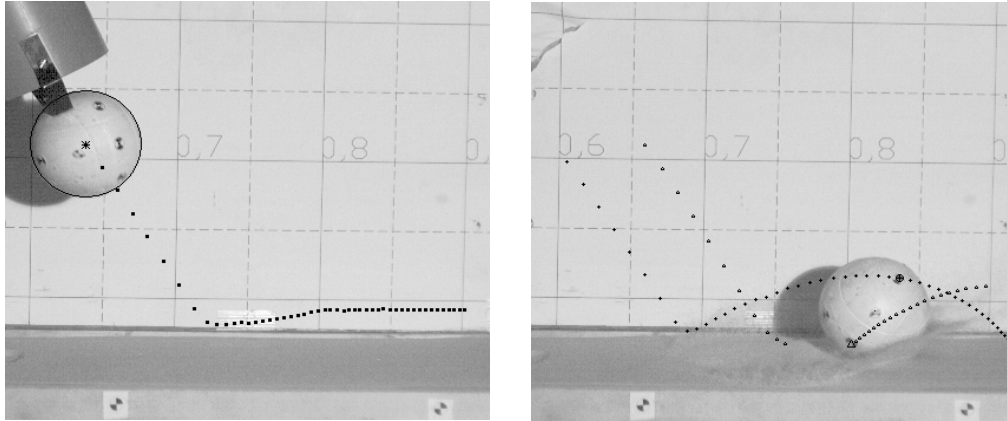


Figure 3.7: Motion analysis with WINalyze for a small-scale test. The centre of the block (left) and two of the targets fixed on its surface (right) are tracked; each dot represents the position of the point in one frame of the film, that means every 1/250 second.

Prior to the presentation of this motion analysis method, two possible sources of error and the compatibility of the method with the system restrictions have to be investigated. In the present case, mainly two problems arise: (1) the reduction of a three-dimensional problem on the image plane x-y, and (2) the accuracy of the object tracking. Both problems are discussed in the following, including the resulting data smoothing problem.

Reduction to 2-D:

Due to the fact that a single camera is used to record the impact, all information concerning the block motion gained from the films are limited to the x-y-plane parallel to the camera plane. In the present case this “motion plane” is assumed to be the vertical plane perpendicular to the ground surface. Therefore, experiments for which a deviation of the block out of the x-y-plane is noted (for example by observation of the traces left on the ground) are invalid and have to be repeated. A strict compliance of this inspection justifies the restriction of the motion analysis to the x-y-plane.

Further, the fact that the block itself is three-dimensional and not planar induces a possible source of error. As aforementioned, the error arises by the projection of a target fixed on the block surface on the x-y-plane of the block centre. Thus, as discussed and showed in Chapter 3.1.3.1, this error is negligible for the small-scale tests.

Accuracy of object tracking:

Also the imprecise tracking of an object can induce an error to the motion analysis. The accuracy depends strongly on the visibility of the tracked object. In general, a sharp contrast enhances drastically the accuracy. For this reason, black and white targets are used and the blocks are coloured white. In case of unsatisfactory tracking results, the program WINanalyze provides several filters to increase the contrast and three different tracking algorithms to either respect or discard the effects of changing illumination, brightness differences or texture structures.

Even if the error is drastically reduced by a correct application of the provided tools, the tracking is never completely free of a random error. This error, generally smaller than a pixel, affects the x- and y-coordinate ($x(t)$ and $y(t)$) of the tracked object. Subsequently, the derived values for the velocity ($x' = v_x(t)$ and $y' = v_y(t)$) and the acceleration ($x'' = a_x(t)$ and $y'' = a_y(t)$) are also affected by the random error. The resulting graphs of velocity and acceleration are scatter-prone, complicating definitely the data analysis. WINanalyze provides a special feature to smooth the scattered graphs. The random noise is removed from the data using a low-pass filter according to the method of Savitzky & Golay [1964]. Pursuant to this method, the values for x' and y' respectively x'' and y'' are calculated directly from the original (non-smoothed) coordinates x and y . As explained in the following, the resulting data are then smoothed using a sort of weighted moving window average. The smoothed data reduce the effect of random errors enhancing in general the accuracy of the motion analysis.

Data smoothing and its effect on velocity and acceleration curves:

In the present case, the smoothing of the data introduces however a new problem: Kernels, being a sort of weighted moving window averages with predefined widths (as explained in the following) are used to smooth the data. Due to the smoothing, an individual peak value - resulting whether of an impact or a measuring error - is faded in its absolute value while its duration is increased. In the case of an error, such an effect can be very helpful for the data analysis. But in the present case of an impact analysis, the exact determination of beginning, duration and end of this event by the acceleration or velocity graph is therefore not straightforward. For the interpretation of the experimental results, this problem is nevertheless very important, the end of the impact being determined by means of the velocity and acceleration graphs (refer to Chapter 3.1.4.2). The following simple example illustrates this problem and shows the adopted solution.

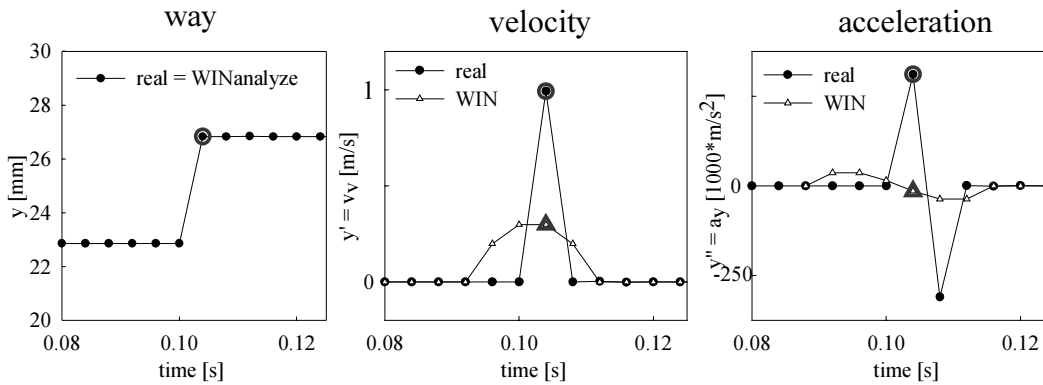


Figure 3.8: Way, velocity and acceleration – “real” values versus smoothed WINanalyze values.

The first diagram in Figure 3.8 plots the y-coordinate versus time of an imaginary object followed by WINanalyze. Each point represents the actual y-coordinate on the corresponding frame. The object is motionless except a sudden movement after $t = 0.1$ s. The velocity and acceleration of the object are illustrated on the following graphs. The circular symbols represent the values computed by a simple derivation of $y(t)$, the triangular symbols denote the results of the data smoothed by WINanalyze. The time when the object first has its new position is highlighted by a larger symbol. The analysis of the plots reveals that the velocity and acceleration graphs anticipate the value changes to come “in future”, the same goes for value changes “in the past”. In case of a measuring error, the smoothing evidently helps to restrict the erroneous peak value. For the determination of beginning and end of a sudden impact, however, the interpretation of the smoothed graphs is not straightforward.

Therefore, the mathematical law for the smoothing has to be considered. It would lead too far to go much into details in the context of this thesis; the interested reader may refer to the very detailed article published by Savitzky & Golay [1964] and Chapter 14 of the book by Press & al. [1992]. As relevant for the following, it just should be mentioned that for the first or second derivation (y' and y'') a data point is smoothed by using a sort of weighted moving window average (so-called “kernel”) by the width of 5 or 7 respectively. As presented in Figure 3.9, the number of points used “to the left” (earlier) of the actually smoothed data point is equal to the number used to its right (later). The smoothing over the respective kernel of 5 or 7 further induces a bias to the smoothed data points, if the underlying function has a nonzero second derivate, as the peak in our example. Consequently, for the smoothed curve of the first derivative y' the influence of the peak can be noted two time steps “before” and one time step “after” the real event (Figure 3.9, left). In the case of the second derivative y'' the data are influenced even three time steps before and two time steps after the event (Figure 3.9, right).

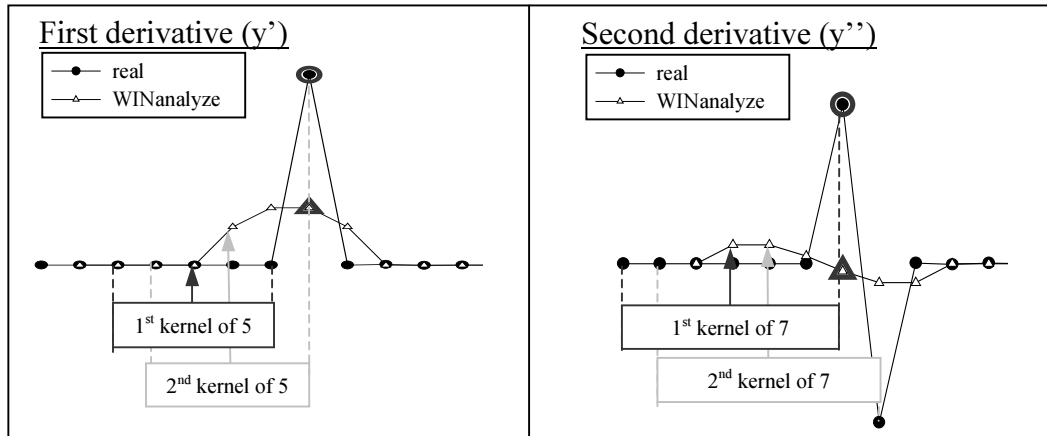


Figure 3.9: Example for a kernel of 5 and 7 for respectively the first and second derivative of the curve $y(t)$.

Applied to the case of a simple shock, this knowledge is essential for the interpretation of the smoothed data curves. Given the fact that a simple shock is completed theoretically at the time when the acceleration becomes zero (refer to Chapter 3.1.4.2), the end of an impact can be determined in the following way: The smoothed acceleration curve (in this example $y'' = a_y$) is analysed for the first frame after the begin of the shock for which the acceleration y'' equals zero. As we have seen above, this time - that is to say the corresponding frame “n” - is not the real end of the impact, but the frame **after** the end of impact. Consequently the preceding frame “n-1” has to be chosen as characteristic frame determining the end of impact. As we will see later on, it is important to mention that for frame “n-1” the preceding peak has no effect on the smoothed velocity curve y' any more (Figure 3.10).

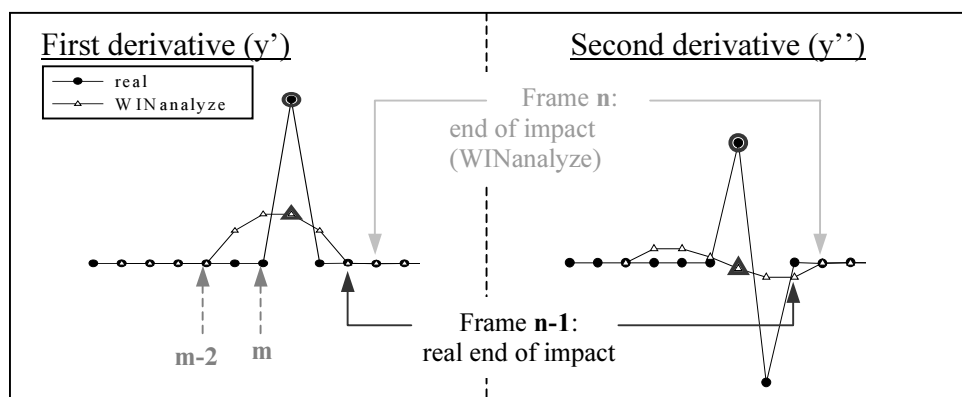


Figure 3.10: Beginning and end of impact – smoothed WINanalyze and real y' and y'' curves.

Before impact, that is to say till $t = 0.1$ s (Figure 3.8) respectively “m” in Figure 3.10 (left), the “real” velocity y' of the object equals zero in the present example. For frame “m”, however, the smoothed value of y' is not equal to zero. According

to the mathematical smoothing law, frame “m-2” (for which the smoothed y' equals zero) has to be used to determine the correct smoothed value of y' (Figure 3.10, left). If a constant acceleration as e.g. gravity acts on the tracked object before its impact (as it is the case for the small- and half scale tests), it can nevertheless be assumed that the increase of the velocity due to gravity between frame “m-2” and “m” is not significant, regarding the time gap of $2 \cdot 1/250$ seconds.

As we will see in Chapter 3.1.4.2, the data smoothing affects strongly the variability of the test results. The considerations above thus are used for all further data processing and have to be respected for the interpretation of the resulting graphs of velocity and acceleration of the tracked blocks.

3.1.4.2 Further data processing

After the motion analysis, WINalyze automatically creates output files containing the data of time, positions, velocities and accelerations in x- and y-directions (corresponding to the camera coordinates) of every tracked object. In the present case these objects are the targets and the centre of the block. For further processing, these data are exported to Excel. By means of the registered successive positions, the translational velocity, acceleration and total energy of each tracked object are computed. The rotation of the block is evaluated by means of the movement of the tracked targets relative to the centre of the block, which is also tracked. The beginning and end of impact are determined (the first optically by means of the film, the latter based on the acceleration of the block centre), to finally calculate the resulting coefficients of restitution. As most trajectory programs use either the couple of coefficients R_n and R_t or the coefficient defined by means of the (total) block energy R_{TE} , and most values in literature are given for these definitions, the three coefficients of restitution are assessed for all performed impact tests.

In the following, the procedure for the further data processing is explained in detail.

Excel routine:

Given the large number of output-files (one for each test!) and the stereotype data processing, several VisualBasic subroutines are used to process the data. The basic main subroutine created by Bisschot [2002] was continuously developed and completed to perform the following steps for every output file:

1. Import of the WINalyze output file in a new Excel file, creating a data sheet for each tracked object (targets and block centre) containing the time

and the respective coordinates x and y (raw data), velocities $x' = v_x$ and $y' = v_y$ (smoothed) and accelerations $x'' = a_x$ and $y'' = a_y$ (smoothed) given by WINalyze.

- For each tracked object the “real” (non-smoothed) values of the velocities and accelerations in x - and y -directions are computed as follows (as control of the values given by WINalyze):

$$v_{x,n} = \frac{(x_n - x_{n-1})}{dt}, \quad v_{y,n} = \frac{(y_n - y_{n-1})}{dt} \quad (3-2)$$

$$a_{x,n} = \frac{(v_{x,n} - v_{x,n-1})}{dt}, \quad a_{y,n} = \frac{(v_{y,n} - v_{y,n-1})}{dt} \quad (3-3)$$

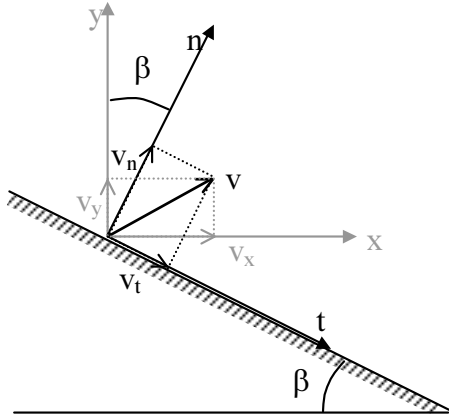


Figure 3.11: Sketch of the relation between the coordinate systems x - y and n - t .

Further, the velocities and accelerations normal and tangential to the ground surface are evaluated for both, the smoothed WINalyze and the “real” values of v_x and v_y (refer to sketch in Figure 3.11):

$$v_n = v_x \cdot \sin\beta + v_y \cdot \cos\beta \quad (3-4)$$

$$v_t = v_x \cdot \cos\beta - v_y \cdot \sin\beta \quad (3-5)$$

$$a_n = dv_n/dt, \quad a_t = dv_t/dt \quad (3-6)$$

- Computation of the angle ψ and the corresponding rotational velocity ω for each visible target (not for the block centre); ψ being the gradient in degree of the straight line between block centre and target:

$$\psi = \arctan \frac{|y_C - y_A|}{|x_C - x_A|} \quad (3-7)$$

y and x being the coordinates of the centre of mass (index C) and the

examined target (index A) respectively. For the small-scale tests, it can be assumed that the gradient of the straight line between centre and target projected in the plane of the gravity centre is the same as the gradient of the spatial connection between centre and target.

The rotational velocity ω is expressed as:

$$\omega = d\psi/dt \quad (3-8)$$

and computed in radians/second. For the further processing and to reduce the oscillation due to random errors, the mean of all values ω computed for different targets is built for every frame.

4. Computation of the translational, rotational and total energies for both, the smoothed WINalyze and the “real” translational respectively rotational velocities of the block’s centre:

$$E_t = 0.5 \cdot m \cdot v_{tot}^2 = 0.5 \cdot m \cdot (v_x^2 + v_y^2) \quad (3-9)$$

$$E_r = 0.5 \cdot \Theta \cdot \omega^2 = 0.5 \cdot \frac{2}{5} \cdot m \cdot r^2 \cdot \omega^2 \quad (3-10)$$

Θ being the moment of inertia about the block centre
(e.g. $\Theta = \frac{2}{5} \cdot m \cdot r^2$ for a solid sphere),

$$E_{tot} = E_t + E_r \quad (3-11)$$

5. Computation of the coefficients of restitution R_t , R_n and R_{TE} for both, the smoothed WINalyze and the “real” velocity data of the block centre:

$$R_t = v_{t,r} / v_{t,i} \quad (3-12)$$

$$R_n = v_{n,r} / v_{n,i} \quad (3-13)$$

$$R_{TE} = E_{tot,r} / E_{tot,i} \quad (3-14)$$

the indices “i” and “r” stand for “incident” and “rebound”, characterizing the velocity or energy at the beginning and the end of the impact. As we will see below, the definition of the impact end is not straightforward and therefore quite difficult to automate. Thus, a time is proposed by the routine for both the “beginning” and the “end”, which has to be controlled by hand.

6. Graphical representation (as exemplified in Figure 3.14) of: the position x-y of all targets and the block centre; the translational velocities and accelerations v_x , v_y , a_x , a_y , v_t , v_n , a_t and a_n of the block centre for WINalyze and “real” values; the mean angular velocity ω and the translational, rotational and total energies E_t , E_r , E_{tot} for WINalyze and “real” values.

The steps 2. to 4. are performed for each time step of 0.004 seconds, corresponding to one frame of the film.

Determination of the instants “before” and “after” impact:

From equations (3-12) to (3-14), the evaluation of the coefficients of restitution is based on the motion characteristics of the boulder before and after its impact with the slope, which thus necessitates the determination of the beginning and the end of the shock. The detection of the beginning of the impact is easily done: a careful frame-by-frame analysis of the film is sufficient to find the instant at which the boulder enters in contact with the ground. The computation of the coefficients of restitution hence is made by means of the incoming velocities and energies just before the boulder gets in contact with the ground.

Contrary to the beginning of the shock, the end cannot be determined visually due to the throwout of ground particles and a generally indistinct rebound of the block (no complete free flight after impact). The solution adopted to solve this difficult point is inspired by the theory of shocks. According to this theory, simple trapezoidal shocks are characterised by a graph of acceleration as a function of time that increases linearly up to a certain value, stays constant for a certain time and decreases again linearly till it reaches the value of zero. As similar graphs are clearly observed in the tests for the block's acceleration component normal to the slope, the end of the shock is defined as the time when the graph of the normal component of acceleration a_n reaches zero (Figure 3.12; in case of a horizontal ground surface - as in the presented case - the normal and vertical acceleration components a_n and a_y are the same!). The graph of the tangential component of acceleration shows a similar shape, but its peak is not as pronounced. In case of bouncing with final free flight, the acceleration must be equal to gravity at the end of the shock. However, as nearly no final free flight of the boulder after impact was observed, the aforementioned definition is used.

As additional decision support, the normal velocity component is consulted. Due to some inevitable imprecision causing oscillations of the velocity and acceleration values, it is sometimes hard to judge whether the instant at which a_n first reaches zero really determines the end of impact or whether it is just an oscillation. In this case, the normal velocity component constitutes a good decision support, v_n reaching per definition a global maximum at the same instant as a_n passes zero. Consulting the local and global development of both the normal acceleration and the normal velocity thus helps to determine definitively the end of impact.

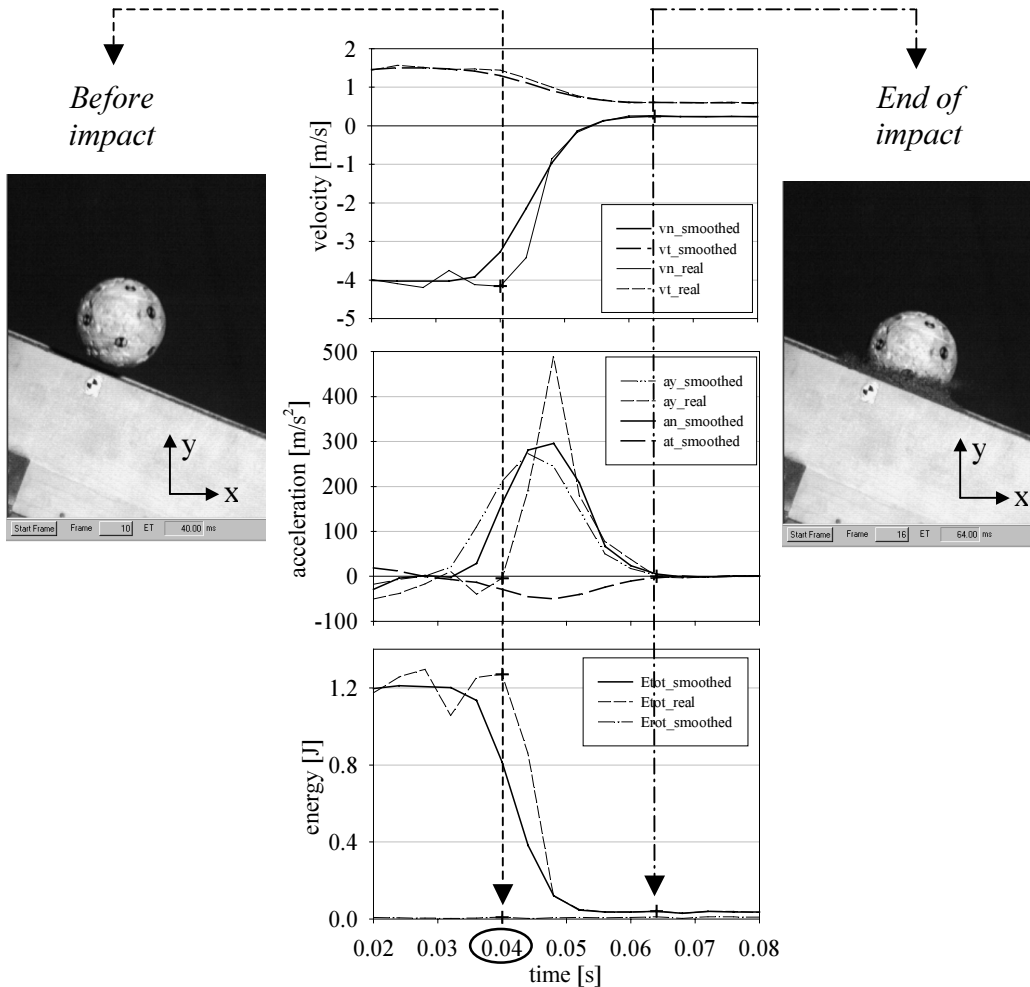


Figure 3.12: Determination of the beginning and the end of impact by means of the not smoothed graph of acceleration.

Variability of the resulting coefficients of restitution:

For the first test series, the coefficients of restitution have been computed by means of the “real” velocities of the block’s centre of mass. As illustrated in Figure 3.13 (left), displaying both the average and standard deviation of values gathered by three similar experiments, the coefficients R_n , R_t and R_{TE} show a large variability. It is due to the oscillation of the “real” velocity values discussed in Chapter 3.1.4.1. Thus, the coefficients of restitution have been evaluated additionally based on the smoothed data provided by WINalyze (Figure 3.13, right). A comparison of the variability of both results reveals clearly more steady results for the latter approach. Consequently the final evaluation of the coefficients of restitution is made by means of the smoothed data.

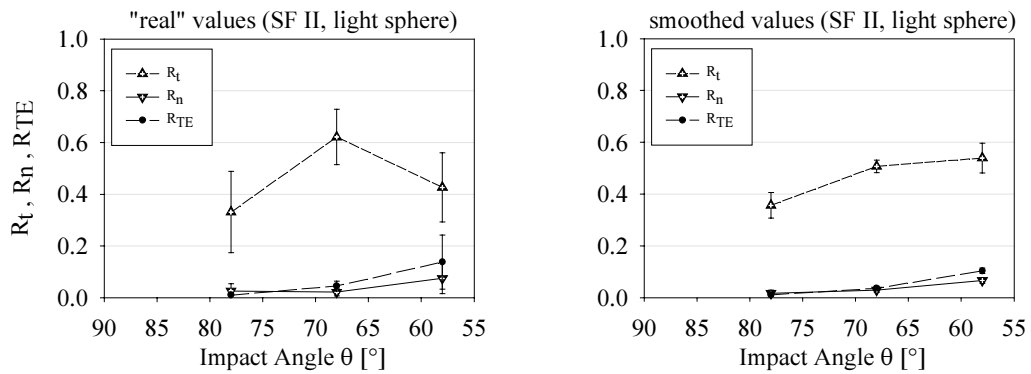


Figure 3.13: Comparison of the standard deviation for values of R_n , R_t and R_{TE} computed by means of "real" (left) and smoothed (right) velocity values for one of the small-scale test series. The reduction of the error bars is evident for the right-hand sided graph.

Representation of the gathered information:

Figure 3.14 (left side) exemplarily shows the data gathered for the position, the velocity, the acceleration and the energy of the block centre for an vertical impact test with the light sphere on a slope ($\beta = 22^\circ$) made of S0-4. The first graph represents the successive positions of the block centre and some of the targets. It shows clearly the change of direction during impact and the instantaneous transition from translation to rotation. The zone where the block overcomes the frontal sand pile formed during impact is identifiable for the graph of the block centre. The following graphs show the real and smoothed values of the normal and tangential velocities and accelerations of the block centre respectively. The crosses at $t_1 = 0.04s$ and $t_2 = 0.064s$ point out the instants before (t_1) and after the impact (t_2). Comparing the smoothed graphs to the "real" (not smoothed) values, the problem arisen by the smoothing of the data can clearly be noted: for the smoothed graphs, the influence of the impact and thus its beginning seems to occur prior to the "real" beginning.

The tangential velocity of the block centre diminishes continuously during impact. After impact it stays constant proving a rolling without acceleration on the slope. The normal velocity meanwhile decreases during impact to zero and changes in sign. At the instant v_n equals to zero, the maximum penetration into the ground material normal to the slope surface is reached and the phase of restitution begins. The impact is completed as soon as v_n reaches its maximum value ($a_n = 0 \rightarrow v_n = \max$). If the trajectory of the block is followed long enough (not the case on the graphs of Figure 3.14), v_n finally reduces to zero in case of rolling or sliding on the slope surface.

Before impact the vertical acceleration a_y takes approximately the value of gravity, that is to say -9.81 m/s^2 . During impact, the graphs of all acceleration components (a_y , a_x , a_n , a_t) show a peak. At impact end, the vertical acceleration a_y equals to zero in case the block stays in contact with the ground surface or takes values up to maximum -9.81 m/s^2 in case of acceleration in negative (downwards) direction and free flight. The smoothed normal and tangential accelerations are computed from the smoothed values of a_y and consequently take the value zero at the same time as a_y .

During impact, the total as well as the translational energy (as E_{rot} is very small during the first phase of impact, E_{trans} nearly equals E_{tot}) decrease rapidly while the rotational energy increases due to the rotation of the block induced by the frictional contact between block and ground. The loss of total energy between beginning and end of impact is clearly to see. In the present case the proportion of rotational energy to total energy after impact is about 20%.

On the right hand side of Figure 3.14, the block position before and after impact and its incident and rebound translational and rotational velocities are represented. Further, the radius line illustrates the rotation of the block between beginning and end of the impact. By means of such graphs, the impact process can be visualised better. Together with the Excel sheets, these graphs constitute the basis for the analysis and interpretation of the test results.

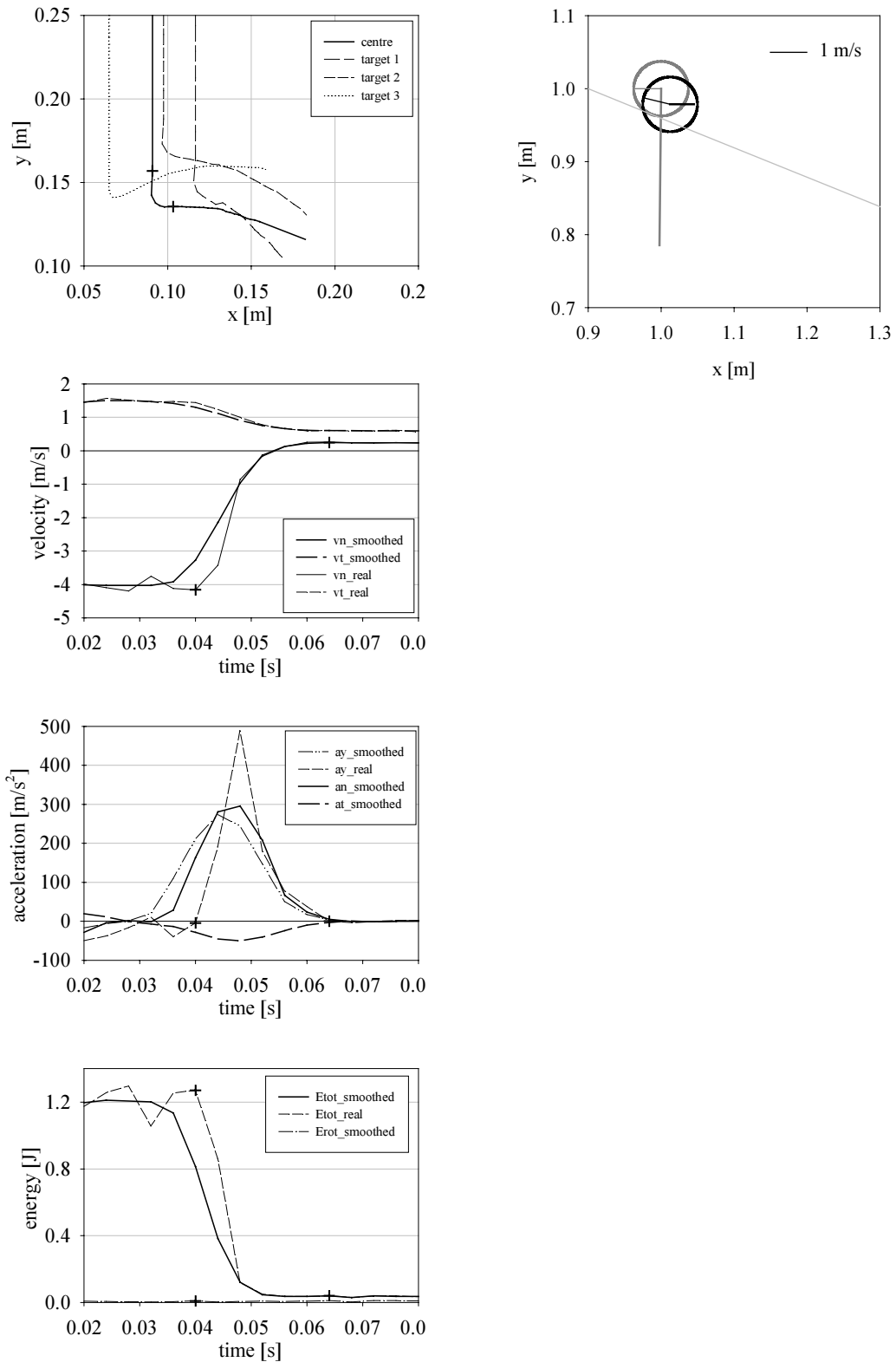


Figure 3.14: left: time versus position, velocity, acceleration and energy for a vertical impact on inclined ground with the light sphere (s9e3L3). A cross highlights the beginning and end of impact.

right: position and velocity vector before (grey) and after (black) impact.

3.1.5 Small-scale test program

All in all, about 210 small-scale tests have been carried out to identify the parameters influencing the bouncing phenomenon. Therefore, several testing series are performed, changing one after the other the following parameters:

- weight of the blocks: 3 spheres with different weight (1300, 3800 and 7500 N) but constant diameter (7.5 cm) to analyse the influence of the mass without changing the diameter.
- slope inclination β : 0° , 12° , 22° , 32° .
- impact direction:
 - a) inclined impact on horizontal ground,
 - b) vertical impact on horizontal or inclined ground,
 - c) inclined impact on inclined ground
 (see Figure 3.15).
- impact angle θ : 90° , 78° , 68° , 58° for impact direction a) and b), for c) the impact angle θ equals $\theta^* - \beta$, with θ^* being 90° , 78° , 68° , 58° .
- slope material: 4 granular cohesionless ($c = 0$) materials with a “critical state” friction angle φ between 32° and 43° ; compacted or bulked, depending on the series (refer to Table 3.1 and Figure 3.3).

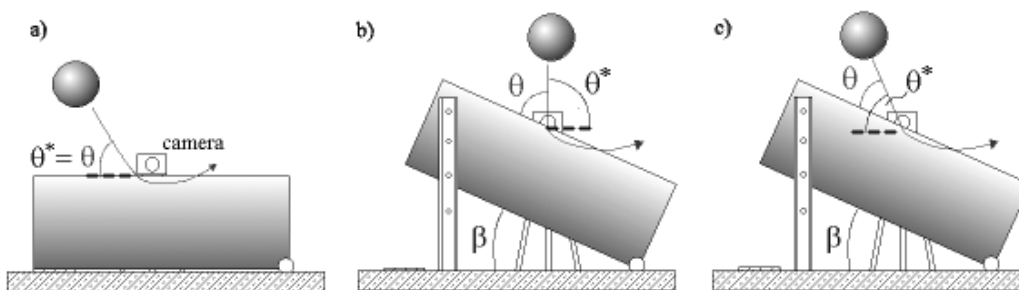


Figure 3.15: Scheme of the small-scale testing device. Inclined impact on horizontal ground (a), vertical impact on inclined ground (b) and inclined impact on inclined ground (c).

The angular aperture between the horizontal and the slope surface defines the slope inclination β . The impact angle θ is defined as the angle between the ground surface and the velocity vector of the block at impact. A further angle, θ^* , is introduced to indicate the direction of the impact velocity vector independently from the slope angle. It is assigned to be the aperture angle between the horizontal and the velocity vector. For all impact tests on horizontal ground, the angle θ^* is equal to θ . All angles are reported in Figure 3.15.

The small-scale tests are organised in different series. A series consists of a sequence of impact tests with only one parameter being changed gradually while all other parameters stay unvaried. Depending on the number of values chosen for the changing parameter (generally three to four), a test series consists in 9 to 12 impact tests.

Clearly not every possible parameter combination can be tested in a limited time; this would have meant to perform some thousand impact tests. So the most interesting combinations are chosen in such way that at least three values for one parameter are tested.

Most of the series are performed with the concrete block weighing 380 grams. On each of the compacted ground materials SF I, SF II and SF I+G, two series are performed changing either the ground inclination β (vertical impact on horizontal and inclined ground ($\beta = 0^\circ - 32^\circ$ while $\theta^* = 90^\circ$)) or the impact angle θ (inclined impact on horizontal ground ($\theta = \theta^* = 78^\circ - 58^\circ$ while $\beta = 0^\circ$)).

In addition, three series of inclined impact tests on inclined ground are performed on SF I. For each of the series, the impact direction θ^* is varied between 78° and 58° while the ground inclination β stays constant at 12° , 22° or 32° .

On the compacted ground material S0-4, only a series of vertical impacts on horizontal and inclined ground is carried out. Moreover, a series of vertical impacts on horizontal and inclined, bulked ground SF I is performed.

The light block (130 grams) is used to perform likewise two series of either vertical (changing β while $\theta^* = 90^\circ$) or inclined (changing θ while $\beta = 0^\circ$) impact tests on the compacted ground materials SF I, SF II and SF I+G. As for the concrete block, no series of inclined but only of vertical impact tests are carried out on the compacted ground material S0-4.

The metal sphere, being with 750 grams the heaviest of the three blocks, is used only on the ground material SF I. A series of vertical impact tests is performed on the bulked ground material, while both a series of vertical and inclined impacts are carried out on the compacted soil. No further tests are performed with the metal sphere having a unit weight of 34 kN/m^3 , which is heavier than any natural rock material.

All performed small-scale test series are listed in Table 3.2 for compacted and Table 3.3 for bulked ground materials.

ground material, compacted	impact direction θ^*	ground inclination β	metal sphere (750 g)		concrete sphere (380 g)		light sphere (130 g)			
SF I	$\theta^* = \theta = 78^\circ$ $\theta^* = \theta = 68^\circ$ $\theta^* = \theta = 58^\circ$	$\beta = 0^\circ$	s1	e1L1-3	s5	e1L1-3	s1	e1L1-3		
				e2L1-3		e2L1-3		e2L1-3		
				e3L1-3		e3L1-3		e3L1-3		
	$\theta^* = 90^\circ$	$\beta = 0^\circ$ $\beta = 12^\circ$ $\beta = 22^\circ$ $\beta = 32^\circ$	s2	e1L1-3	s6		s2	e1L1-3		
				e2L1-3		e2L1-3		e2L1-3		
				e3L1-3		e3L1-3		e3L1-3		
				e4L1-3		e4L1-3		e4L1-3		
	$\theta^* = \theta = 78^\circ$ $\theta^* = \theta = 68^\circ$ $\theta^* = \theta = 58^\circ$	$\beta = 0^\circ$			s10 (cf. s5) ¹	e1L1-3 e2L1-3 e3L1-3				
	$\theta^* = 78^\circ, \theta = 66^\circ$ $\theta^* = 68^\circ, \theta = 56^\circ$ $\theta^* = 58^\circ, \theta = 46^\circ$	$\beta = 12^\circ$			s11	e1L1-3 e2L1-3 e3L1-3				
	$\theta^* = 78^\circ, \theta = 56^\circ$ $\theta^* = 68^\circ, \theta = 46^\circ$ $\theta^* = 58^\circ, \theta = 36^\circ$	$\beta = 22^\circ$			s12	e1L1-3 e2L1-3 e3L1-3				
	$\theta^* = 78^\circ, \theta = 46^\circ$ $\theta^* = 68^\circ, \theta = 36^\circ$ $\theta^* = 58^\circ, \theta = 26^\circ$	$\beta = 32^\circ$			s13	e1L1-3 e2L1-3 e3L1-3				
	SF II	$\theta^* = \theta = 78^\circ$ $\theta^* = \theta = 68^\circ$ $\theta^* = \theta = 58^\circ$	$\beta = 0^\circ$			s1	e1L1-3 e2L1-3 e3L1-3	s4	e1L1-3 e2L1-3 e3L1-3	
		$\theta^* = 90^\circ$	$\beta = 0^\circ$ $\beta = 12^\circ$ $\beta = 22^\circ$ $\beta = 32^\circ$			s2	e1L1-3 e2L1-3 e3L1-3 e4L1-3	s3	e1L1-3 e2L1-3 e3L1-3 e4L1-3	
		SF I+G	$\theta^* = \theta = 78^\circ$ $\theta^* = \theta = 68^\circ$ $\theta^* = \theta = 58^\circ$	$\theta = 78^\circ$ $\theta = 68^\circ$ $\theta = 58^\circ$			s4	e1L1-3 e2L1-3 e3L1-3	s6	e1L1-3 e2L1-3 e3L1-3
$\theta^* = 90^\circ$			$\beta = 0^\circ$ $\beta = 12^\circ$ $\beta = 22^\circ$ $\beta = 32^\circ$			s3	e1L1-3 e2L1-3 e3L1-3 e4L1-3	s5	e1L1-3 e2L1-3 e3L1-3 e4L1-3	
S0-4			$\theta^* = 90^\circ$	$\beta = 0^\circ$ $\beta = 12^\circ$ $\beta = 22^\circ$ $\beta = 32^\circ$			s9	e1L1-3	s9	
								e2L1-3		e2L1-3
					e3L1-3	e3L1-3				
					e4L1-3	e4L1-3				

¹ The series of inclined impact tests on the horizontal ground SF I with the concrete sphere is carried out twice. Since for the series s10 to s13 an other camera with a higher frame resolution and a slightly different operating speed is used, the comparison of the test results for series s5 and s10 allows to verify the functioning of the new system.

Table 3.2: List of all small-scale test series performed on compacted ground materials. Series = s, test = e, release of block = L.

ground material, bulked	impact direction θ^*	ground inclination β	metal sphere		concrete sphere		light sphere	
SF I	$\theta^* = 90^\circ$	$\beta = 0^\circ$	s7	e1L1-3	s8	e1L1-3		
		$\beta = 12^\circ$		e2L1-3		e2L1-3		
		$\beta = 22^\circ$		e3L1-3		e3L1-3		
		$\beta = 32^\circ$		e4L1-3		e4L1-3		

Table 3.3: List of all small-scale test series performed on bulked ground material. Series = s, test = e, release of block = L.

3.2 Qualitative interpretation of the small-scale tests

In the following, the observations made visually (by viewing the films) and by a first analysis are given. Further, the qualitative influence of the tested parameters on the coefficients of restitution is presented.

3.2.1 Observations during small-scale tests

After release, the block follows its flight path linearly and generally without rotation. As soon as the block enters in contact with the ground, it is abruptly slowed down. During the ground penetration, the block is subjected to resistance due to soil bearing capacity. The penetration depth and the shape of the induced crater therefore depend highly on the ground material. For impacts of solid blocks on granular materials, the impact energy is too small to cause plastic deformations to the blocks. The blocks therefore are assumed to be rigid and behave perfectly elastic. The ground material – having a much lower strength than the block – meanwhile is deformed elastically and plastically by the impact energy. The motion of the block after impact depends highly on the impact characteristics and covers motion types as sliding, rolling and free flight.

By sifting the films visually, some general observations are made for different impact configurations. They are stated in the following.

Vertical impact on horizontal ground (compacted ground material)

The vertical impact on horizontal ground causes generally no or just a light rebound in vertical direction depending on the mass of the block and the compaction degree of the soil. The velocity after impact is in general purely translational, rotation after impact is not observed. However, in case of an initial rotational velocity of the block before impact, rotation after impact can occur. The initial rotation of the block resulting from the coincidental contact between block and releasing tube can not always be avoided. In this case, a rolling movement of the block in direction of the initial rotation can be observed after impact. As for

the influence on the coefficient of restitution, such releases are not used for further analysis but repeated.

A typical pattern for a vertical impact is illustrated below for the light sphere impacting SF I (Figure 3.16). Independent of the ground material, a disturbed zone appears right after the block gets in contact with the ground. During this phase and depending on the block weight and the ground compaction, more or less sand is projected. At impact end, a crater round the sphere is clearly visible.

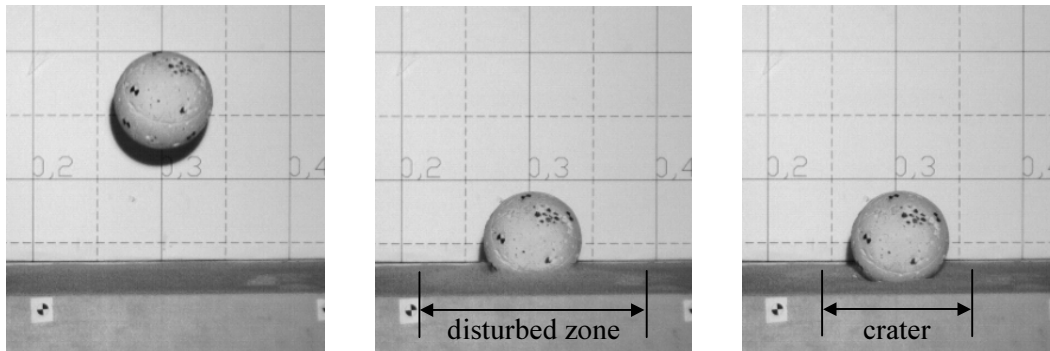


Figure 3.16: Vertical impact of the light sphere on compacted, horizontal SF I (s2e1L3)

Vertical impact on inclined ground (compacted ground material)

The main difference between vertical impacts on horizontal and inclined ground is the post-impact rotation of the block. As soon as the ground is inclined, the incident purely translational movement of the spherical block is transformed to a pure rolling or a combination of rolling and sliding. The more the ground is inclined, the more distinct is the rotation of the block during impact. Spheres with higher unit weight generally seem to have a smoother transition between pure translation (free flight) and rolling (after first contact with the ground). Even if the block begins to develop a rolling motion at the first contact with the ground, it slides at the same time. During impact, the combined rolling-sliding motion is transformed in pure rolling.

The disturbed zone and the crater formed during the impact are extended in dipping direction of the slope. While the block penetrates the ground and begins to roll downhill, a sand pile is formed in front of the block. If the energy restituted to the block is sufficient (as in case of the light sphere), the block rolls over the sand pile and even can take off the ground. In case of high energy dissipation during impact (as e.g. for the metal sphere), the block can be stopped by the pile. The rolling velocity after impact depends highly on the depth of the formed crater.

In case of slope angles close to the internal friction angle of the ground material the slope is at its limit equilibrium (e.g. $\beta = 32^\circ$). Impact on such slopes provokes sliding of the superficial ground material. This effect is observed for all four ground materials and is most pronounced for SF I+G and SF I. The heavier the block, the more pronounced is this sliding effect, taking along the rolling block. In this case, the resulting translation of the block is due to the sliding of the sand and not to a sliding of the block itself.

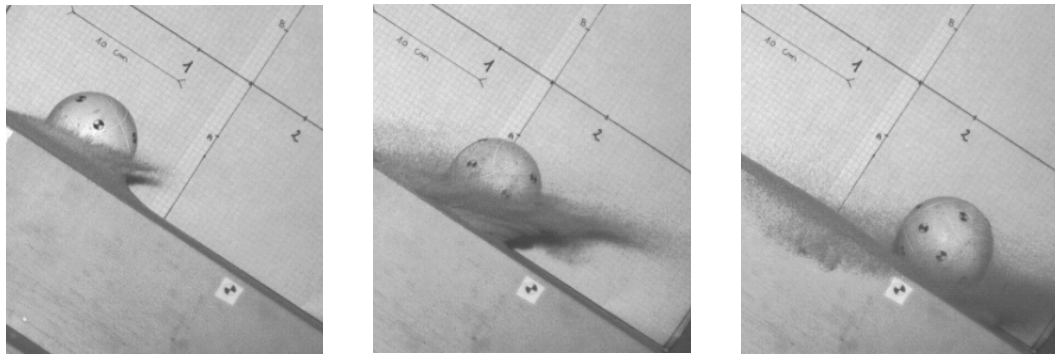


Figure 3.17: Concrete sphere impacting SF II inclined at 32° . The block seems to be “carried” by the projected sand while overcoming the sand pile.

Vertical impact on inclined ground (bulked ground material)

Only two test series are performed on bulked ground material constituted of SF I, both for the constellation “vertical impact on inclined ground”. The metal and the concrete spheres are used for the tests. The general observations made for the compacted soil apply also for the tests on bulked soil.

The main difference to the impact tests on compacted ground is the volume of the crater and the diameter of the disturbed zone, being both much larger on bulked ground. For all impacts, also the volume of projected sand is larger than for the compacted soil. Due to the lower compaction degree, the sand has a lower frictional resistance. Thus sliding of the sand occurs more easily.

In general, no rebound at all is observed, the blocks stop after impact. Only for maximum slope inclinations a slight rolling motion after impact is stated for the concrete block. The sliding sand takes the slightly rolling concrete sphere with it (Figure 3.18).

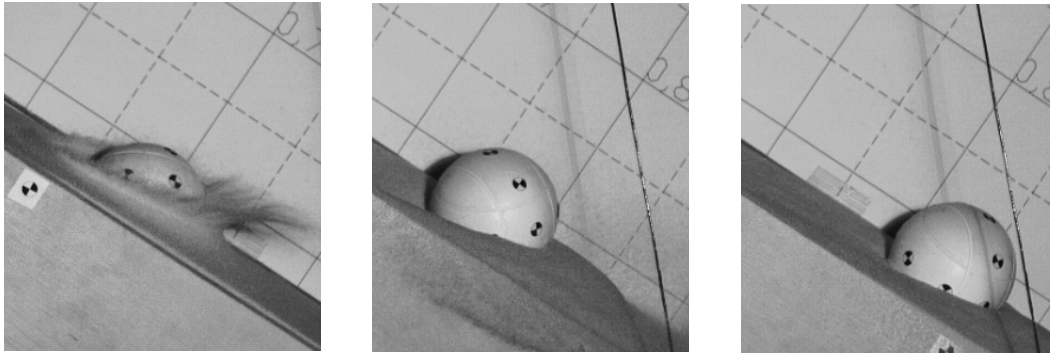


Figure 3.18: Projection and sliding of the sand, taking the slowly rolling concrete sphere with it.

An important observation valid for both blocks (metal and concrete) is the fact that the transition from pure translation to either no motion at all or rolling seems to develop slower than on compacted ground. Even on inclined surface the blocks make their way into the sand with only little rotational movement and quite a lot sliding. Figure 3.19 illustrates the low rolling ratio exemplarily for the concrete sphere.

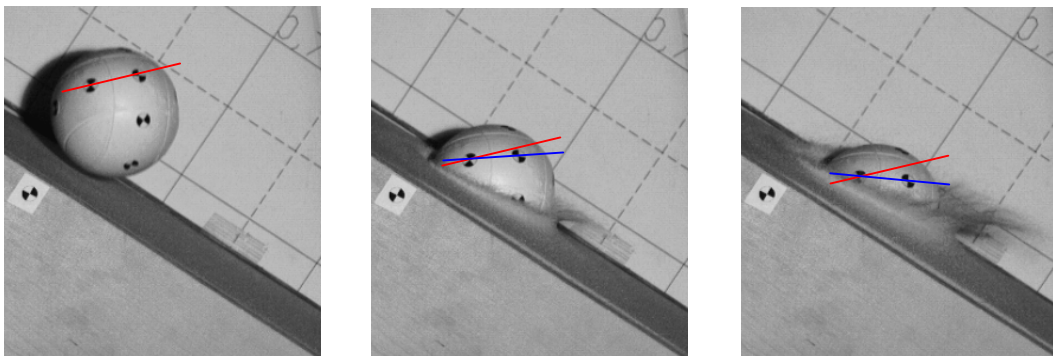


Figure 3.19: First impact phase of the concrete sphere on bulged SF I inclined at 32° . The initial red and the actual blue connection line between two targets illustrate the low rolling ratio.

Due to the enormous sand projection and the deep penetration in the sand, the analysis of the block's motion is very difficult and sometimes even not possible at all for an important part of the trajectory. For this reason, no inclined impact tests were performed on the non-compacted soil.

Inclined impact on horizontal ground (compacted ground material)

The inclined impact tests on horizontal soil are performed for impact angles $\theta = \theta^*$ of 78° , 68° and 58° . The first sifting of the films reveals no significant differences to the corresponding vertical impact tests on inclined soil. In general, the blocks stop more easily after impact due to the lack of the slope inclination

favouring a post-impact rolling motion. The smaller the impact angle and the lighter the block, the more pronounced is the block's motion (rolling or rebound) after impact.

Also for inclined impacts on horizontal soil, the motion of the impacting sphere changes from translation to a combined translation and rotation by the time the block gets in contact with the ground surface. As for vertical impacts on inclined ground, the transition takes longer the heavier the block is. As stated above, the disturbed zone and the crater formed during the impact are extended in direction of the initial motion. For all soils and impact angles their extension is systematically larger the heavier the block. During ground penetration, a sand pile similar to the ones observed for the impacts on inclined soil is created in front of the block.

Corresponding to the observations made above, the rolling length increases with decreasing impact angles. On SF I the blocks systematically roll further than on SF II for all impact angles.

Inclined impact on inclined ground (compacted ground material)

The observations stated above correspond in general to those made for the inclined impact tests on inclined ground. It is observed that the transition from pure translation to rolling takes longer the more tangential the impact is to the slope surface. Also the volume of projected sand increases with increasing slope angles and decreasing impact angles.

As observed for the tests described above, the rolling length after impact is maximal for the maximum slope inclination and increases the more tangential the impact is to the slope surface.

Figure 3.20 illustrates an inclined impact of the concrete sphere on a slope made of SF I.

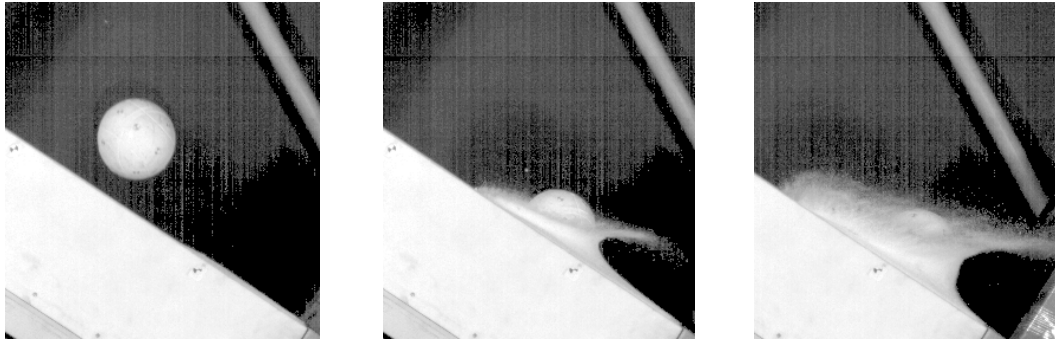


Figure 3.20: Inclined impact ($\theta = 78^\circ$) on inclined SF I ($\beta = 32^\circ$) for the concrete sphere.

For all impact tests the following observations are made:

i) crater and disturbed zone

- The heavier the block (keeping the same diameter!!), the deeper it penetrates into the ground. The resulting crater and the disturbed zone thus increase in volume and diameter for increasing unit weight of the block.
- With increasing slope angles, the diameter of the disturbed zone stays almost constant for the same ground material. While for vertical impacts on horizontal ground the shape is axis-symmetric (circular), its shape shifts in direction of the slope or the incident velocity as soon as impact direction and ground surface are not orthogonal, keeping however the same width.
- The length of the disturbed zone is maximal on SF I+G and minimal on SF II.
- For inclined impacts on horizontal ground the disturbed zone is systematically smaller (shorter) than for vertical impacts on inclined ground.

ii) maximum penetration depth d_{max}

The penetration depth d_{max} is evaluated by both direct measurement and calculation. By means of the normal position of the block centre relative to the slope surface, the maximum penetration depth is evaluated as the maximum difference between the position at begin and during the impact process. The values acquired by direct measurement and by calculation agree very well. The following observations are made relative to the penetration depth:

- The penetration depth decreases with increasing compaction of the ground material.

- For all impact tests, the penetration depth d_{max} is generally maximal on SF I+G (Figure 3.21).
- For constant block diameter, the maximum penetration depth d_{max} increases with increasing block weight (Figure 3.21 to Figure 3.23).
- The change of either slope angle β or impact angle θ causes only little variation to d_{max} . Except for some tests the maximum penetration depth is reached on slopes inclined at 12° to 22° for vertical impacts and at impact angles of 78° to 68° on horizontal ground (Figure 3.22).
- The penetration values coincide quite well for vertical impacts on inclined ground and inclined impacts on horizontal ground (Figure 3.23).

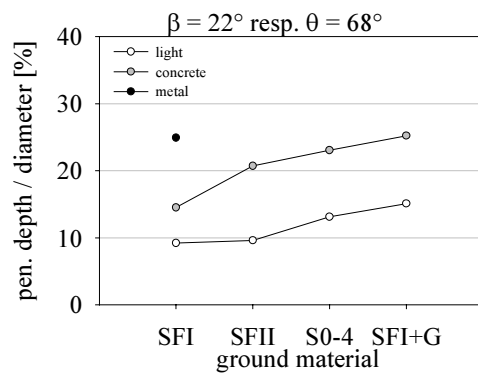


Figure 3.21: Mean values of the maximum penetration depth relative to block diameter [%] for vertical impacts on slopes at $\beta = 22^\circ$ for all four ground materials

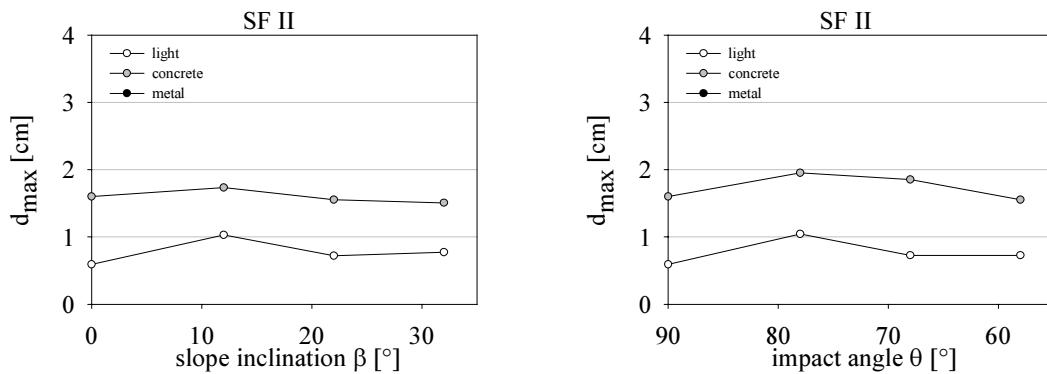


Figure 3.22: Slight change of maximum penetration depth d_{max} [cm] with variation of the slope angle β (left) and the impact angle θ (right) on SF II

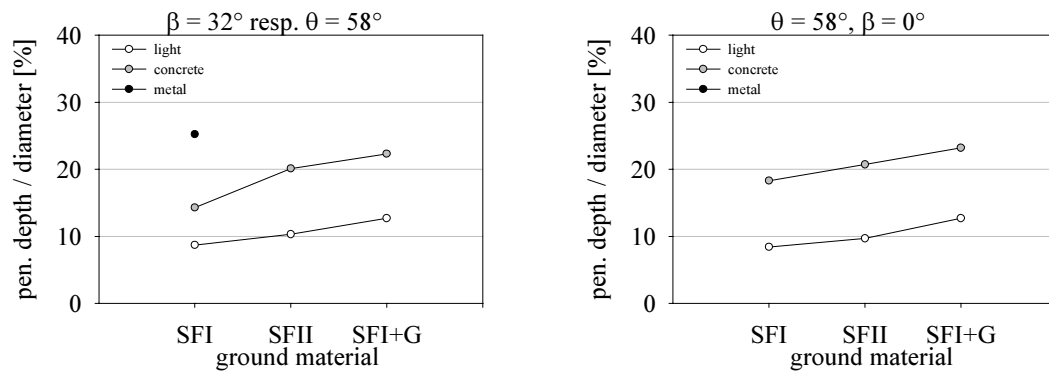


Figure 3.23: Maximum penetration depth relative to block diameter [%] for vertical impacts on slopes at $\beta = 32^\circ$ (left) and inclined impacts at $\theta = 58^\circ$ on horizontal ground (right).

iii) rebound

- A real rebound in sense of “no contact between block and ground” is observed only for impacts of the light and concrete block on compacted SF I+G. On all other ground materials, the blocks never loose contact with the ground surface.
- The rebound height increases for increasing slope and / or decreasing impact angles as well as decreasing block weight.

iv) sand projection

- In general the volume of sand thrown out by the impact increases with the block weight.
- The same goes for increasing slope and / or decreasing impact angles.

v) rolling after impact

- The rolling motion of the block after impact is highly influenced by the penetration depth and the height of the sand pile formed in front of the block. Thus, the lighter the block, the shallower are crater and frontal sand pile and the longer is the rolling path.
- In general, the blocks roll further on slopes than on horizontal ground.
- The more tangential the impact is to the slope surface, the longer takes the transition from translation to rotation.

3.2.2 Sensibility of the coefficients of restitution to the tested parameters

The visual sifting of the films and the observations made during the tests allow a first interpretation of the experimental campaign. The analysis and comparison of the results from the different testing series enable the determination of the most

significant parameters and a first rough quantification of their influence on the coefficients of restitution.

The calculation is performed as described in chapter 3.1.4.2. The resulting coefficients of restitution R_t , R_n and R_{TE} are compared for the different series and analysed for trends induced by the change of the impact parameters. Since the aim of the small-scale tests was not to perform exact scaled tests, the scaling laws are not fully respected. Thus, the values of the evaluated coefficients of restitution have to be considered as qualitative and cannot be compared directly to results gained e.g. by *in situ* tests. A list of all coefficients of restitution R_n , R_t and R_{TE} gathered for the small-scale tests can be found in Appendix I.

As one could expect from the observations stated above, the characteristics of the slope material as friction angle and compaction degree influence the block movement during and after impact as well as the coefficients of restitution. The experiments emphasise also a clear dependency of the latter on parameters characterising the kinematics (e.g. impact angle and impact direction) and the block itself (e.g. weight).

In the following, the influence of the tested parameters on the three coefficients of restitution R_t , R_n and R_{TE} are discussed. The hurried reader will find an overview over the basic trends in Chapter 3.2.3.

Friction angle φ

The influence of the friction angle on the three coefficients of restitution R_t , R_n and R_{TE} is illustrated exemplarily for vertical impacts of the light sphere on compacted slopes inclined at 12° , 22° and 32° (Figure 3.24) and of the concrete sphere (Figure 3.25) on a compacted slope of 22° . No clear difference appears between the two pure foundry sands SF I ($\varphi = 35^\circ$) and SF II ($\varphi = 43^\circ$). However, for both the mixture of sand and graphite SF I+G ($\varphi = 32^\circ$) and the natural material S0-4 ($\varphi = 33^\circ$), the following trends are noted: while R_{TE} remains quite constant, an increase of R_n and a decrease of R_t can clearly be stated, corresponding to a more pronounced block movement in normal direction. These results correspond very well to the observations made during the testing campaign, the motion of the blocks after impact being more parallel to the slope for the pure sands SF I and SF II than for the mixture SF I+G and the natural material S0-4. The same trend of a more pronounced normal block restitution on SF I+G and S0-4 is also observed for heavier blocks (Figure 3.25).

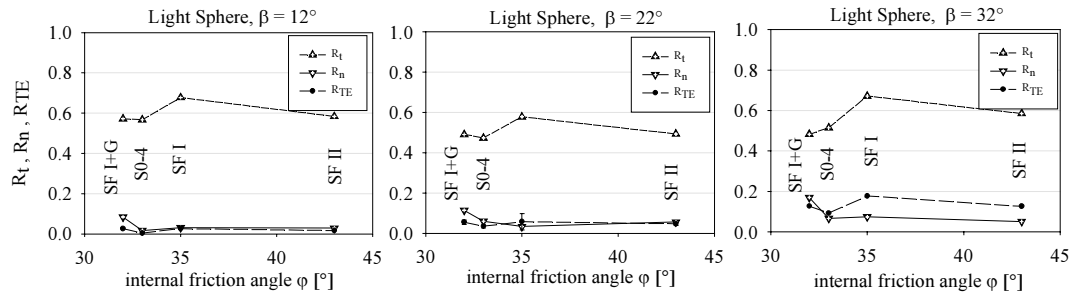


Figure 3.24: Influence of the friction angle ϕ on the coefficients of restitution R_t (triangle up, short dash), R_n (triangle down, solid line) and R_{TE} (circle, long dash) for vertical impacts of the light block on slopes inclined at $\beta = 12^\circ$, 22° and 32° .

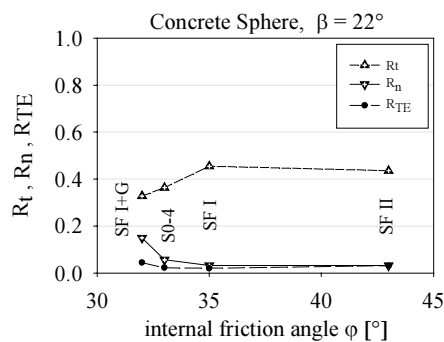


Figure 3.25: Influence of the friction angle ϕ on the coefficients of restitution R_t (triangle up, short dash), R_n (triangle down, solid line) and R_{TE} (circle, long dash) for vertical impacts of the concrete block on a slope inclined at $\beta = 22^\circ$.

It has to be mentioned that by the change of the ground material not only the internal friction angle but also other parameters as the unit weight and the modulus of deformation are altered (refer to Table 3.1). The soil characteristics of the ground materials compared above differ most for the granulometry and unit weight of SF I+G and S0-4. A clear delimitation of the influencing parameters is thus not possible. Therefore, the pronounced change of the coefficients of restitution between SF I+G and SF I could also be due to the higher elasticity of SF I+G and S0-4.

Compaction degree of the ground material

The comparison of impact tests on bulked and compacted slope materials indicates that the compaction degree has a significant influence on the rebound phenomenon. As expected and as illustrated in Figure 3.26, the block penetrates deeper in bulked ground, inducing higher plastic deformation to the ground corresponding to higher energy loss. This leads consequently to smaller coefficients of restitution. Figure 3.27 plots the difference in R_t , R_n and R_{TE} for

series of impacts on bulked and compacted foundry sand SF I with the concrete block. The influence is more pronounced for the tangential coefficient of restitution R_t than for the others, confirming the observation of further post-impact motion particularly in tangential direction made on compacted soil. Since an impact on bulked ground generates a deeper crater and a higher sand pile ahead of the boulder, this result can be explained by the increasing mass of soil offering resistance to the block motion in tangential direction.

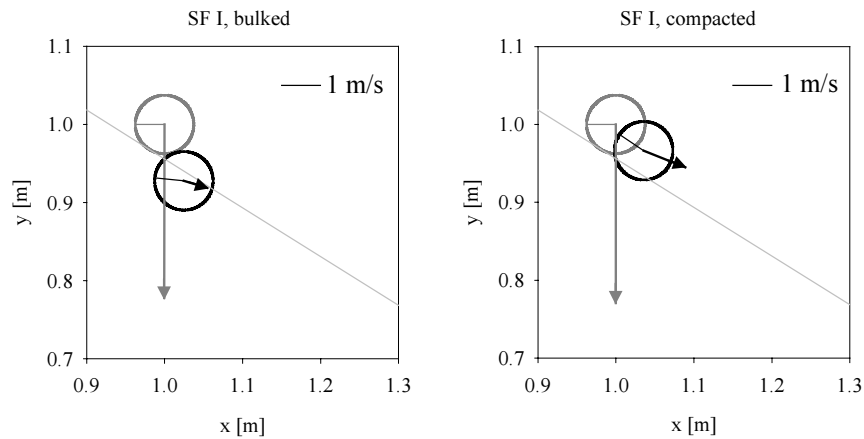


Figure 3.26: Position of the concrete block before (grey) and after (black) its impact on bulked (left) and compacted (right) ground materials inclined at 32° . The grey and black arrows indicate the velocity vector before and after impact respectively; the rotation of the block is given by the radius-line.

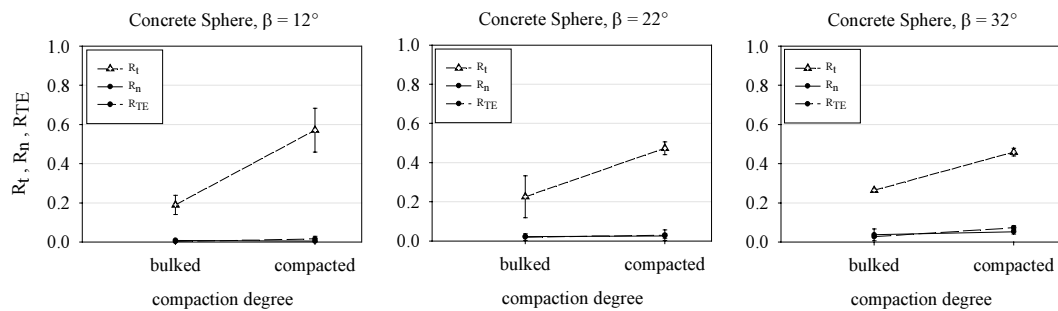


Figure 3.27: Influence of the compaction degree on R_t (short dash), R_n (solid line) and R_{TE} (long dash) determined from vertical impacts of the concrete bowl on bulked and compacted foundry sand (SF I).

Impact angle θ and slope inclination β

Figure 3.28 shows typical results of the coefficients of restitution R_t , R_n and R_{TE} taken from tests series with the concrete block dropped on compacted SF I+G. The graph on the left is for inclined impacts on horizontal ground while the graph

on the right is for vertical impacts on inclined ground. For all test series, decreasing impact angles θ , respectively increasing slope inclinations β , cause a very clear increase of R_n and R_{TE} . In other words: the more normal the impact is to the slope surface, the more energy is dissipated during impact and the less the block rebounds in normal direction. Concerning the tangential component of the coefficient of restitution R_t , the data do not warrant a clear trend.

These conclusions are supported by the results of the inclined impact tests on inclined ground (Figure 3.29). The graph shows exemplarily the influence of the slope angle β on the coefficients R_t , R_n and R_{TE} for impacts with the concrete block on SF I under an impact angle of $\theta = 58^\circ$. The increase of R_n and R_{TE} for increasing slope angles is clearly visible while R_t stays constant. In case the slope angle is closed to the internal friction angle of the ground material ($\varphi_{SF I} = 35^\circ$ whereas $\beta = 32^\circ$), sliding of ground material at impact is observed, leading to a post-impact block movement more tangential and less normal to the slope surface. This observation is confirmed by the increase of R_t and the decrease of R_n for the maximum slope inclination.

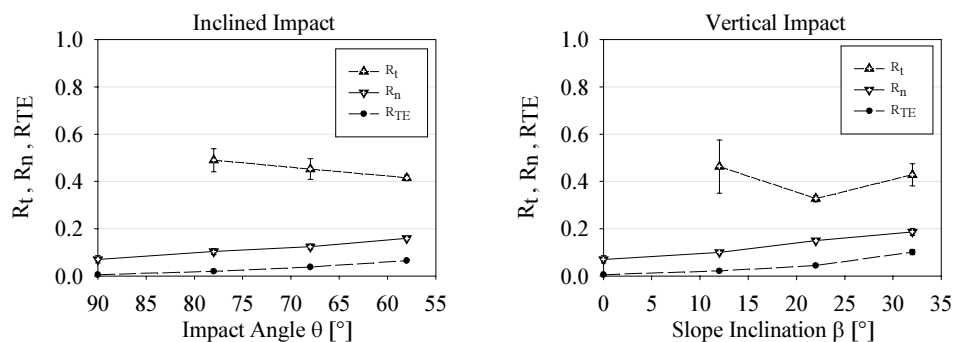


Figure 3.28: Influence of the impact angle θ (respectively the slope inclination β) on R_t (short dash), R_n (solid line) and R_{TE} (long dash). The data are gathered from impacts of the concrete block on SF I+G.

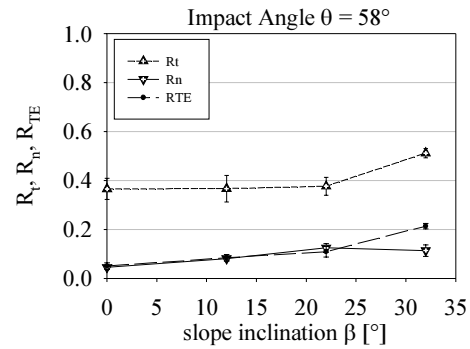


Figure 3.29: Influence of the slope inclination β for impacts under $\theta = 58^\circ$ on R_t (short dash), R_n (solid line) and R_{TE} (long dash). The data are gathered from inclined impacts of the concrete block on SF I.

In Figure 3.28 no values of the coefficient R_t are given for normal impacts ($\beta = 0^\circ$ and $\theta = 90^\circ$). For such impacts, being perfectly normal to a horizontal slope surface, the tangential coefficient of restitution R_t is not defined and makes no sense, as the tangential velocity components before and after impact both equal zero ($R_t = 0/0$). For these impact configurations, the values of R_t thus are not represented in the graphs.

It is interesting to note that these trends for impacts on granular soil slopes are rather coherent with recent results obtained at the Hong-Kong Polytechnic University [Chau & al., 2002] from small-scale impact tests of spherical boulders on rock slopes (refer to Chapter 2.5.3).

Further, the variability of results obtained from tests under the same impact conditions (error bars in Figure 3.28 and Figure 3.29) points out a much larger variability for the tangential component of the coefficient of restitution R_t than for R_n and R_{TE} . However, the scatter of data seems less pronounced for impacts more tangent to the ground surface. This observation is rational, bearing in mind that the accuracy of the measurement becomes higher as the tangential component of the velocity increases.

Impact direction

Very interesting information is gained by means of the small-scale tests on the influence of the impact direction on the coefficients of restitution. The test results illustrate, that besides the impact angle θ , the impact direction has a certain influence on the motion of the block, especially for slopes with inclinations close to their friction angle. This is best illustrated in Figure 3.30 comparing the coefficients of restitution presented in Figure 3.28 for both impact directions (inclined impact on horizontal ground versus vertical impact on inclined ground).

The graph reveals no clear difference in R_n and R_{TE} provided that the slope angle β ($\theta = 90^\circ - \beta$) remains small compared to the friction angle of the slope material (in the present case: $\varphi_{SF\ I+G} = 32^\circ$). However, as already stated above, for slopes near their limit equilibrium state, being characteristic for natural slopes below cliffs, the failure of the ground under the block is easier and less energy consuming, causing R_n and R_{TE} to increase. This trend is however not obvious for the tangential component of the coefficient of restitution R_t due to rather scattered data.

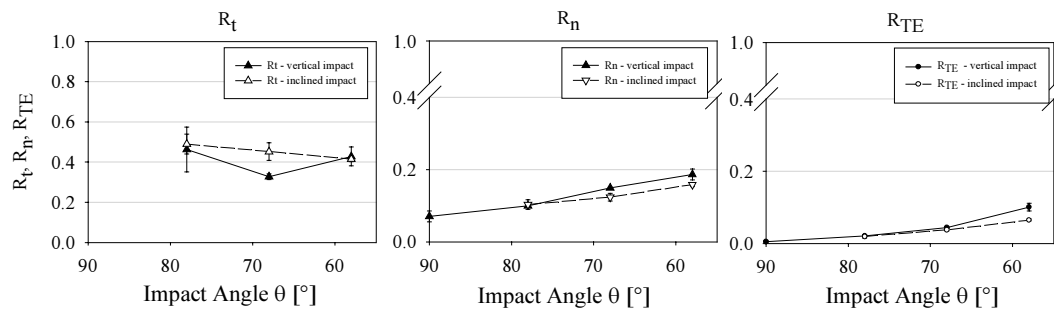


Figure 3.30: Influence of the impact direction on R_t (left), R_n (middle) and R_{TE} (right). The solid lines are for vertical impacts on inclined ground and the dashed lines for inclined impacts on horizontal ground.

Block weight

The unit weight of rocks varying in a very limited range of values, field or laboratory testing campaigns with natural boulders do not allow to differentiate the respective influence of block weight and block size on the rebound phenomenon. For that reason, several tests of the experimental campaign are performed with spheres of same diameter but different weight.

As example, Figure 3.31 plots the coefficients of restitution R_t , R_n and R_{TE} versus different block weights (1300, 3800 and 7500 N) gathered from inclined impacts ($\theta = 58^\circ$) on a horizontal surface of compacted foundry sand SF I. For similar impact conditions, due to their higher incoming energy ($E = \frac{1}{2}mv^2$), heavier blocks penetrate deeper in the ground (Figure 3.32), inducing more plastic deformations and energy loss in the soil. This explains lower rebounding velocities of the boulder and therefore smaller coefficients of restitution R_t , R_n and R_{TE} .

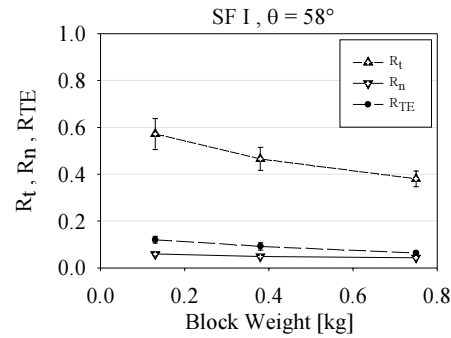


Figure 3.31: Influence of the block weight on R_t (short dash), R_n (solid line) and R_{TE} (long dash).

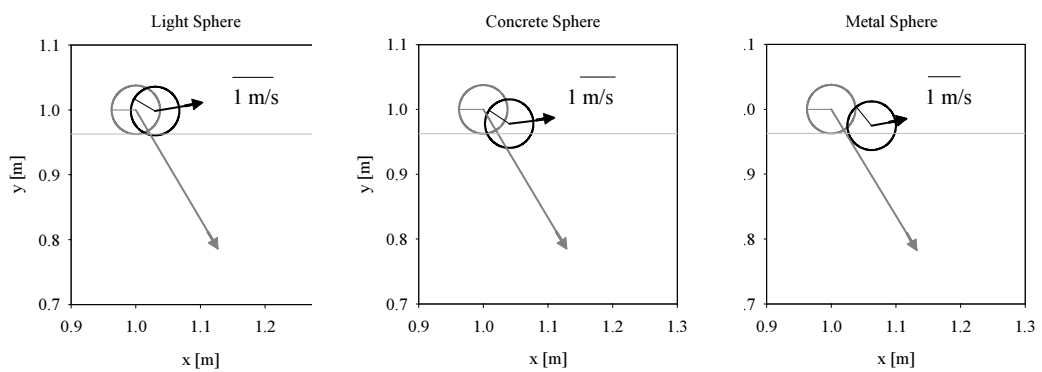


Figure 3.32: Influence of the block weight: deeper penetrations and smaller rebounding velocities are observed for heavier blocks (from the left to the right). The black circles indicate the position of the block at the end of the impact, the black arrows its rebounding velocity.

As stated above, the initial pure translation of the block is transformed into a combination of rotation and translation. For small-scale test conditions, the ratio between the rotational energy and the total kinetic energy after impact averages approximately 20% and depends on parameters related to the slope material (e.g. friction angle) and to the block kinematics (impact angle). Figure 3.33 exemplarily shows the rotational rate induced during impacts for vertical drops of the concrete sphere on inclined slopes of compacted ground material SF I+G.

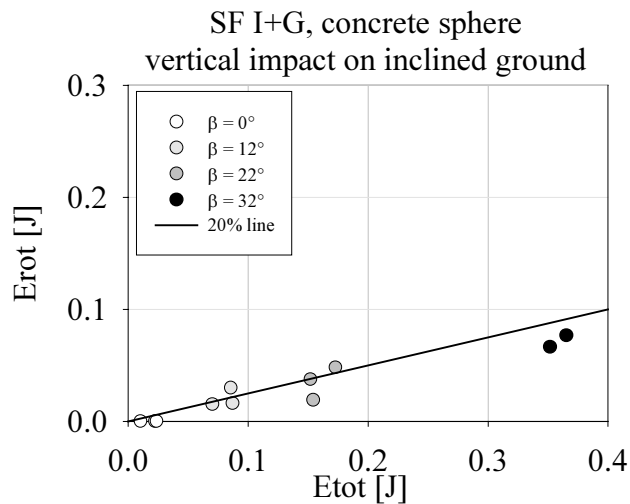


Figure 3.33: Ratio of rotational energy (E_{rot}) to total kinetic energy (E_{tot}) after impact for vertical impacts of the concrete block on inclined slopes of compacted SF I+G.

3.2.3 Summary

To sum up the results of the observation, the following points should be retained:

- The less the ground is compacted, the larger is the disturbed zone at impact, the deeper the block penetrates in the soil and therefore is slowed down by the sand pile formed in front of it leading to a less pronounced movement (rolling or bouncing) after impact.
- For increasing ground inclinations β and decreasing impact angles θ the same tendency is observed: for steady impact directions θ^* the length of the disturbed zone stays quite constant for all slope inclinations, but is shifted in “downhill” direction for steeper slopes. For steady slope inclinations, the same phenomenon is observed for decreasing impact angles θ .
- The penetration depth is rather independent of the slope or impact angle. For $\beta = 12^\circ$ and 22° respectively $\theta = 78^\circ$ and 68° the penetration depth seems to take slightly higher values than for the other configurations. However, a clear decrease of the penetration depth is observed for increasing compaction of the ground material.
- The steeper the slope or the flatter the impact angle, the more pronounced is the motion after impact. For vertical impacts on inclined ground, the motion after impact is more pronounced than for the corresponding inclined impact on horizontal soil.
- The influence of the block weight for constant diameters is very clear: with the weight of the block, the length of the disturbed zone and the penetration depth increase systematically for all test configurations

(inclined impact and vertical impact), whereas the motion after impact is less pronounced for the heavier blocks.

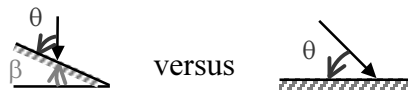
The experimental results confirm very clearly the dependency of the coefficients of restitution not only on characteristics of the ground material but also on different factors related to the kinematics and to the block. The following clear trends are observed:

Influence of the parameters related to the ground characteristics:

- Internal friction angle φ of granular materials \nearrow (and other characteristics of the ground material changed for changing material, as unit weight or modulus of deformation)
 - uniformly graded materials (SF I, SF II): $R_n, R_t, R_{TE} \cong \text{const.}$
 - mixed and natural materials (SF I+G, S0-4): rebound more normal to the slope
- Ground compaction \nearrow
 - $R_n \nearrow, R_t \nearrow \nearrow, R_{TE} \nearrow$
- Slope inclination $\beta \nearrow$
 - $R_n \nearrow, R_t \cong \text{constant}, R_{TE} \nearrow$

Influence of the parameters related to the kinematics:

- Impact angle $\theta \searrow$ (resp. slope angle $\beta \nearrow$ for vertical impacts on inclined ground)
 - $R_n \nearrow, R_t \cong \text{constant}, R_{TE} \nearrow$
- Impact direction: vertical impacts on inclined ground versus inclined impacts on horizontal ground



for $\beta \ll \varphi$: $R_n, R_t, R_{TE} \cong \text{similar values for both configurations}$
 for $\beta \cong \varphi$: $R_n \nearrow, R_t \cong \text{similar}, R_{TE} \nearrow$ for impacts on slopes

Influence of the parameters related to the block:

- block weight \nearrow
 - $R_n \searrow, R_t \searrow, R_{TE} \searrow$

The small-scale experimental campaign ascertains the influence of several parameters related to ground, kinematics and block on the rebound of the block

and the coefficients of restitution commonly used to compute the rebounding velocity (R_n , R_t) and energy (R_{TE}). Comparing data from different testing series the following dependencies are stated:

Concerning the slope material characteristics, the motion of the block during and after impact is moderately influenced by the friction angle and significantly by the compaction degree. The experiments emphasise also a clear dependency of the coefficients of restitution on parameters characterising the ground as the slope inclination β and the kinematics as the impact angle θ and the impact direction θ^* . They point out for instance that the more normal the impact is to the slope surface, the less the block rebounds, as observed already by Chau & al. [2002] on rock slopes. Finally, testing series performed with spheres of same diameter but different weight show a certain dependency of the rebound and consequently of the coefficients of restitution on the block weight (or incoming energy as $E = \frac{1}{2} mv^2$).

3.3 Scale effects

The small-scale experimental campaign is very helpful for the understanding of rockfall phenomenology and in defining the most important parameters. However, the quantitative interpretation of the results is not straightforward, owing to the difficulty in matching the similitude requirements for all parameters involved.

In the present case, each unit used in context of the impact analysis, as e.g. velocity, acceleration, energy, linear momentum, stress etc., depend on three fundamental physical parameters, length L [m], time T [s] and stress σ [N/mm^2], the force [N] = [$kg \cdot m/s^2$] relating the mass [kg] to the parameters L [m] and T [s]. Thus, all units can be reduced to the independent units meter, second and kilogram. To scale a model matching the similitude requirements, the basic scales have to be defined parting from simple relations. This is possible e.g. as follows:

- $A = L/L_M$ (geometrical scale), L being the geometrical size of the prototype *in situ* and L_M being the geometrical size in the model (e.g. diameter of the spherical blocks),
- $\Sigma = \sigma/\sigma_M$ σ and σ_M being the stress in prototype and model, respectively, and
- $T = T/T_M$ (time scale), T being the time span in reality and T_M in the model.

With the definitions given above, the scale for each physical parameter can be computed (refer to Table 3.4).

Certain naturally given restrictions limit the choice of scale and define the relation between the three basic scales. In case of impact tests in free conditions (no centrifuge), gravity represents a naturally fixed parameter, which stays constant for both prototype and model. With $g = g_M$, g and g_M being gravity in prototype and model, respectively, the scaling laws thus yield a relation between the time scale T and the geometrical scale A :

$$\frac{g}{g_M} = \frac{\text{ms}^{-2}}{\text{ms}^{-2}} = \frac{LT^{-2}}{L_M T_M^{-2}} = AT^{-2} \stackrel{!}{=} 1 \quad \Rightarrow \quad T = A^{1/2} \quad (3-15)$$

A further relation is enforced if the same material is used in model and prototype, having thus the same unit weight $\gamma = \gamma_M$:

$$\frac{\gamma}{\gamma_M} = \frac{\text{Nm}^{-3}}{\text{Nm}^{-3}} = \frac{\sigma L^{-1}}{\sigma_M L_M^{-1}} = \Sigma A^{-1} \stackrel{!}{=} 1 \quad \Rightarrow \quad \Sigma = A \quad (3-16)$$

By means of the restrictions stated above, the following relations apply for the evaluation of the scale:

parameter	notation	unit	scale
acceleration	a	[m/s ²]	1
gravity	g		
length	L	[m]	Λ
time	t	[s]	$T = \Lambda^{1/2}$
stress	σ		
modulus of subgrade reaction	M_E	[N/m ²]	$\Sigma = \Lambda$
Young's modulus	E_s		
mass	m	[kg] = [N/m ²] · [s ² ·m]	$\Sigma T^2 \Lambda = \Lambda^3$
unit weight	γ	[N/m ³]	$\Sigma \Lambda^{-1} = 1$
mass density	ρ	[kg/m ³]	$\Lambda^3 \Lambda^{-3} = 1$
force	F		
weight	W	[N]	$\Sigma \Lambda^2 = \Lambda^3$
translational velocity	v	[m/s]	$T = \Lambda^{1/2}$
rotational velocity	ω	[rad/s]	$T^{-1/2} = \Lambda^{-1/2}$
linear momentum	p	[kg·m/s]	$\Sigma T \Lambda^2 = \Lambda^{7/2}$
energy	E	[J] = [kg·m ² /s ²] = [Nm]	$\Sigma \Lambda^3 = \Lambda^4$
deformation / strain	ε	[-]	1
Poisson's ratio	ν	[-]	1
internal friction angle	φ	[rad]	1
coefficients of restitution	R_n, R_t, R_{TE}	[-]	1 ?????

Table 3.4: Scale factor of several physical parameters, maintaining gravity and using the same ground material on a small- and full-scale.

Being the same material, it is rather difficult to match the similitude requirements for the deformation modulus M_E , which should be Λ times $M_{E,M}$ of the model.

According to the scaling laws stated above (Table 3.4), the scale factor amounts to $\Sigma = \Lambda$ for stresses, strength and modulus of deformation. Even if the choice of purely granular materials ($c = 0$) allows matching the condition for the strength criterion, the laboratory experiments do not satisfy the similarity requirement for the modulus of subgrade reaction M_E . Yet, the compaction degree respectively the subgrade modulus M_E of the ground was found to affect strongly the rebound of the blocks and the coefficients of restitution. During deceleration of the block, energy is accumulated in the ground, which is restored to the block during its acceleration after impact. Thus it is likely that the coefficients of restitution determined by small-scale experiments do not match those evaluated in field fall

occurrences. The error induced by the scale effect is however less significant for a scaling factor of $\Lambda = 2$ (half-scale) than for $\Lambda \gg 10$ (small-scale). For that reason, the realisation of full- or half-scale tests remains essential for a correct quantification of the bouncing of rock blocks on natural slopes.

To investigate the influence of the downscaling on the coefficients of restitution, some of the coefficients evaluated by small-scale tests are compared to the results of half-scale tests (refer to Chapter 4). The similitude requirements match best for the tests given in Table 3.5. On a small-scale, the corresponding tests are performed with the light sphere (130 g, $r = 0.0375$ m) dropped vertically from 1 m height on an inclined ground (S0-4). On a half-scale, the same inclined ground material is used, whereas the spherical block (150 kg, $r = 0.365$ m) is dropped from 10 m height.

parameter		scale factor	value (small-scale)	value (half-scale)	Λ	$\Gamma = 1$
block	mass m [kg]	Λ^3	0.13 kg	152 kg	$(m/m_M)^{1/3} = 10.53$	-
	radius r [m]	Λ	0.0375 m	0.365 m	$(r/r_M) = 9.73$	-
	unit weight γ_b [kN/m ³]	1	5.88 kN/m ³	7.46 kN/m ³	-	$(\gamma/\gamma_M) = 1.27$
ground	unit weight γ_g [kN/m ³]	1	12 kN/m ³	12 kN/m ³	-	≈ 1
	subgrade modulus M_E	Λ	500 kN/m ²	500 kN/m ²	$\approx 1 \neq \Lambda$!!!	-
	internal friction angle φ [°]	1	33°	33°	-	-
kinematics	drop height H [m]	Λ	1 m	10 m	$(H/H_M) = 10$	-
	impact energy E [J]	Λ^4	1.2753 J	14911.2 J	$(E/E_M)^{1/4} = 10.4$	-
	velocity v [m/s]	$\Lambda^{1/2}$	4.4 m/s	14 m/s	$(v/v_M)^2 = 10.12$	-
	linear momentum p [kg m/s]	$\Lambda^{7/2}$	0.572 kg m/s	2128 kg m/s	$(p/p_M)^{2/7} = 10.48$	-

Table 3.5: Relationship between small-and half-scale tests for several variables verified for the geometrical scale Λ (explanation in the text).

Thus, the geometrical scale factor Λ (being equal to Σ) between small- and half-scale tests is verified to be about 10 in this case. It is respected for all physical variables, except for the particle size of the ground and the subgrade modulus M_E

(using the same ground material). Two other series approximately match in scale: The vertical impacts on inclined ground (S0-4) performed with the concrete sphere ($m = 0.38$ kg, $H = 1$ m) on a small-scale match the half-scale tests performed with the 100 kg sphere (weighing exactly 117 kg) dropped from a height of $H = 5$ m (with a scaling factor of approximately $\lambda = 5$) and the 550 kg sphere dropped from $H = 10$ m ($\lambda = 10$).

Comparing the results achieved for those impact tests on a small- and half-scale, one finds that several measured characteristics match the scaling laws while others don't. Concerning the maximum penetration depth d_{\max} (measured in vertical direction), the maximum normal acceleration $a_{n,\max}$ during impact and the duration of the acceleration peak (t_{peak}) as well as of the total impact process (t_{tot}) (both definitions concerning the duration will be introduced in Chapter 4), the following observations are made:

- maximum penetration depth d_{\max} : For all three mentioned examples the particular scaling factor λ (10 respectively 5) applies very well.
- maximum value of the normal acceleration $a_{n,\max}$ of the block centre: As the scale factor for acceleration and gravity is fixed to be 1, $a_{n,\max}$ should have the same value for both small- and half-scale tests. However, the real scale factor ranging between 1.4 and 2.5 (the maximum acceleration being 1.4 to 2.5 times larger for the half than the small-scale tests), the similitude requirements are not fulfilled.
- duration of the peak (t_{peak}) and of the complete impact process (t_{tot}): whereas the scale factor T should equal to $\lambda^{1/2}$ (3.2 for $\lambda = 10$ and 2.2 for $\lambda = 5$), the results show generally smaller factors (1.8 to 2.6 instead of 3.2 and 1.7 instead of 2.2). That means that the impact duration on a half-scale is comparatively shorter than on a small-scale.

The fact that the maximum acceleration and the impact time do not match the similitude requirements could be explained as follows. The analysis of the tendencies noted for the maximum acceleration (being larger for half-scale tests) and the impact duration (being shorter for half-scale tests) shows that the blocks are slowed down more abruptly during half- than during small-scale tests. As the deceleration of the block during impact and the duration of impact both depend directly on the ground deformability, this illustrates that the ground material reacts different for impacts at small- and large scale. It is supposed that this effect is due to the fact that the resilient modulus M_E does not match the scaling laws (M_E is not λ times bigger on a half- than on a small-scale, as the same material is used at both scales!).

Bearing these results in mind, it is not surprising that the coefficients of restitution evaluated on a small- and half-scale do not match the similitude requirements as

well. Being unit-less, they should have the same value at both scales. However, a mathematical evaluation of the scale factor for the main values of R_n , R_t and R_{TE} leads to the following ratio:

		Scaling factors evaluated between small- and half-scale								
		0.13 kg \leftrightarrow 150 kg H = 1 m \leftrightarrow 10 m			0.38 kg \leftrightarrow 100 kg H = 1 m \leftrightarrow 5 m			0.38 kg \leftrightarrow 550 kg H = 1 m \leftrightarrow 10 m		
		small scale	half scale	<i>ratio</i> <i>hs/ss</i>	small scale	half scale	<i>ratio</i> <i>hs/ss</i>	small scale	half scale	<i>ratio</i> <i>hs/ss</i>
R_n	12° / 10°	0.018	0.045	2.6	0.021	0.036	1.7	0.021	0.047	2.3
	22° / 20°	0.060	0.053	0.9	0.056	0.045	0.8	0.056	0.057	1.0
	32° / 30°	0.066	0.061	0.9	0.056	0.089	1.6	0.056	0.084	1.5
R_t	12° / 10°	0.563	0.363	0.6	0.437	0.352	0.8	0.437	0.347	0.8
	22° / 20°	0.473	0.378	0.8	0.364	0.318	0.9	0.364	0.346	1.0
	32° / 30°	0.515	0.485	0.9	0.494	0.438	0.9	0.494	0.417	0.8
R_{TE}	12° / 10°	0.004	0.008	2.0	0.010	0.004	0.4	0.010	0.005	0.5
	22° / 20°	0.034	0.024	0.7	0.022	0.018	0.8	0.022	0.020	0.9
	32° / 30°	0.092	0.055	0.6	0.068	0.060	0.9	0.068	0.046	0.7

Table 3.6: Scaling factors evaluated between comparable small- and half-scale tests for the coefficients of restitution R_n , R_t and R_{TE} . The factor should theoretically equal 1.

As given in Table 3.6, the scale factor for the coefficients of restitution, which should equal 1, ranges between 0.4 and 2.6. For nearly normal impact tests ($\beta = 10^\circ$ resp. 12°) the similitude is not verified very well in case of the normal coefficient of restitution R_n (1.7 to 2.6 instead of 1). Except for this configuration, the coefficients of restitution R_n and R_t evaluated on a small-scale are in general slightly larger ($\approx 25\%$) than the corresponding coefficients evaluated on a half-scale. The same goes for the coefficient of restitution R_{TE} , however, the difference between small- and half-scale test results amounts to approximately 40%.

The dependency of the coefficients of restitution on the scale of the model emphasises clearly the importance of large- or half-scale tests for a qualitative verification as well as an exact quantification of these coefficients. Owing to the difficulty in matching all similitude requirements for the small-scale tests performed in the framework of the present thesis, a half-scale experimental campaign is additionally carried out. The aim of the half-scale tests is to verify the qualitative conclusions drawn from the small-scale tests and, above all, to quantify properly the influence of various impact parameters. By means of the half-scale test results, new mathematical expressions shall be developed, modelling adequately the block rebound.

The half-scale tests performed in the framework of this thesis and the results are explained and evaluated in the following chapter.

4 Half-scale experimental campaign

Owing to the difficulty in matching all similitude requirements for the small-scale tests, a half-scale experimental campaign is carried out. The aim of the half-scale tests is to verify the qualitative conclusions drawn from the small-scale tests and, above all, to quantify properly the influence of various impact parameters. By means of the half-scale test results, new mathematical expressions for the coefficients of restitution are developed. Their subsequent implementation in rockfall computer codes should lead to a better prediction capacity for rock block trajectories and to a better delineation of areas at risk (hazard maps).

The following chapter is composed of three main sections. In the first one, the experimental set-up, the measuring devices and the data processing for the comprehensive half-scale test campaign is described. The second section gives a qualitative overview on the test results. The parameters guiding the movement of the block at impact end and thus the coefficients of restitution are determined and their influence is analysed qualitatively. In the third section, the mechanisms of impact are analysed in detail. The characteristics found to influence the impact process and the movement of the block at impact end are quantified by mathematical formulations. Based on the gathered knowledge on ground failure during impact, new mathematical formulations are proposed for the coefficients of restitution. The results gathered by these formulations are compared to the test results.

4.1 Physical modelling

4.1.1 Motivation

As discussed in Chapter 3.3, the similitude requirements are not fully respected for the small-scale tests. Therefore, a half-scale experimental campaign is carried out. The tests are performed as well in laboratory allowing a thorough control of the parameters. The term “half-scale” is chosen to emphasise the fact, that the size and weight of the blocks (max. 10 kN) and the impact energy (up to 100 kJ) of the tests can be compared to natural low-energy events but still don't match the energy scale of bigger natural rockfall events.

Irrespective of these still limited values, the half-scale tests allow nevertheless to verify the qualitative conclusions drawn from the small-scale test results and – what's most important – a quantification of the influence of various impact parameters within the range of applied energies on the coefficients of restitution.

4.1.2 Experimental set-up

The half-scale tests are performed in one of the laboratory's halls ("Halle Fosse") being equipped with an overhead crane and a circular shaft of 8 m depth. The diameter of the shaft being only 5 m, the working space is quite limited requiring a good arrangement of the set-up and several optical "special features" as stated in the following.

As for the small-scale tests, the experimental set-up consists of an inclinable container filled with ground material. Ground inclinations from 0° up to 40° are possible, the maximum depending on the friction angle of the ground material. By means of the overhead crane, masses up to 1 ton can be released from different heights to perform a vertical free fall of maximum 10 m. As the blocks, the container is manoeuvred by the overhead crane. The impact is filmed with the camera described in Chapter 3.1.3.1 at an operating speed of 250 frames per second.

About 175 impact tests have been performed. They are organised in series to systematically isolate and investigate the influence of several parameters. In the following, the different parts of the testing device and the used test materials are described in detail. Chapter 4.1.3.1 gives details of the measuring devices for the motion analysis.

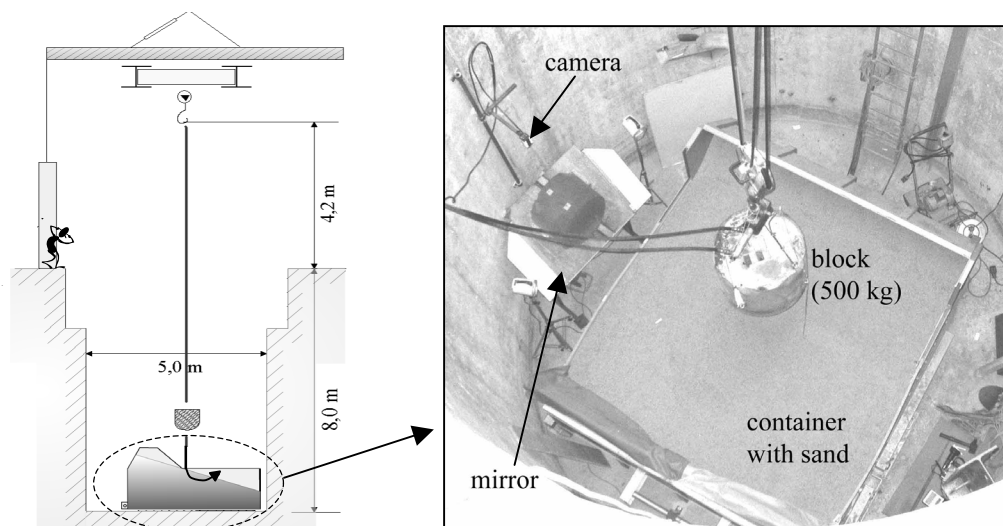


Figure 4.1: Scheme and photo of the test site in the Halle Fosse (EPFL).

4.1.2.1 Testing device

Container

To create an artificial slope for the impact tests, an inclinable container was designed by the author of this thesis (Figure 4.2). Due to different constraints concerning the restricted space in the circular test shaft, the rigidity of the system during impact, the minimal dimensions of the container required to avoid boundary effects and the possibility to build a compacted slope, a thorough study was performed to find the optimal form and inclination system for the container. The dimensions in length, width and height of the resulting container are 3.25 m x 2.7 m x 1 m. The width, corresponding to three times the diameter of the largest block, is chosen to minimize the influence of the container boundaries on the ground behaviour during impact. A cut-off in the sidewalls of the container guarantees the unblocked lateral visibility of the slope surface (Figure 4.2, top middle). The ground material is held back laterally by means of changeable wooden boards sloped on the upper edge from 0° to 40° corresponding to the possible ground inclinations (Figure 4.2, top right).

The end of the container is equipped with a rotational axis, which is fixed to the shaft foundation. The container is inclined along this axis by means of the overhead crane. Two pairs of stilts in different length on both sides of the container support it in each of the inclined positions.

To protect the container wall at the lower end of the slope against shock, several layers of foam mats are positioned.

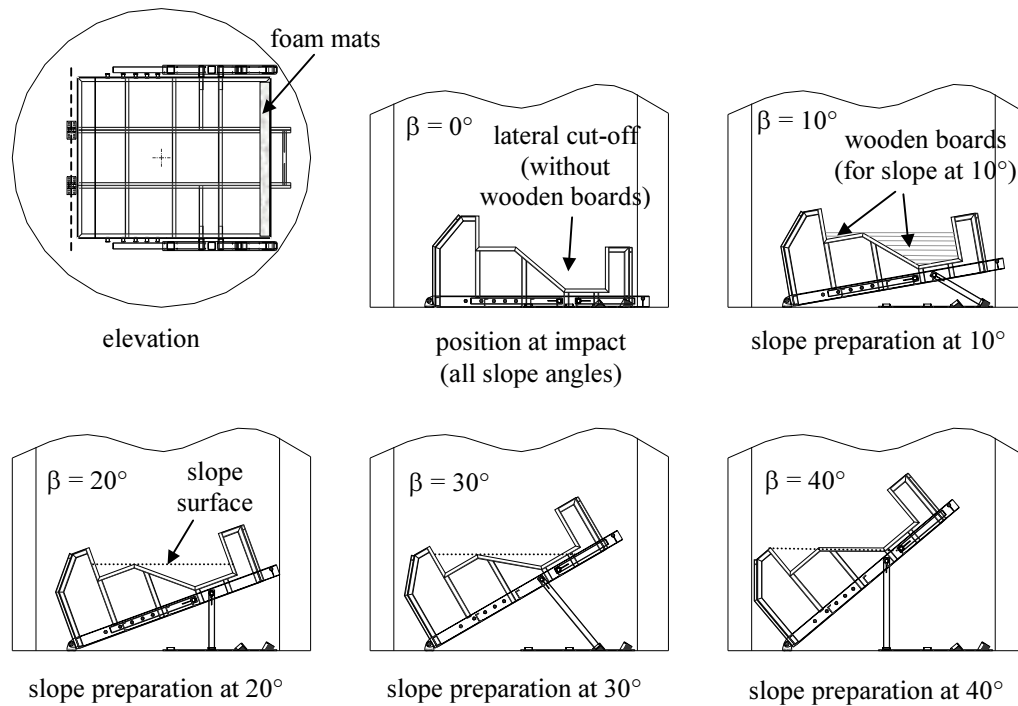


Figure 4.2: Elevation and lateral view of the container in the shaft. To prepare the ground material, the container is inclined. During the impact test, however, it is posed on the ground (position $\beta = 0^\circ$).



Figure 4.3: Hydraulic block releasing system

Block releasing

The blocks are manoeuvred and brought into releasing position by means of the overhead crane. A block releasing system consisting of a hydraulic cylinder which is fixed to the crane hook is used to either grip or release the cable from which the block is hung (Figure 4.3). The clearance between block and ground surface is measured by means of a cord fixed to the base of the block. The cord eases also the collimation of the container centre.

Mirror

Due to the limited space in the shaft it was not possible to place the camera far enough from the impact point to get a full view of the impact process. Therefore, the camera was equipped with a wide-angle lens and installed vertically on the shaft wall by means of an arrangement of rods, which can be moved against each other to change the position of the camera. The camera was adjusted to face a mirror situated underneath and inclined at 45° so that the

image of the impacting block is deflected directly onto the camera. Thus a sufficiently large field of view can be observed. At the same time, the camera is safe from blasting particles provoked by the impact.

4.1.2.2 Materials

Blocks

For the half-scale tests blocks of different shape, weight and size are used. The first set of blocks has already been used for previous impact tests on a rock-shed model [Montani-Stoffel, 1998]. The blocks are made of a steel shell filled with concrete to avert block bursting during impact. The shape is cylindrical with a spherical base (see Table 4.1) and corresponds to the shape of impact blocks used for rockfall tests in Japan [Yoshida & al., 1988]. All three blocks have a constant ratio between the mass of the cylindrical section and the total block mass. The ratio between the height and the diameter of the cylindrical section is constant as well.

Additionally a second set of purely spherical blocks is used. They also consist of a steel shell and all but one are filled with concrete. The diameter of the spherical blocks is chosen to match that of the cylindrical blocks.

Table 4.1 resumes the characteristics of all used blocks.

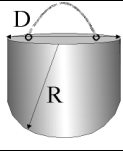
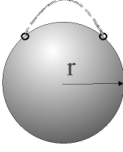
Block shape	Block weight W [kN]	Unit weight γ [kN/m ³]	Diameter D [m]	Radius R or r [m]
	1	25.8	0.42	R = 0.30
	5	25.6	0.72	R = 0.52
	10	26.2	0.90	R = 0.60
	1.17	30.1	0.42	r = 0.210
	1.52	7.5	0.73	r = 0.365
	5.53	27.1	0.73	r = 0.365

Table 4.1: Characteristics of the impact blocks used for the half-scale tests

Ground material

As ground material the same natural sand S0-4 as for the small-scale tests is used. Its characteristics can be found in Chapter 3.1.2.2. As the capacity of the container is about 9m³, the ground material clearly cannot be replaced after each impact test, inducing a dynamic ground compaction with the ongoing tests. This compaction is controlled using a dynamic cone penetration test called PANDA. Further details on this test can be found in Chapter 4.1.3.2.

4.1.2.3 Procedure for the impact tests

On a half-scale, only vertical impact tests on horizontal or inclined ground are performed. The first tests are carried out on horizontal ground. Therefore, wooden sidewalls with a horizontal upper border are positioned in the provided cut-off in the lateral container walls before the placement of the ground material. The container is completely filled so that the thickness of the sand layer is 1 m (after compaction). The ground surface then is compacted by means of a vibrating plate. The compaction of the ground material resulting from the vibration and – later on – by the dynamic compaction during the tests is controlled regularly (Chapter 4.1.3.2).

To prepare a slope, the container is inclined up to the requested slope angle (Figure 4.2, $\beta = 10^\circ$ to 40°). In the inclined position of the container, the ground material is spread out horizontally and compacted by the vibrating plate. The upper border of the wooden sidewalls (which have to be changed to correspond to the requested slope inclination) acts as horizontal calibration line. After the compaction of the slope surface, the container is replaced on the base of the shaft (Figure 4.2, position at impact, $\beta = 0^\circ$).

In general, the compacting of the ground material is performed previous to each test series. As described in Chapter 4.1.5, a tests series is defined as the sequence of three similar impact tests for each falling height ($H = 1, 2, 5, 10\text{m}$, beginning with the smallest and increasing H gradually) with one and the same block on a certain slope. Between the impact tests for one test series, the ground material only replaced and compacted “by hand” (see last section of this Chapter). However, for impacts on horizontal ground and small slopes (up to 10°), the ground has not to be re-compacted after the test series with small blocks $< 500\text{ kg}$.

To avoid a rebound of the whole container due to the impact impulsion during the test, the free end (right hand side end in Figure 4.2) is screwed tightly to the foundation. Bearing solidly to the shaft base, the influence of the container on the block rebound is limited and the impact tests are carried out.

To perform an impact test, the block is manoeuvred into the releasing position by the overhead crane. A cord fixed to the base of the block serves as measure for the falling height and as pointer for the impact position. All blocks are positioned in such way as to have 1 m of ground cushion beneath the impact position (Figure 4.4). For the heaviest block (10 kN), all impacts are performed in the middle of the container while for the smaller blocks two impact tests can be accomplished next to each other. Before releasing the block, the camera is prepared for recording. As for the small-scale tests, the trigger is set to 100% to record the last

four seconds before its operation. The block then is released and the impact is filmed with 250 f/s. The filmed scene is controlled and the impact-relevant part of the film (generally about 120 frames) is saved under the individual series' name and ready for further data processing.

After each impact tests, the block is removed so that the dimensions of the crater left in the sand can be measured. The ground then is prepared for the next impact test by refilling the crater with sand, compacting it in layers by stamping and finally flattening it with a rake. For impacts on horizontal ground or slopes of 10° , this re-preparation of the slope can be made without inclining the container. For larger slope angles, however, the container has to be inclined. Further, as for larger slope angles ($\beta \geq 20^\circ$) the blocks roll down the slope after impact, the traces left in the sand are more important and demand a larger re-preparation of the slope.

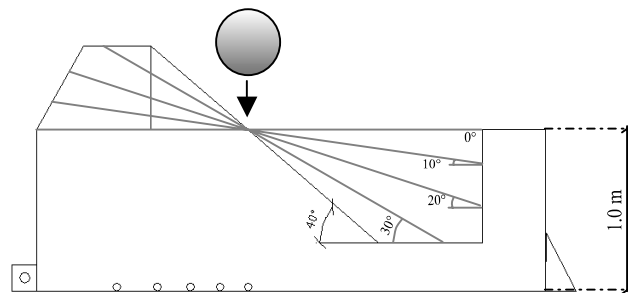


Figure 4.4: Same impact position for all slope inclinations

4.1.3 Measuring devices

4.1.3.1 Capturing of the block motion

Camera

The same digital high-speed video camera as for the small-scale tests is used to film the trajectory of the blocks during impact. The operating speed is set at 250 f/s, allowing an optimal resolution of the frames (480 x 420 pixel). The maximum recording time is four seconds. Due to the restricted space in the test shaft, the camera cannot be installed perpendicularly to the block motion plane, but films the impact using a mirror installed next to the container (see Chapter 4.1.2.1).

Lens

As mentioned above, the restricted working space requires the use of a wide-angle lens. The chosen 6 mm C-mount lens (corresponding approximately to a 20 mm photo lens) causes a radial distortion to the film. Previous to the motion analysis,

the distorted films have to be corrected requiring the determination of the camera and lens specific parameters. The procedure adopted for the camera calibration and the correction of the films is discussed in more detail in Chapter 4.1.4.1.

Targets

As for the small-scale tests, photographic targets are fixed on the blocks and the structure. Due to the difference in size between the small- and the half-scale blocks, the area captured by the camera on a half-scale is about six times bigger than the small-scale display window. Thus the area displayed in one pixel is minor on a small-scale (about 0.8 x 0.8 mm) than on a half-scale (about 5 x 5 mm). This illustrates why the targets used for the half-scale tests differ from those used at small scale.

Applying the calculation of errors presented in Chapter 3.1.3.1 (equation (3-1)) on the films of the half-scale tests, the maximal error Δx for a minimal distance Z of 3.0 m and a maximum block radius r and distance X of 0.45 m each, is about 6.7 cm. A pixel displaying the size of about 5 x 5 mm, this error evidently has to be taken into account. To avoid this problem, the targets are not fixed on the surface of the half-scale blocks but on their sides, so that they are in the same moving plane as the centre of gravity of the block and move parallel to the image plane. Only the mass centre of the cylindrical blocks is marked with an additional target on the block surface (Figure 4.5).

The shape and size of the targets used for the half-scale tests is chosen to be a black square of 1 x 1 cm. By this size, the target is pictured by about four pixels. Preliminary tests revealed this shape as optimal to limit the random error induced by the motion analysis.



Figure 4.5: Targets fixed in the same moving plane as the centre of gravity of the block and – only for cylindrical blocks (right) – at height of the mass centre of the half-scale blocks.

4.1.3.2 Ground compaction

Due to its volume (9m³!), the ground material used for the half-scale tests is not removed and replaced after each impact. Thus, unlike the small-scale tests, the half-scale tests imply a dynamic ground compaction with ongoing series.

To determine the dynamic compaction of the ground material over the ongoing test series, a dynamic cone penetrometer test (PANDA) is used. This penetrometer was developed in France in the early 1990 and since has become widely used especially in France but also in Central Europe. By means of the PANDA test, the ground resistance to a cone is investigated, giving information on the compaction and layering of a ground profile of up to 6 meters depth.

The dynamic cone penetrometer test is carried out by driving a cone with an area of 2, 4 or 10 cm² (in the present case a cone of 2 cm² is used) on the end of a set of rods into the ground using a fixed weight hammer. A microprocessor records two parameters for each blow of the hammer: the impact speed and the cone penetration depth. The impact speed is measured by an accelerometer on the head of the tool while a retractable tape captures the depth of penetration. The microprocessor uses the depth of penetration and the energy for each blow of the hammer to calculate the dynamic cone resistance q_d using the following modified “Dutch Formula” [Cassan, 1998]:

$$q_d = \frac{1}{A} \cdot \frac{\frac{1}{2}mv^2}{1 + \frac{p}{m}} \cdot \frac{1}{x_{90^\circ}}, \quad (4-1)$$

where A is the area of the cone, m and p being the striking (hammer) and the struck (tool) mass respectively, v being the impact speed of the hammer and x_{90° being the penetration due to one blow of the hammer on a 90° cone. The recorded data are transferred to a computer to plot the values of the dynamic cone resistance q_d against depth using the PANDA software.

Studies have proved the reliability of the results obtained by the PANDA test by comparison to other standard *in situ* tests [Juran & al., 1999]. In the framework of

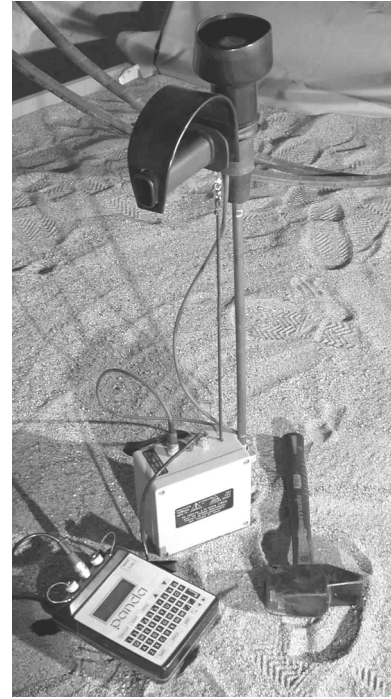


Figure 4.6: The dynamic cone penetrometer tool PANDA.

the present thesis, the test is employed with regard to the possibility to its use in field tests due to its light weight, easy handling and aptitude to be employed also in difficult terrain as rockfall cones or mountain sides. Even if the measured ground resistance q_d cannot be compared directly to a subgrade modulus M_E , it allows nevertheless a rough estimation of the ground compaction.

To assess the dynamic compaction of the ground material during the half-scale test series, the PANDA test is performed at several stages of the testing programme (refer Table 4.4 and Table 4.5) in the middle of the container and repeated about 20 cm aside.

A comparison of the dynamic cone resistance q_d with deformability properties of the slope material (e.g. subgrade modulus M_E) was not possible in the framework of this thesis. Indeed, such a comparison would have meant to perform a plate-bearing test after each impact or impact series of three tests additionally to the PANDA tests. As the preparation for a plate-bearing test in the test shaft takes in general at least one day, less impact tests would have been performed in total.

However, at the end of the impact test series, three plate-bearing tests were performed: one directly on the impact point in the middle of the container (N° 1), one in the roll-out-zone (N° 2) and one in a zone, where no impact tests were performed (N° 3). As the counter bearing for the test (a steel beam) is mounted transversally, the emplacement of the tests is not exactly in the moving axis of the blocks (Figure 4.7). The results of the plate bearing tests are given in Table 4.2. $M_{E,1}$ represents the initial loading modulus, whereas $M_{E,2}$ gives the modulus for the reapplication of the load.

	$M_{E,1}$ [MN/m ²]	$M_{E,2}$ [MN/m ²]
N° 1	0.3	1.8
N° 2	0.5	1.2
N° 3	6.0	20.4

Table 4.2: Results of the plate-bearing tests performed at the end of the impact test series.

Comparing these results with the results gathered from the PANDA tests performed afterwards at the same locations, one realises that the low value of M_E for test N° 1 (impact point) is due to the low compaction of the upper soil layer (up to 40 cm depth). This observation corresponds very well to the PANDA test results gathered during the test series. For both locations where no impact tests have been performed previously, the profile of the ground resistance q_d does not show such change. Consequently, the measured plate-bearing modulus M_E is higher for these locations. As it can be seen in Figure 4.7, for test N° 2 the upper

layers of the ground are softer than for test N° 3 due to the shift of sand in front of the block during impact. As no relocated sand can be found on the locations of test N° 3 (above the impact tests), both, plate bearing modulus as well as PANDA, show higher values. Comparing the test results for the spots N° 2 and N° 3 show that the plate bearing modulus is most influenced by the upper layer of the ground: for the first 30 cm of depth (measured from ground surface) the values evaluated by means of the PANDA tests are smaller at N° 2 than N° 3, consequently $M_{E,N^{\circ}2}$ is smaller than $M_{E,N^{\circ}3}$. However, for depth > 30 cm, the dynamic ground resistance evaluated for both tests is nearly the same.

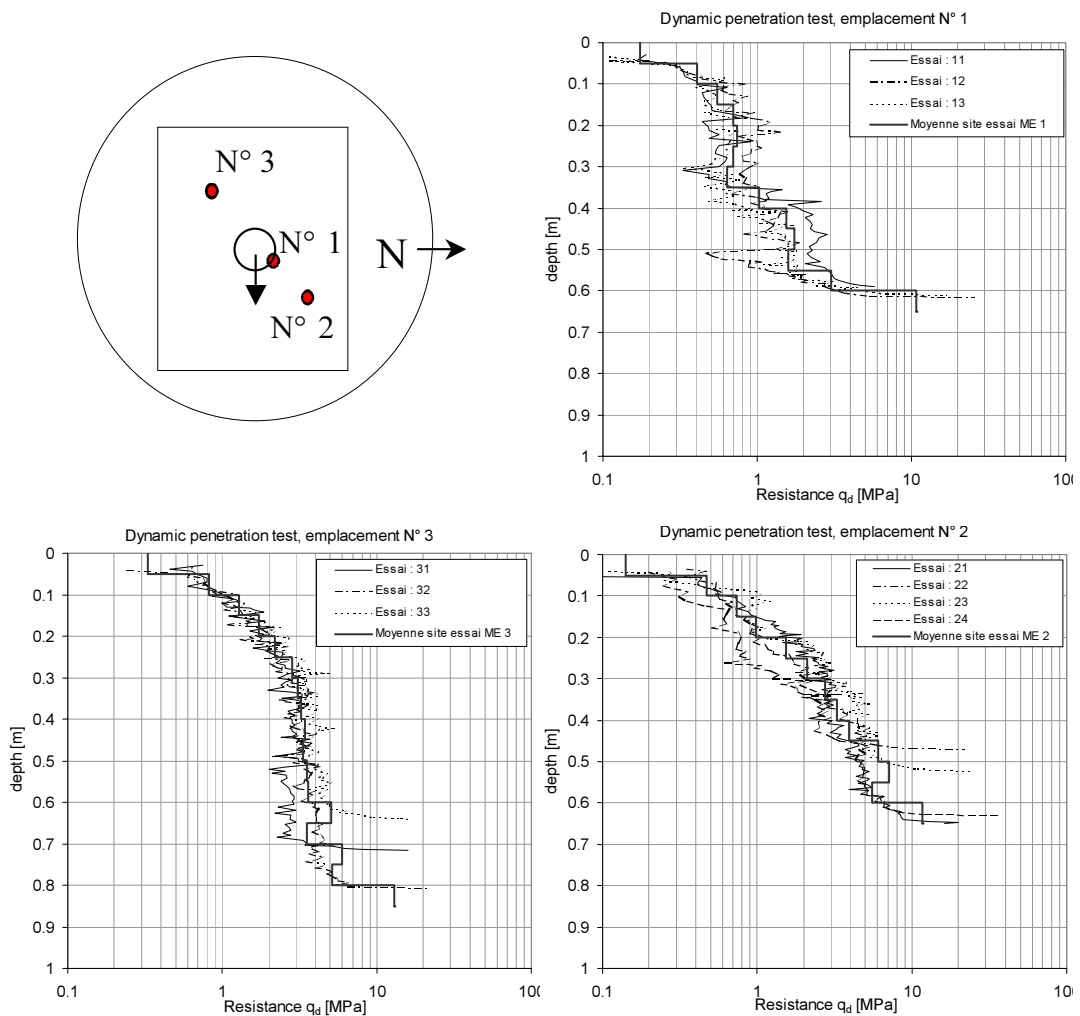


Figure 4.7: Location of the plate-bearing tests N° 1-3 and the results of the corresponding PANDA-tests. For each emplacement, 3 to 4 PANDA tests are performed, the mean values are represented by the thick line.

4.1.3.3 Measurement of traces

As for the small-scale tests, the diameters of the crater and of the crater rim are measured lengthwise and in transverse direction. In case of rolling or sliding of the block, the width and every eventual deflection of the rolling trace are recorded. The maximum depth is measured at the middle of the crater in vertical direction beginning at surface level.

4.1.4 Data acquisition and data processing

4.1.4.1 Correction of distorted films

Due to the wide-angle lens used to film the half-scale tests, the resulting films suffer a radial distortion. Prior to any motion analysis, these films have to be corrected to avoid miscalculations of the position, velocity and acceleration of the block. Such correction requires the determination of the exact camera calibration parameters being (a) the external or extrinsic parameters which depend upon the 3-D position and orientation of the camera frame relative to a certain world coordinate system, and (b) the internal or intrinsic parameters which are the camera geometrical and optical parameters (as focal length, other lens parameters, radial and tangential distortion parameters, etc.).

Two different camera calibration tools, the machine vision software HALCON of MVTec [Halcon 6.0, 2000], and a Matlab Toolbox specially conceived for this kind of application [Camera Calibration Toolbox for Matlab 6.5] were tested. The choice has finally fallen on the latter mainly due to the fantastic user support and the easy application of the calibration results for both single frame and film sequence corrections. Even if the camera parameters resulting from the two calibration techniques cannot be compared directly due to their slightly different definition, the “converted” parameters agree fairly well. In the following, the procedure of camera calibration and film correction by means of the Matlab Toolbox is presented.

The calibration procedure is basically inspired by the technique proposed by Zhang [1999] using images of a planar pattern shown at a few different orientations. For the toolbox, also non-planar calibration rigs could be used. The computation method of the intrinsic parameters differs slightly from Zhang and is based on that used by Heikkilä & Silvén [1997]. This calibration procedure is an extension to the classic two-step approach where the initial camera parameter values are computed linearly by a closed form solution (to accelerate and simplify the computational burden of a nonlinear minimization) and the final values are obtained by minimizing a nonlinear error function. An image correction is

performed additionally to the two previous steps, using an implicit model that interpolates the correct image points based on the physical camera parameters derived in previous steps [Heikkilä & Silvén, 1997]. For more details on the mathematical algorithm used for the camera calibration, refer to the cited articles and the Matlab Toolbox.

The intrinsic camera parameters resulting from the calibration are defined by the following parameters:

- fc_1, fc_2 : focal length (being a unique value in mm), expressed in units of horizontal (fc_1) and vertical (fc_2) pixels and stored in the 2x1 vector fc . For square pixels, the aspect ratio fc_2/fc_1 equals 1.
- cc_1, cc_2 : coordinates of the principal point (where the distortion in all directions is zero) in horizontal (cc_1) and vertical (cc_2) direction, stored in the 2x1 vector cc ,
- α_c : skew coefficient, defining the angle between the x and y sensor axes (α_c equals 0 for rectangular pixels),
- kc : vector storing the radial and tangential distortions.

The distortion model first introduced by Brown [1966] expresses the normalized pinhole projection of a point P (x, y) on the image plane, combined with the correction for the radial and tangential distortion components which are not taken into account by a simple pinhole model, by the vector x_d :

$$x_d = \begin{bmatrix} x_{d1} \\ x_{d2} \end{bmatrix} = \left(1 + kc_1 \cdot r^2 + kc_2 \cdot r^4 + kc_5 \cdot r^6\right) \cdot \begin{bmatrix} x \\ y \end{bmatrix} + dx \quad (4-2)$$

where kc_1, kc_2 and kc_5 are coefficients for the radial distortion, $r^2 = x^2 + y^2$ (pinhole projection) and dx is the tangential distortion vector with the tangential distortion coefficients kc_3 and kc_4 :

$$dx = \begin{bmatrix} 2 \cdot kc_3 \cdot x \cdot y + kc_4 \cdot (r^2 + 2x^2) \\ kc_3 \cdot (r^2 + 2y^2) + 2 \cdot kc_4 \cdot x \cdot y \end{bmatrix}. \quad (4-3)$$

The tangential distortion is due to imperfect centering of the lens components or other manufacturing defects as the camera assembly.

The proper camera model for accurate calibration can therefore be written in the following form:

$$\begin{bmatrix} x_p \\ y_p \\ 1 \end{bmatrix} = \mathbf{KK} \cdot \begin{bmatrix} x_{d1} \\ x_{d2} \\ 1 \end{bmatrix} \quad (4-4)$$

with x_p , y_p as horizontal and vertical coordinates of the point P in the distorted image and the camera matrix \mathbf{KK} as follows:

$$\mathbf{KK} = \begin{bmatrix} fc_1 & \text{alpha_c} \cdot fc_1 & cc_1 \\ 0 & fc_2 & cc_2 \\ 0 & 0 & 1 \end{bmatrix}. \quad (4-5)$$

In this model the set of intrinsic parameters (fc_1 , fc_2 , alpha_c , cc_1 and cc_2) is augmented with the distortion coefficients kc_1 to kc_5 . The explicit camera calibration procedure performed by the Toolbox determines the optimal values for these parameters based on image observations of a known 3-D target, in this case the planar chessboard pattern shown at several different orientations (Figure 4.8).

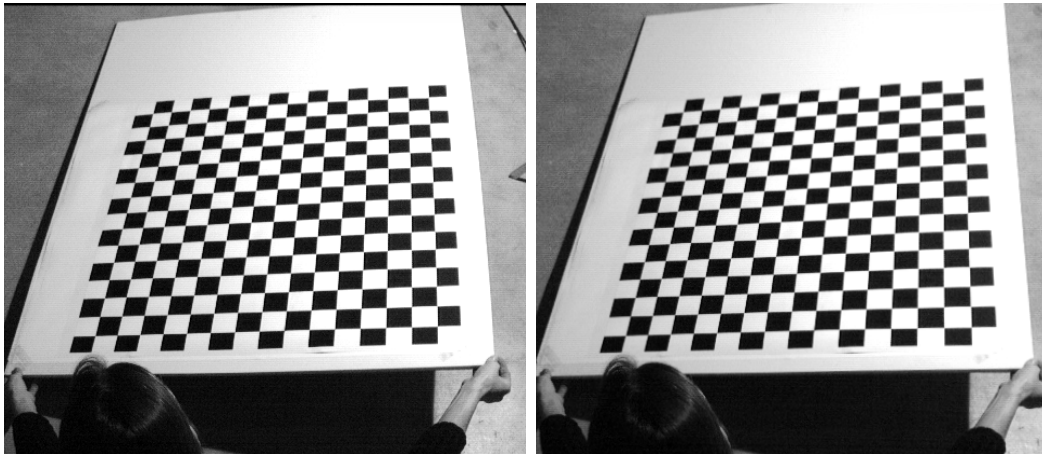


Figure 4.8: Planar chessboard pattern used for the camera calibration: original (distorted) image (left) and undistorted result (right).

In the present case, the calibration of the camera parameters is based on a total of about 30 calibration images. The intrinsic camera parameters resulting of the iterative calibration process are given in Table 4.3. The distortion effect can be visualized to show the importance of the radial versus the tangential component of distortion (Figure 4.9). Each arrow in the complete distortion model represents the effective displacement of a pixel induced by the lens distortion. The centre of distortion is given by the circle while the x marks the physical centre of the CCD sensor. The points in the corners of the image are displaced by as much as 16 pixels showing clearly the importance of the correction. Even if the complete and the radial distortion model look quite similar on the first sight, a closer look points

out the importance of the tangential component, in the present case induced by the imperfect centering of the CCD sensor (maximum displacement greater than 2 pixels).

	x, y	error $\pm [\Delta x, \Delta y]$
Pixel error	[0.1459, 0.1753]	
Focal length f_c	(814.644, 838.211)	[2.402, 2.363]
Principal point c_c	(237.898, 248.625)	[2.665, 3.001]
Skew α_c	0	0
Radial coefficients $kc_{1,2,5}$	(-0.2963, -0.2602, 0)	[0.009472, 0.06866, 0]
Tangential coefficients $kc_{3,4}$	(-0.007303, 0.0007856)	[0.0004772, 0.0004292]

Table 4.3: Calibration results used for the correction of the distorted films. x and y correspond to the horizontal and vertical coordinates of a point in the image, the centre of the upper left pixel of the image being the origin [0;0].

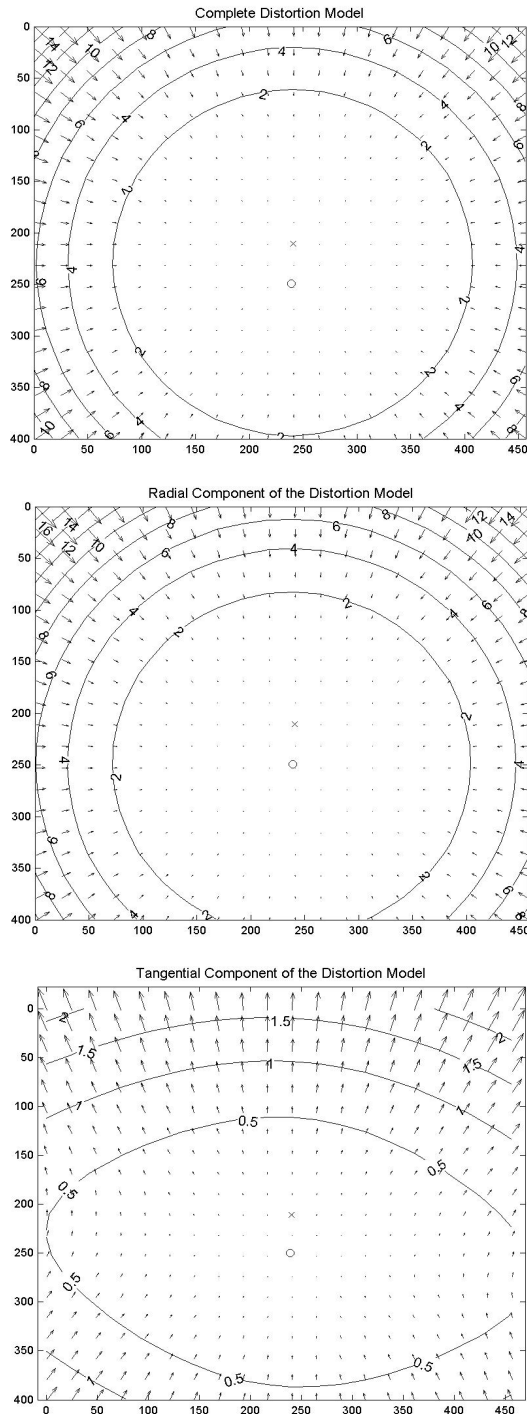


Figure 4.9: Visualization of the complete (top), radial (centre) and tangential (below) distortion model.

4.1.4.2 Data acquisition and processing

The same procedure as for the small-scale tests is applied. The error arising by the reduction of the reality to 2-D is avoided on a half-scale by fixing the targets in

Subsequently to the calibration of the camera parameters, the correct, undistorted position of the block can be achieved by two ways: Either the distorted film is analysed and the resulting (distorted) coordinates of the block are corrected, or the complete film is corrected prior to its analysis so to deliver directly the undistorted coordinates. As several preliminary tests have shown, both methods yield the same result. Clearly the computing time for the first solution is shorter than for the second as only a couple of coordinates are corrected. However, by the distortion of the film, the tracking of the centre of the spherical blocks by means of the block circumference becomes less exact. Therefore, the second method is applied.

The correction of a whole film is made frame by frame. Prior to the correction process, the film is decomposed in single numerated frames, which are fed through the iteration of the “undistort”-function of the Toolbox. After the correction, the film is recomposed by means of the Adobe software “Premiere 6.0” and ready for a motion analysis by WINalyze.

the block motion plane. The accuracy of object tracking and the data-smoothing problem described in Chapter 3.1.4.1 also apply for the half-scale tests.

The data processing is performed as described in Chapter 3.1.4.2 for the small-scale tests.

4.1.5 Half-scale test programme

Similarly to the small-scale tests, the half-scale tests are organised in series. Within one series only one parameter, the falling height, is varied from 1 to 10 m while all other parameters (block, slope inclination, etc...) remain constant. A series therefore consists of three to four impact tests, performed thrice each, with the same block released from increasing height (1 m, at times 2 m, 5 m and 10 m). The same series then is repeated with another block weight or form, increasing from series to series, starting with the lightest block of 1 kN to the heaviest of 10 kN.

The same pattern of tests is performed on horizontal ground (slope inclination $\beta = 0^\circ$) and on three slopes ($\beta = 10^\circ, 20^\circ, 30^\circ$). Table 4.4 and Table 4.5 summarize the performed impact tests for the cylindrical and spherical blocks respectively.

The asterisks before or after a test name in the tables below indicate the realization of a dynamic cone penetrometer control (PANDA) respectively before or after the series of impact. The dynamic ground compaction becoming less important with ongoing impact tests, the frequency of the compaction measurement is reduced more and more.

A complete list respecting the cycle of the tests and quoting all slope replacements as well as the name of the PANDA tests can be found in Appendix II.

Ground inclination β [°]	Falling height H [m]	1 kN		5 kN		10 kN	
0°	1m	C1	* e1L1-3	D1	* e1L1-3	M1	* e1L1-3
	2m		* e2L1-3		* e2L1-3		* e2L1-3
	5m		* e3L1-3		* e3L1-3		* e3L1-3
	10m		* e4L1-3		* e4L1-3		* e4L1-3 *
10°	1m	C2	* e1L1-3	D2	* e1L1-3	M2	e1L1-3
	2m		e2L1-3		e2L1-3		e2L1-3
	5m		e3L1-3		e3L1-3		e3L1-3
	10m		e4L1-3		e4L1-3		e4L1-3
20°	1m	C3	e1L1	D3		M3	e1L1-3
	2m						e2L1-3
	5m				e3L1		e3L1-3
	10m						e4L1-3
30°	1m				M4	e1L1-3	
	5m					e3L1-3	
	10m					e4L1-3	

Table 4.4: Test series performed with the cylindrical blocks. Series = C, D or M, test = e, release of block = L.

Ground inclination β [°]	Falling height H [m]	1.17 kN		1.52 kN		5.53 kN	
10°	1m	o2	e1L1-3	H2	e1L1-3	O2	e1L1-3
	5m		e3L1-3		e3L1-3		e3L1-3
	10m		e4L1-3		e4L1-3		e4L1-3
20°	1m	o3	e1L1-3	H3	* e1L1-3	O3	e1L1-3
	5m		e3L1-3		e3L1-3		e3L1-3
	10m		e4L1-3		e4L1-3		e4L1-3 *
30°	1m	o4	* e1L1-3	H4	e1L1-3	O4	e1L1-3
	5m		e3L1-3		e3L1-3		e3L1-3
	10m		e4L1-3		e4L1-3		e4L1-3

Table 4.5: Test series performed with the spherical blocks. Series = o, H or O, test = e, release of block = L.

4.2 Qualitative interpretation of the half-scale tests

In the first instance, the results of the half-scale tests are interpreted qualitatively and the evaluated trends are compared to the ones observed on a small-scale. In a further step, the observed trends are quantified (Chapter 4.3).

4.2.1 Observations during half-scale tests

As for the small-scale tests, a first sifting of the films allows to investigate the visible differences and common points between the different tests. In general, the spherical blocks show an impact behaviour similar to the one observed on a small-scale for vertical impacts on horizontal and inclined compacted ground material. During impact, the ground around the block is disturbed and a sand pile is formed in front of the impacting block (Figure 4.10). The initial pure translation of the block is transformed during impact into a combined rotational and translational movement. Depending on block size, slope inclination and falling height, the spherical block overcomes the frontal sand pile and rolls further on or rolls back into the formed crater. On the slope inclined at 10° , only the hollow block rolls further on for the maximum drop height of 10 m. All other blocks either stay put or roll back into the crater. At $\beta = 20^\circ$, however, rolling as far as the end of the slope is observed nearly for all impact tests with spherical blocks. On slopes inclined at 30° , without exception all spherical blocks roll further on.

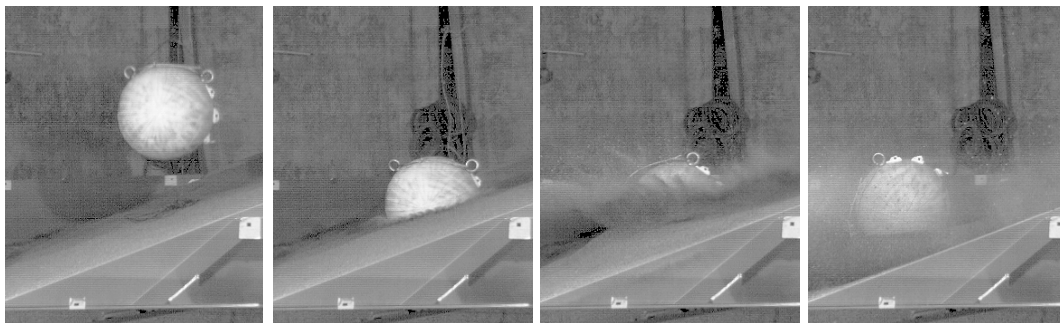


Figure 4.10: Spherical block (100 kg) impacting a slope inclined at 20° after a free fall of 10 m. The development of a frontal sand pile is visible in the third picture.

Due to their spherical base, the cylindrical blocks show the same behaviour as the spheres during the first phase of impact. For impacts on slopes, the incident pure translation is changed quite suddenly to a rolling movement as soon as the block touches the ground (Figure 4.11). The block then rolls on its spherical base till the edge of the cylindrical block shaft enters in contact with the ground. Being not able to roll on continuously, the blocks then have tendency to slide a short way down in this position before toppling over (for slopes inclined at $\beta = 20^\circ$ and steeper) and sliding on the cylindrical part of the block.

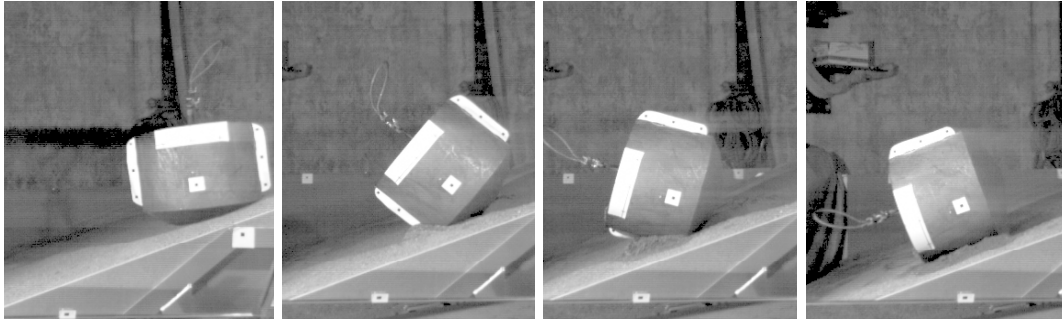


Figure 4.11: Cylindrical block (100 kg) impacting the slope inclined at 20° after a free fall of 1 m. The transition of rolling to sliding is illustrated in the last three pictures.

As for the small-scale tests, higher impact energies (by increase of block mass and / or falling height) provoke a deeper penetration of the block into the ground causing the throw-out of more sand material during impact. The comparison of the crater depth for the spheres “100 kg” (117 kg) and “150 kg” (152 kg) having nearly the same mass but different diameters (0.42 m versus 0.73 m) emphasises the influence of the block area in contact with the ground during impact: whereas the smaller block penetrates very deep into the ground, the larger block induces a much shallower crater for same falling heights.

As the crater depth, and similarly to the small-scale tests, the diameter of the crater increases with increasing impact energies (block mass and / or falling height), also the height of the crater rim increases with the impact energy.

No real rebound (no contact between block and ground) is observed for the half-scale tests. However, the rolling trace left in the sand by the hollow sphere (150 kg) for impacts from 5 and 10 m on slopes inclined at 30° becomes thinner indicating a slight tendency to bounce off the ground.

4.2.2 Closer investigation of several important characteristics

In the following, the influence of the impact conditions on some impact and rebound relevant characteristics is investigated qualitatively.

4.2.2.1 Maximum penetration depth d_{\max}

As for the small-scale tests, the penetration depth d_{\max} is evaluated by both *in situ* measurement and calculation based on the films. The values acquired by both methods agree very well, assuring the correct calculation and measurement. In addition to the parameters found to influence the penetration depth on a small-scale, that is to say the block weight (for constant diameter), the ground material

and its compaction, the maximum penetration depth is found to depend on the following parameters and their products:

- block weight W (for *constant unit weight* γ of the blocks, that is to say the radius increases with the block weight as $W = \gamma V = \gamma \cdot 4/3\pi r^3$. This applies also for the shaft radius of the cylindrical blocks, see Figure 4.12),
- block radius r (spheres) respectively R (cylinders) (for blocks with *similar block weight* but different radius. The radius r resp. R is the radius of the block at contact point, called “contact radius” in the following.),
- falling height H ,
- impact energy E ($E_{\text{pot}} = mgH$), being the combination of the block weight ($W = mg$) and the falling height H .

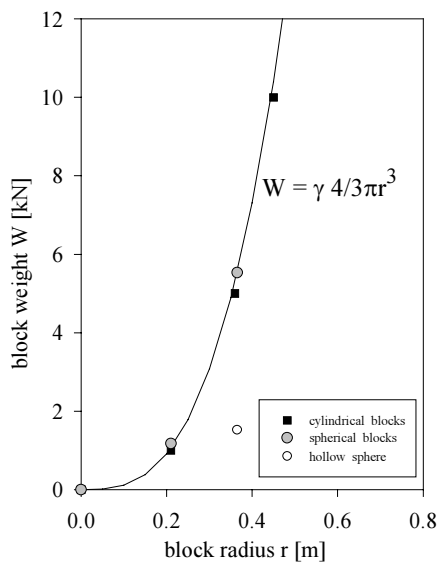


Figure 4.12: Relationship between weight W and radius r (shaft radius for cylindrical blocks) for all concrete filled blocks.

To compare the penetration depth of the different blocks irrespective of their size, the penetration rate, being the ratio between maximum penetration depth and block diameter (shaft diameter for the cylindrical blocks), is evaluated. The penetration rate is given in percent and plotted against the drop height for each block. It is found that the penetration rate increases with increasing falling height H (Figure 4.13).

Further, as illustrated in Figure 4.13, for blocks with similar unit weight the penetration rate is quite comparable. For a change in unit weight the penetration rate increases or decreases with increasing or decreasing unit weight, respectively. These trends are observed for all slope inclinations.

Thus, as observed for the small-scale tests, for the same block diameter but different unit weight (150 kg \leftrightarrow 550 kg spheres), the heavier block penetrates deeper into the ground. For rather similar block weights but different diameters (117 kg \leftrightarrow 152 kg spheres, $r_{117\text{kg}} = 0.21$ m \leftrightarrow $r_{152\text{kg}} = 0.365$ m), combination not investigated on a small-scale, the small block shows a much higher penetration rate than the large block.

Comparing the penetration rate of the cylindrical blocks, the same trend as for the spheres with similar unit weight is observed for all slope inclinations.

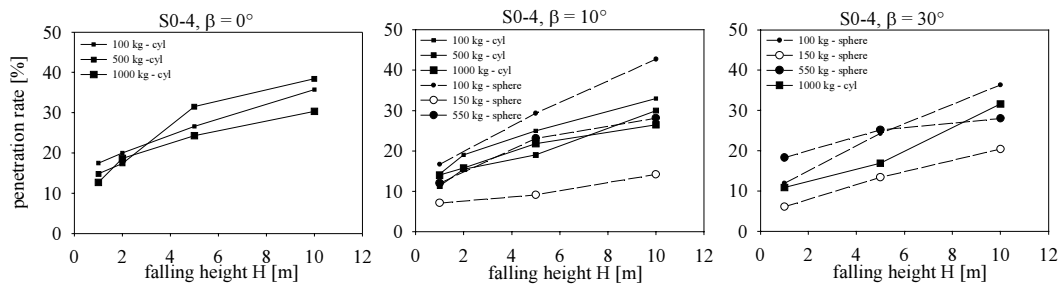


Figure 4.13: Penetration rate (being the ratio between maximum penetration depth and block/shaft diameter), being comparable for blocks with similar unit weight and increasing with increasing falling heights.

Similarly to the penetration rate, the absolute value of the maximum penetration depth d_{\max} increases with increasing falling height. This trend is observed for each block. These trends are confirmed by those stated by Montani-Stoffel [1998] for vertical impacts on horizontal ground. For small slope angles and blocks with similar unit weight, d_{\max} increases with the block weight and thus with the block radius, whereas for large slope angles ($> 20^\circ$) and small falling heights (≤ 5 m) a penetration maximum is reached for the 550 kg sphere. As observed on a small-scale, increasing slope angles thus provoke no straight proportional trend to d_{\max} . As we will see later on, this phenomenon is directly related to the rolling movement of the block.

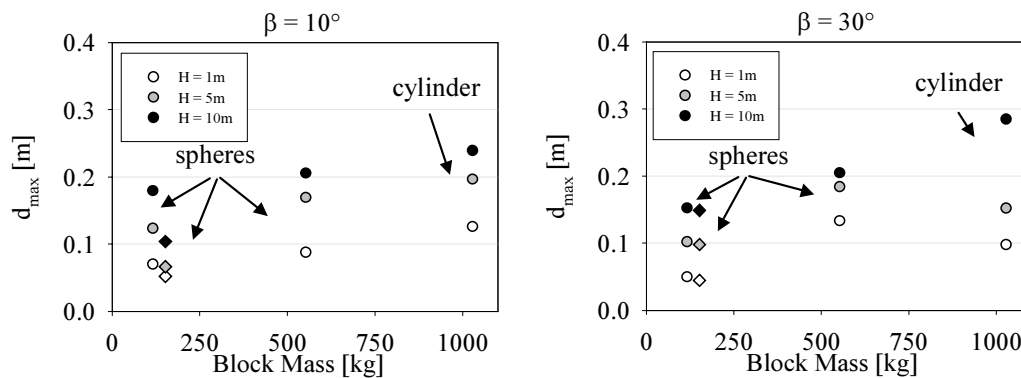


Figure 4.14: Influence of the block mass on d_{\max} . Left: nearly linear trend for small slope angles (10°); right: no linear trend for large slope angles (30°) and small falling heights. The spherical symbols represent blocks with similar unit weight, the diamond-shaped symbols stand for the 150 kg block with lower unit weight.

Accordant to the statement of Montani-Stoffel [1998] for vertical impact tests on horizontal ground material, for the same impact energy the penetration depth d_{\max} is highest for the smallest block (e.g. 100 kg sphere dropped from 10 m versus 1000 kg cylinder dropped from 1 m, see Figure 4.14).

4.2.2.2 Block acceleration during impact

During free flight, the block is subjected to a constant negative (downwards) acceleration by gravity. As soon as it gets in contact with the ground surface and during the entire impact process, the block then is decelerated in positive (upwards) direction. As observed for the small-scale tests, the waveform of the impact induced block acceleration corresponds to a peak (Figure 4.15, left). This corresponds to the observations made by Yoshida & al. [1988] and Montani-Stoffel [1998] for vertical half-scale impact tests on horizontal soft sand with sphere- or cone-base weights. For both small- and half-scale tests, the peak generally is followed by a kind of plateau (Figure 4.15, right). The occurrence, the length and height of the plateau depend on several factors, which will be discussed later on (Chapter 4.3.1).

To analyse and interpret the impact tests, both the normal (a_n , normal to the slope surface) as well as the vertical (a_y , parallel to gravity) block acceleration components are investigated. As both values are related by the slope angle β ($a_n = a_y \cdot \cos \beta$), the trends observed and described in the following are valid for both components. For the largest slope angle $\beta = 30^\circ$ the maximal difference in value between a_n and a_y is about 13%, whereas the waveform remains similar.

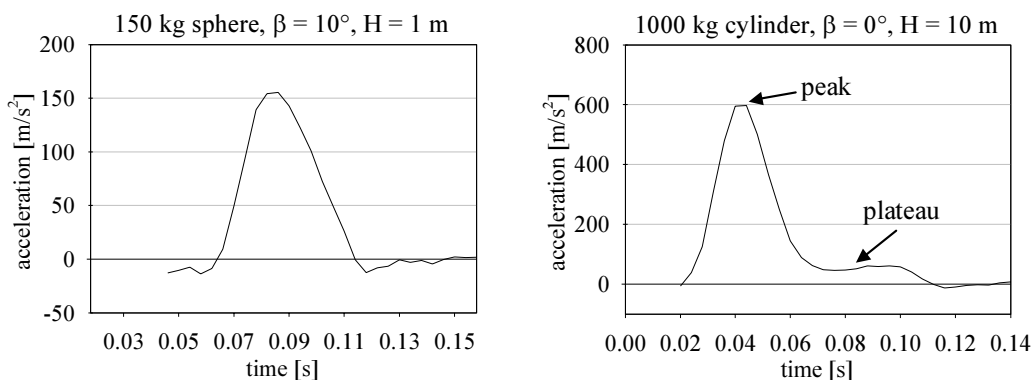


Figure 4.15: Typical wave form for the block acceleration normal to the ground surface without (left) and with plateau (right).

Maximum acceleration (peak value):

For both small- and half-scale tests the maximum deceleration of the block during impact $a_{n,max}$ is found to be relatively independent of the slope inclination β , as to see in Figure 4.16 exemplarily for impact tests with the 1000 kg block (left, black plot).

The comparison of the maximum acceleration for blocks with different weight but same diameter (150 kg versus 550 kg sphere) dropped from the same height

reveals that $a_{n,max}$ increases with decreasing unit weight (clearly to observe comparing the acceleration values for same falling heights given in Figure 4.17). This means that for same block radius and same impact velocity a lighter block is decelerated more abruptly than a heavy one. A same but less distinct trend is observed for the small-scale tests. For blocks with rather similar weight but different diameters (117 kg versus 150 kg sphere), higher peak values are achieved for the block with larger diameter (Figure 4.17). Both results show that blocks with lower unit weight undergo a stronger deceleration than blocks with higher unit weight. This result is coherent with the duration of the acceleration peak (discussed in the following), showing shorter peak duration for the 150 kg sphere than for all other blocks, which have similar unit weights.

Whereas Yoshida & al. [1988] state that the maximum acceleration decreases with increasing block weight (for similar unit weight of the blocks), by the present tests this trend is not confirmed as for similar unit weight of the blocks the maximum acceleration $a_{n,max}$ is not influenced by changing block weights.

Further, the maximum acceleration normal to the slope surface is found to increase strongly with increasing falling height H (Figure 4.16 right, black plot). Furthermore, the maximum acceleration is noted to be strongly related to the maximum penetration depth d_{max} (Figure 4.17). As both characteristics, falling height H and maximum penetration depth d_{max} , are found to depend on each other, this observation is consequently logic.

Acceleration plateau:

For nearly all impact tests performed on a half-scale the acceleration wave shows a plateau after the initial acceleration peak (Figure 4.15, right). Some exceptions where no acceleration plateau is observed are found for impact tests with low impact energies (block weight up to 500 kg, falling heights up to 5 m). Inspired by this observation, the question for which limit energy value an acceleration plateau occurs is revealed and will be discussed later on (Chapter 4.3.1.2).

In case an acceleration plateau occurs, its mean value $a_{n,plateau}$ is found to decrease with increasing slope inclinations (Figure 4.16, left, white plot and Figure 4.18, left). As discussed later on, the value of the plateau probably corresponds to the force needed to create global shear failure in the ground material (Chapter 4.3.1.2). Hence the observed tendency is plausible bearing in mind that for steeper slope inclinations the bearing capacity of the ground material is lower than for small slope angles.

Further, the value of the acceleration plateau $a_{plateau}$ increases slightly with increasing falling height H up to a limit value, remaining constant for further

impact velocity increase (Figure 4.16 for $a_{n,plateau}$, right; white plot and Figure 4.18 for $a_{y,plateau}$, right). A similar trend is observed for the relation between the value of the acceleration plateau and the maximum penetration depth d_{max} . As d_{max} depends on the falling height H (as stated above), the observed clear relation between $a_{plateau}$ and d_{max} , denoting a limit value of $a_{plateau}$ for large penetration depths, is logic.

As is can be seen from Figure 4.18, the value of $a_{plateau}$ further depends on the block itself and thus from its mass, radius and volume weight.

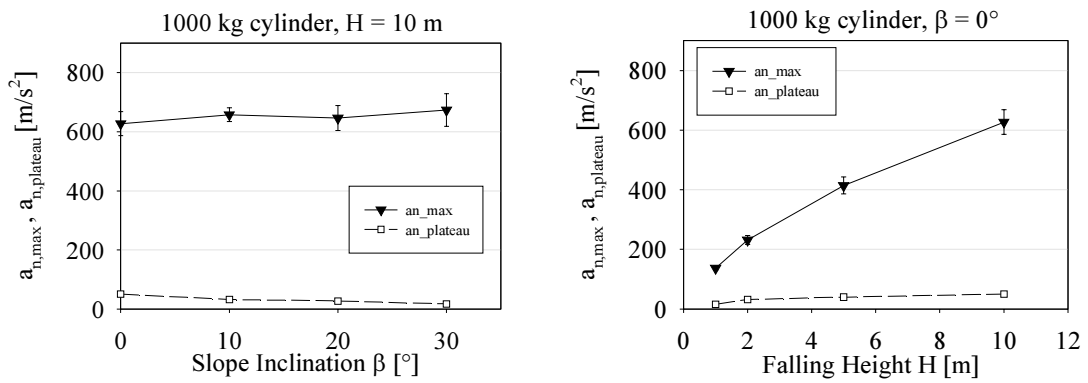


Figure 4.16: Influence of slope inclination and falling height on the maximum acceleration $a_{n,max}$ and the acceleration plateau $a_{n,plateau}$

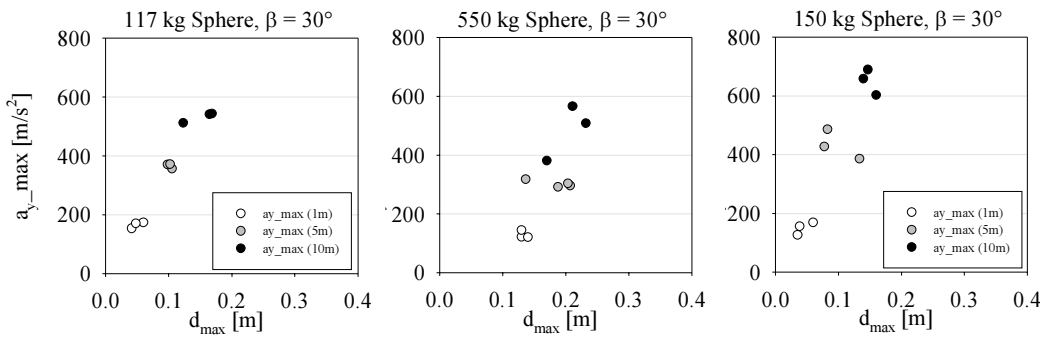


Figure 4.17: Evidence of a relation between the maximum acceleration (here: vertical acceleration component $a_{y,max}$) and the maximum penetration depth d_{max} .

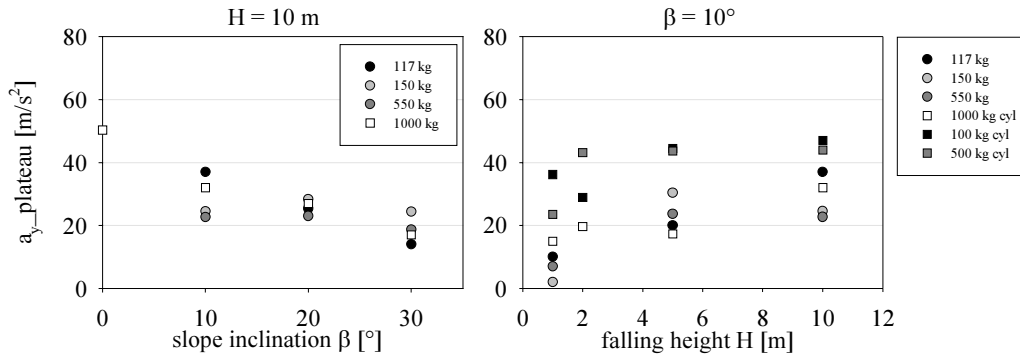


Figure 4.18: Dependency of the mean vertical acceleration plateau value $a_{y_plateau}$ on the slope inclination (left) and the falling height (right).

4.2.2.3 Impact time

The total impact time is the sum of the duration of both the acceleration peak and the acceleration plateau (Figure 4.19). The separate investigation of these components reveals the following trends:

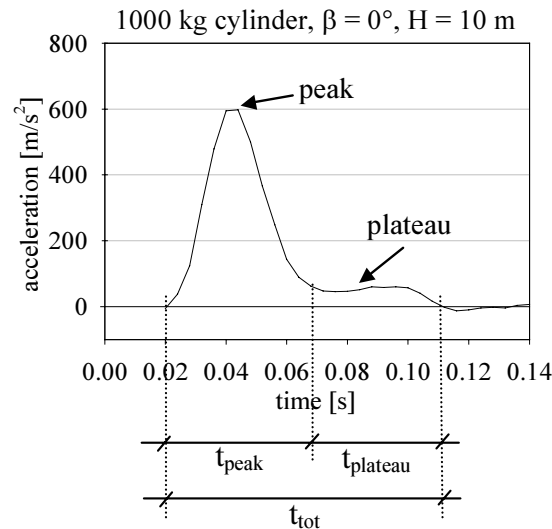


Figure 4.19: Duration of the acceleration peak t_{peak} , the acceleration plateau $t_{plateau}$ and the total impact time t_{tot} .

t_{peak} : The duration for the peak of acceleration $t_{an,peak}$ is found to be independent of both slope angle (as observed on a small-scale) and falling height (Figure 4.20). Further it seems to be quite constant for different block weight and size (only a very slight increase with increasing block size; contrary to the observations reported by Montani-Stoffel [1998], stating a slight but clear increase of the impact time with increasing block size), provided that the blocks have a similar

unit weight. For decreasing unit weight, the duration of the acceleration peak decreases slightly.

t_{plateau} : The time span during which the acceleration takes a constant value $t_{\text{an,plateau}}$ shows no clear dependency on the slope angle β but increases with increasing falling height H . Further, the duration of the plateau increases strongly with increasing block size.

t_{tot} : Being the sum of t_{peak} and t_{plateau} , the total impact time shows no clear dependency on the slope angle, but increases with increasing falling height. For blocks with similar unit weight but increasing size and weight, the total impact time is found to increase. Whereas the latter statement corresponds to the results presented by Montani-Stoffel [1998], no increase of the total impact duration with increasing falling heights is observed. However, as Montani-Stoffel considers only the acceleration peak for the evaluation of the impact duration, this observation confirms the independence of t_{peak} on the falling height (as stated above).

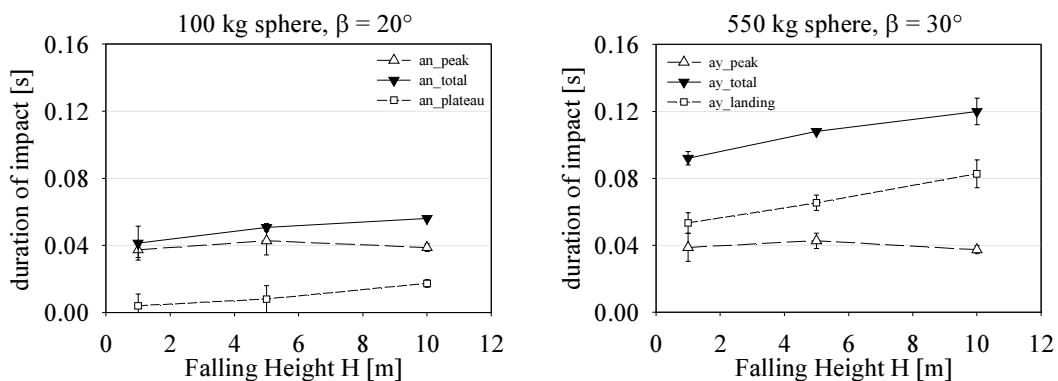


Figure 4.20: Both average and standard deviation for the impact duration of the acceleration peak, the plateau and the total impact process for the 100 kg (left) and the 550 kg sphere (right) dropped from different heights on a slope inclined at 20° and 30° , respectively.

4.2.2.4 Impulse or linear momentum p

During impact, the block induces an impulse p to the ground. As the impulse is the product of mass and velocity, its value is time-dependent. The total impulse induced by the block to the ground during impact thus is the sum of the block velocity times the block mass over all time increments Δt between beginning and end of impact. This corresponds to the integration of the block acceleration during impact times the block mass (Figure 4.21). As the acceleration during impact

shows a plateau for most of the impact tests performed on a half-scale, two values are evaluated for the impulse: the value of the total impulse between the beginning of the impact and either the end of the acceleration peak (p_{peak}) or the end of the impact (p_{tot}).

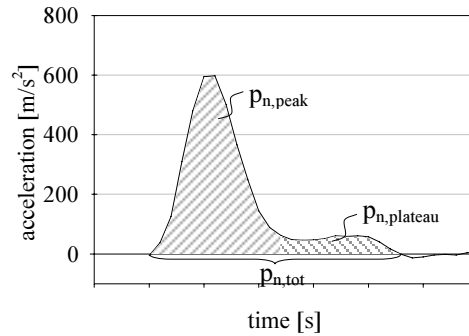


Figure 4.21: Meaning of the impulsion values p_{peak} , p_{plateau} and p_{tot} evaluated for each impact test.

An investigation of the values gathered for the normal component of the impulse $p_{\text{n,peak}}$ and $p_{\text{n,plateau}}$ relative to the slope surface reveal the following dependencies.

$p_{\text{n,peak}}$: The impulse acting during the acceleration peak shows a very slight decreasing trend for increasing slope inclinations β (Figure 4.22, left). As this trend is minimal and not observed for all tests, it is consequently supposed that $p_{\text{n,peak}}$ is independent of the slope angle. However, $p_{\text{n,peak}}$ increases with increasing falling height H (what is evident as the impact velocity increases with the square root of the falling height: $v = (2gH)^{1/2}$) and quite linearly with increasing block mass (what is also evident as $p = mv$) (Figure 4.22, right).

$p_{\text{n,plateau}}$: As observed for $p_{\text{n,peak}}$, the impulse acting during the acceleration plateau is quite independent of the slope angle. Having values close to zero for small falling heights and block masses, as no or only little acceleration plateau occurs, it increases with increasing falling height and increasing block weight.

$p_{\text{n,tot}}$: $p_{\text{n,tot}}$ being the sum of $p_{\text{n,peak}}$ and $p_{\text{n,plateau}}$, its value consequently is also quite independent of the slope angle and increases with H and m (Figure 4.22).

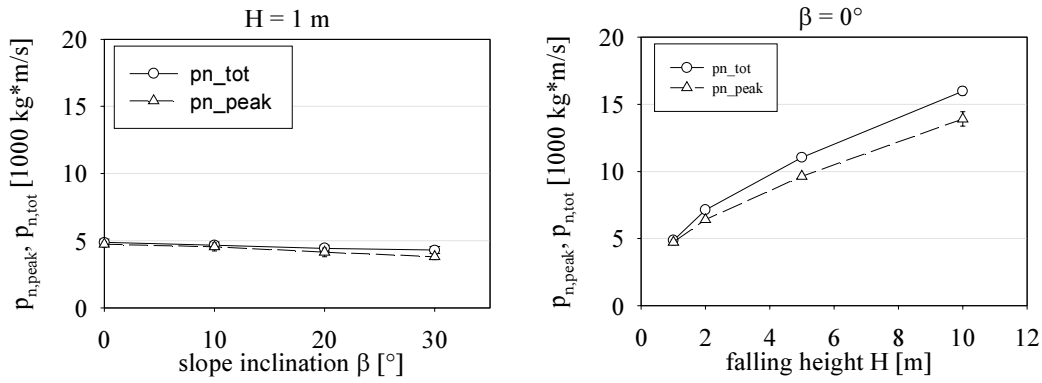


Figure 4.22: Influence of the slope inclination β (left) and the falling height H (right) on the normal component of the impulse $p_{n,peak}$ and $p_{n,tot}$ for the 1000 kg cylindrical block. The value of $p_{n,plateau}$ corresponds to the difference between $p_{n,peak}$ and $p_{n,tot}$.

4.2.3 Sensibility of the coefficients of restitution to the tested parameters

In the following, the influence of each tested parameter on the coefficients of restitution is investigated, changing successively one parameter at once. The observed tendencies are reported below. The trends are compared to the observations made on a small-scale, taking into account especially the impact tests on the natural ground material S0-4 that is used for both small- and half-scale tests. The results are as well compared to the trends asserted in literature. A list containing the coefficients of restitution R_n , R_t , and R_{TE} as well as the maximum acceleration, the acceleration during the plateau and the maximum penetration depth evaluated for all half-scale tests can be found in Appendix III.

4.2.3.1 Slope inclination β (respectively impact angle θ)

As for the small-scale tests, all test series performed on a half-scale reveal for each block and each falling height a clear increase of R_n and R_{TE} for increasing slope inclinations β (corresponding at the same time to decreasing impact angles θ), whereas the tangential component of the coefficient of restitution R_t does not warrant a clear trend (Figure 4.23). The increase of R_{TE} and R_n means that for steeper slopes (eventually near their limit of equilibrium) the block loses less energy during impact and rebounds relatively more normal to the slope surface. These trends confirm the observations made by authors who have investigated the influence of the slope inclination on the coefficients of restitution as discussed in Chapters 2.5.2. and 2.5.3. (as e.g. by Wu [1985] and Chau & al. [2002]).

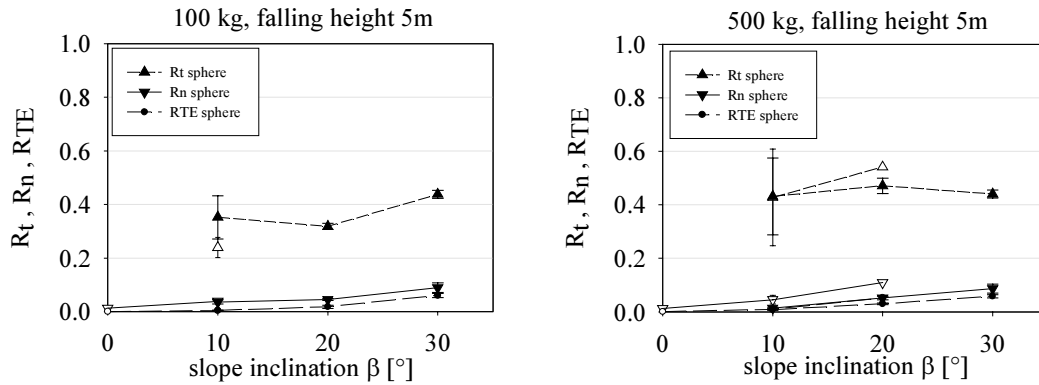


Figure 4.23: Influence of the slope angle β on the coefficients of restitution R_n , R_t and R_{TE} for the blocks weighing about 100 kg (left; black symbols: sphere (117 kg), white symbols: cylinder (103 kg)) and about 500 kg (right; black symbols: sphere (550 kg), white symbols: cylinder (511 kg)).

A closer investigation of the trend observed for R_n reveals a different behaviour for spherical and cylindrical blocks: whereas R_n increases nearly linearly with slope inclinations increasing from 10° to 30° for spherical blocks and all falling heights, a sudden increase of R_n is observed for slope angles larger than 20° for the cylindrical block of 1000 kg (Figure 4.24, left). At the same time, the tangential component of the coefficient of restitution R_t for the cylindrical block, increasing strongly between $\beta = 10^\circ$ and 20° , changes sharply to a constant trend. Both observations are most pronounced for small impact velocities and gradually attenuate for higher impact velocities (Figure 4.24, left to right).

As only few impact tests have been performed on slopes at $\beta = 20^\circ$ and none for $\beta = 30^\circ$ with smaller cylindrical blocks, it is not possible to prove that this phenomenon occurs for all cylindrical blocks. However, it is highly probable that this trend emerges for all cylindrical blocks due to the following considerations: The phenomenon is most pronounced for small impact velocities. In this case, the penetration into the ground is small. Therefore the ground material offers low lateral resistance to the block during the impact process. Consequently, the block rotation is high due to both, the lack of rolling resistance and the large radius of the spherical base. The large base radius has in fact two combined effects: on the one hand, it decreases the penetration depth of the block, on the other hand, the eccentricity to the vertical centre line of the point of first contact between block and ground is about 30% higher than for the corresponding spherical block (Figure 4.34). Due to the toppling (see Figure 4.11) and the higher rotation rate, the velocity component tangential to the slope increases intensely, explaining the sharp increase of R_t between $\beta = 10^\circ$ and 20° . Such effect is not observed for spherical blocks: having a smaller radius than the cylinder base, they penetrate deeper into the ground and have a lower rotation rate than the cylindrical blocks for same falling heights (see Chapter 4.2.3.3).

For slopes inclined at 30° , a mechanism similar to the one described for $\beta = 20^\circ$ takes place. R_t consequently remains nearly constant at a high level between $\beta = 20^\circ$ and 30° (the gain of tangential rebounding velocity is counterbalanced by the incident tangential velocity increasing with the slope angle as $v_{t,i} = v_i \cdot \sin\beta$). However, at $\beta = 30^\circ$, the rotation induced to the block during impact is higher than for $\beta = 20^\circ$ due to a larger eccentricity between first contact point and vertical centre line. The rotational energy causes the block to roll over the ground material accumulated in moving direction more than to displace it downwards. This causes the rebound direction to be more normal to the slope surface compared to the nearly slope-parallel rebound for $\beta = 20^\circ$, resulting in an increase of R_n .

These effects are observed for impact velocities up to 9.9 m/s (corresponding to a free fall of 5 m). For higher impact velocities the block penetrates deeper into the ground, resulting in a higher lateral resistance, which reduces the rotation of the block and thus the effects described above.

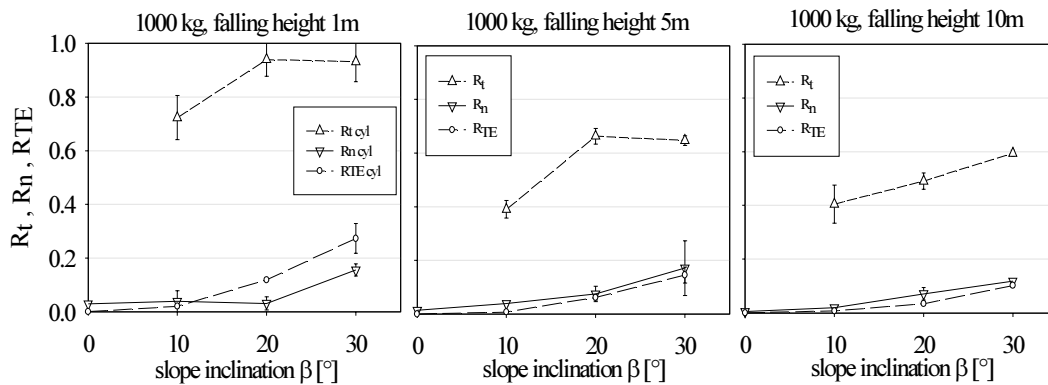


Figure 4.24: Observations for cylindrical blocks: for small impact velocities (left diagram) important change of trend for R_t from $\beta = 10^\circ$ (increasing) to 30° (constant), R_n (sharp rise for $\beta = 30^\circ$) and R_{TE} (sharp rise for $\beta \geq 20^\circ$). These effects gradually attenuate for higher impact velocities (middle and right diagrams).

Another effect observed for slope inclinations of 20° and more is the increase of the total energy restitution (R_{TE}), being particularly sharp for the cylindrical block (Figure 4.24: cylinder; Figure 4.25, upper graphs: sphere). As stated above, also this effect attenuates for increasing impact velocities (Figure 4.25 left to right). A closer investigation reveals that in case of the cylindrical blocks it is due to the sharp increase of R_t for $\beta = 20^\circ$, which is generated by the decrease of frontal resistance for steep slopes (including the instability of the slope itself at $\beta \geq 30^\circ$). In case of the spherical blocks, the increase of R_{TE} is due to the same factors except for the increase of R_t , which remains nearly constant for all slopes. As mentioned above, the attenuation of the effect is due to the deeper penetration of

the block into the ground for higher impact velocities, creating a higher frontal resistance to the downhill motion of the block.

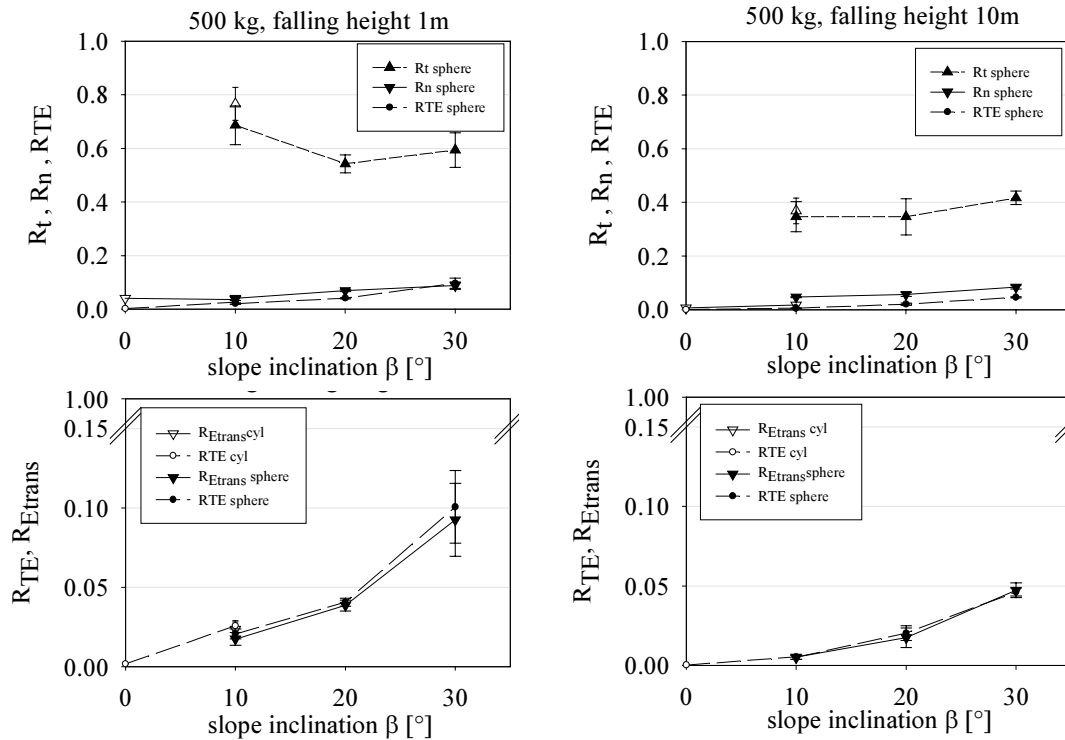


Figure 4.25: upper graphs: change of trend for R_{TE} (rise for $\beta \geq 20^\circ$) observed for spherical blocks at small impact velocities (left). The effect gradually attenuates for higher impact velocities (right).

lower graphs: increase of the rotational energy of the spherical block with increasing slope angles for small falling heights (left: 1m), effect which is not observed for large falling heights (right: 10 m). R_{Etrans} is the translative component of the coefficient of restitution R_{TE} .

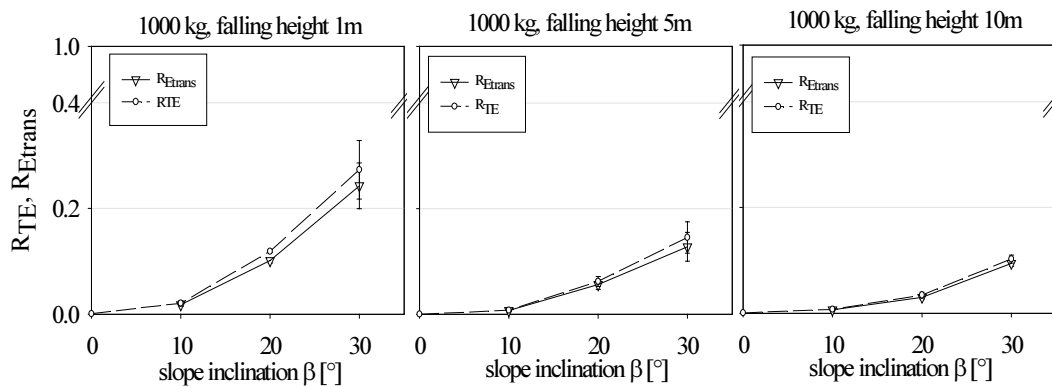


Figure 4.26: Increase of rotational energy for the cylindrical block (1000 kg) as function of the slope inclination. The rotational energy is the difference between the total (R_{TE}) and the translational (R_{Etrans}) energy restitution of the block: the effect is most pronounced for small impact velocities (left) and attenuates for increasing falling heights (middle and right).

4.2.3.2 Block weight W

The unit weight of rocks varying in a very limited range of values, field or laboratory testing campaigns with natural boulders do not allow to differentiate the respective influence of block weight and block size on the rebound phenomenon. For that reason, several tests of the experimental campaign are performed to differentiate the respective influence of block size and block weight on the coefficients of restitution.

The results for impact tests performed with blocks having different unit weight but the same diameter or similar weight but different diameters are investigated. The results for impact tests with changing unit weight are compared to the corresponding small-scale test results.

Constant diameter, increasing block weight:

Two of the spherical blocks used for the impact tests on a half-scale have the same diameter (0.73 m) but different block masses of 150 kg and 550 kg respectively. Comparing the coefficients of restitution gathered for both blocks for similar impact conditions, the following trends are observed:

As experienced for the small-scale tests, the heavier block is observed to penetrate deeper into the ground, causing more plastic deformation to the soil and thus losing more energy during impact than a lighter block with same diameter. The higher accumulation of ground in front of the block further creates a higher resistance in downhill direction. At impact end, the heavier block therefore has a lower rotational and translational velocity than the light one, especially for low impact velocities. Consequently, the coefficient of restitution R_{TE} is higher for the 150 kg sphere than for the 550 kg sphere. As for the small-scale tests, the difference is most pronounced for large slope inclinations.

The normal and tangential coefficients of restitution R_n and R_t , however, don't show the same coherent decreasing trend for increasing block weight observed on a small-scale. In fact, the trends observed on a half-scale inverse for increasing impact velocities: whereas for small falling heights ($H = 1$ m) the 550 kg block undergoes a higher tangential and lower normal restitution than the 150 kg block for all slope inclinations, it is the contrary for large falling heights ($H = 10$ m) (Figure 4.27). A parallel study of the rebound velocity direction (Figure 4.28) reveals that for low impact velocities ($v = 4.4$ m/s) the light block rebounds more normal to the slope surface than the heavy block, whereas for high impact velocities ($v = 14$ m/s) the inverse trend is observed. This is valid for all slope inclinations. The first part of this statement (concerning falling heights of 1 m) corresponds to the observations made for impact tests on a small-scale with blocks

of same diameter but different weight. As no impact tests with increasing falling heights are performed on a small-scale, it is not known if such inversion of the rebound direction for higher impact velocities occurs also on a small-scale.

An explanation can be found by analysing the acceleration graphs of both blocks. Whereas one observes an acceleration plateau indicating a shear failure of the ground (as it will be discussed in Chapter 4.3.1.1) for all impact tests with the 550 kg block, in case of the 150 kg block an acceleration plateau appears only for falling heights of 10 m (and exceptionally 5 m). In case shear failure occurs, the ground offers less frontal resistance to the block causing it to move more tangential to the slope. This could explain why the light block rebounds more normal to the slope than the heavy block in case of low impact velocities but has the same rebound direction in case of high impact velocities ($H = 10$ m).

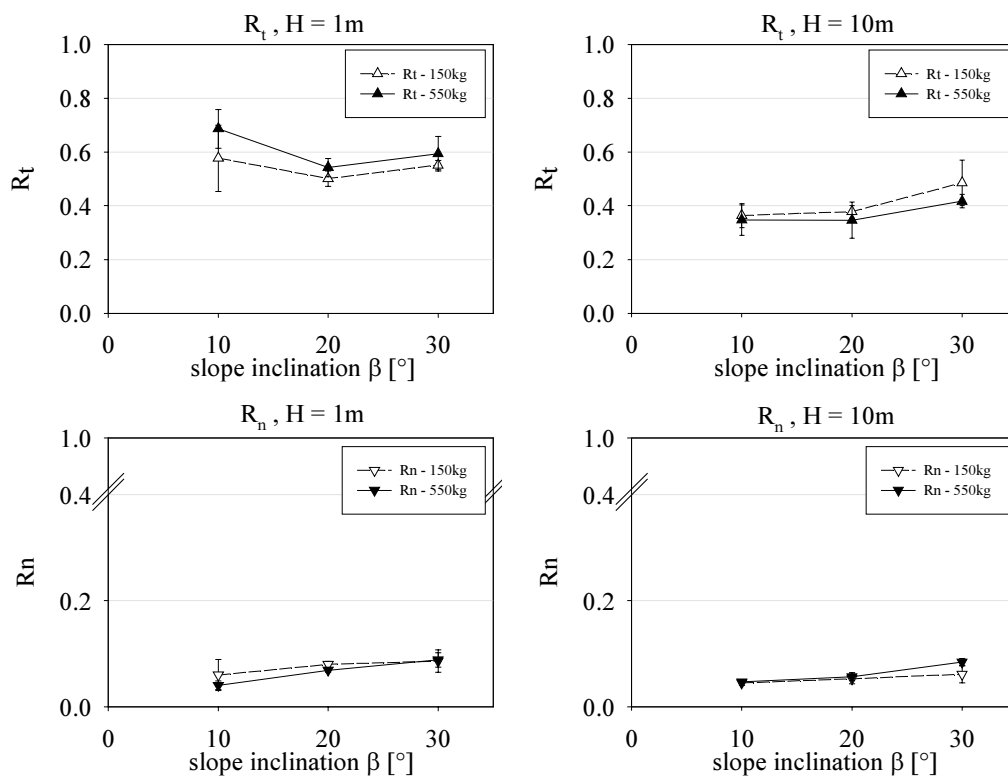


Figure 4.27: Inversion of the trends for R_n and R_t with increasing falling heights:

$H = 1$ m: $R_t(550 \text{ kg}) > R_t(150 \text{ kg})$ and $R_n(550 \text{ kg}) < R_n(150 \text{ kg})$;

$H = 10$ m: $R_t(550 \text{ kg}) < R_t(150 \text{ kg})$ and $R_n(550 \text{ kg}) > R_n(150 \text{ kg})$

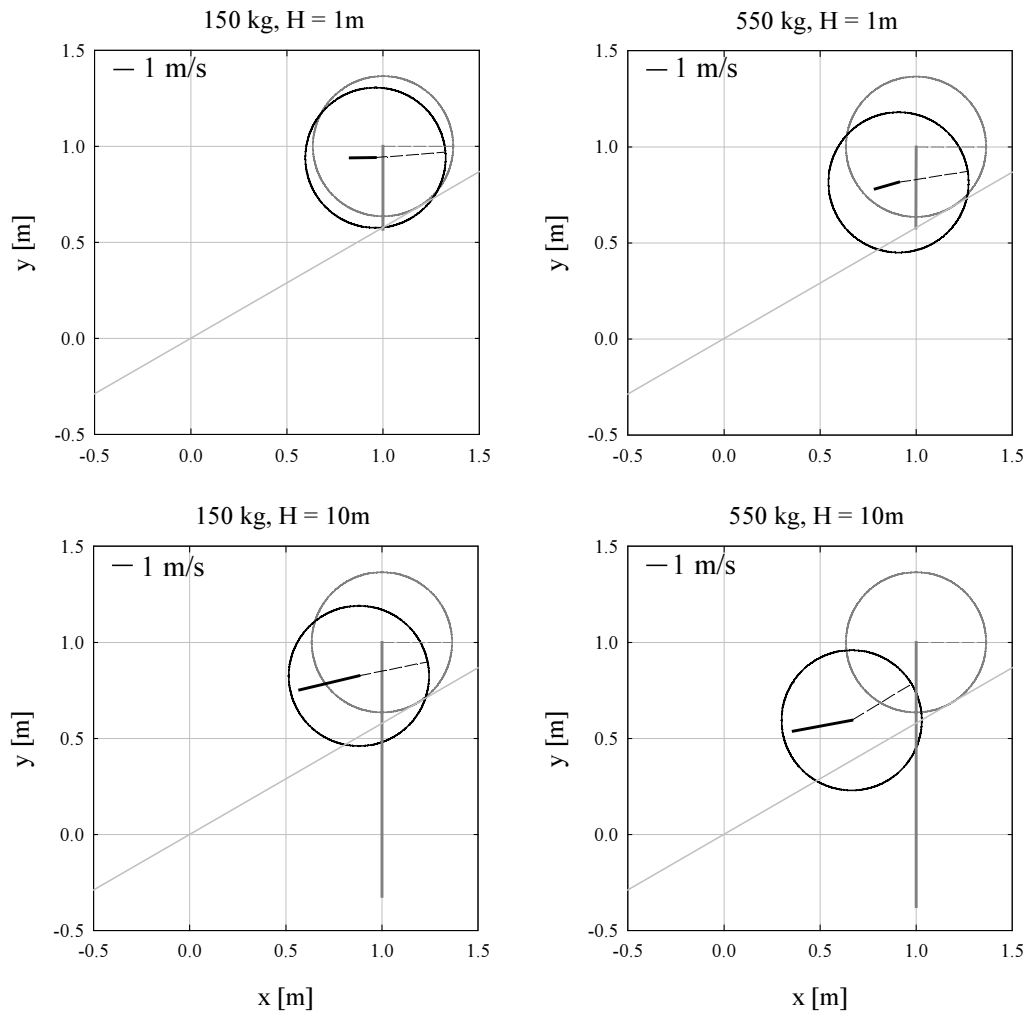


Figure 4.28: Position and velocity vectors (scale in the upper left corner; grey: before impact, black: after impact) of the 150 kg and the 550 kg sphere for impact tests on a slope inclined at 30° from different falling heights (upper row: $H = 1$ m, lower row: $H = 10$ m).

Constant weight, increasing diameter:

The real block masses of the “100 kg” (\varnothing 0.42 m) and the “150 kg” (\varnothing 0.73 m) spheres being of 117 and 152 kg respectively, the difference in weight corresponds to 30% whereas the difference in diameter is larger than 70%. Thus, a comparison of the restitution coefficients gathered for both blocks allows to reveal the influence of a change in diameter for nearly constant block weights.

For comparable impact conditions one observes that the small 117 kg sphere penetrates deeper into the ground during impact than the large 150 kg sphere. This is the logical consequence of the increase of contact surface, causing the observed lower penetration rate of the 150 kg block. This effect is most pronounced for falling heights larger than 1 m. In this case the smaller block, penetrating deeper into the soil than the larger block, dissipates more energy during impact and meets

more ground resistance in moving direction. Consequently, the coefficients of restitution R_t , R_n and R_{TE} are lower for the small than for the large sphere for impacts with falling heights larger than 1 m (Figure 4.29, right hand side).

For a falling height of 1 m, however, the tangential coefficient of restitution R_t is higher for the small than for the large block, independently of the slope inclination (Figure 4.29, left hand side). For a slope angle of 30° , the small block additionally has a larger restitution in normal direction than the large block (Figure 4.29, left). Analysing the rebound direction for $H = 1$ m by means of the velocity vectors (e.g. $\beta = 10^\circ$, Figure 4.30), one realizes that for any slope inclination, in spite of a deeper penetration into the ground, the small block rebounds more tangential to the slope surface than the large block. This is due to the ground shear failure occurring for all impacts from 1 to 10 m height (with sparse exceptions at $\beta = 20^\circ$) with the small block, favouring a tangential block motion. For the corresponding impact tests with the large sphere, no acceleration plateau and thus no ground shear failure is observed.

Summarizing the influence of the block diameter, it is stated that independently of falling height and slope inclination a smaller block loses more energy during impact than a larger block with similar weight. This means that a block supposed to have e.g. an elliptical shape with a contact radius R (flat side) and a contact radius r (pointed side; with $R > r$) loses more energy during impact and rebounds less if it hits the ground with the more “pointed” part than if it impacts the ground with its flat side (supposing that the centre of gravity of the block in both cases is exactly vertical over the contact point, otherwise the impact configuration has probably an additional important influence). Further, a smaller block rather tends to provoke shear failure of the ground and thus rebounds more tangential to the slope than a larger block with similar weight.

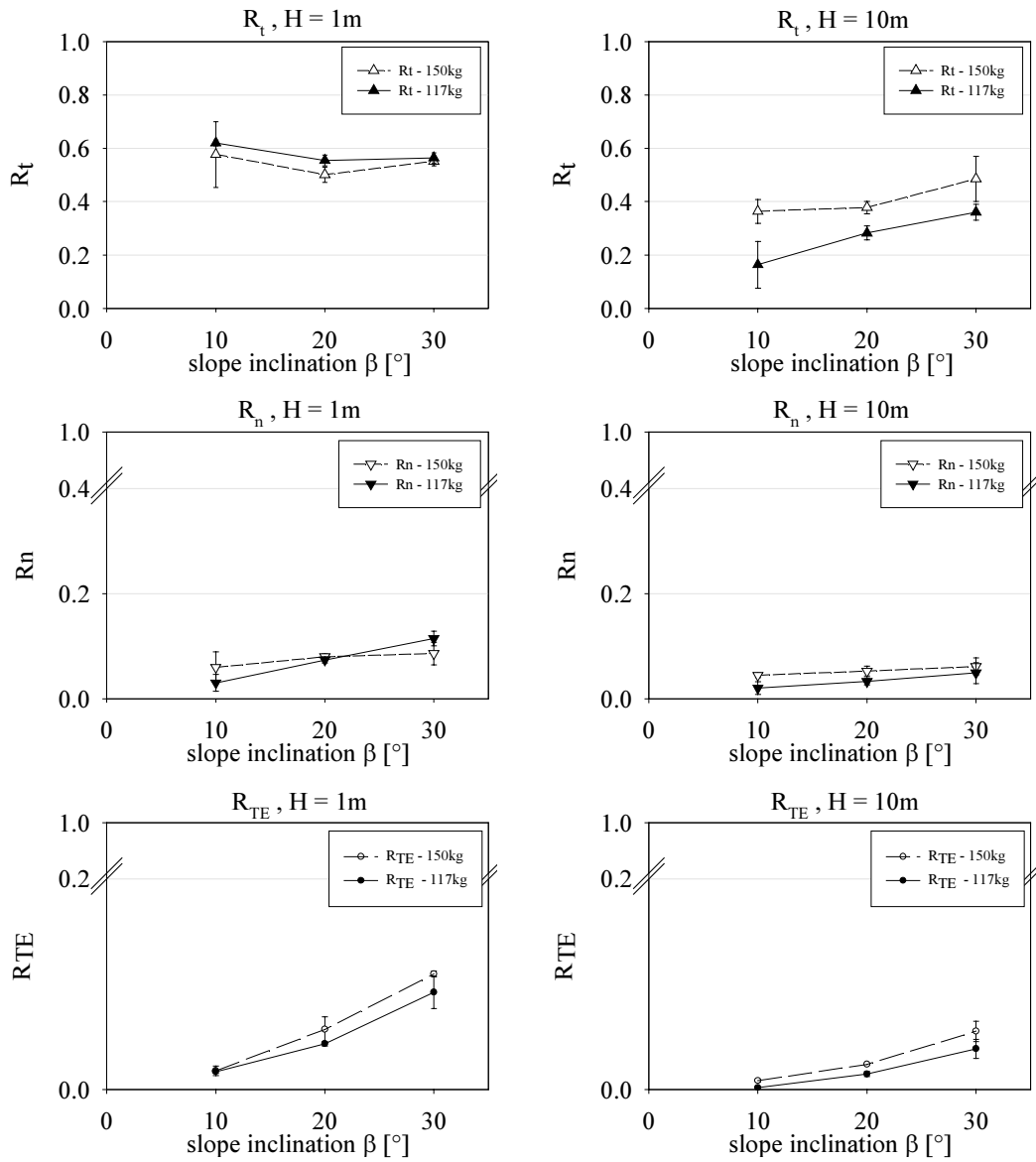


Figure 4.29: Comparison of the coefficients of restitution R_t , R_n and R_{TE} for the small (117 kg) and the large (150 kg) sphere: trend inversion for R_t between $H = 1$ m and $H = 10$ m.

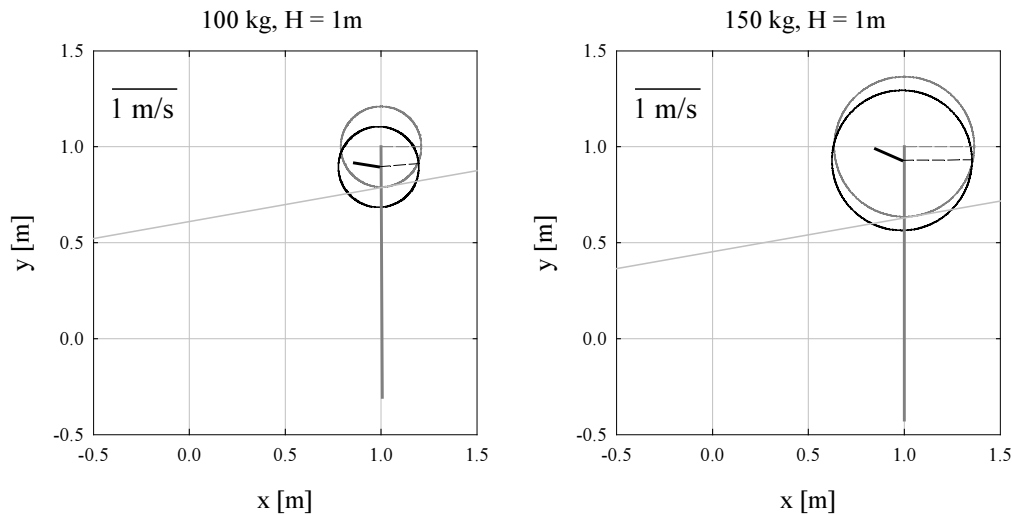


Figure 4.30: More tangential rebound in spite of deeper penetration of the small (117 kg) sphere (left) compared to the large (150 kg) sphere (right) for impacts from $H = 1$ m.

Constant unit weight, increasing weight and diameter (all spheres and cylindrical blocks except the 150 kg sphere):

For blocks with similar unit weight the characteristics mass and size are coupled. Thus, an increase of the radius implies an increase of the block weight. Consequently, the coefficients of restitution gathered for impacts under similar conditions but increasing block weights and sizes combine the effects stated above:

- Spherical blocks, small falling heights ($1 \text{ m} \leq H \leq 5 \text{ m}$): As stated above, for increasing block weight but same diameter the coefficients of restitution R_n and R_{TE} decrease slightly and R_t increases (Figure 4.27, left), whereas an increase of block diameter (maintaining constant the block weight) causes contrarily an increase of R_n and R_{TE} and a decrease of R_t (Figure 4.29, left). Thus, for increasing block weight and size and for slope angles larger than 10° , the opposed trends of R_n , R_t and R_{TE} observed for each parameter cancel each other. The coefficients thus remain constant as long as the block diameter and thus the contact area between block and ground increase at a rate corresponding to the increase of block weight (Figure 4.31). For small slope angles ($\beta = 10^\circ$), however, an increase of R_t and thus of R_{TE} are observed.
- Spherical blocks, large falling heights ($5 \text{ m} \leq H \leq 10 \text{ m}$): As stated above, for increasing block weight but same diameter the coefficients of restitution R_t and R_{TE} decrease slightly and R_n increases, whereas an increase of block diameter (maintaining constant the block weight) causes all three coefficients to increase. The increasing trend for R_t and R_{TE} with the block size being stronger than the decrease with the block weight, for large falling heights, R_t increases slightly with the coupled increase of

block weight and size. An increasing trend is observed as well for R_n (Figure 4.32).

- Cylindrical blocks, small slope angles ($\beta \leq 10^\circ$): Similar to the observations made for spherical blocks and small slope angles, a combined increase of block weight and diameter (constant unit weight) causes the coefficients of restitution R_t and R_{TE} to increase whereas R_n reveals a constant to slightly decreasing trend (Figure 4.33). A slight decrease of R_n is observed in case of a simultaneous strong increase of R_t for a block mass increase from 100 kg to 500 kg. This signifies a more tangential rebound behaviour of the 500 kg block which is due to its toppling. Also the slight decrease of R_t observed for a block mass increase from 500 kg to 1000 kg and small falling heights ($H \leq 5$ m) shows that the 500 kg cylinder tends to topple more easily than the 1000 kg cylinder due to the higher penetration rate of the latter. This assumption is supported by the rotational rate which is slightly higher for the 500 kg than for the 1000 kg cylinder for $\beta \leq 10^\circ$ and $H \leq 5$ m.

As for slope angles steeper than 10° no test series were performed with the 100 kg and 500 kg cylinder, no trend for increasing block weight can be reported.

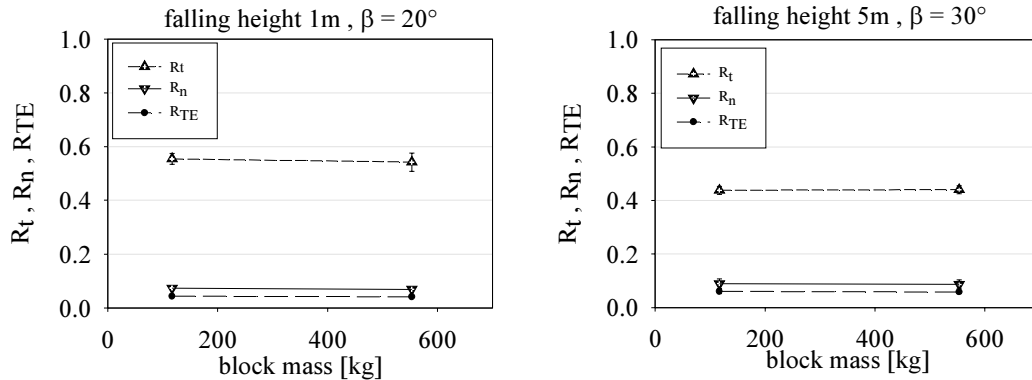


Figure 4.31: Spherical blocks, low falling heights: R_n , R_t and R_{TE} remain constant for a coupled increase of block weight and diameter (constant unit weight).

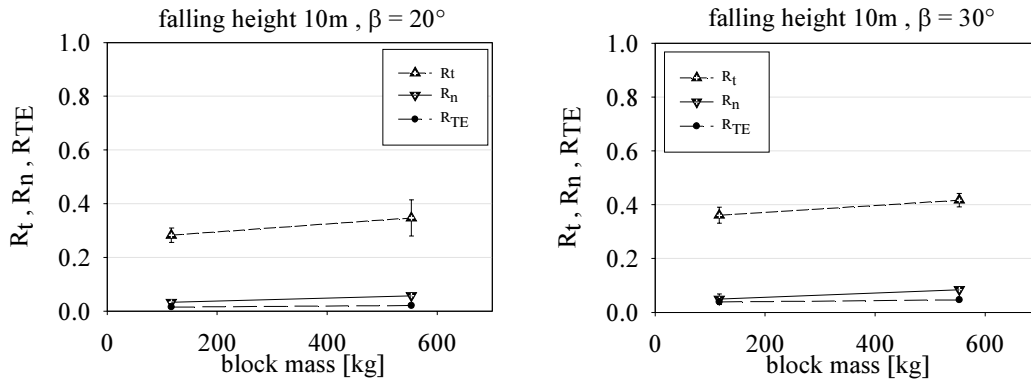


Figure 4.32: Spherical blocks, large falling heights: R_n , R_t and R_{TE} increase for a coupled increase of block weight and diameter (constant unit weight).

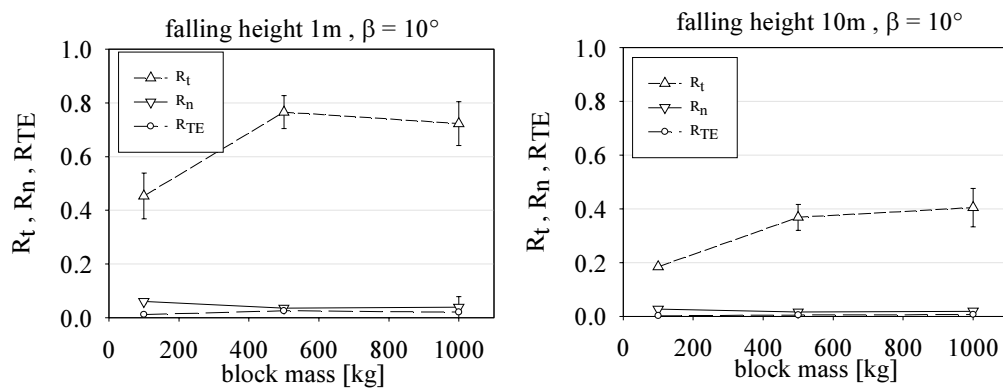


Figure 4.33: Trends observed for R_n , R_t and R_{TE} for a coupled block mass and diameter increase for cylindrical blocks impacting flat slopes (constant unit weight).

4.2.3.3 Block shape

Comparing the coefficients of restitution evaluated for both the cylindrical and the spherical blocks, no clear tendency is observed for $\beta = 10^\circ$. On slope angles larger than 10° , however, all three evaluated coefficients of restitution R_n , R_t and R_{TE} are higher for cylindrical blocks than for spheres (as to see in Figure 4.23 for 500 kg blocks). In case of R_t and R_{TE} this is due to the behaviour explained above in the paragraph “*slope inclination β* ”: The spherical base having a larger radius than the corresponding spherical block, at same impact velocity the cylinder penetrates less into the ground, promoting its tangential propagation during impact (low lateral ground resistance) as well as its normal rebound velocity. Consequently, the tangential and normal components of the coefficient of restitution are larger than the ones evaluated for spherical blocks. Further, due to the low penetration rate, less energy is dissipated during impact by plastic ground deformation. Together with a higher rotational energy component the coefficient of total energy restitution R_{TE} is higher than for the corresponding spherical blocks.

The higher rotation rate is due to a larger eccentricity between the vertical centre line and the first contact point for cylindrical than for spherical blocks (Figure 4.34) and the lower lateral rolling resistance due to a smaller penetration rate. Figure 4.35 illustrates the observation of higher rotational energy rates for cylindrical than for spherical blocks for slope angles of 20° and steeper.

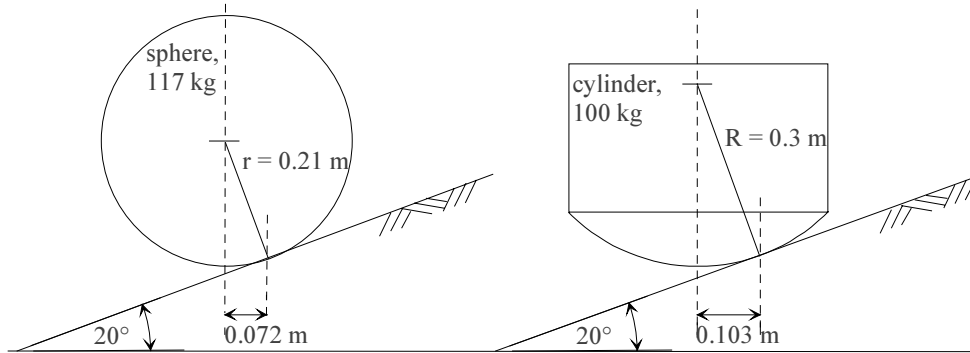


Figure 4.34: Eccentricity between the vertical centre line and the first contact point with the slope (illustrated for $\beta = 20^\circ$): larger for cylinder than for sphere, inducing more rotation of the cylindrical blocks

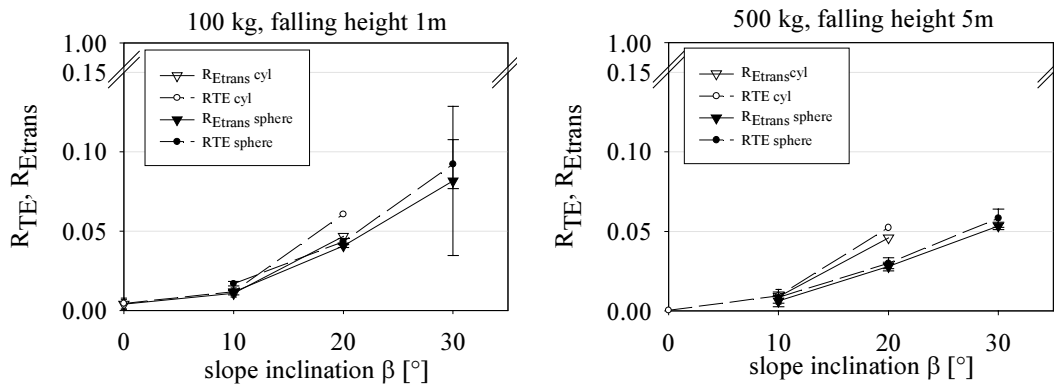


Figure 4.35: Comparison of the coefficient of restitution for the translational part of the block energy (R_{Etrans}) and the total energy (R_{TE}) for both spherical (black symbols) and cylindrical (white symbols) blocks. The difference between R_{TE} and R_{Etrans} indicates the rotational energy rate: the larger the difference, the higher the block rotation at impact end.

Summarizing it can be stated that the block form, varying between a sphere and a cylinder with spherical base, has no influence on the rebound for small slope angles ($\beta \leq 10^\circ$). On slope angles larger than 10°, however, cylindrical blocks have higher coefficients of restitution and a higher rotation rate.

4.2.3.4 Falling height H

On a small-scale, no tests were performed to investigate the influence of the falling height and thus of the impact velocity on the rebound of the blocks. On a half-scale, the trends described in the following are observed for increasing falling heights keeping all other parameters constant. As some particularities concerning specially R_n are observed for cylindrical blocks, the trends are analysed successively for both block forms.

Cylindrical blocks:

The vertical impacts performed on horizontal ground ($\beta = 0^\circ$) with cylindrical blocks show that R_n and R_{TE} decrease both with increasing falling heights (corresponding to increasing impact velocities). However, no statement can be made for the dependence of R_t on the impact velocity, as for perpendicular impacts the tangential coefficient of restitution is not defined ($R_t = v_{t,r}/v_{t,i} \approx 0/0$).

For impacts on slopes, likewise, a decrease of R_{TE} is observed for increasing falling heights, whereas the constantly decreasing trend of R_n for perpendicular impacts is observed only for large falling heights ($H \geq 5\text{m}$). In case of the cylindrical blocks dropped from four different heights (1, 2, 5 and 10 m), a clear increase of R_n is observed for small falling heights. For the blocks of 100 kg and 500 kg, R_n increases from $H = 1\text{ m}$ to $H = 2\text{ m}$, whereas for the heaviest block of 1000 kg, R_n increases even up to $H = 5\text{ m}$ (Figure 4.36). As simultaneously the tangential coefficient of restitution R_t decreases strongly (Figure 4.36), this means that the moving direction after impact of cylindrical blocks becomes more and more normal to the slope surface for falling heights increasing from $H = 1$ to 2 m (respectively 5 m for the largest cylindrical block). This effect is caused by the penetration depth, which increases with increasing impact velocities (respectively falling heights). The resulting increasing ground resistance in front of the block forces the block to rebound more normal to the slope. This explanation is confirmed by the gradually abating decrease of R_t with increasing impact velocities observed for all impact tests on slopes.

The decrease of R_{TE} with increasing falling heights results from the same mechanism: with increasing impact velocities, the block penetrates deeper into the ground material provoking larger plastic deformations of the latter and thus loses more energy during impact. The increasing frontal ground resistance further reduces the rotational energy rate of the block. Consequently, the higher the impact velocity, the lower is the total energy restitution as well as the rotational energy rate of the block at impact end. This is observed likewise for cylindrical and spherical blocks for all slope inclinations, as illustrated in Figure 4.38.

Spherical blocks:

Whereas the coefficients of restitution R_t and R_{TE} show similar decreasing trends for both cylindrical and spherical blocks, the graphs for R_n differ from the ones observed for the cylindrical blocks. For small slope inclinations ($\beta = 10^\circ$), R_n tends to be constant for changing falling heights (Figure 4.37, left). However, for larger slope angles ($\beta = 20^\circ$ and 30°), a decrease of R_n is observed (Figure 4.37, middle and right), being more pronounced for the lighter (100 kg) than for the heavier (550 kg) block.

As no impact tests were performed with spherical blocks from falling heights of 2 m, it is possible that the rise of R_n , observed for impact heights increasing from 1 to 2 m for the corresponding cylindrical blocks, is not detected. The quite constant behaviour of R_n between falling heights of 1 to 5 m supports this assumption. In case this assumption is right, the rebounding behaviour for increasing impact velocities is similar for spheres and cylinders.

Summarizing the upper considerations it can be stated that for increasing impact velocities (respectively falling heights) the tangential coefficient of restitution R_t reacts most sensible and decreases strongly (the decrease attenuates for higher impact velocities), whereas R_n and R_{TE} show in general a slighter decreasing trend. Whereas for small falling heights ($H = 1$ m) the downhill rolling of the block is imposing the rebound direction (quite tangential to the slope surface, means small R_n , large R_t), the increasing resistance of the ground accumulated in front of the block for increasing falling heights forces the block to rebound more normal to the slope (initial increase of R_n , strong decrease of R_t). The energy dissipation, resulting from the ground plastification and the rolling and sliding friction, thus initially increases as well with increasing falling heights, to be followed by a decreasing trend for higher impact velocities.

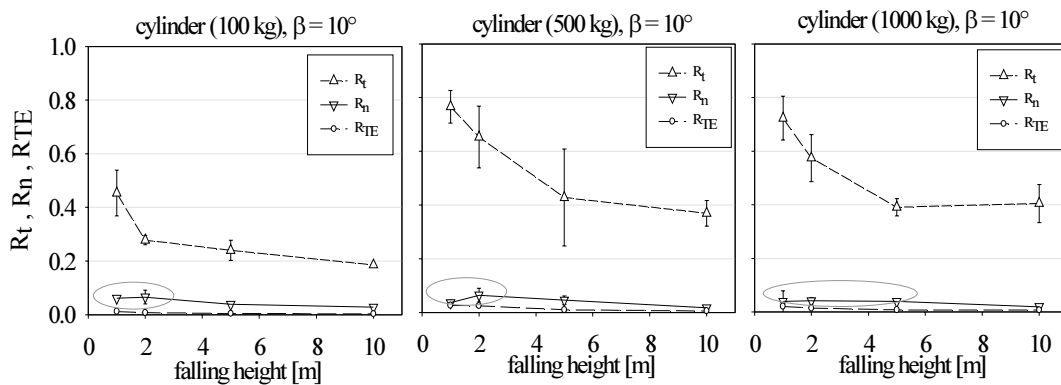


Figure 4.36: Increasing trend for R_n for impacts on slopes with small falling heights for cylindrical blocks (see ovals!).

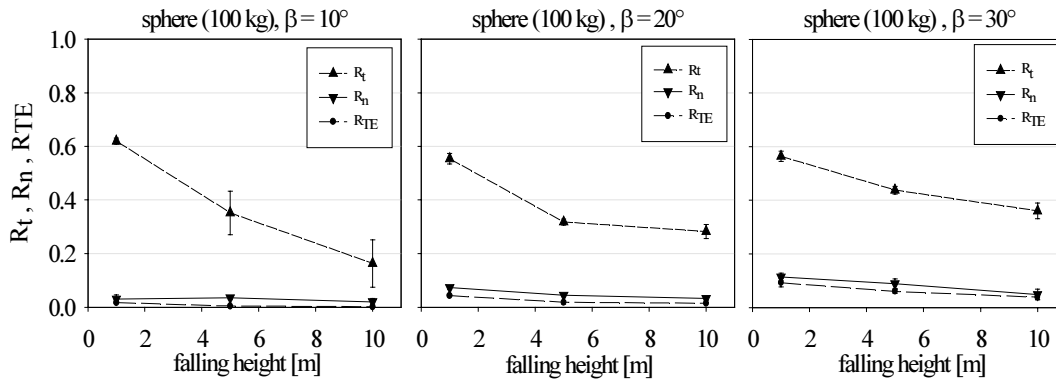


Figure 4.37: Decreasing trend for R_t and R_{TE} for impacts on slopes with spherical blocks. The constant trend for R_n on flat slopes changes to a decreasing trend for steeper slopes (left to right).

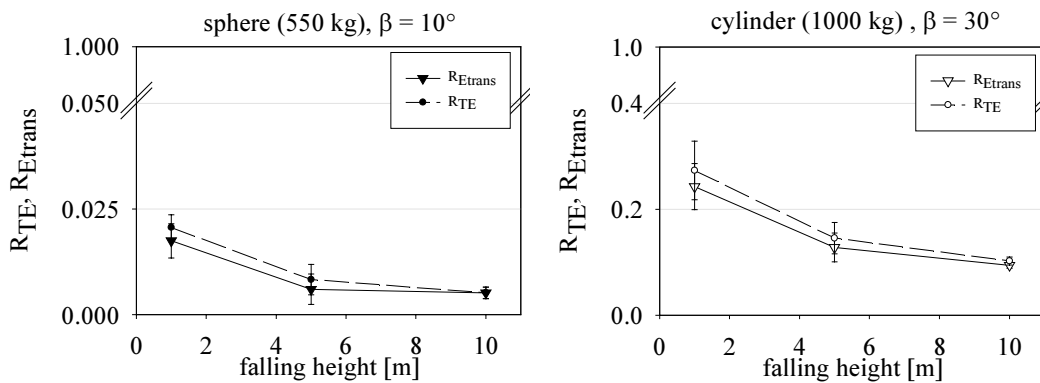


Figure 4.38: Decrease of the rotational energy rate with increasing impact velocity respectively falling height observed for both spheres (left) and cylinders (right). The rotational energy rate is expressed by the difference between the value of the coefficient of restitution of the total (R_{TE}) and the translational (R_{Etrans}) energy.

The observed trend of R_t being more sensible to the impact velocity than the normal component R_n confirms the observations made by Urciuoli [1988]. Agreeing observations are stated by some more authors (as e.g. Hutchings & al. [1981]). The only controversial observation reported by Ushiro & al. [2000] and stating that R_t is insensitive to the impact velocity, is based on impact tests on rock and concrete, not on soft soil.

4.2.3.5 Impact energy E

As the impact energy is the product of the block mass, the falling height and the gravity ($E = mgH$), the trend of the coefficients of restitution with increasing impact energy is the product of the trends observed for each of the parameters block mass and falling height. Analysing the change of the coefficients of restitution with changing impact energy for a certain block, the result corresponds

to the trend observed for the change of the corresponding falling height (see paragraph above). As already mentioned above, for blocks weighing 500 kg and more (corresponding to high impact energy levels), the decreasing trend of R_n observed for light blocks attenuates to a nearly constant value (Figure 4.39). A similar observation is stated by Chau & al. [1998b] as reported in Chapter 2.5.3.: the authors observe a decrease of R_n with increasing impact energy for low energy levels, whereas for higher energy levels, the impact energy has no influence on R_n . The trends for R_t and R_{TE} are as well confirmed by the tests performed by Chau & al. [1998b] or Wong & al. [2000].

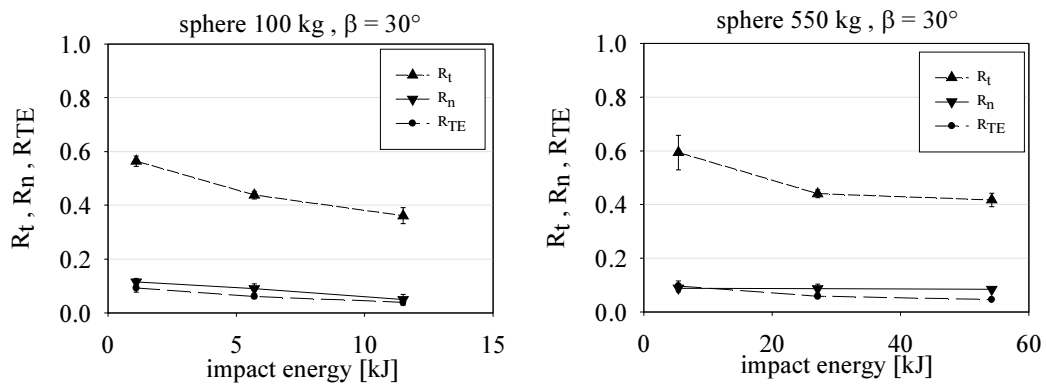


Figure 4.39: Attenuation of the decreasing trend of R_n with increasing block mass (left to right).

A comparison of the coefficients of restitution obtained for the same impact energy but different blocks and falling heights reveals the following trends:

Same impact energy for blocks with constant diameter but different weight:

Assuming a constant diameter, at same impact energy, the tangential coefficient of restitution R_t is clearly lower for a light block (150 kg) than for a heavy block (550 kg) (Figure 4.40). The normal component R_n is quite similar for small impact energies and shows a slight increasing trend for increasing block mass for higher impact energies. Thus, a light block rebounds more normal to the slope surface than a heavy block with same diameter. As the coefficient of energy restitution R_{TE} is lower for the light block than for the heavy block, the light block loses more energy during impact than the heavy one. Knowing that at same impact energy the light block has a higher impact velocity than the heavy block and nearly the same maximum penetration depth as the latter, this result is coherent with the trends stated above.

For blocks with same diameter but different weight it can thus be stated that at same impact energy a block with higher mass rebounds more tangential to the slope surface and loses less energy during impact than a lighter block.

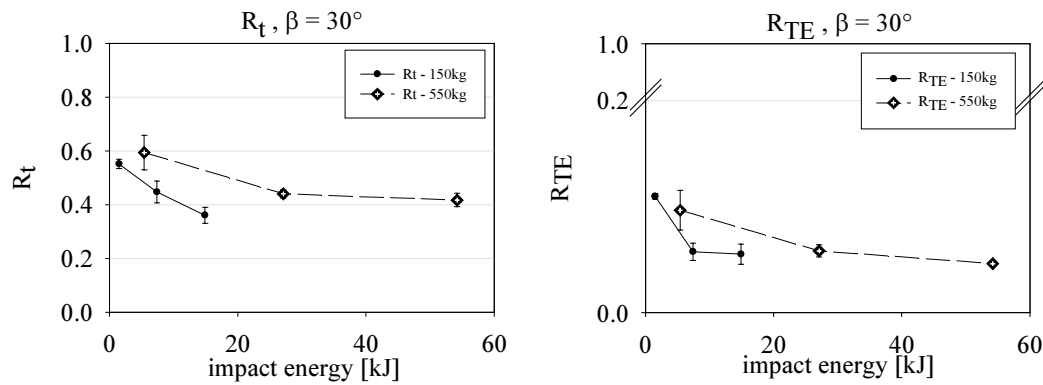


Figure 4.40: At same impact energy, R_t and R_{TE} both are lower for a light block (150 kg) than for a heavy block (550 kg) with same diameter.

Same impact energy for blocks with constant weight but different diameter:

For blocks with nearly the same weight but different diameter, for same falling heights the same impact energy is achieved. Comparing the coefficients of restitution acquired for same impact energies, one realizes that for both blocks the coefficients R_t and R_{TE} are similar for small impact energies, whereas for large impact energies both values R_t and R_{TE} are larger for the big block (150 kg, \varnothing 0.73 m) than for the small block with almost the same weight (117 kg, \varnothing 0.42 m) (Figure 4.41). This effect attenuates for increasing slope angles. The normal coefficient R_n as well is larger for a larger block, the difference however is very small.

Thus, for blocks with same mass but different diameters applies the following: at same impact energy a block rebounds more normal to the slope surface and loses more energy during impact, the smaller its radius is at the impact point.

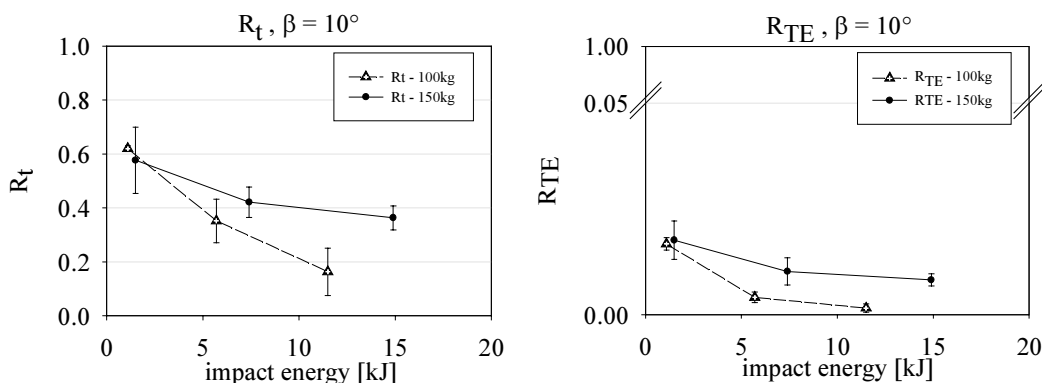


Figure 4.41: Increasing difference between the coefficients of restitution R_t (left) and R_{TE} (right) for increasing impact energy: R_t and R_{TE} both achieve higher values for a large block (150 kg) than for a small block (117 kg, called "100 kg" in the legend) with almost the same weight.

Same impact energy for blocks with constant unit weight but changing mass and diameter:

For blocks with constant unit weight, a change of block weight implies a simultaneous change of its diameter. Analysing the influence of both parameters on the coefficients of restitution, one realizes that at same impact energy heavy blocks have in general a higher restitution in normal and tangential direction as well as in terms of energy than light ones (Figure 4.42). The impact direction further is observed to be more normal to the slope the smaller and lighter the block is. This is valid for the tested block forms and all slope angles and signifies that large blocks with low impact velocities rebound more tangential to the slope surface and loose less energy during impact than smaller blocks with corresponding higher impact velocities.

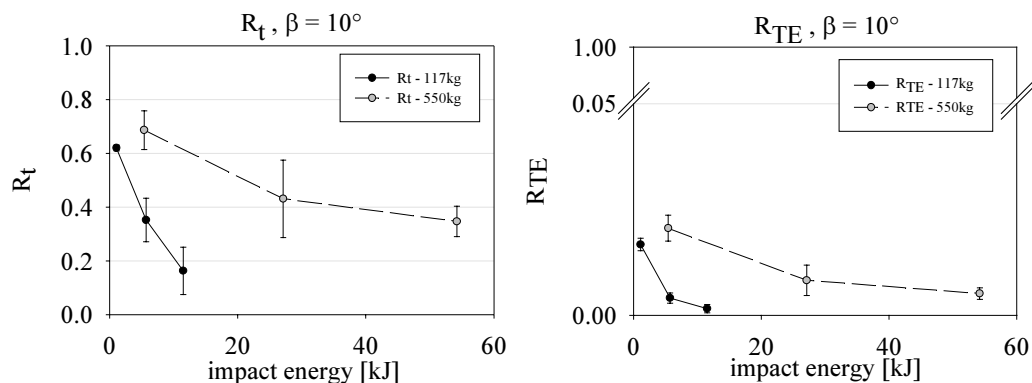


Figure 4.42: Higher R_t and R_{TE} being for larger and heavier blocks than for smaller and lighter ones, at same impact energy.

4.2.3.6 Impulse p

Comparable to the impact energy, the impulse depends on the parameters mass and falling height (the latter as square root). A qualitative interpretation of the influence of the impulse on the coefficients of restitution reveals the same trends as stated in the subheading 4.2.3.5, as only the scale of the horizontal axis changes. Consequently, also the comments concerning the trends of R_n , R_t and R_{TE} for constant energy but changing block diameter and / or mass apply fully for impacts at same impulse. As stated for similar impact energies achieved for different impact conditions, one can summarize that for the same value of impulse at impact the block with higher incident velocity has a lower post-impact velocity, rebounds more normal to the slope and loses more energy during impact.

Comparison between the influence of impact energy E and impulse p

As the impact energy E and the impulse p , depend on the block mass and the impact velocity, respectively the falling height, it is interesting to know, which of these parameters has a stronger influence on the coefficients of restitution.

The coefficients of restitution of different blocks are compared for impacts with same impulse or impact energy. The difference between the values of the coefficients of restitution is called ΔR . Evaluating ΔR for a certain impulse p ($\Delta R(p)$) as well as for the corresponding impact energy E ($\Delta R(E)$) reveals the following trend: $\Delta R(p)$ is found to be systematically larger than $\Delta R(E)$ for the tangential (Figure 4.43), the normal and the energetic coefficient of restitution (except for some values of R_n and R_{TE}). This signifies that for a change of block mass, the impulse at impact has more influence on the block restitution than the impact energy. In other words: at constant impulse, an increase of the block mass provokes a larger increase of the restitution coefficients and thus a more pronounced rebound than the same increase of block mass at constant impact energy. This result is in agreement with the observations made above, stating a lower rebound for small and light blocks having a high impact velocity than for large and heavy blocks having a low impact velocity.

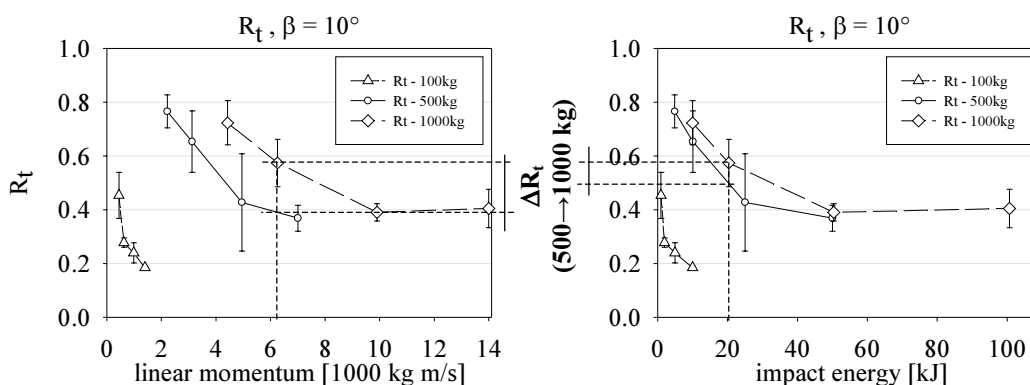


Figure 4.43: Comparison of ΔR_t achieved for same impulse respectively same impact energy but different mass of the block (in the present case for cylinders): ΔR_t is smaller for the impact energy than for the impulse.

4.2.4 Synopsis: parameters found to influence the coefficients of restitution

As for the small-scale tests, the half-scale test series reveal very clearly the dependency of the coefficients of restitution on parameters related to the ground, the block and the kinematics. Summarizing the observations discussed above and changing only the parameter mentioned in the headline, the following trends are stated:

Influence of the parameters related to the ground characteristics:

- Slope inclination $\beta \nearrow$ (respectively impact angle $\theta \searrow$)
 $R_n \nearrow$, $R_t \cong \text{constant to } \nearrow$, $R_{TE} \nearrow$

Influence of the parameters related to the kinematics:

- Falling height $H \nearrow$, corresponding to impact velocity $v \nearrow$
 - Sphere: $R_n \searrow$ (most pronounced for steep slopes and light blocks, attenuating for increasing block weight),
 $R_t \searrow$ strongly, $R_{TE} \searrow$
 - Cylinder: $R_n \searrow$ (but \nearrow for simultaneous strong decrease of R_t in case of $1 \text{ m} \leq H \leq 5 \text{ m}$ for all slope inclinations),
 $R_t \searrow$ (strongly for $H \leq 5 \text{ m}$, slight for $H > 5 \text{ m}$)
 $R_{TE} \searrow$

- Impact energy $E \nearrow$: see “Falling height H ” for the corresponding block

- Constant impact energy:

Block diameter \nearrow , constant block weight:

At same impact energy a block rebounds more tangential to the slope surface and loses less energy during impact, the larger its radius at impact point ($R_n \nearrow$ slightly, $R_t \nearrow$, $R_{TE} \nearrow$).

Block weight \nearrow , constant diameter:

At same impact energy a block with higher mass rebounds more tangential to the slope surface and loses less energy during impact than a lighter block ($R_n \nearrow$ slightly, $R_t \nearrow$, $R_{TE} \nearrow$).

Block weight \nearrow , diameter \nearrow (constant unit weight):

For impacts at same energy, heavy blocks having low impact velocities have higher coefficients of restitution than light blocks with high impact velocities ($R_n \nearrow$ slightly, $R_t \nearrow$, $R_{TE} \nearrow$).

- Impulse $p \nearrow$: see “Falling height H ” for the corresponding block
- Constant impulse: see “Constant impact energy”

Influence of the parameters related to the block:

- Block weight \nearrow , constant diameter (different unit weight)
 - 1 m \leq H \leq 5 m: $R_n \searrow$ slightly, $R_t \nearrow$, $R_{TE} \searrow$ slightly
 - 5 m $<$ H \leq 10 m: $R_n \nearrow$ slightly, $R_t \searrow$ slightly, $R_{TE} \searrow$ slightly

- Block diameter \nearrow , constant weight (different unit weight)
 - 1 m \leq H $<$ 5 m: $R_n \nearrow$ (but \searrow for $\beta = 30^\circ$), $R_t \searrow$ slightly, $R_{TE} \nearrow$
 - 5 m \leq H \leq 10 m: $R_n \nearrow$, $R_t \nearrow$, $R_{TE} \nearrow$

- Block weight \nearrow , diameter \nearrow (same unit weight)
 - Sphere:
 - 1 m \leq H \leq 5 m and $\beta \leq 10^\circ$: $R_n \cong$ constant, $R_t \nearrow$, $R_{TE} \nearrow$
 - $\beta > 10^\circ$: $R_n, R_t, R_{TE} \cong$ constant
 - 5 m \leq H \leq 10 m: $R_n \nearrow, R_t \nearrow$ slightly, $R_{TE} \nearrow$ slightly

 - Cylinder:
 - 1 m \leq H \leq 10 m and $\beta \leq 10^\circ$: $R_n \cong$ constant (\searrow in case of simultaneous strong increase of R_t),
 $R_t \nearrow$, $R_{TE} \nearrow$ slightly

- Block form: sphere versus cylinder with spherical base
 - $\beta \leq 10^\circ$: no clear difference
 - $\beta > 10^\circ$: R_n, R_t, R_{TE} (cylinder) $>$ R_n, R_t, R_{TE} (sphere)

4.3 Quantitative interpretation of the half-scale tests

In the following, the influence of the parameters found to control the rebound phenomenon and the coefficients of restitution, which till now has been interpreted only qualitatively by giving trends, is quantified. Therefore, first the failure mechanisms occurring during impact are analysed in detail and the conditions for their occurrence are investigated. Parting from this knowledge, the characteristics describing the impact phenomenon physically, as the maximum penetration depth, the maximum acceleration of the block during impact and the rotational velocity at impact end are investigated and quantified. Based on the knowledge of the failure mechanisms in the ground material occurring during the impact process and the idea of impulse conservation, the normal and tangential coefficients of restitution R_n and R_t are quantified. The results gathered by means of the proposed formulations are compared to the measured values. Finally, the coefficient R_{TE} , defined by the ratio of the total energy of the block after and before impact, is expressed in dependence on the proposed formulations of R_n , R_t and the rotational velocity at impact end.

4.3.1 Impact mechanisms

As we have seen in section 4.2.2, the movement of the block after impact depends on a very complex interaction of several parameters related to block, ground and kinematics. To get a better knowledge of the rebound mechanism, the main mechanisms occurring during impact are analysed in the following.

For impacts on granular slopes ($\beta \neq 0^\circ$) from *small falling heights* with blocks of a distinct contact radius (no projectile form), the “impact” looks alike a “deposition” of the block on the ground surface. Without creating a deep crater, the block begins to roll on the ground surface. The impact mechanism thus resembles somewhat to impacts on hard ground materials, where almost no deformation of the ground surface occurs.

For *larger falling heights* or impacts on horizontal ground, the block penetrates in the soft ground material creating a distinct crater and causing local or even global failure of the ground material. As the crater rim hinders the rolling of the block, the translational motion of the block is preponderant in this case.

For impacts on soft granular materials hence two main mechanisms can be distinguished: the rolling of the block on the ground surface and the penetration of the block into the ground (translation). As described above, those mechanisms are “antagonistic”: the deeper the block penetrates the ground, the more the rotation is hindered. On the other hand, a block with a rotation gained after ground contact or

with an initial rotation (this test configuration was not analysed within the framework of this thesis) tends to roll on the surface and to penetrate less into the ground. For impacts on slopes near their limit of equilibrium, a further mechanism occurs: the ground material begins to slide at the surface as soon as the block gets in contact with it.

The ground characteristics as well as the block shape and its kinematics decide, which movement type prevails for an impact. The information on the block movement gained during the impact tests allow to identify the following measured values as very important for the determination of the impact mechanism:

- the acceleration in function of time, yielding the values for a_{\max} and a_{plateau} ,
- the limit criterion for which a plateau occurs,
- and the maximum penetration depth d_{\max} .

Mathematical relations are proposed in the following for those values. It should be mentioned that the validity of the proposed formulations are only verified for the tested impact conditions. Further tests (other energies, blocks, impact configurations etc.) on other ground materials should be performed to verify eventual extrapolations of the presented formulations.

4.3.1.1 Ground failure during impact

To be able to investigate the impact phenomenon on granular materials and to describe it mathematically, it is of the utmost important to gather the best possible knowledge on the ground behaviour and its failure mode during impact. The intensive study of the parameters evaluated for the impact tests (especially initial velocity, acceleration maximum and plateau value, rotation rate after impact, maximum penetration depth, block and slope characteristics) revealed the problem to be a very complex combination of different failure modes. In the following a possible interpretation of the failure process due to vertical and lateral loading by impacts is proposed.

During impact, the ground material undergoes an impulsive loading. As mentioned by authors who have studied dynamic loading phenomenon on sandy ground materials (as e.g. Selig & McKee, 1961), the ground reaction and failure mode differ for static and dynamic loading. Whereas for static loading the ground material generally fails along clearly defined shear surfaces, Selig & McKee [1961] observed no clearly defined shear surface for dynamic loading tests. The failure pattern corresponds more to the ground distortion occurring during static loading of loose sand (Figure 4.44). Only after repeated impulsive loading of the footing, a clear shear failure pattern was observed.

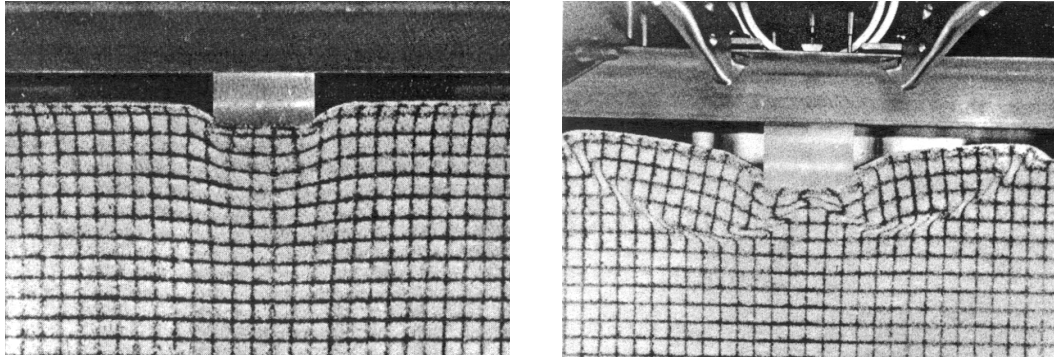


Figure 4.44: Failure pattern for dynamically (left) and statically (right) loaded dense, dry sand. Whereas the static load provokes a global failure (right), the dynamic load distorts the ground locally (left); after Selig & McKee [1961].

Applied to the present case of impact tests on slightly compacted, dry sand, these results and the occurrence of a residual acceleration value (plateau) suggest the assumption of the following ground failure mode being a combination of two stages:

In a first phase, the ground material is loaded impulsively, that is to say with a very high load (mostly much higher than the maximum bearing capacity of the ground material) in a very short time. In this phase, a ground compaction with **local shear failure** resulting in a ground distortion (as described by Selig & McKee [1961], Figure 4.44, left) takes place right under the block as it penetrates the ground. Additionally, the sand directly beyond the block is displaced down- and sideways by the block penetrating the ground. After the paroxysm of the shock, the block is still but less decelerated by the resistance of the ground material and continues to penetrate the ground. The maximum penetration depth (measured in vertical direction) is thus reached after the paroxysm of the shock for the instant at which the normal velocity component v_n equals to zero. In this post-paroxysm phase, two different phenomena are observed:

- Either the normal velocity (being defined as negative for approaching the ground and positive for separation) of the block increases quite linearly, passes through zero (changing direction) and increases further linearly till it reaches its maximum (positive) value for which the impact is defined to be terminated. In this case, no residual acceleration in form of a plateau is observed (Figure 4.45, left).
- In the second case, the normal velocity increase shows two phases: a first with intense increase and a second with quite linear, less intense increase (Figure 4.45, right). This signifies a lower decreasing rate of the approaching velocity as well as a phase of quite constant deceleration of the block. Evidently, from this time on, the ground offers less resistance to

the block. In case this phenomenon occurs, a second ground failure mechanism is supposed to take place, beginning with the formation of the acceleration plateau: the **global shear failure** (Figure 4.44, right) along a clearly defined shear surface. The justification of this assumption is presented in the following.

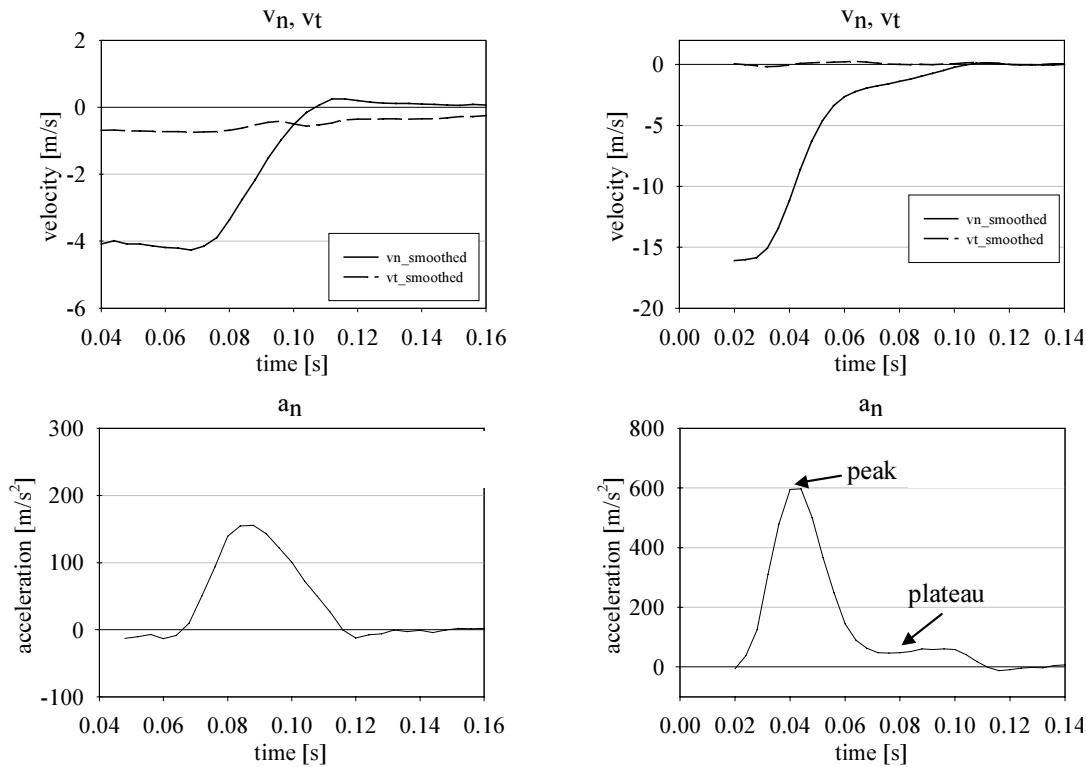


Figure 4.45: Typical forms of the acceleration wave and the corresponding velocity versus time observed for the impact tests on a small- and half-scale: low energy impact without acceleration plateau (left, H2e1L3) and high energy impact with acceleration plateau (right, M1e4L1).

A comparison of the maximum bearing capacity of the ground for circular footings with the radius of the block at maximum

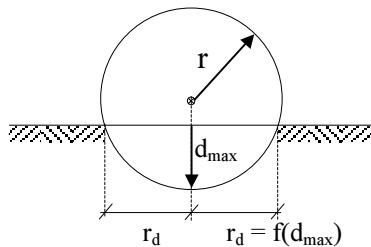


Figure 4.46: Dependency of the penetration radius r_d on the penetration depth d_{max} .

penetration depth r_d ($r_d = \sqrt{2 \cdot r \cdot d_{max} - d_{max}^2}$;

Figure 4.46) after the method proposed by Lang & Huder [1990] reveals a surprisingly good correlation between the theoretically evaluated bearing capacity and the force acting on the ground during the acceleration plateau phase (Figure 4.47).

The acting force $F_{plateau}$ equals the product of the block mass m and the mean acceleration value for the plateau. The maximum bearing capacity is evaluated after Lang & Huder [1990] by means of

the formula given in equation (4-10), which is based on the bearing capacity theory of Terzaghi for infinite long, rectangular foundations. The maximum bearing stress σ_f is defined to be:

$$\sigma_f = c \cdot N_c + (\gamma t + q) \cdot N_q + \frac{1}{2} b \cdot \gamma \cdot N_\gamma \quad (4-6).$$

As the cohesion c is equal to zero and the lateral load is assumed to be zero as well, equation (4-6) is simplified to:

$$\sigma_f = \gamma t \cdot N_q + \frac{1}{2} b \cdot \gamma \cdot N_\gamma \quad (4-7)$$

with γ being the unit weight of the ground material, t being the foundation depth from sole to ground surface for buried foundations, b being the foundation width and the bearing capacity factors N_q and N_γ being given by the following formulations:

$$N_q = e^{\pi \cdot \tan \varphi} \cdot \tan^2 \left(45^\circ + \frac{1}{2} \varphi \right) \quad (4-8)$$

$$N_\gamma \approx 1.8 \cdot (N_q - 1) \cdot \tan \varphi = 1.8 \cdot \left(e^{\pi \cdot \tan \varphi} \cdot \tan^2 \left(45^\circ + \frac{1}{2} \varphi \right) - 1 \right) \cdot \tan \varphi \quad (4-9)$$

with φ being the internal friction angle of the soil in degree [°]. The equation (4-9) represents the upper limit of the values given for N_γ in literature. To respect the shape and the finite length of the foundation and special features as inclined load, inclined sole or inclined ground surface, five factors s , d , i , g and b' are used:

$$\sigma_f = \gamma t \cdot N_q \cdot s_q \cdot d_q \cdot i_q \cdot g_q \cdot b'_q + \frac{1}{2} b \cdot \gamma \cdot N_\gamma \cdot s_\gamma \cdot d_\gamma \cdot i_\gamma \cdot g_\gamma \cdot b'_\gamma \quad (4-10)$$

with s_q and s_γ being form factors, d_q and d_γ being factors accounting for the depth, i_q and i_γ being load inclination factors, g_q and g_γ being factors accounting for the slope inclination and finally b'_q and b'_γ being factors for the sole inclination.

In the present case, the foundation chosen to represent the block is assumed to be a circular disk. By this simplification, the spherical shape of the foundation sole is neglected. As a planar sole offers higher resistance to ground penetration than a spherical one, the maximum bearing capacity evaluated for this assumption is higher than in reality. Further, the radius of the foundation is assumed to equal the radius r_d of the block at ground surface level for the maximum penetration depth (Figure 4.46). In case of a horizontal ground surface, the foundation depth t is

assumed to be $d_{\max}/2$ to account for the spherical shape of the block base. The correction factors for N_q are evaluated according to Lang & Huder [1990] to:

$$s_q = 1 + \frac{b}{l} \cdot \tan \varphi = 1 + \tan \varphi \quad \text{for } b = l = 2r_d \text{ for circular foundations,}$$

$$d_q = 1 + 0.035 \cdot \tan \varphi \cdot (1 - \sin \varphi)^2 \cdot \arctan \frac{t}{b}$$

$$i_q = \left[1 - \frac{\frac{1}{2}T}{N + \frac{\bar{b} \cdot \bar{l} \cdot c}{\tan \varphi}} \right]^5 = \left[1 - \frac{1}{2} \cdot \tan \delta_R \right]^5$$

$$g_q = g_\gamma = \left(1 - \frac{1}{2} \tan \beta \right)^5$$

$$b'_q = e^{(-0.035 \cdot \alpha^\circ \cdot \tan \varphi)}$$

For inclined ground surfaces, the foundation depth t is assumed to equal zero, corresponding to a foundation placed on the ground surface. This assumption is admissible as the foundation depth on the “weak” side (downhill side) is very small. By this assumption the factor N_q , accounting for the gain of bearing capacity by the weight of the ground surrounding a foundation buried at a certain depth t , becomes zero. With these assumptions and with the foundation width $b = 2r_d$, the equation (4-10) is simplified to:

$$\sigma_f = r_d \cdot \gamma \cdot N_\gamma \cdot s_\gamma \cdot d_\gamma \cdot i_\gamma \cdot g_\gamma \cdot b'_\gamma \quad (4-11)$$

with (after Lang & Huder [1990]):

$$s_\gamma = 1 - 0.4 \cdot \frac{b}{l} = 0.6 \quad \text{for } b \text{ (width)} = l \text{ (length)} = 2r_d \text{ for circular foundations,}$$

$$d_\gamma = 1$$

$$i_\gamma = \left[1 - \frac{\left(0.7 - \frac{\alpha^\circ}{450^\circ}\right) T}{N + \frac{\bar{b} \cdot \bar{l} \cdot c}{\tan \varphi}} \right]^5$$

with α being the sole inclination relative to the horizontal, N and T the normal and tangential forces in the foundation plane and \bar{b} and \bar{l} the effective width and length in case of eccentric loading. With $c = 0$ (no cohesion) and $T/N = \tan \delta_R$, δ_R being the direction of the resulting force (relative to the normal) acting on the foundation sole, the load inclination factor equals to:

$$i_\gamma = \left[1 - \frac{\left(0.7 - \frac{\alpha^\circ}{450^\circ}\right) T}{N} \right]^5 = \left[1 - \left(0.7 - \frac{\alpha^\circ}{450^\circ}\right) \cdot \tan \delta_R \right]^5$$

$$g_\gamma = \left(1 - \frac{1}{2} \tan \beta \right)^5$$

$$b'_\gamma = e^{(-0.047 \cdot \alpha^\circ \cdot \tan \varphi)}$$

The maximum bearing capacity is evaluated for each impact configuration (different blocks, different slope angles...) after equations (4-10) ($\beta = 0^\circ$) respectively (4-11) ($\beta = 10^\circ$ - 30°) with the corresponding values for the correction factors. The internal friction angle φ of the ground material is assumed to equal the critical state friction angle (33° for the material S0-4). As the initial impact direction of the blocks is vertical, the sole inclination α is assumed to be zero (sole normal to impact direction). Also the load inclination δ_R is assumed to equal zero due to the fact that the vertical acceleration component a_y is used to calculate the acting force F_{plateau} . The corresponding maximum bearing load R_f is calculated to:

$$R_f = \sigma_f \cdot \pi r_d^2 \quad (4-12)$$

with r_d being the radius of the block at maximum penetration depth.

For the assumptions stated above and slope angles between 10° and 20° , the bearing load R_f corresponds very well to the force $F_{\text{plateau}} = m \cdot a_{y,\text{plateau}}$ applied to the ground during the acceleration plateau. Figure 4.47 exemplarily represents the correlation between the theoretical static bearing capacity R_f (calculated using the measured values of d_{max}) and the force $F_{\text{plateau}} = m \cdot a_{y,\text{plateau}}$ (calculated using the measured values of $a_{y,\text{plateau}}$) for the 100 kg sphere at slope inclinations of 10° and 20° , the 500 kg cylinder at $\beta = 10^\circ$ and the 1000 kg cylinder at $\beta = 20^\circ$. The straight line represents perfect agreement. The data having zero values for F_{plateau} correspond to impacts without observed acceleration plateau.

In case of $\beta = 30^\circ$, the acting force F_{plateau} is slightly higher than the theoretical bearing capacity (Figure 4.48). This effect probably is due to the fact that for $\beta = 30^\circ$ the slope is near its limit equilibrium. Thus, the ground failure corresponds more to a slope stability problem than to a ground bearing capacity. The formulation proposed by Lang & Huder probably reaches its limits of applicability, underestimating the ground volume offering resistance to failure (Figure 4.49).

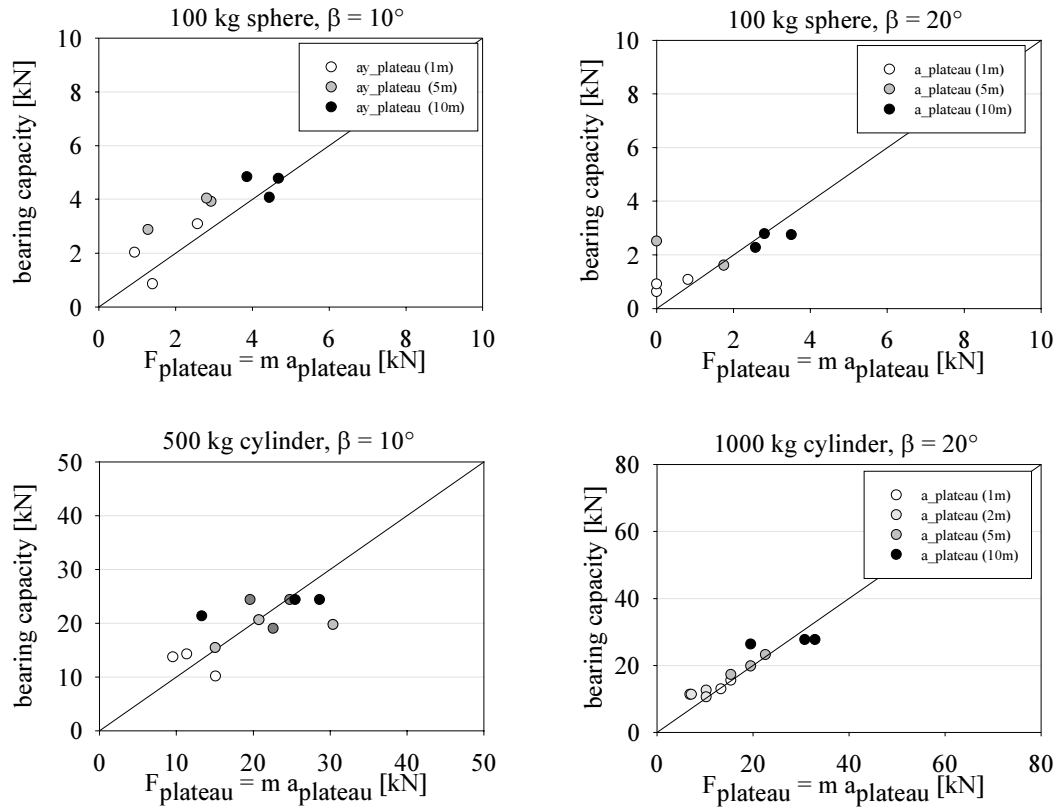


Figure 4.47: Correlation between maximum theoretical bearing capacity for circular footings loaded statically in vertical direction and the force $F_{plateau}$ acting between block and ground during the acceleration plateau.

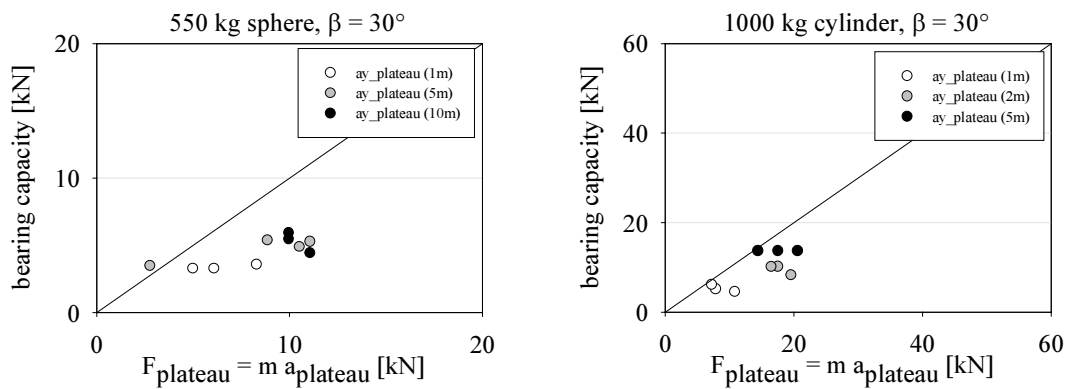


Figure 4.48: Correlation between R_f and $F_{plateau}$ for slopes inclined at 30° .

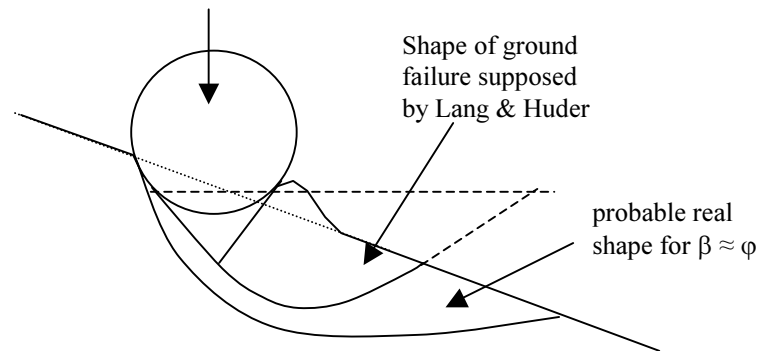


Figure 4.49: Sketch illustrating the difference in ground failure modes for the theory proposed by Lang & Huder for shallow foundations (valid for small slope angles) and the ground failure mode probably occurring for slopes at the limit of equilibrium ($\beta \approx \varphi$).

For vertical impacts on horizontal ground ($\beta = 0^\circ$), the calculated bearing capacity is systematically much larger than the observed acting force F_{plateau} (Figure 4.50, upper graphs). The following possible explication is provided:

A vertical impact on horizontal ground corresponds to a perfectly vertically loaded individual circular foundation. In this case ground failure is likely to occur all around the footing. This means that the ground failure can't no longer be stated as a two-dimensional problem but its three-dimensional form has to be respected. According to Terzaghi, Lang & Huder [1990] propose to account for a symmetrical ground failure either by reducing the parameters c (cohesion) and φ (friction angle) by one third (corresponding to a local shear failure problem respectively a local failure coming to the ground surface) or by substituting the foundation width b by a fictive value b^* being about half of the geometric width ($b^* \approx 1/2 \cdot b$).

Applying either the first or the second proposed correction to the present case, one observes a very good correlation in both cases (Figure 4.50 for $2/3 \cdot \varphi$, lower graphs).

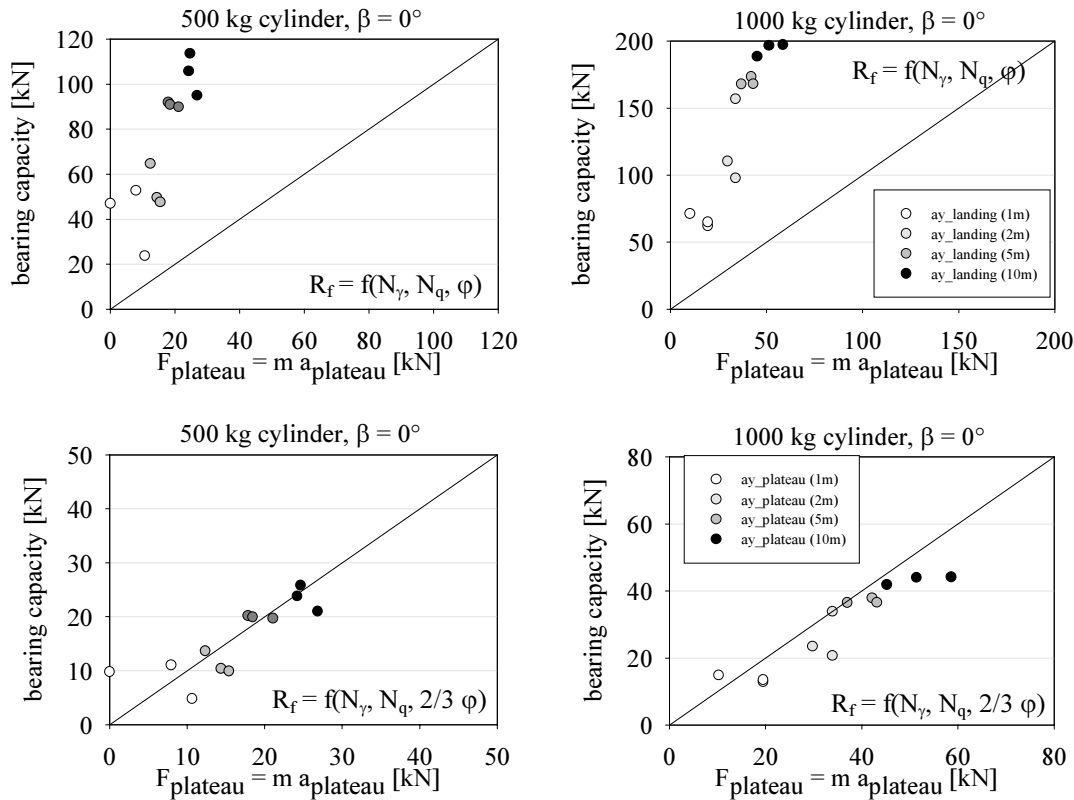


Figure 4.50: Impacts on horizontal ground: Very good correlation between bearing capacity R_f and F_{plateau} for a reduction of the friction angle φ by one third (lower line) to account for the rather local failure (coming to the ground surface).

These results signify that for the proposed assumptions the resisting force R_f corresponds to the acting force F_{plateau} . It is thus very likely that for impacts showing an acceleration plateau global shear failure occurs in the ground material. In case that no acceleration plateau occurs, the impact of the block provokes only local shear failure right under the block.

4.3.1.2 Conditions for which global shear failure occurs

The fact that global shear failure occurs in the ground for certain impacts (showing an acceleration plateau) but not for others (showing only an acceleration peak without distinct plateau) raises the question which conditions are necessary to provoke the ground to fail globally.

A systematic analysis of the half-scale test results on different criteria which are imaginable to provoke global shear failure for values exceeding a certain limit (as impulse, energy, penetration depth, block size etc.) reveals a clear limit criterion for the incident energy (Figure 4.51). In case of the performed impact tests, the impact energy equals the potential energy E_{pot} .

For impacts on horizontal ground ($\beta = 0^\circ$) with concrete filled blocks, global ground failure occurs systematically for an incident energy exceeding about 6 kJ. A transition zone can be defined for energies between about 3 and 5 kJ. Here, ground failure occurs twice for three tests, only for one of three tests no acceleration plateau is observed.

As the bearing capacity of a ground decreases with increasing slope angles, it is expected that the limit energy needed to provoke global ground failure decreases. This effect is clearly observed, as for slope angles of 20° an acceleration plateau is observed already once out of three tests for an energy level of about 1 kJ for the 117 kg sphere, whereas for slope angles of 30° the ground fails for all impact tests with concrete filled blocks.

However it is surprising that for $\beta = 10^\circ$ ground failure occurs for all tests with concrete filled blocks. Possibly this apparently contradictory finding is due to the different rebound mechanism for blocks on slopes of 10° and 20° : On slopes inclined at 10° most of the impact energy is transferred to the ground, only a small portion of it coming back to the block as restituted energy (elastic reaction of the ground). In this case, as we will see further on (Chapter 4.3.2.4), only a small part of the energy is transformed into rotation of the block. Thus, for slope angles of 10° , the impact energy transferred to the ground is sufficient to overcome the bearing capacity of the slope. For slope angles of 20° , however, a higher percentage (even a maximum one for falling heights up to 5 m) of the initial energy is transformed into rotation. Especially for small falling heights, the block movement changes abruptly from translation to a combination of rotation and translation as soon as the block enters in contact with the slope surface. Thus, in case of small falling heights, less energy is transferred to the ground material. As consequence the energy required to provoke global ground failure is not reached. For small falling heights, thus an energy limit comparable with the one observed on horizontal ground is noted.

In contrast, on slopes inclined at 30° (approaching the natural angle of limit equilibrium of the sand material) the low percentage of energy not transformed into rotation but transferred directly to the ground is sufficient to provoke global ground failure. Thus, all impact tests with concrete filled blocks exceed the limit energy.

The fact that only sparse cases of global ground failure are observed for the 150 kg sphere for falling heights up to 5 m on slopes larger 10° supports this thesis: As the 150 kg block has a much lower unit weight than the concrete filled blocks, during impact it penetrates less into the ground and consequently acquires a large rotational energy. The part of the incident energy transferred to the ground

in case of small falling heights this is not sufficient to provoke a global ground failure.

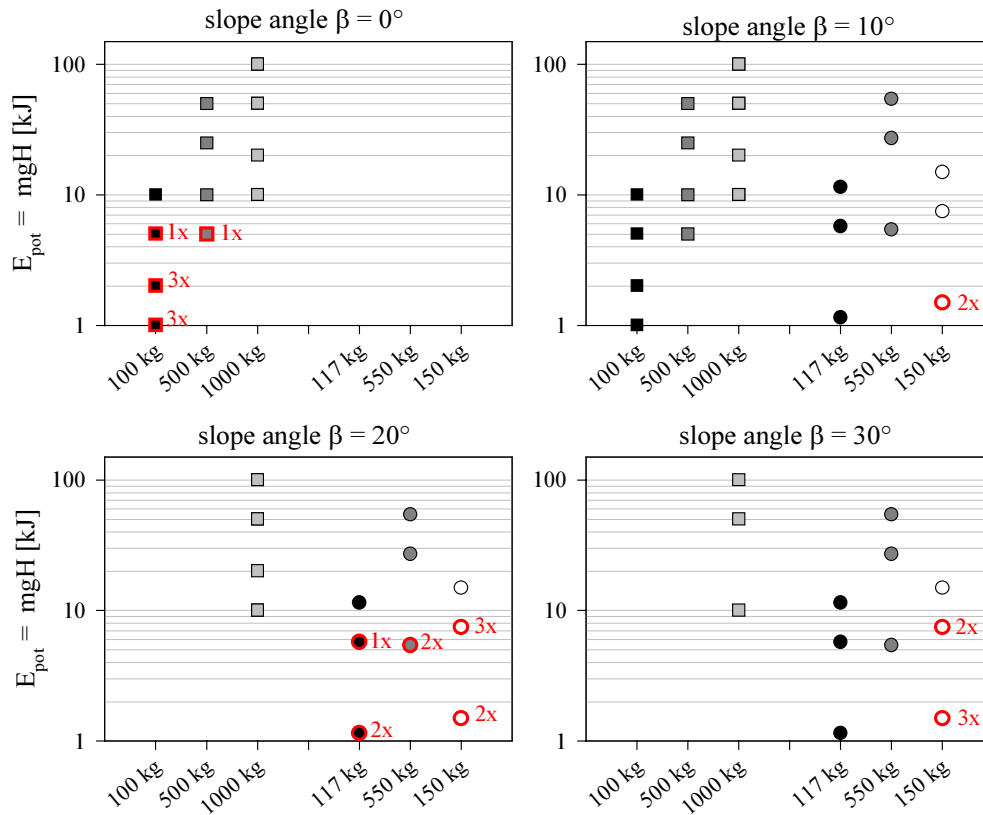


Figure 4.51: Critical impact energy for which global ground failure occurs: the red plots indicate the tests and the frequency (out of three tests) for which no acceleration plateau is observed.

As the bearing capacity R_f of a ground material and thus the occurrence of local or global ground failure depend strongly on the geomechanical characteristics of the soil (cohesion, friction angle, compaction, etc.), the limit energy values given in Figure 4.51 apply only for the used cohesionless sand material S0-4. The small-scale tests confirm this remark, as one notes for similar impact conditions different limits for global ground failure for different materials SF I, SF II and S0-4. Figure 4.52 reveals this difference for the materials S0-4 and SF I.

Comparing the energy limit found for the material S0-4 for small- and half-scale tests (half-scale (Figure 4.51): approx. 6 kJ, small-scale (Figure 4.52): > 4 J) illustrates that the block size has a non-negligible influence.

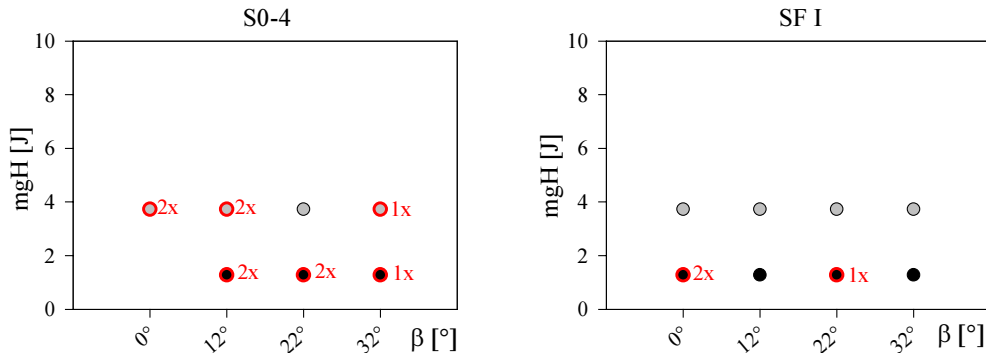


Figure 4.52: Variation of the critical impact energy for different granular materials (S0-4 and SF I) observed for the small-scale tests with the light (black plots) and the concrete (grey plots) sphere.

4.3.2 Quantification of some impact characteristics

4.3.2.1 Evaluation of d_{\max} through energy consideration

To determine the maximum penetration depth d_{\max} of a block into the ground material during impact, several propositions are stated in literature. These formulations are based on the assumption that the impact can be classified either as purely elastic, plastic or elastic-perfectly plastic [Montani-Stoffel, 1998]. For **purely elastic impacts**, the following formulations are stated:

- Hertz [1881] / Goldsmith [1960]:

$$d_{\max} = \left(\frac{5 \cdot m \cdot g \cdot H}{2\kappa} \right)^{2/5} \quad \text{with} \quad \kappa = \frac{4\sqrt{r}}{3\pi k} = \frac{4\sqrt{r} \cdot E}{3 \cdot (1 - \nu^2)} \quad (4-13),$$

m being the block mass, r its radius and E and ν the elasticity and the Poisson's ratio of the ground material. Comparing the vertically measured penetration values d_{\max} to the values calculated by means of this formulation, one finds a quite good correlation for impacts on horizontal ground, $\nu = 0.25$ and $E = 5000 \text{ kN/m}^2$ (Figure 4.53, left). However, the elasticity modulus E measured at the end of the impact tests amounts only to about 370 kN/m^2 (as $E = \frac{1}{4} \cdot \pi \cdot M_E \cdot (1 - \nu^2)$, with $M_E = 500 \text{ kN/m}^2$). Further, the influence that has been observed for a change of the slope inclination cannot be accounted for by means of this formulation. Consequently, the formulation proposed by Hertz and modified by Goldsmith cannot be applied without further consideration.

- Lang [1974]:

$$d_{\max} = \left(\frac{m \cdot g \cdot H}{M_E \cdot r} \right)^{1/2} \quad (4-14),$$

g being gravity, H the falling height, m and r the mass and radius of the block and M_E the plate bearing modulus. Also this formulation produces quite good correlations with the measured values of d_{\max} for impact tests on horizontal ground and a plate bearing modulus of 1000 kN/m^2 (Figure 4.53, right). The plate bearing modulus measured after the impact series, however, amounts only to about 500 kN/m^2 . Also here, the influence of the slope angle is not included. Thus, also this formulation cannot be applied without further considerations and correction factors.

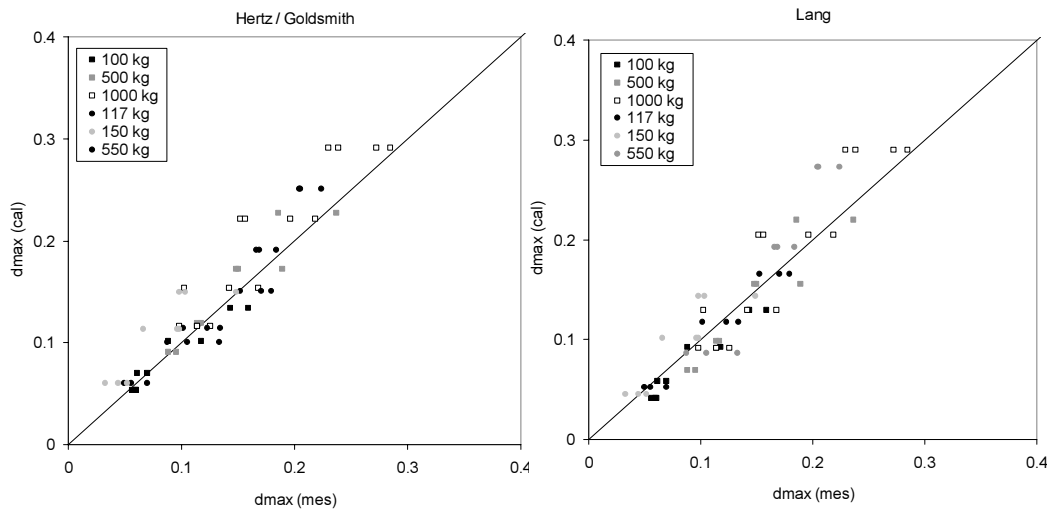


Figure 4.53: Correlation between values for d_{\max} measured for impact tests on horizontal ground and calculated after the method proposed by Hertz and Goldsmith (left) and Lang (right).

For **perfectly plastic** behaviour of the ground material, Heierli [1984] proposes a formulation based on the proposition of Habib [1979] for an impact of a hard block on a soft ground cushion. By drawing an energy balance, Heierli compares the impact energy $E_{\text{pot}} = mgH$ with the ground deformation energy $E_i = \delta \cdot R_f \cdot d_{\max}$:

$$d_{\max} = \frac{m \cdot g \cdot H}{R_f} \cdot \frac{1}{\delta} \quad (4-15),$$

with δ being a parameter depending on the impact velocity v_i and R_f being the bearing capacity of the ground for static loads.

To calculate the maximum ground penetration during impact supposing **elasto-plastic** ground behaviour, Azimi & Desvarreux [1988] propose the following

expression, which calculates the penetration depth without considering the energy loss during the plastic deformation of the ground material:

$$d_{\max} = 0.52 \cdot \left(\frac{m \cdot g \cdot H}{k} \right)^{1/2} \quad \text{with} \quad k = \frac{\pi}{2} M_E \cdot r \cdot \left(1 + \frac{r}{e} \right) \quad (4-16),$$

with e being the thickness of the damping ground layer.

Further, the Army [Poncelet; Lang, 1974; Zivilschutz, 1964] proposes an **empiric formulation** to determine the maximum penetration of a spherical projectile into the ground:

$$d_{\max} = \frac{1}{2} \cdot \frac{m}{A \cdot b} \cdot \sqrt{2gH} \quad (4-17),$$

with A being the area of the cross section of the projectile and b an empirically determined constant of the ground material ($b = 35$ for sandy soils). It has to be mentioned that, in terms of units, this formulation is not homogeneous.

As it can be seen from the cited formulations, the maximum penetration depth depends on the impact energy defined by the block mass m and the falling height H . The ground stiffness is taken into account by all formulations either by means of an elasticity modulus E , a plate bearing modulus M_E or an empirical factor related to a certain ground material. Table 4.6 lists the exponents stated for the parameters proposed to influence the penetration depth.

Exponent b	impact energy $E_{\text{pot}} = mgH$	block radius r	other parameters
Hertz / Goldsmith	2/5	-1/5	$E: -2/5, \nu: 2/5$
Lang	1/2	-1/2	$M_E: -1/2$
Heierli	1	(by R_f)	$R_f, \delta: -1$
Azimi & Desvarreux	1/2	-1/2	$M_E: -1/2$
Poncelet	$m: 1; gH: 1/2$	-2	b

Table 4.6: Exponents stated in literature expressing the relation between d_{\max} and the impact energy E_{pot} , the radius r of the block and further parameters describing the elasticity or strength of the ground material.

To develop an expression for d_{\max} , the theory of energy conservation is used. Similarly to the proposition made by Heierli [1984], an energy balance is drawn. However, not the resistance of the ground R_f but the energy dissipated during impact is compared to the incident energy of the block. Assuming a perfectly

plastic impact ($v_r = 0$ after impact), the integral of the dissipated energy $m \cdot a_y(t) \cdot d(t)$ equals the potential energy of the block E_{pot} . Using the product of the maximum values of both a_y and d , the equation $m \cdot a_{y,max} \cdot d_{max} = E_{pot}$ is not performed, as the maxima of the acceleration and the block penetration do not occur simultaneously. However, based on the hypothesis of a perfectly plastic impact on a spring-mass-oscillator, Lang [1974] and Montani-Stoffel [1998] prove the proportionality between the product of the maximum values $m \cdot a_{y,max} = F_{y,max}$ and d_{max} and the impact energy E_{pot} to be as follows:

$$m \cdot a_{y,max} \cdot d_{max} = F_{y,max} \cdot d_{max} = f \cdot E_{pot} \quad (4-18),$$

where the multiplication factor f equals 2 for both extremes: a damped and an undamped oscillator. This proportionality is stated also by other authors, using slightly different multiplication factors:

- Parting from the theory of contacts developed by Hertz [1881], one finds proposes a factor f of 2.5.
- For impacts on a gallery roof covered with a damping material, Heierli [1984] proposes different factors depending on the thickness e of the damping layer ($e = 1\text{m}$: $f = 1.86$; $e = 0.5\text{m}$: $f = 1.63$), the acceleration being measured on the surface of the gallery roof.
- Based on the results gained by impact tests on different damping layers, Montani-Stoffel [1998] proposes a factor f of 1.6 for impact tests on cushions covering a protection gallery model and $f = 1.5 \cdot \exp(r/(1.5 \cdot e))$ for impacts on a soil layer reposing on firm ground. The latter expression shows that f depends on the thickness of the damping layer e as well as on the radius of the block.

Further, Montani-Stoffel mentioned a slight influence of the plate bearing modulus M_E on the factor f , which is however stated to be quasi insignificant. As M_E has an influence on both the maximum penetration and the maximum acceleration during impact, it could happen that by the multiplication of both factors the influence of M_E disappears.

Comparing the product of $F_{y,max} \cdot d_{max}$ with the potential energy E_{pot} of the block at impact for all tests performed on a half-scale, one finds indeed a linear relation between both terms. The multiplication factor f ranges between 0.7 and 1.7 depending on the various impact tests.

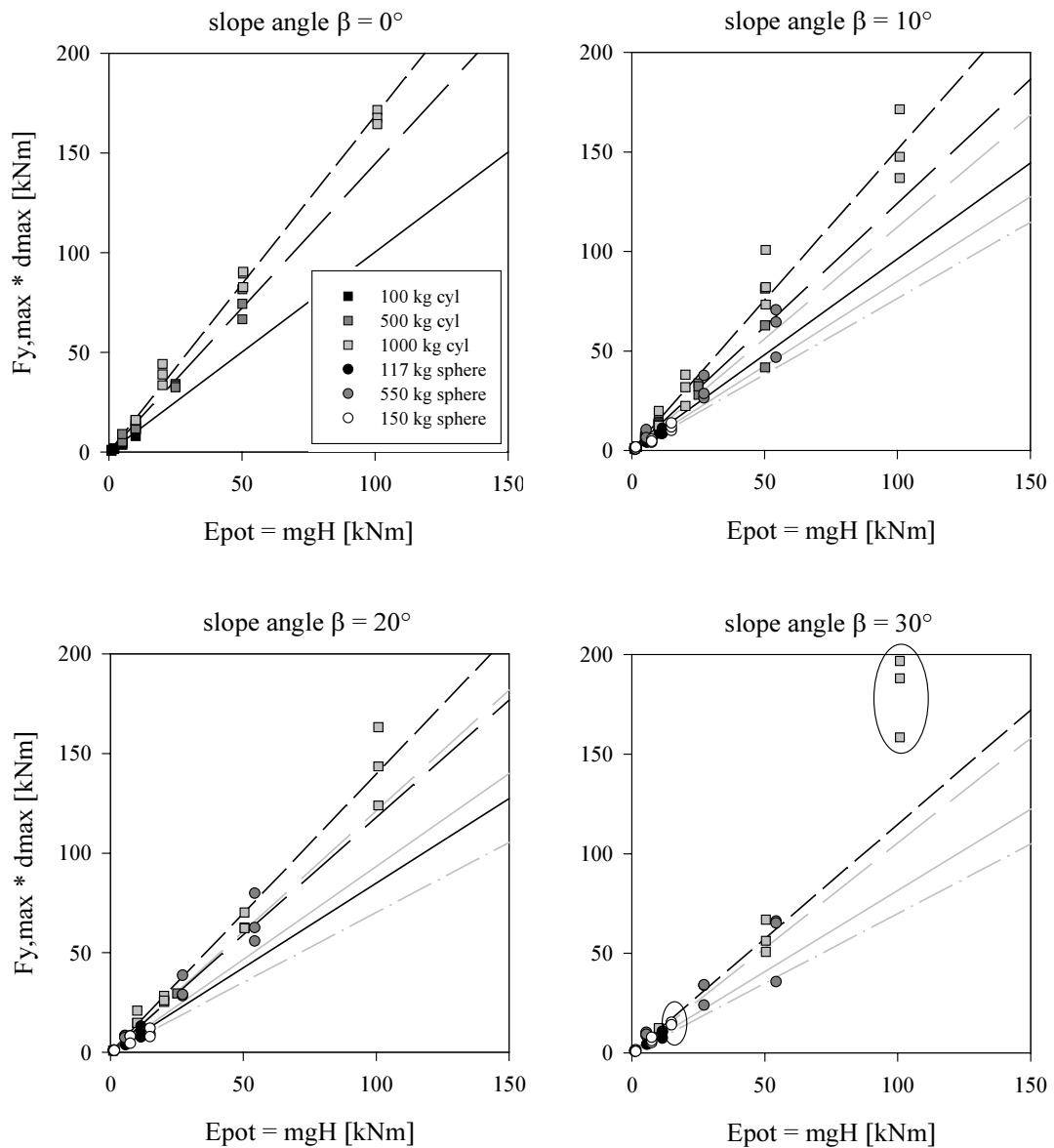


Figure 4.54: Relation between $F_{y,max} * d_{max}$ and the potential energy E_{pot} for tests on different slope inclinations.

As it can be seen from Figure 4.54, the multiplication factor f depends not only on the block characteristics (mass and radius) but also on the slope angle β . For the impact tests with large falling heights ($H = 10$ m) on the slope inclined at 30° , a change in the rebound mechanism can be stated for the cylindrical 1000 kg block and the spherical 150 kg block (oval marks in Figure 4.54). This divergence is due to a change in the rotational energy rate of the blocks: The higher the impact velocity, the deeper the blocks penetrate into the ground and the lower is the rotation induced during the impact. As it will be presented further on (Figure 4.66), in case of the discussed values the rotational rate in fact is found to be very low, justifying this hypothesis.

Analysing the influence of the block mass m and the block radius r on the factors f evaluated for all impact tests, one finds that m has an exponent between 0.16 and 0.42 (Figure 4.55). A clear difference can be found between the values gathered for the cylindrical blocks and the spheres: the mean value of the exponent for the block mass for all slope angles is 0.2 for the three cylinders (left diagram), whereas for the two concrete filled spheres it is 0.17 (right diagram). For spheres with same diameter but different unit weight (lower graph), the mean exponent is about 0.34. In case of blocks with constant unit weight, the exponent for the radius is about three times the exponent of the mass. As $m = 4/3 \cdot \pi \cdot r^3 \cdot \rho$, the evaluated exponents prove to be logical.

It should be mentioned, that the form of the function $f = a \cdot m^b$ was chosen as it fits very well the trends observed for the cylindrical blocks. As for all investigations concerning the spherical blocks only two data points are available (see left and lower diagrams of Figure 4.55), any function would produce a perfect fit ($R^2 = 1$). However, it was decided to keep the same form of function adopted for the cylindrical blocks.

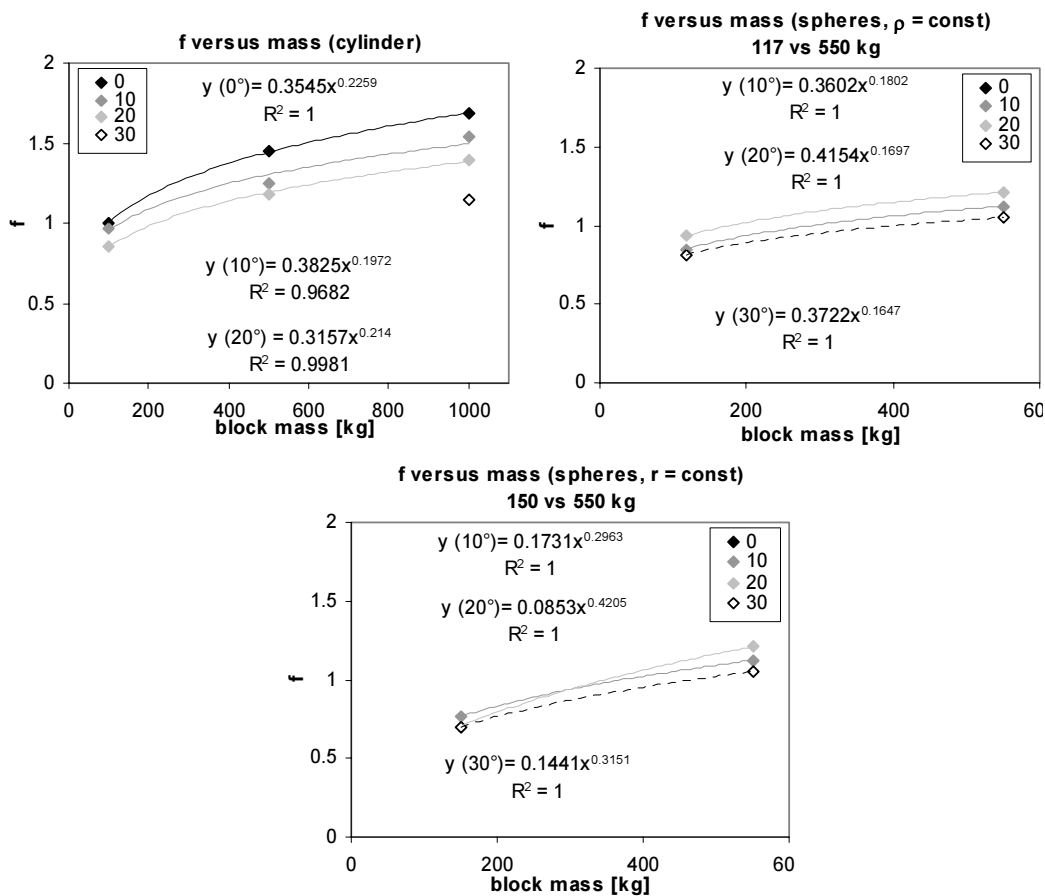


Figure 4.55: Influence of the block mass m on the factor f : the exponent quantifying the block mass influence depends on the block geometry.

To simplify the problem, the exponent for the mass m is fixed to 0.2, even though by this simplification the very complex relation between the block mass m and its radius r is not perfectly sorted out in case of blocks with different unit weights. As none of the used blocks have exactly the same weight but different diameters and only two blocks with perfectly same radii but different weights are used for the impact tests, the lack of information on the respective influence of m and r hinders a more precise quantification. The correlation between the measured data and the curves fitted to them in form of a function $f = C_1 \cdot m^{0.2}$ is still very good, even if in case of the spheres the excellent correlation is not surprising as only two data points are available (Table 4.7: determination coefficient R^2).

Table 4.7 further shows the values evaluated for C_1 . A close investigation of the constant C_1 reveals its dependence not only on the slope angle β , but also on the block geometry: whereas the slope inclination has only little influence on the spheres, for cylindrical blocks a clear decrease is stated. This is due to the eccentricity of the point of first contact between block and slope surface, being larger for the cylindrical than for the spherical blocks. This provokes a larger rotational rate of the cylindrical blocks compared to the spheres, which is most distinct for steep slopes (see Chapter 4.3.2.4). That means that for cylindrical blocks on steep slopes a higher proportion of the initial impact energy is directly transmitted into rotational energy and does not participate in the creation of the crater.

As the internal friction angle φ limits the natural slope angle β , it seems logical to create a relation between both parameters. Thus, the function describing the dependency of C_1 on changing slope angles is expressed by the ratio of β to φ . As shown in Figure 4.56, a linear relation can be stated between C_1 and β/φ .

$f = C_1 \cdot m^{0.2}$	cylinder ($\rho = \text{const}$)		sphere ($\rho = \text{const}$)		sphere ($r = \text{const}$)	
	C_1	R^2	C_1	R^2	C_1	R^2
$0^\circ / 33^\circ = 0$	0.4166	0.99				
$10^\circ / 33^\circ = 0.303$	0.3768	0.96	0.3214	0.99	0.3040	0.90
$20^\circ / 33^\circ = 0.606$	0.3446	0.99	0.3488	0.97	0.3112	0.74
$30^\circ / 33^\circ = 0.909$	0.2967 ¹	-	0.3038	0.96	0.2820	0.87

Table 4.7: Constants C_1 and standard deviation R evaluated for different block forms for all slope angles β .

¹ As only tests with the 1000 kg cylinder are performed on a slope of 30° , this value is evaluated for the concrete filled spheres and the largest cylinder, supposing similar behaviour for both block forms. This assumption can be justified by the general trend of C_1 being very close for all block forms on $\beta = 30^\circ$ (refer to Figure 4.56).

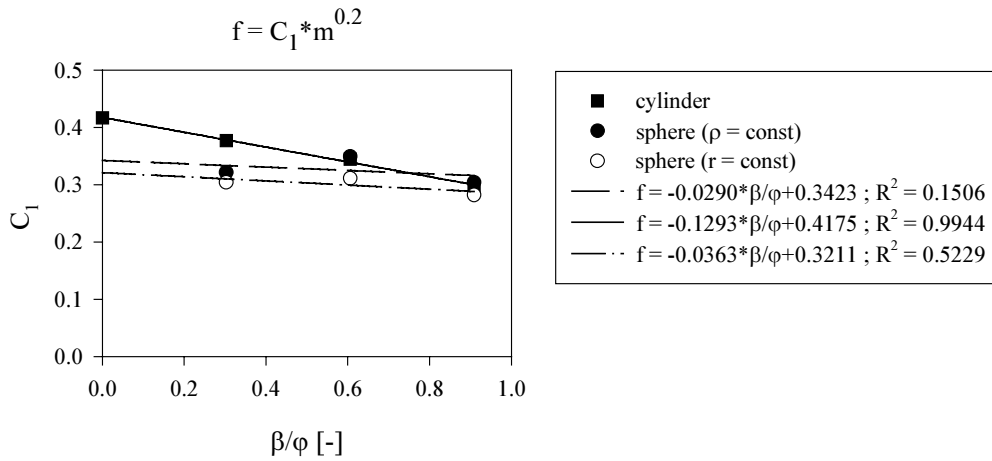


Figure 4.56: Linear regression between C_1 and the ratio β/φ , showing clearly the dependence on the block geometry.

By means of the gathered information, the following formulation is proposed to express the multiplication factor f :

$$f = m^{0.2} \cdot \begin{cases} \left(-0.029 \cdot \frac{\beta}{\varphi} + 0.3423 \right) & ; \text{ sphere} \\ \left(-0.1293 \cdot \frac{\beta}{\varphi} + 0.4175 \right) & ; \text{ cylinder} \end{cases} \quad (4-19)$$

This formulation is valid for $\beta/\varphi < 1$ and a block density of about 2500 kg/m^3 (as it is the case for the concrete filled blocks). For other densities or irregular block forms, this formulation cannot be applied without further consideration. For instance, as to see in Figure 4.56, the multiplication factor f is slightly lower for blocks with same diameter but decreasing density (700 kg/m^3 , hollow circles) compared to concrete filled blocks (2500 kg/m^3 , black circles).

Therefore, it is very likely that the multiplication factor f decreases with an increase of the ratio r/ρ which can be due either to a change of block radius or volume mass. A quantification of this effect by means of the present tests results is not reasonable as only two blocks with different volume masses are used. Further impact tests should therefore be performed to quantify correctly the influence of the volume mass on the multiplication factor f .

Applying the expressions given in equation (4-19) to the performed impact tests, one finds a very good correlation between the calculated values (according to equation (4-19)) of the multiplication factor f and the values calculated from the measurements (Figure 4.57).

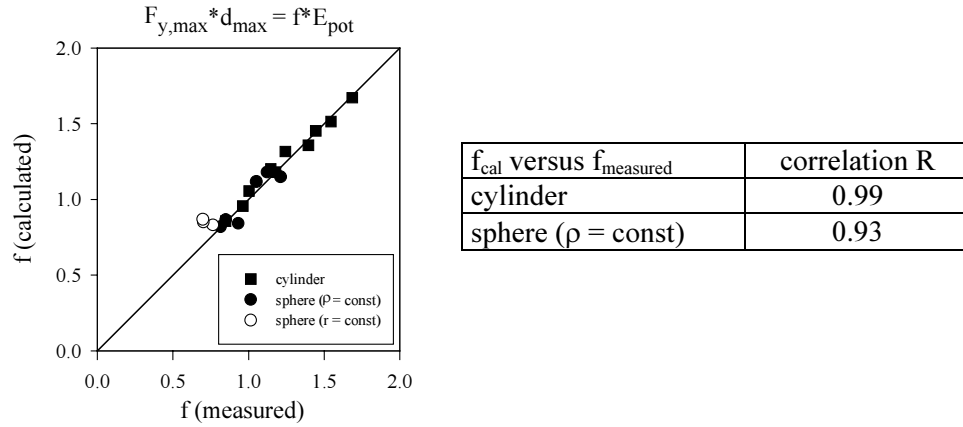


Figure 4.57: Correlation between the calculated and measured values of the multiplication factor f . The resulting correlations are given in the table (right). The values of $f_{measured}$ are calculated from measurements.

In terms of units, the proposed formulation is unfortunately not homogeneous. In the framework of this thesis it was not possible to find a homogeneous formulation fitting the measured data and being at the same time physically meaningful. To fulfil the homogeneity of the relation, further research could investigate two possibilities:

The first is to bring the block mass m in relation to the mass of the ground moving during the impact. This would lead to an expression of the form $\frac{\rho_{block} \cdot V_{block}}{\rho_{ground} \cdot V_{ground}}$, ρ

being the density and V the volume of block and ground respectively. The problem occurring here is the determination of the ground volume moving during the impact, which reveals to be difficult to assess.

The other possibility is to use a relation between the acting and resisting forces by an expression of the form $\frac{m \cdot g}{M_E \cdot A}$, g being the gravity, M_E the plate bearing

modulus and A a surface which would have to be determined.

However, up to now, no meaningful solution could be found for both propositions.

Introducing the expression for f (equation (4-19)) in equation (4-18) yields the following equation for d_{max} :

$$d_{max} = \frac{E_{pot}}{F_{y,max}} \cdot m^{0.2} \cdot \begin{cases} \left(-0.029 \cdot \frac{\beta}{\varphi} + 0.3423 \right) & ; \text{ sphere} \\ \left(-0.1293 \cdot \frac{\beta}{\varphi} + 0.4175 \right) & ; \text{ cylinder} \end{cases} \quad (4-20)$$

In the following section 4.3.2.2, a relationship will be presented to express $F_{y,\max}$ by means of the potential energy and the ground stiffness. Substituting $F_{y,\max}$ in equation (4-20) by the expression proposed later on (equation (4-25)), d_{\max} can be written as follows:

$$d_{\max} = \frac{(mgH)^{0.4}}{1.15 \cdot M_E^{0.4} \cdot r^{0.6}} \cdot \begin{cases} \left(-0.029 \cdot \frac{\beta}{\varphi} + 0.3423 \right) & ; \text{ sphere} \\ \left(-0.1293 \cdot \frac{\beta}{\varphi} + 0.4175 \right) & ; \text{ cylinder} \end{cases} \quad (4-21)$$

As the formulation proposed for $F_{y,\max}$ is **not homogeneous** relative to the units, equation (4-21) neither is. The correlation with the measured values, however, is very good (Figure 4.58, left).

Reducing equation (4-21) to a **homogeneous** formulation yields a slightly different expression of the maximum penetration of spherical or cylindrical blocks impacting a granular slope:

$$d_{\max} = 1.3 \cdot \left(\frac{mgH}{M_E \cdot r^{0.5}} \right)^{0.4} \cdot \begin{cases} \left(-0.029 \cdot \frac{\beta}{\varphi} + 0.3423 \right) & ; \text{ sphere} \\ \left(-0.1293 \cdot \frac{\beta}{\varphi} + 0.4175 \right) & ; \text{ cylinder} \end{cases} \quad (4-22)$$

The first term of the homogeneous expression is very similar to the one proposed by Lang. Main differences are the exponent of the radius (0.5 instead of 1 due to the global exponent of 0.4) and of the first term (0.4 instead of 0.5 proposed by Lang) as well as the multiplication factor accounting for block shape and slope angle. On the other hand, the exponent of 0.4 corresponds to the one proposed by Hertz for the ratio between potential energy and ground stiffness.

Figure 4.58 represents the correspondence between measured and calculated values of d_{\max} for both the non-homogeneous (equation (4-21), left graph) and the homogeneous (equation (4-22), right graph) formulations. Even if the fit for the non-homogeneous formulation is better ($R^2 = 0.91$), the homogeneous formulation yields as well very good results ($R^2 = 0.87$). For the latter, only about 10 % of the calculated data don't meet the error interval of the order of approximately ± 2.5 cm, represented as dotted lines.

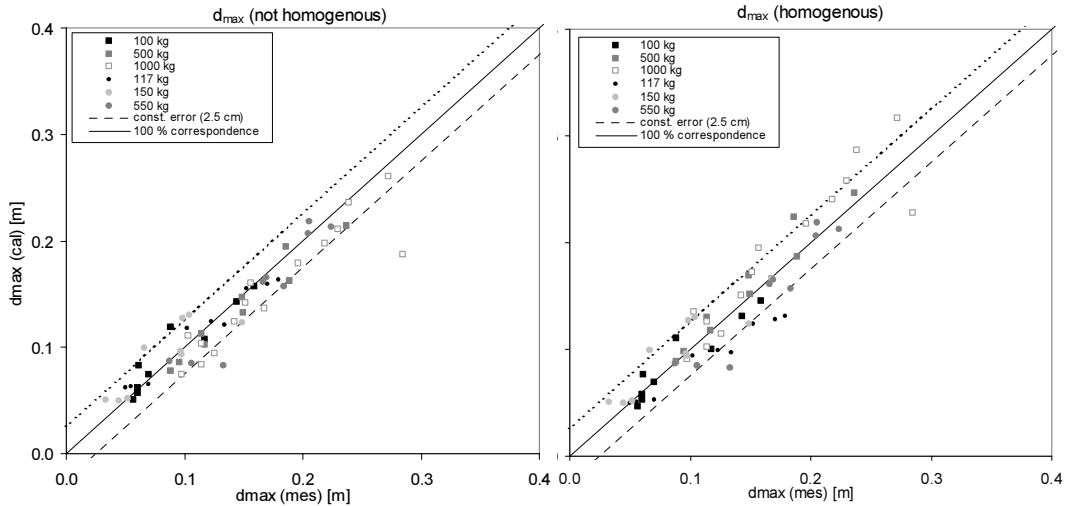


Figure 4.58: Correlation between measured and calculated values of the maximum penetration depth d_{max} . Left: non-homogeneous formulation (equation (4-21)), right: homogeneous formulation (equation (4-22)).

4.3.2.2 Evaluation of the acceleration force $F_{y,max}$ and the acceleration $a_{y,max}$

To be able to determine the maximum acceleration $a_{y,max}$ and the corresponding maximum force $F_{y,max} = m \cdot a_{y,max}$ acting between block and ground at the acceleration peak, a formulation is developed expressing $F_{y,max}$ in dependence of the incident energy of the block. For the performed tests, the energy of the blocks at impact equals the potential energy $E_{pot} = mgH$ (pure translation). Quantifying the influence of the falling height and thus of the potential energy on the maximum acceleration force $F_{y,max}$, one finds an exponent of 0.6 for E_{pot} . This corresponds to the influence of E_{pot} on the impact force proposed by Hertz for elastic impacts of two spheres. Also Montani-Stoffel [1998] found 0.6 as exponent for E_{pot} for impact tests performed on granular materials resting on a concrete slab.

Further, it seems logical that the maximum acceleration of the block and thus $F_{y,max}$ depends on the stiffness of the ground material: the impact of a hard sphere on a hard ground results in a much shorter contact time and a higher maximum acceleration of the block than a comparable impact on a soft material. As for the present half-scale impact tests only one ground material is used, the influence of the plate bearing modulus M_E can not be quantified directly based on the test results. In Montani-Stoffel's thesis [1998], the influence of M_E on the maximum force acting on the block during the acceleration peak has been evaluated by means of a distinct element model and validated by means of the performed impact tests. The same influence of M_E is supposed to be valid for the present

tests, i.e. with an exponent of 0.4. The acceleration force $F_{y,\max}$ thus can be written as:

$$F_{y,\max}^{(E_{\text{pot}})} = C_1 \cdot M_E^{0.4} \cdot (mgH)^{0.6} \quad (4-23).$$

For this expression the factor C_1 and thus $F_{y,\max}$ is found to be independent on the slope inclination β (Figure 4.59) for all concrete filled blocks. A very slight increase of C_1 and thus $F_{y,\max}$ can be noted for the hollow sphere (150 kg) for increasing slope angles: due to its low density, the hollow sphere penetrates only little in the ground material, promoting the transition from pure translation to rolling movement already for small slope angles (as described in Chapter 4.2.1). As result, a part of the impact energy is transferred directly into rotation, explaining the lower acceleration force at the paroxysm of the shock. As the influence is very low (exponent of 0.1), this effect is neglected in the following.

Further, C_1 depends on the block mass m as well as on its radius r at the impact point (contact radius). The separate influence of block mass, radius and density could only be verified by means of the tests performed with two blocks: comparing the acceleration measured for the 150 and the 550 kg spheres (same radius!) allows to evaluate the pure influence of the mass, whereas the (nearly pure) influence of the radius is evaluated comparing the test results of the 117 and the 150 kg sphere (nearly same mass, different radius). Therefore, further studies should be performed to verify the formulation proposed in (4-24) with respect to the particular influence of the block mass and the radius.

After an accurate fitting process, the best correlation between the measured and calculated values of $F_{y,\max}$ is found for the following expression of C_1 :

$$C_1 = 1.15 \cdot m^{0.2} \cdot r^{0.6} \quad (4-24)$$

With such a factor C_1 the equation (4-23) is not homogeneous relative to the units. However, it was not possible to find an equivalent homogeneous formulation, for which the influence of the block mass and the contact radius is respected nearly as accurately as for the presented formulation.

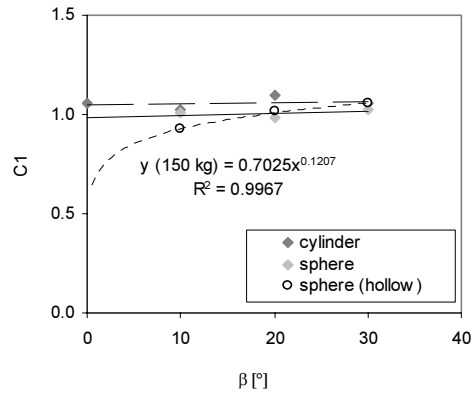


Figure 4.59: Independence of the factor C_1 on the slope angle β for all concrete filled blocks.

The resulting **non-homogeneous** formulation for $F_{y,\max}$ depending on the potential energy E_{pot} thus can be written as:

$$F_{y,\max}^{(E_{\text{pot}})} = 1.15 \cdot m^{0.2} \cdot r^{0.6} \cdot M_E^{0.4} \cdot (E_{\text{pot}})^{0.6} \quad (4-25).$$

This formulation is very similar to the one proposed by Montani-Stoffel [1998] (refer to equation (2-42)) for impacts on granular material resting on a concrete slab. Unlike the formulation proposed in equation (4-25), the formulation proposed by Montani-Stoffel is homogeneous. However, the latter is valid only for blocks with a constant relation between mass and contact radius, whereas the equation given above allows to distinguish the respective contributions of mass and impact radius. Furthermore, it could be shown that the slope angle has no significant influence on the maximum acceleration force.

The correlation between measured and calculated values of $F_{y,\max}(E_{\text{pot}})$ is excellent and is presented in Figure 4.60.

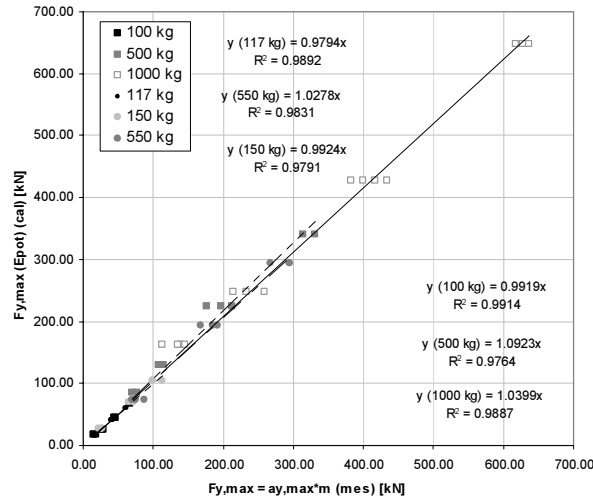


Figure 4.60: Correlation between the values of $F_{y,max}$ derived from the measured maximum acceleration $a_{y,max}$ times the block mass (x-axis), and calculated by means of equation (4-25) (y-axis).

4.3.2.3 Relation between acceleration force $F_{y,max}$ and block penetration d_{max}

Parting from the formulations given in (4-22) and (4-25), the maximum acceleration force can be expressed in function of the maximum penetration d_{max} . The resulting formulation presents itself as follows:

$$F_{y,max}^{(d_{max})} = 0.77 \cdot m^{0.2} \cdot r^{0.9} \cdot d_{max}^{1.5} \cdot M_E \cdot \begin{cases} \left(-0.029 \cdot \frac{\beta}{\varphi} + 0.3423 \right)^{-1.5} & ; \text{ sphere} \\ \left(-0.1293 \cdot \frac{\beta}{\varphi} + 0.4175 \right)^{-1.5} & ; \text{ cylinder} \end{cases} \quad (4-26)$$

Verifying the correlation between the values calculated for $F_{y,max}(d_{max})$ by means of this formulation and the “measured” ones (Figure 4.61), one realises a much lower correlation than the one observed for $F_{y,max}(E_{pot})$. This is due to the fact, that the values calculated for d_{max} using equation (4-22) do not correlate perfectly with the measured values.

The proposed formulation corresponds rather well to the one proposed by Montani-Stoffel [1998] (refer to equation (2-44)), evaluated for vertical impact tests on horizontal layers of granular material reposing on a concrete slab: also here, the plate bearing modulus M_E of the ground material has an exponent of 1 and the maximum penetration depth d_{max} with an exponent of 1.5. The formulation proposed in equation (4-26) adds a slight dependence of $F_{y,max}$ on the ratio between slope angle β and internal friction angle φ as well as a dependency

on the block mass and the contact radius by means of the factors $m^{0.2} \cdot r^{0.9}$. Both relations have in fact been observed for $F_{y,\max}(d_{\max})$ during the fitting process. As formulation (4-25) is not homogeneous relative units, the same goes for the present formulation.

To control the exponent b of the penetration depth, indicated to equal 1.5 by equation (4-26), the maximum force $F_{y,\max}$ derived from the measured maximum acceleration $a_{y,\max}$ is plotted versus the measured maximum penetration depth d_{\max} . Figure 4.62 reveals that the exponent of d_{\max} ranges between values of 1 and 2, the mean value for all impact tests being in fact 1.5. By a further investigation, the exponent b is found to be independent of the slope inclination β but to depend slightly on the block mass m (Figure 4.63). The dependency on the block radius corresponds to the one observed for the block mass.

To account for this dependency of the exponent b of the penetration depth d_{\max} on the block mass, the following expression could be introduced instead of the constant value of 1.5 (Figure 4.63). It was evaluated for the mean values of b over all slope angles β :

$$b = 0.3554 \cdot m^{0.23} \quad (4-27)$$

It is interesting to note that according to the theory of elastic impacts developed by Hertz, the maximum force depends on the penetration depth with an exponent of 1.5. Developing the same type of formulation (parting from vertical impact tests on horizontal granular soil material), Montani-Stoffel [1998] found an exponent of 1.5 for impacts on compacted ground material (gravel) reposing on a slab, whereas for impacts on the same material reposing directly on the shaft foundation an exponent of 2 is found. In case that the ground material reposing on the shaft foundation is not compacted, the exponent decreases to 1.5, being the same value found for impacts on the slab. This shows that not only the stiffness of the subjacent structure has an influence on the exponent of d_{\max} , but also the stiffness of the ground material. This seems logic as a compacted ground material reacts more elastic than a non-compacted one. However, quantification is not possible at the present stage of the research, as only impact tests on one ground material are performed on a half-scale.

However, as shown by Montani-Stoffel for impacts on different compacted ground materials, a further dependence on M_E is highly probable. As this influence cannot be quantified by means of the present impact test results, this expression is not yet introduced in the formulation given above. However, this is a very interesting point to investigate by means of further impact tests.

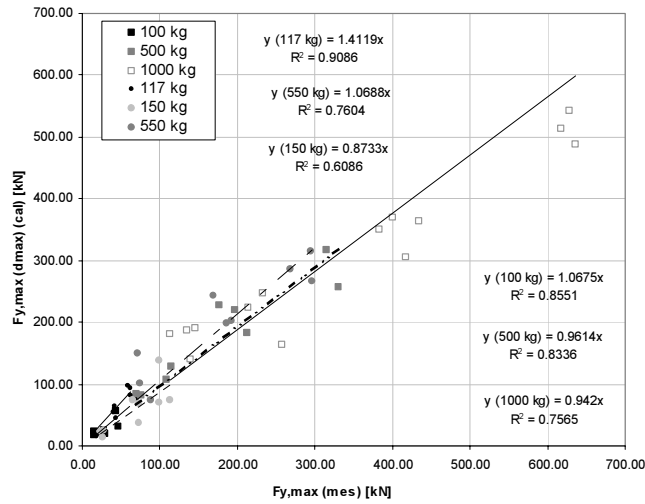


Figure 4.61: Correlation between “measured” and calculated values of $F_{y,max}(d_{max})$.

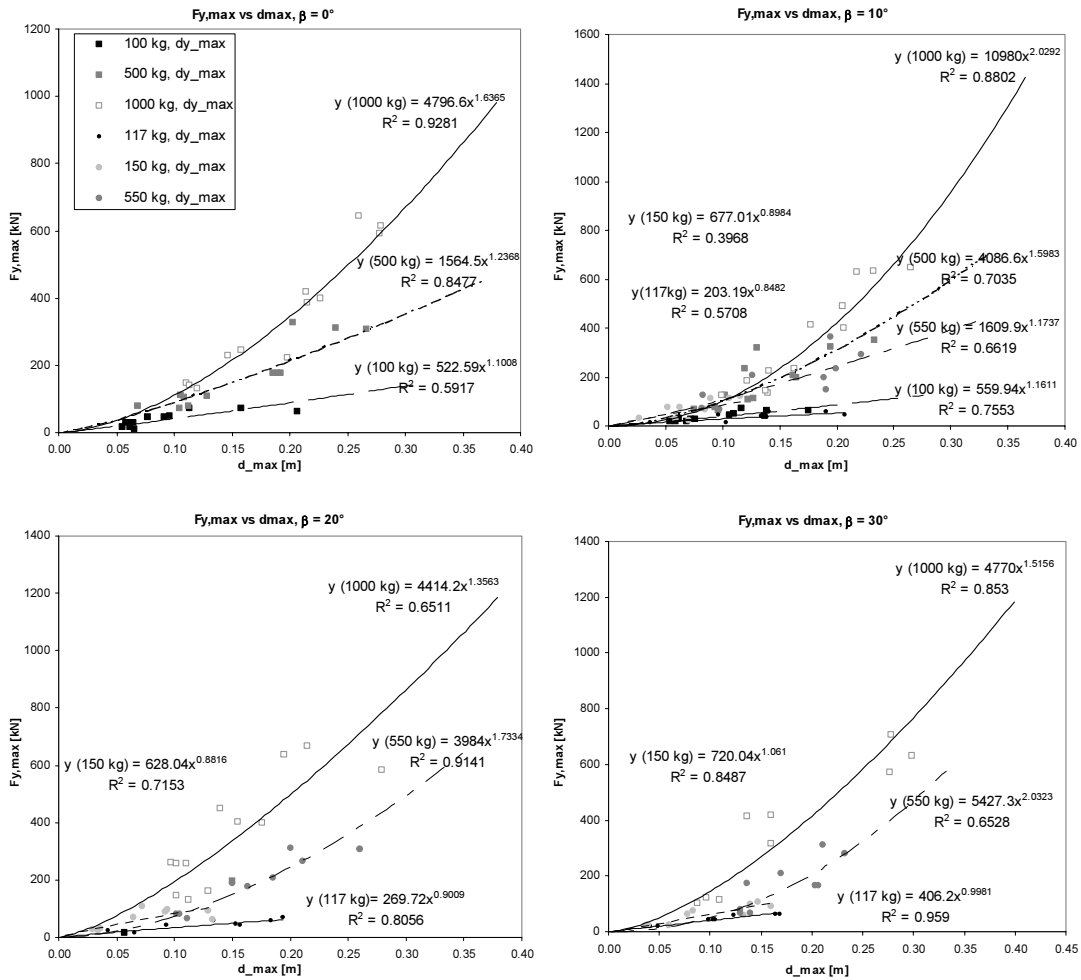


Figure 4.62: Relation between measured $F_{y,max}$ and d_{max} : The exponent of the penetration depth d_{max} varies between 1 and 2.

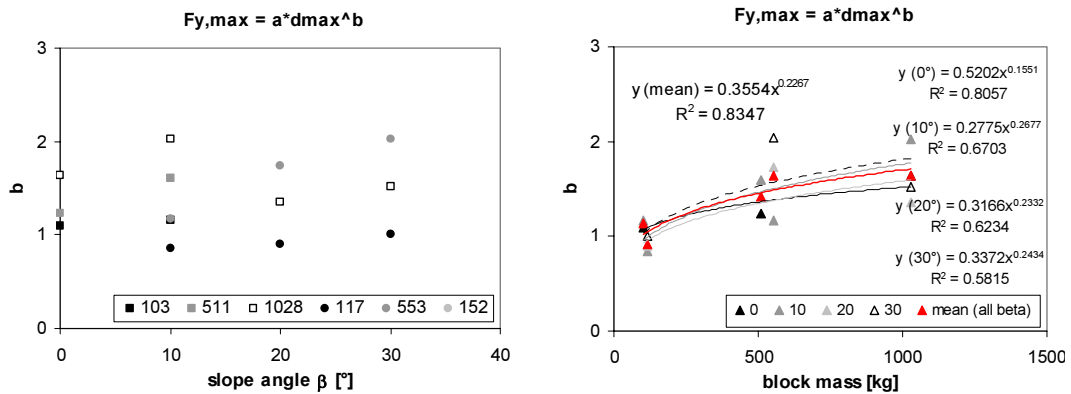


Figure 4.63: Dependence of the exponent b of d_{\max} on the slope angle β (left) and the block mass (right).

4.3.2.4 Relation between rotational and translational energy at the end of impact

As already mentioned above, for impacts on granular material some sliding occurs between block and ground surface during the impact process. The impact thus has to be defined as “partially sliding” impact. Moreover, the friction in the contact surface induces a rotation to the block so that its movement changes gradually from pure translation before impact to rotation and translation after impact.

In case of impacts on a hard ground surface, the rotational rate induced during impact depends on the roughness and thus the friction coefficient of the contact surfaces. As in the present case the ground material is a soft granular material and no hard surface, the rotation velocity is highly influenced by the depth of the crater formed at impact. For penetration depths exceeding a certain value, the crater rim hinders the rotation of the block. As the crater depth is directly related to the falling height, a dependency of the rotational energy of the block after impact on the falling height is expected. This clear dependence of $E_{r,\text{rot}}$ on the falling height H is observed in Figure 4.64: Plotting the ratio of rotational energy after impact to the impact energy ($E_{r,\text{rot}}/E_{i,\text{tot}}$) versus the falling height, one notes with increasing falling heights a very clear decrease of the percentage of energy transformed into rotation during impact. As on large slope inclinations the block rotation is maximal, this effect is most pronounced for $\beta = 30^\circ$.

Authors who have experienced impacts on *hard* ground surfaces [Japan Road Association JRA; Chau & al., 2002] state an independence of the rotational energy after impact ($E_{r,\text{rot}}$) on the boulder mass and the impact energy. As reported above and illustrated in Figure 4.64, this statement does not at all apply to the

present performed impact tests. The effect reported above thus is a very interesting result, obviously occurring only for impacts on soft or granular slopes.

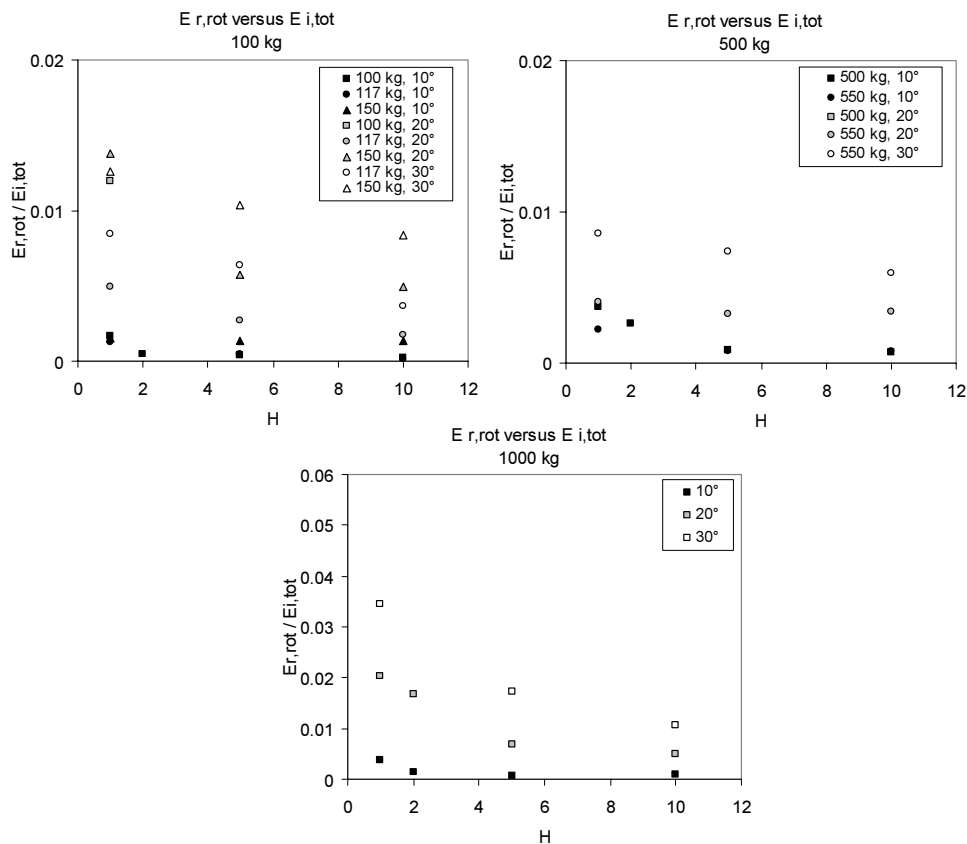


Figure 4.64: Dependence of the ratio $E_{r,rot}/E_{i,tot}$ on the falling height H : For increasing impact heights the percentage of energy transformed into rotation decreases very clearly.

Concerning the relation α between the rotational and the translational energy of the block after impact ($\alpha = E_{r,rot}/E_{r,tot}$), the Japan Road Association stated a maximum value $\alpha = 40\%$ evaluated for *in situ* impact tests on rock slopes. This upper bound for spherical boulder impacts on rock slopes corresponds very well to the one found for the present impact tests on granular slopes (Figure 4.65, 40%-line). However, the mean ratio between $E_{r,rot}$ and $E_{r,tot}$, proposed by JRA to be mainly $< 10\%$ on rock slopes, is found to be slightly higher and to depend on the slope inclination. This observation corresponds to the one stated by Chau & al. [2002] for small-scale impacts on hard slopes (refer to Chapter 2.6). The graphs represented in Figure 4.66, plotting the ratio $\alpha = E_{r,rot}/E_{r,tot}$ versus the slope inclination β , reveal the influence of β which differs for increasing impact velocities respectively falling heights.

Analysing the data separately for each falling height, one realises especially for small impact velocities ($H = 1$ to 5 m) a maximum of $E_{r,rot}/E_{r,trans}$ for $\beta = 20^\circ$

(Figure 4.66, $H = 1$ and 5 m). This corresponds to the observations made during the analysis of the limit impact energy for which global ground failure occurs: for slope angles of 20° , this energy limit is distinctly higher than on slopes inclined at 10° or 30° . The explanation proposed above for this phenomenon, to be due to the transfer of a more important part of the impact energy to rotational energy, is confirmed by this observation. Further, the decrease of the ratio of rotational energy induced to the block during impact for slope angles larger than 20° corresponds to the slope stability. The slopes at $\beta = 30^\circ$ are very close to the limit of equilibrium (as the internal friction angle φ of the sand is 33°). At impact, the sand thus is destabilised and begins to slide locally and superficially under the block. The sliding sand takes the block with it, leading to a proportionally larger translational than rotational motion of the block after impact than for stable slopes (e.g. $\beta = 20^\circ$).

The assertion made by Chau & al. [2002] that on hard ground materials the ratio $E_{r,rot}/E_{r,trans}$ increases with the slope (or impact) inclination up to a certain limit value ($\beta \approx 40^\circ$) and decreases for slopes steeper than this limit (transition from sticking impact to sliding impact on hard slopes) is thus as well valid for impacts on granular slopes for small falling heights (even if on granular slopes no perfect “sticking” impact is possible). For stable slopes the rotation of the block after impact increases with increasing β . As soon as the slope angle approaches the limit equilibrium ($\beta \approx \varphi$), the ground fails locally or even globally at impact and the rotation induced to the block decreases with further increase of the slope angle.

For falling heights ≥ 5 m, the impact energy is in general high enough to provoke global ground failure, especially on steeper slopes (except for the hollow 150 kg). In combination with the deep crater formed during impact hindering the rotation, the failure of the ground provokes an increase of the translation relative to the rotation with increasing slope angles. The ratio α hence decreases (Figure 4.66, $H = 10$ m). For large falling heights, the maximum rotational rate $E_{r,rot}/E_{r,trans}$ is in general reached already for very small slope angles ($\beta = 10^\circ$ in the present case).

Chau & al. [2002] propose a simple theoretical model describing the first rising part of the energy ratio $\alpha = E_{r,rot}/E_{r,trans}$ with β . Assuming that the rotational velocity after impact equals $\omega_r = v_i \cdot \sin\beta/r$ (no slip at impact point and no frictional loss), α is expressed as function of the slope angle β and the normal and tangential coefficients of restitution R_n and R_t :

$$\alpha = \frac{E_{r,rot}}{E_{r,trans}} = \frac{2}{5} \cdot \frac{\sin^2 \beta}{(R_t^2 \cdot \sin^2 \beta + R_n^2 \cdot \cos^2 \beta)} \approx \frac{1.6 \cdot \tan^2 \beta}{1 + 2.56 \cdot \tan^2 \beta} \quad (4-28).$$

In obtaining the last equation, it is supposed that $R_t \approx 0.8$ and $R_n \approx 0.5$, being mean values that apply for the small-scale impacts tests on solid materials performed by Chau & al. [2002].

Yet, as discussed above, for impacts on granular material the ratio α depends not only on the slope angle but also on the ground stiffness and the falling height (influencing the maximum penetration), the internal friction angle of the soil and the block itself (shape, weight,...). These parameters should therefore be implemented in a reasonable formulation describing α . Furthermore, the form of the function proposed by Chau & al. has a upturned concave form. The form of a curve supposed to start from point (0; 0) (as for horizontal ground and vertical fall no rotation is induced to the block) and passing by the data points given in Figure 4.66, however, seems to be linear or even down-turned concave. The formulation (4-28) proposed by Chau & al. [2002] thus does not apply for impacts on soft granular slopes.

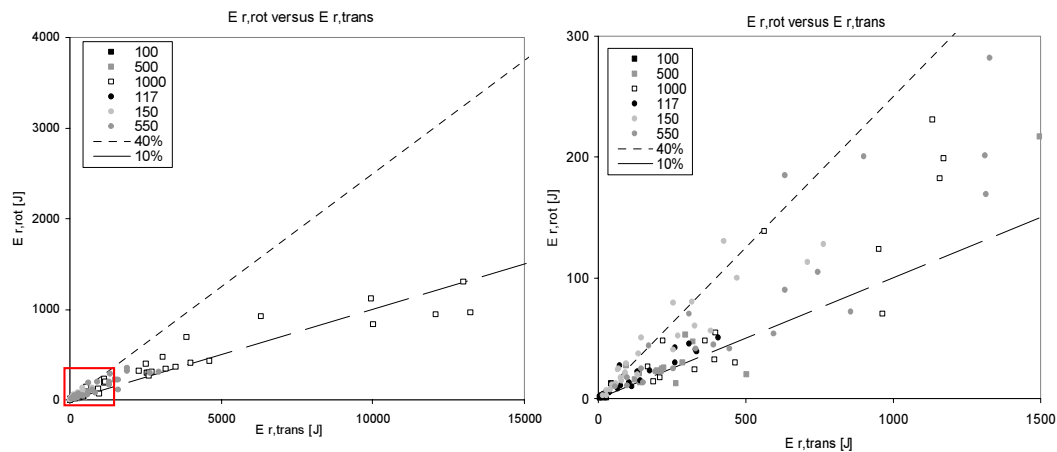


Figure 4.65: $E_{r,rot}$ versus $E_{r,trans}$ for all impact tests: the 40% line (short dash) reported by JRA to represent the upper bound of the ratio $E_{r,rot}/E_{r,trans}$ for impacts of spherical boulders on rock slopes fits very well the present data. The 10% line (long dash), reported by JRA to be fallen short of by more than 50% of the data, is illustrated by the long dash. The graph on the right is a zoom on the zone marked left.

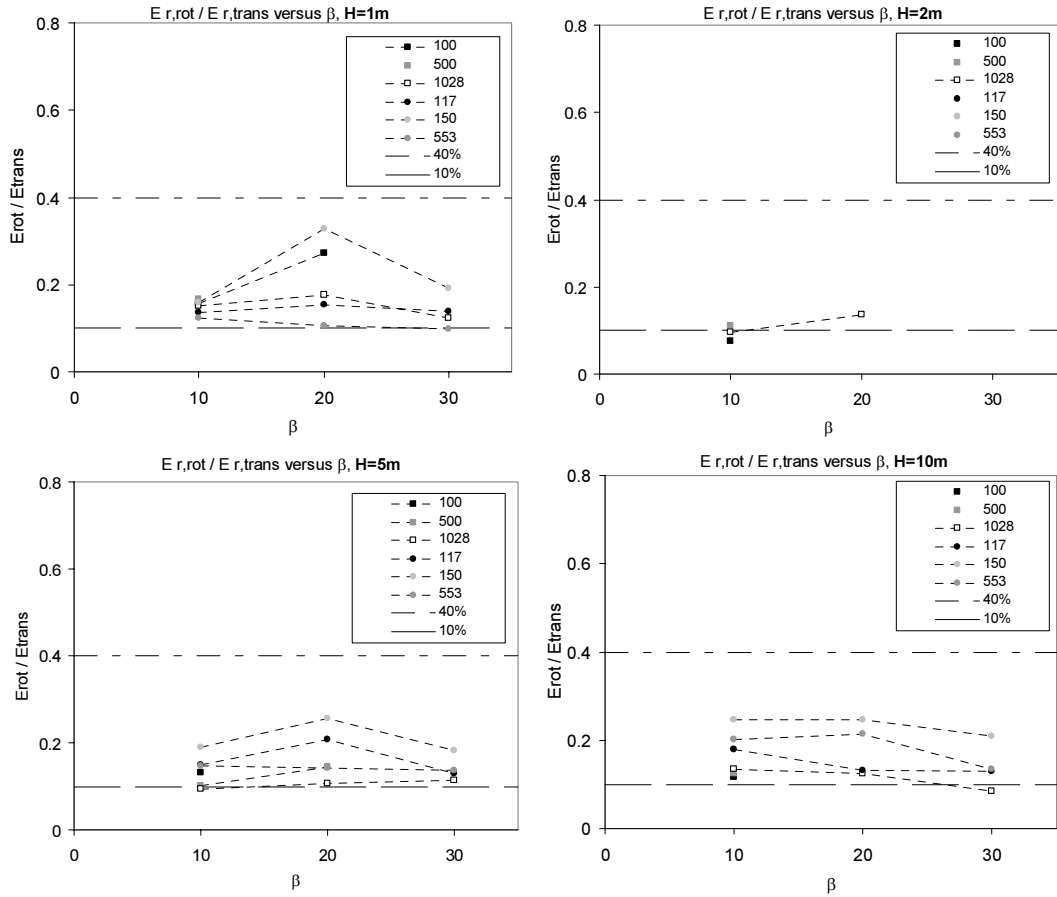


Figure 4.66: Influence of the slope angle β on the ratio $E_{r,rot}/E_{r,trans}$ plotted for the mean values of each impact test series. The 10% and 40% lines are given as reference. The square plots represent the data gathered for cylindrical blocks, the circles represent spheres.

As we have seen above, for impacts on granular, soft material, the rotational energy depends strongly on the impact height and – consequently - on the crater depth. To quantify the rotational velocity ω_r of the block after impact, in a first step the obviously existing dependency of ω_r on the ratio of the falling height H to the penetration depth d_{max} (Figure 4.67) is quantified. As we have seen above that the crater depth has a crucial influence on the rotation of the block, its implementation in the expression for ω_r seems very logic. By means of d_{max} also the plate bearing modulus M_E of the ground as well as the radius and mass of the block are taken into account. It is found that the relation between ω_r and H/d_{max} can be written as:

$$\omega_r = a \cdot (H/d_{max})^b \quad ; \quad \text{with } b = 0.45 \tag{4-29}$$

The exponent b , being nearly independent on the block shape and mass, is fixed to the mean value for all test series, that is to say $b = 0.45$. The factor a then is evaluated for $b = 0.45$ by means of curve fitting. The resulting values for a are

listed in Table 4.8. Plotting the factor a versus the ratio β/φ , a linear relation is found, the gradient of which depends on the block. However, as no clear trend is found, in a first approach the gradient is supposed to equal 0.66, corresponding to the gradient of the linear regression for the mean values of a (given in the last line of Table 4.8). The resulting first proposal to express ω_r in dependency on the falling height H can be written as follows:

$$\omega_r = 0.66 \cdot \frac{\beta}{\varphi} \cdot \left(\frac{H}{d_{\max}} \right)^{0.45} \quad (4-30).$$

Comparing the resulting values calculated for ω_r to the measured values one realised that the simplifications made above (as fixing the gradient on the mean value 0.66 irrespective of its dependence on the block itself) falsifies the results as a residual influence of the block still persists. Analysing the resulting linear regression curves between $\omega_r(\text{measured})$ and $\omega_r(\text{calculated})$ for each block reveals a dependency of the gradients $C(\omega_r)$ on the block shape itself. Due to the eccentricity of the point of first contact, being larger for the cylindrical than for the spherical blocks, this result is logical. For that reason, the factor 0.66 is changed to 1.2 for cylinders, producing the best correspondence between measured and calculated values. The final formulation to calculate ω_r hence is proposed to be:

$$\omega_r = \left(\frac{H}{d_{\max}} \right)^{0.45} \cdot \frac{\beta}{\varphi} \cdot \begin{cases} 1.2 & ; \text{cylindrical blocks} \\ 0.7 & ; \text{spherical blocks} \end{cases} \quad (4-31)$$

The correlation between measured and calculated values of ω_r , represented in Figure 4.68, is very convincing.

However, the study of the factors a given in Table 4.8 reveals its persisting slight dependency on the block mass and radius for spherical blocks and slope angles of 20° and 30° . A possible explanation could be, that the supposition that the exponent b is independent of the block mass and radius (as no trend with m or r has been discovered), is not exactly right. Further impact tests from more than three different falling heights should consequently be performed to confirm or not this assumption.

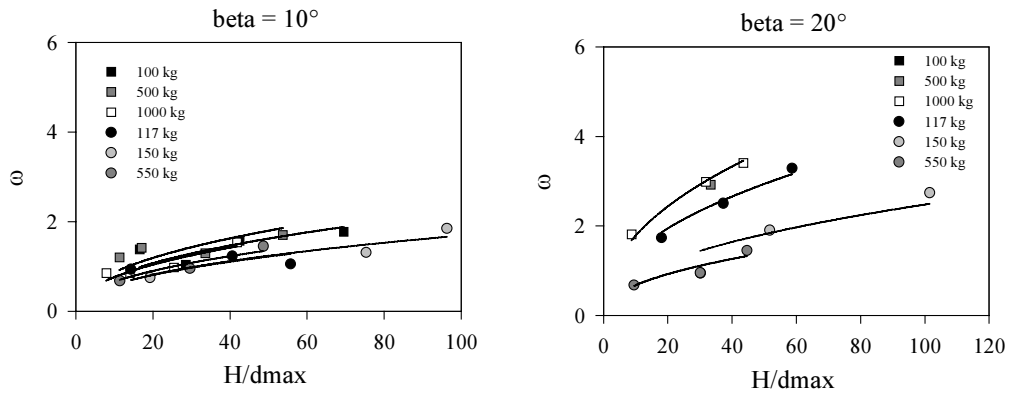


Figure 4.67: Dependency between ω_r and the ratio H/d_{max} for an exponent b fixed to 0.45, exemplarily illustrated for $\beta = 10^\circ$ and 20° .

$\omega_r = a \cdot (H/d_{max})^{0.45}$	$\beta = 10^\circ$	$\beta = 20^\circ$	$\beta = 30^\circ$
100 kg, cylinder	0.279		
500 kg, cylinder	0.309		
1000 kg, cylinder	0.270	0.633	0.973
117 kg, sphere	0.210	0.505	0.580
150 kg, sphere	0.213	0.312	0.487
550 kg, sphere	0.234	0.240	0.242
mean (all blocks)	0.2525	0.4225	0.5705

Table 4.8: Values for the factor a resulting from a curve fitting with $\omega_r = a \cdot (H/d_{max})^{0.45}$.

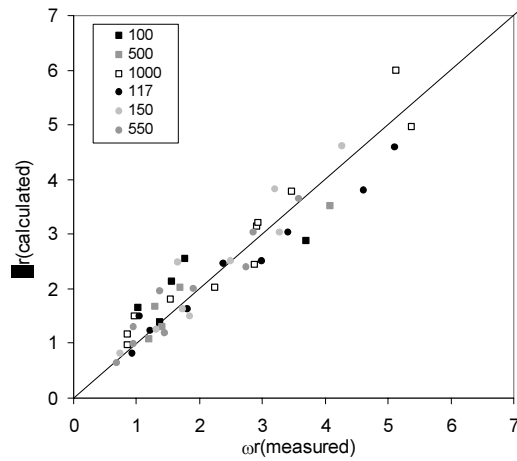


Figure 4.68: Correlation between measured and calculated values of ω_r in [rad/s].

4.3.3 Quantification of the coefficients of restitution

As discussed in Chapter 4.2.3, the coefficients of restitution R_n , R_t and R_{TE} are found to depend on several of the tested parameters. Summarising the results of Chapter 4.2.3, it can be stated that the coefficients are function of the following basic parameters:

$$\begin{aligned} R_n &= f(\beta, \theta, H, m, r), \\ R_t &= f(H, m, r), \\ R_{TE} &= f(\beta, \theta, H, m, r). \end{aligned}$$

Consequently, all combinations of these basic parameters as e.g. the impact energy $E_{v,i} = mgH$ (for vertical impacts without initial rotation) or the impulse $I_{v,i} = mv$ have as well an influence on the coefficients of restitution.

In literature, only few dependencies of the coefficients of restitution on impact parameters are stated and mainly concern the impact velocity respectively the falling height (Hoek [1987], Urciuoli [1988], Pfeiffer & Bowen [1989], Ushiro & al. [2000]). A statement treating the impact angle is published by Wu [1985], proposing a linear relation between the normal and tangential components R_n and R_t to the impact angle θ . However, none of the propositions given in literature express the coefficients of restitution directly as function of a combination of the cited parameters.

To develop a formulation incorporating all parameters on which a dependency has been found in the small- and half-scale experimental campaigns, a new approach is chosen. The idea is based on the conservation of momentum: During impact, the rock block of mass m hits the ground material with an initial impact velocity v_i . During the shock, a certain volume of ground material of mass M gets involved in the impact event and undergoes a certain displacement. According to the theory of momentum conservation, the ratio between the impacting block mass m and the total of masses in movement after impact (block mass m and ground mass M) is used to characterise the coefficients of restitution. In the following sections, formulations for the normal and tangential components of the coefficient of restitution R_n and R_t are developed based on this proposed basic idea.

4.3.3.1 Normal component of the coefficient of restitution R_n

Parting from the basic idea presented above to define the coefficient of restitution by means of the ratio of mass(es) in motion before and during the impact, the basic formulation for R_n has the form

$$R_n = \frac{m}{m + M_{R_n}} \quad (4-32),$$

m being the mass of the block and $M_{R_n} = \rho_{\text{ground}} \cdot V$ the mass of the ground set in motion during the impact. As shown in Chapter 4.3.1.1, for most of the impact tests performed in the framework of this thesis, global shear failure occurs in the ground material. In a first approach, the volume of the ground involved in the shear process is supposed to correspond to the moving ground mass M . Simplifying our problem to the case of a circular foundation with its sole at a depth corresponding to the maximum penetration depth of the block d_{max} , the volume of the failing ground is a function of the section $A_d = \pi r_d^2$ of the foundation and the depth d_{max} . In case of a spherical “foundation”, the section A_d corresponds to the section of the sphere at the level of the ground surface, r_d being the radius of this section (Figure 4.69).

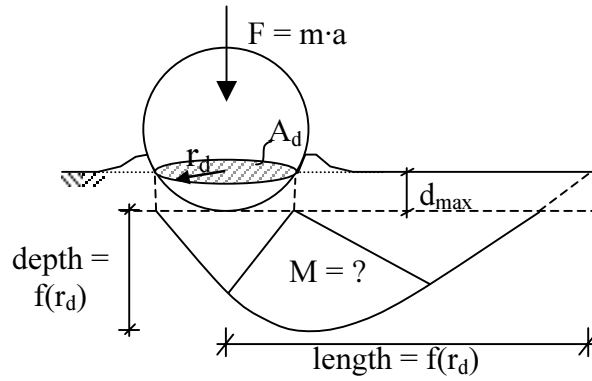


Figure 4.69: Scheme of the ground volume involved in a one-sided shear failure of the ground during impact.

Among several possibilities of describing the volume of the displaced ground material (e.g. in terms of r_d^3 , $d_{\text{max}} \cdot r_d^2$, $d_{\text{max}}^2 \cdot r_d$, d_{max}^3 , ...), the following expression is found the most promising:

$$M_{R_n} = \rho_{\text{ground}} \cdot V_{R_n} = \rho_{\text{ground}} \cdot C_1 \cdot (d_{\text{max}} \cdot r_d^2) \quad (4-33),$$

with ρ_{ground} being the density of the ground material, C_1 being a factor related to the geometry of the involved ground volume and the foundation radius r_d being described by:

$$r_d = \sqrt{2 \cdot r \cdot d_{\text{max}} - d_{\text{max}}^2} \quad (4-34).$$

To verify the supposed dependency of the ground mass M_{R_n} on a volume being function of $d_{\max} \cdot r_d^2$ and to determine the factor C_1 , a back-analysis is performed: For each impact test, the corresponding ground volume V_{R_n} is evaluated by means of the “measured” value of R_n derived from the measured normal component of velocity before and after impact. For this purpose equation (4-33) is implemented in equation (4-32) and the resulting formulation is solved for the ground volume V , yielding:

$$V_{R_n} = \frac{m \cdot (1 - R_n)}{R_n \cdot \rho_{\text{ground}}} \quad (4-35)$$

Plotting the ground volume V evaluated by this formulation for each impact configuration versus the product $d_{\max} \cdot r_d^2$ calculated from the measured value of d_{\max} , one finds a linear correlation for each slope inclination (Figure 4.70). Due to the scattering of the data, the regression coefficient R^2 is quite poor for slope angles of 20° and 30° . The general trend however is very well represented by the linear correlation. The gradient of the regression lines displayed in Figure 4.70 corresponds to the factor C_1 introduced in equation (4-33).

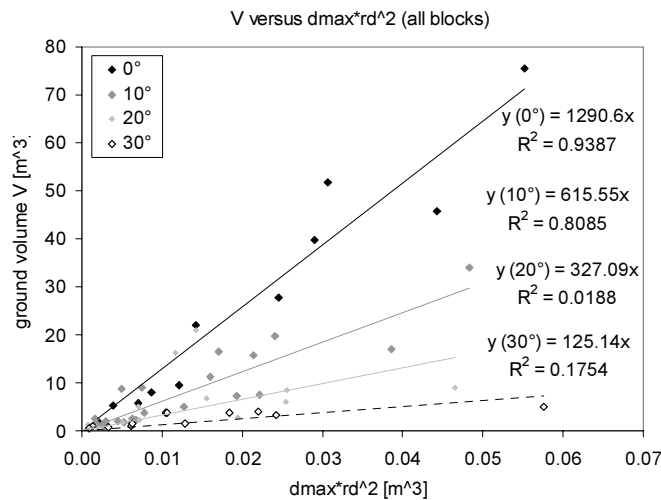


Figure 4.70: Linear relation between the ground volume V (evaluated by equation (4-35) from the “measured” data of R_n) and the product $d_{\max} \cdot r_d^2$ (evaluated from the measured values of the maximum penetration depth d_{\max}) for each slope inclination.

Figure 4.70 represents the correlations for the entire test results for all blocks. A separate representation of the data gathered for the spherical and the cylindrical blocks reveals however slightly different gradients. For comparison with the values gathered for all blocks, the gradients as well as the regression coefficient R^2 are given in Table 4.9.

Gradient C_1	$\beta = 0^\circ$		$\beta = 10^\circ$		$\beta = 20^\circ$		$\beta = 30^\circ$	
	C_1	R^2	C_1	R^2	C_1	R^2	C_1	R^2
all blocks	1290.6	0.94	615.6	0.81	327.1	0.02*	125.1	0.18*
cylinders	1290.6	0.94	633.6	0.83	330.8	0.58*	102.6	0.37*
spheres, full	-	-	505.9	0.38*	316.1	0.51*	214.4	0.77
sphere, hollow	-	-	412.6	0.08*	299.6	0.03*	137.8	0.07*

* Due to the scattering of the data, the regression is very low. The general trend is however represented by the regression line!

Table 4.9: Gradients of the linear regression lines (C_1) and the corresponding regression coefficient R^2 found for the correlation between V and $d_{\max} \cdot r_d^2$ (with **measured** values of the maximum penetration depth d_{\max}), evaluated once for all blocks (as illustrated in Figure 4.70) and once for each block type separately.

The fact that different factors C_1 are found for different slope angles shows that the volume of the ground depends on the slope inclination β . The decreasing trend for increasing slope angles, presented in Figure 4.70 and Table 4.9, is rather logical for two reasons: firstly, the shape of the ground failure (illustrated schematically in Figure 4.69 for a horizontal ground surface, i.e. $\beta = 0^\circ$) changes for changing surface inclinations. It seems logical that the volume of the ground moved during shear failure should diminish with increasing slope angles. This corresponds to the decrease of the gradients illustrated in Figure 4.70. Secondly, as presented in Chapter 4.2.3, an increase of R_n is observed for increasing slope angles. If the volume V is found to decrease with increasing β , the coefficient of restitution R_n , evaluated by means of a formulation of the form proposed in equation (4-32), increases. This corresponds to the trend of R_n observed above.

To quantify the influence of the slope angle β on the ground volume V moved during the impact process, the gradients C_1 evaluated for each slope angle and given in Table 4.9 are plotted versus the ratio β/φ . This ratio is used instead of β to account for the internal friction angle of the ground material. Further, the ratio β/φ facilitates the development of a homogeneous formulation of R_n . The resulting dependency is illustrated in Figure 4.71 separately for each block type.

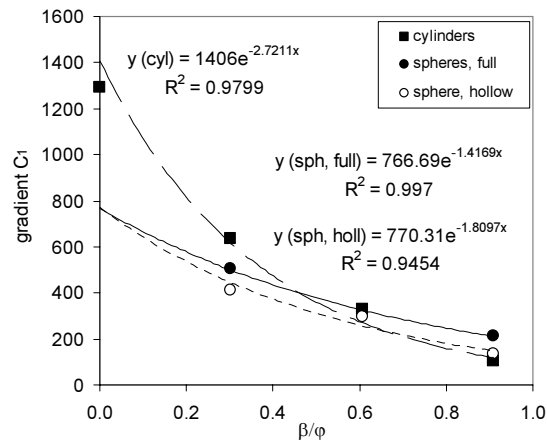


Figure 4.71: Exponential correlation between the gradient C_1 (separately for the cylindrical, the spherical concrete filled and the spherical hollow blocks; refer Table 4.9) and the ratio β/ϕ .

Figure 4.71 reveals a very good correlation for an exponential regression curve of the form $C_1 = a \cdot e^{-b \cdot \beta/\phi}$. The values for b and a differ for spherical and cylindrical blocks. Analysing Figure 4.71 it becomes clear that the shape of the block has an influence on the gradient C_1 and thus on the volume V displaced during the impact process. Further, the influence of the unit weight of the spherical blocks is not perfectly accounted for by the expression developed to quantify the normal coefficient of restitution R_n , as the curves in Figure 4.71 differ slightly for the concrete filled and the hollow spheres.

The values of a and b are evaluated based on an investigation by curve fitting. The values for which the best coefficients of determination R^2 are found are illustrated in Figure 4.71. Based on a further fitting process (results see Table 4.10), b is finally chosen to equal 1.5 for spherical blocks, corresponding to parallel curves for different unit weights. For the cylindrical blocks, a very good fit is found for b equal to 2.5. The difference arising by the block shape thus is taken into account by means of the factor b .

In case of the spherical blocks, the factor a , being larger for concrete filled than for hollow blocks, represents the residual influence (apart from the block mass m) of the unit weight of the blocks. That signifies that the gradient C_1 is larger for concrete filled than for hollow blocks, causing R_n to increase with decreasing unit weight. This has in fact been observed during the impact tests.

$C_1 = a \cdot e^{b \cdot \beta / \varphi}$	b = 1.5		b = 2		b = 2.5	
	a	R ²	a	R ²	a	R ²
cylinders	1136	0.89	1239.9	0.98	1306.7	0.995
spheres (full)	798.0	0.997	981.4	0.89	-	-
sphere (hollow)	662.5	0.944	815.9	0.89	-	-

Table 4.10: Regression coefficient R^2 evaluated for different values of the factors a and b (b being fixed to the indicated value and a being determined by fitting) defining the function $C_1 = a \cdot e^{b \cdot \beta / \varphi}$.

According to this choice, R_n can be calculated by means of the following formulation:

$$R_n = \frac{m}{m + \rho_{\text{ground}} \cdot (d_{\text{max}} \cdot r_d^2)} \cdot C_1 \quad (4-36),$$

with

$$C_1 = \begin{cases} 798 \cdot e^{-1.5 \frac{\beta}{\varphi}} & , \text{ concrete filled spheres} \\ 662 \cdot e^{-1.5 \frac{\beta}{\varphi}} & , \text{ hollow sphere} \\ 1307 \cdot e^{-2.5 \frac{\beta}{\varphi}} & , \text{ cylinders} \end{cases} \quad (4-37)$$

To verify the aptitude of this formulation, the measured values of R_n are compared to the ones calculated by equation (4-36). For a first comparison, the *measured* values of d_{max} are used to calculate R_n (Figure 4.72). This allows to evaluate the correspondence between calculated and measured values of R_n without any influence of errors resulting from other sources as d_{max} : As the fit between $d_{\text{max}}(\text{measured})$ and $d_{\text{max}}(\text{calculated})$ of course is not exactly perfect, an error is induced to $R_n(\text{calculated})$ by d_{max} and r_d (the latter depending directly on d_{max}^2 , refer to equation (4-34)).

In a second step, the coefficient R_n is calculated according to equation (4-36) using the *calculated* values of d_{max} using equation (4-22). The correspondence between the measured values of R_n and the ones calculated with d_{max} evaluated by means of equation (4-22) is represented in Figure 4.73. The solid black line represents perfect correspondence (100%), the dashed lines enclose all values having a constant error of ± 0.025 . The apparently bad correspondence between $R_n(\text{calculated})$ and $R_n(\text{measured})$ displayed in both figures is discussed hereafter.

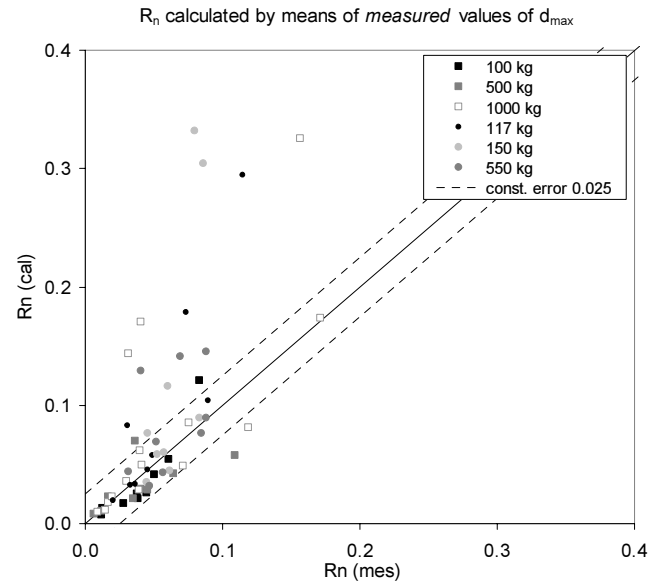


Figure 4.72: Correspondence between measured and calculated values of R_n evaluated according to equation (4-36). R_n (cal) is calculated by means of the **measured** data of d_{max} .

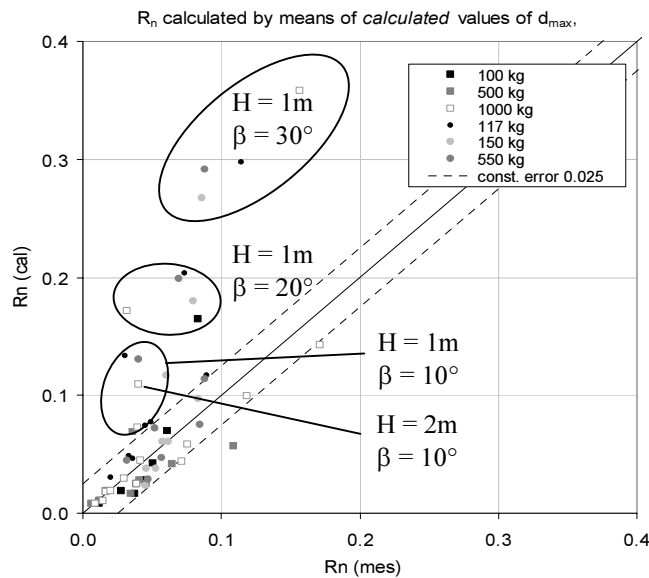


Figure 4.73: Correspondence between measured and calculated values of the normal coefficient of restitution. R_n is calculated according to equation (4-36) and by means of **calculated** values of d_{max} . The proposed formulation overestimates R_n for small falling heights and slope angles $\geq 10^\circ$ (data points selected by ellipses).

As to see in both graphs, the normal component of the coefficient of restitution R_n is clearly overestimated for certain cases. A closer investigation reveals that the concerned values all originate from impact tests on slopes ($\beta \neq 0^\circ$) with small falling heights (H in general 1 m, once 2 m; see ellipses in Figure 4.73). This underlines once more the fact that different impact conditions lead to different “rebound” mechanisms of the block. As already mentioned, for small falling heights, the impact energy is too low to provoke a deep crater in the ground

material. As soon as the block gets in contact with the ground surface, it begins to roll on the surface, creating only a small crater. As discussed previously, a higher percentage of the initial impact energy is transformed into rotation of the block than for impacts from larger falling heights. This kind of mechanism strains the ground material quite differently than the mechanism for impacts at higher energy levels (no global ground failure, rather superficial load). Bearing this in mind, it is not surprising that the developed formulation for R_n (which is based on the idea of a ratio of masses involved in the impact process corresponding to the theory of momentum conservation) overestimates the restitution for small falling height especially in case of large slope angles. The transfer of a part of the impact energy to rotation is neglected.

For impacts causing a clear crater, however, the impact mechanism corresponds to the one assumed to govern R_n . Consequently, R_n is well represented for impacts with falling heights > 1 m by the proposed formulation, which is finally written as follows:

$$R_n = \frac{m}{m + C_1 \cdot \rho_{\text{ground}} \cdot (d_{\text{max}} \cdot A_d)} \quad (4-38),$$

$$\text{with } C_1 = \begin{cases} 254 \cdot e^{-1.5 \frac{\beta}{\varphi}} & , \text{ concrete filled spheres} \\ 211 \cdot e^{-1.5 \frac{\beta}{\varphi}} & , \text{ hollow sphere} \\ 416 \cdot e^{-2.5 \frac{\beta}{\varphi}} & , \text{ cylinders} \end{cases}$$

with m being the block mass, β being the slope angle relative to the horizontal, φ being the “critical state” friction angle and ρ_{ground} the density of the granular ground material, d_{max} being the maximum penetration depth in vertical direction and $A_d = \pi \cdot r_d^2$ the section of the block at level of the ground surface for the maximum penetration depth (Figure 4.69).

The fact that a differentiation has to be made for C_1 for the concrete filled and the hollow spherical blocks shows that the proposed formulation does not yet represent perfectly the influence of the unit weight of the blocks. Further, the differentiation between spheres and cylinders shows that the development of one single formulation of R_n applicable for all block forms is probably not possible.

The proposed equation (4-38) hence has to be seen as a tool which produces good results in case of vertical impacts on horizontal granular materials (for all tested

falling heights, as no rotation occurs) and in case of impacts on slopes for falling heights > 1 m. Eliminating therefore the values of R_n calculated for impacts on slopes ($\beta \neq 0^\circ$) with small falling heights ($H = 1$ m), corresponding to the data highlighted by the ellipses in Figure 4.73, the resulting correspondence between measured and calculated coefficients R_n is more convincing (Figure 4.74).

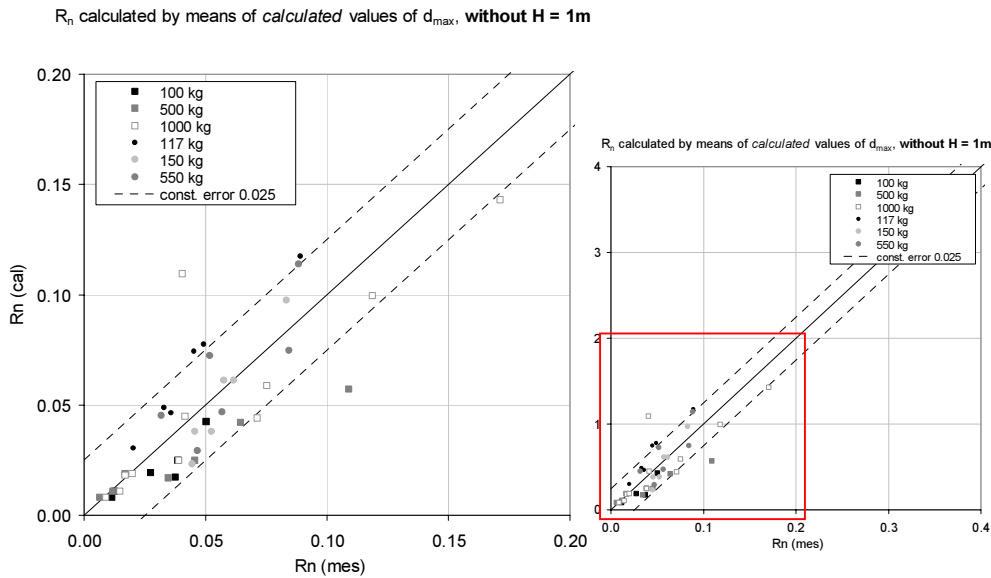


Figure 4.74: Correspondence between R_n (calculated, with d_{max} calculated) and R_n (measured) for all impact tests *except* the ones from $H = 1$ m on slopes ($\beta \neq 0^\circ$). The graph on the left is the zoom on the highlighted part of the right graph.

The worst predictions are the data for impact tests with the 1000 kg cylinder on a slope of 20° from $H = 2$ m (blank square) and for the 500 kg cylinder dropped from 5 m on a slope of equally 20° (grey square). In the first case, it can be argued, that the falling height of 2 m is still very small and thus still a rolling mechanism takes place at impact, excluding the applicability of the formulation proposed for R_n . In case of the 500 kg block it has to be noted, that only a single impact has been performed on a slope of 20° and a falling height of $H = 5$ m. The data point thus is not perforce reliable.

4.3.3.2 Tangential component of the coefficient of restitution R_t

To quantify the tangential coefficient of restitution R_t , the philosophy presented above for R_n , that is to say the ratio between the masses moved during impact process, is retained according to the idea of the conservation of momentum:

$$R_t = \frac{m}{m + M_{R_t}} \quad (4-39)$$

As for R_n , the mass M_{R_t} of the ground material involved in the mechanism has to be determined. In a first approach, the corresponding volume V_{R_t} is assumed to equal the one retained for R_n . However, it is found that the correspondence between the volume calculated by means of an equation analogue to (4-35) (with R_t instead of R_n) and the volume obtained by a formulation of the form $V_{R_t} = f(d_{\max} \cdot r_d^2)$ is not very good. The gradients C_2 obtained of the linear regression for each block still show a clear dependence on the block mass and radius (Figure 4.75).

This signifies that the ground volume influencing R_t is not the same as for R_n . This seems logical as the coefficients R_n and R_t are governed by different mechanisms. An impact load in normal direction effects a state of stress in the ground that finally provokes a global base failure (Figure 4.69), whereas a tangential impact load causes shear failure. Thus, other possibilities have to be found to represent the involved ground volume. The following three possibilities are imaginable:

- depending solely on the maximum penetration depth, $V = f(d_{\max}^3)$;
- depending solely on the radius of the corresponding foundation, $V = f(r_d^3)$;
- or depending on both d_{\max} and r_d combined as follows: $V = f(d_{\max}^2 \cdot r_d)$.

The analysis of all three propositions reveals that V_{R_t} is best represented by the last expression. This result seems logical, as the volume expressed by a function of the form $V_{R_t} = C_2 \cdot d_{\max}^2 \cdot r_d$ implicates both, the force resisting to the shear movement R (being function of d_{\max}^2 , refer to Figure 4.76) as well as the diameter $D_d = 2r_d$ of the block at ground surface level (corresponding to the third dimension). The formulation for R_t hence is developed based on the following expression for the interested ground mass M_{R_t} :

$$M_{R_t} = \rho_{\text{ground}} \cdot V_{R_t} = \rho_{\text{ground}} \cdot C_2 \cdot (d_{\max}^2 \cdot r_d) \quad (4-40)$$

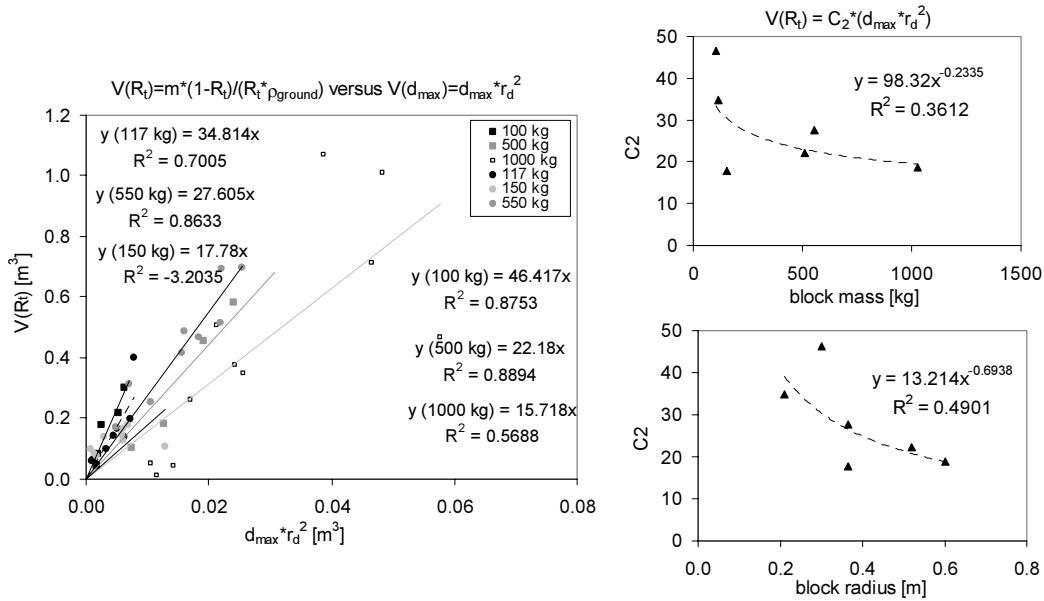


Figure 4.75: For a ground volume calculated by $V_{Rt} = d_{max} \cdot r_d^2$ (with **measured** values of d_{max}), the influence of block mass m and radius r are not ideally accounted for: this is shown by the dependence of the gradient C_2 (left graph) on m and r (graphs on the right hand side).

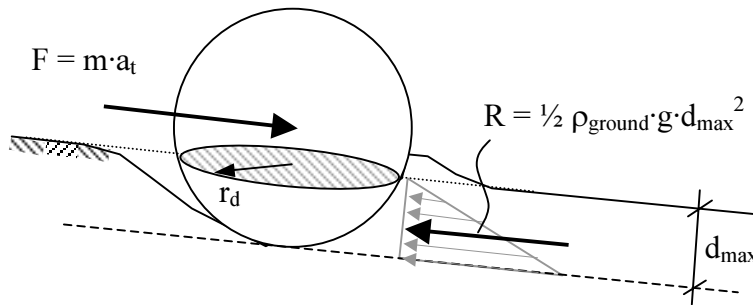


Figure 4.76: Scheme of the shear failure mechanism. The ground volume resisting to the block motion is a function of $d_{max}^2 \cdot r_d$.

Plotting the ground volume V_{Rt} evaluated by means of the chosen formulation $V_{Rt} = C_2 \cdot d_{max}^2 \cdot r_d$ versus the volume $V(R_t) = m \cdot (1 - R_t) / (R_t \cdot \rho_{ground})$ assessed from the tangential coefficient of restitution, the correlations presented in Figure 4.77 are found. As noted on the same figure, one of the data points for the 1000 kg block seems to diverge. A close investigation of the test results shows that this divergence is due to the value of the maximum penetration depth d_{max} , which seems to be too high. This assumption is supported by the fact that d_{max} normally is smaller for slopes inclined at 30° than 20° . In case of the 1000 kg block and a drop height of 10 m, a reverse trend is observed. As the value in question originates from extreme impact conditions (all impact parameters are extreme: the block mass, the slope inclination and the drop height), it is possible that another

mechanism takes place, which is not observed for less extreme impact conditions. Hence, the value in question is eliminated for the further data processing. The resulting gradients and their correlation are given in Table 4.11.

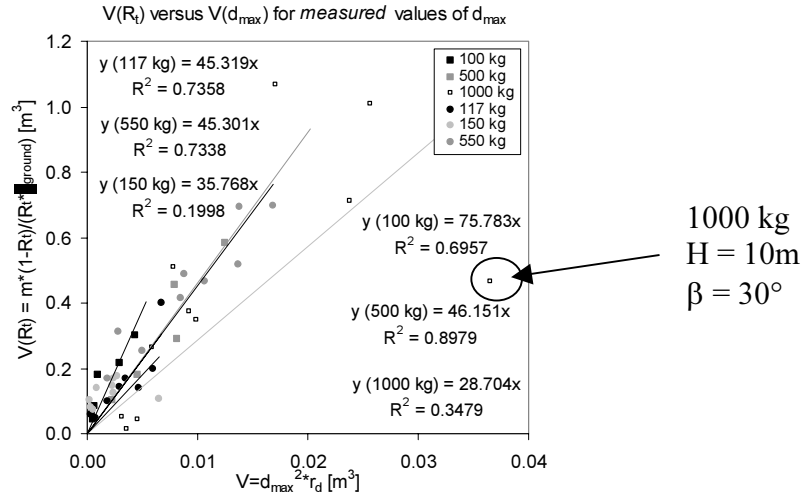


Figure 4.77: Correlation between the calculated ($V(R_t)$, y-axis) and the “measured” (x-axis) values of V_{Rt} . V_{Rt} “measured” is evaluated by means of the **measured** values of d_{max} . As discussed in the text, the highlighted data point for the 1000 kg block is eliminated for further data processing.

$V_{Rt} = C_2 \cdot (d_{max}^2 \cdot r_d)$	C_2	R^2
100 kg, cylinder	75.8	0.696
500 kg, cylinder	46.2	0.898
1000 kg, cylinder	40.2 ²	0.782 ²
117 kg, sphere	45.3	0.736
550 kg, sphere	45.3	0.734
150 kg, sphere	35.8	0.200*

* Due to the scattering of the data, the correlation is very low. The general trend however is respected.

Table 4.11: Gradient C_2 and regression coefficient R^2 evaluated by means of Figure 4.77.

Plotting the values of C_2 presented in Table 4.11 versus the block mass m and its radius r reveals that for formulation (4-40) the ground volume V_{Rt} is almost independent on the impacting block. It is interesting to note that for all but one block, the factor C_2 averages 43. Only exception is the 100 kg cylinder for which C_2 equals nearly the double. As the correlation presented in Figure 4.77 does not show any extreme values (as for the 1000 kg block), the reason for the much bigger value of C_2 has to be found elsewhere. As it seems that the ground volume calculated by means of R_t is generally overestimated, it can be argued that in case

² The gradient C_2 and the correlation R^2 do not correspond to Figure 4.77, as the “out of range” value for $H = 10\text{ m}$ and $\beta = 30^\circ$ is eliminated as discussed in the text.

of the 100 kg cylindrical block the real failure mechanism does not correspond to the proposed one.

As for all but the 100 kg cylinder C_2 averages 43, this value is adopted as final solution. Eliminating the value found for the 100 kg cylinders, the dependence of C_2 and thus of V_{Rt} on the block mass and radius is completely eliminated (Figure 4.78). As no other dependency on either the slope angle or other parameters are found, the following formulation is proposed to assess the tangential coefficient of restitution R_t :

$$R_t = \frac{m}{m + 43 \cdot \rho_{\text{ground}} \cdot (d_{\text{max}}^2 \cdot r_d)} \quad (4-41)$$

The correspondence between the measured values of R_t and the ones calculated according to equation (4-41) is illustrated in Figure 4.79 for $R_t = f(d_{\text{max}}, \text{measured})$ and in Figure 4.80 for $R_t = f(d_{\text{max}}, \text{calculated according to (4-22)})$. Comparing both graphs, the accumulation of errors for $R_t = f(d_{\text{max}}, \text{calculated})$ becomes evident by the larger scatter of the data. Further, as already observed for the normal coefficient of restitution R_n , the proposed formulation generally overestimates the restitution for impacts from small drop heights ($H = 1$ m) and slope inclinations equal and larger than 10° . The corresponding values are highlighted in both graphs. The same kind of explanation as for R_n is proposed. Hence, for small falling heights the impact mechanism corresponds to a rolling of the block on the slope surface, the crater left in the ground is comparatively flat. As the mechanism proposed above to govern the value of R_t occurs only for impacts provoking a more significant penetration, the formulation (4-41) is not valid for impacts provoking only very flat craters. For more significant falling heights and crater depth, however, the formulation is acceptable.

Concerning the general medium correspondence, it has to be mentioned that the values measured for R_t show a very large scatter. This is even more pronounced for impacts on small slope angles (as a small deviation provokes a large error for nearly vertical impacts). Bearing this in mind, the correlations are not too bad.

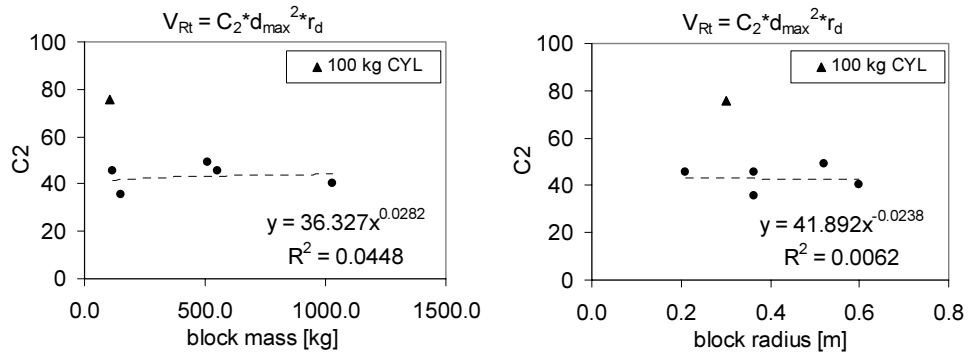


Figure 4.78: Except for the value of C_2 evaluated for the 100 kg cylinder (triangle), V_{Rt} can be stated to be independent on the block mass and block radius. This signifies that the ground mass M_{Rt} involved in the impact process is well represented by the formulation proposed in equation (4-40).

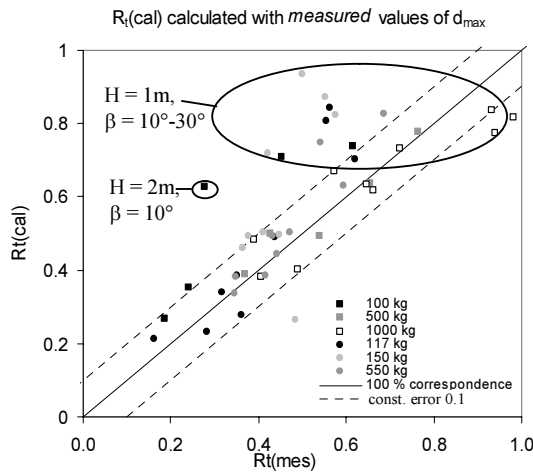


Figure 4.79: Correspondence between measured and calculated values of R_t using the formulation proposed in (4-41) and **measured** values of d_{max} .

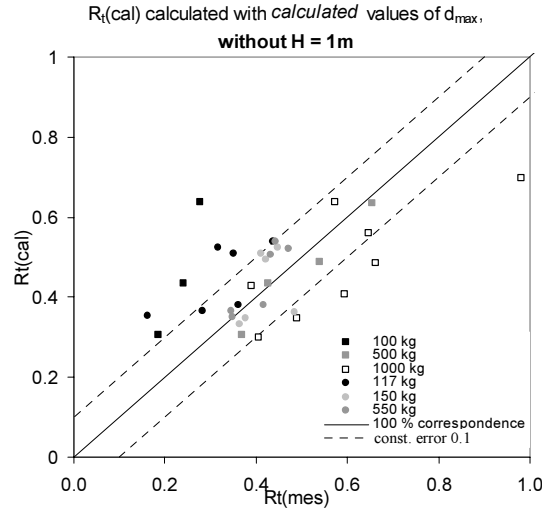


Figure 4.80: Correspondence between measured and calculated values of R_t using the formulation proposed in (4-41) and *calculated* values of d_{max} .

4.3.3.3 Coefficient of restitution R_{TE} defined by means of the ratio $E_{r,tot}/E_{i,tot}$

The coefficient of energy restitution is expressed by the ratio of the total energy at the end of impact to the total energy before impact. The total energy herein is the sum of translational and rotational energy of the block. Contrary to the normal and tangential components of the velocity restitution R_n and R_t , R_{TE} accounts for the rotation of the block. As it is observed during real rockfall events, the rotation of the block can reach important values during the trajectory and thus should not be neglected during simulation.

Knowing the translational and rotational impact velocities v_i and ω_i and expressing the rebound velocity components $v_{n,r}$ and $v_{t,r}$ by means of R_n and R_t , R_{TE} can be written as follows:

$$R_{TE} = \frac{m \cdot \left[(R_t \cdot v_{t,i})^2 + (R_n \cdot v_{n,i})^2 \right] + I \cdot \omega_r^2}{m \cdot v_i^2 + I \cdot \omega_i^2} \quad (4-42)$$

The coefficients of restitution R_n and R_t can be calculated according to the proposed formulations (4-38) and (4-41), the same goes for the rotational velocity at impact end ω_r (equation (4-31)).

The correlation between measured and calculated values for R_{TE} is presented in Figure 4.81. As the expressions proposed for R_n and R_t are not valid for impacts from small drop heights on slopes, the values calculated for R_{TE} for $H = 1\text{m}$ and $\beta = 20^\circ$ and 30° do not fit the measured values. In case of $H = 1\text{m}$ and $\beta = 10$, the

calculated values show a constant error of about 0,025 (dashed line in Figure 4.81). For all other cases, the correspondence between measured and calculated values is good.

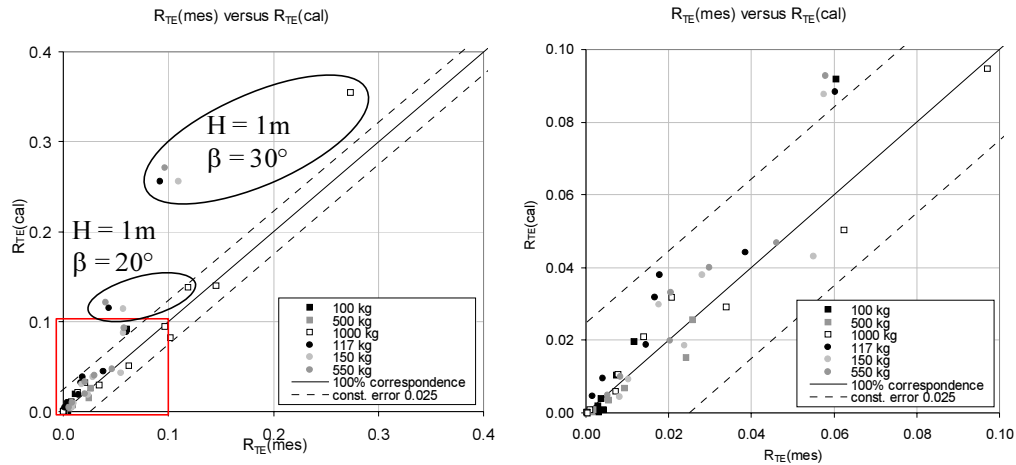


Figure 4.81: Good correspondence between measured values of R_{TE} and values calculated by means of formulation (4-42) and calculated values of R_n , R_b , d_{max} and ω_r . Only in case of small drop heights and large slope angles (highlighted values) the correspondence is low due to the fact that R_n and R_i are not valid for these impact combinations. The right hand graph represents a zoom.

4.3.4 Synopsis and domain of validity

The interpretation of the half-scale impact tests on granular material has contributed to explain the mechanisms occurring during impact and guiding the motion of a rock block during and after impact. During impact, the movement of the block is mainly guided by three mechanisms: the penetration into the ground material (translation in vertical resp. normal direction), the translation in lateral direction (due to the superficial sliding of the ground material if the slope angle approaches the internal friction angle and / or the displacement of the ground during global base failure) and the rotation induced during impact. It is found however that all three mechanisms are related and influence the movement of the block at impact end. The movement type that finally preponderates and guides the impact depends on the impact conditions (drop height, slope angle, block shape and size). For example for vertical impacts on horizontal ground, no lateral and rotational block movements can occur (if the block has no initial block rotation). For vertical impacts from small drop heights on a slope, the rotational movement of the block is important due to the eccentricity of the resulting ground reaction on the rock block (Figure 4.82, left graph). In case of more important falling heights on the same slope, the translation becomes more important, as firstly the crater hinders the rotation and secondly the eccentricity of the resultant acting on the

block is smaller (Figure 4.82, right graphic). If the slope is near its limit equilibrium, the lateral translation becomes very important, as at impact the slope fails superficially and begins to slide, taking the block with it.

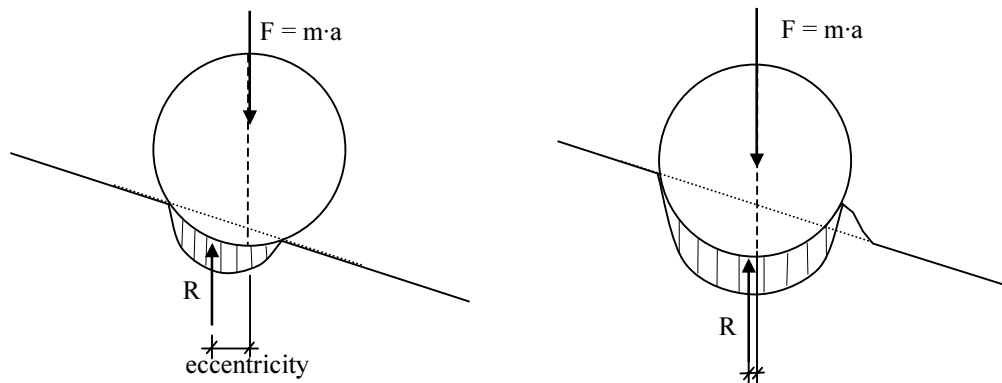


Figure 4.82: Increase of eccentricity of the resulting ground resistance R with the penetration depth, i.e. for increasing impact velocities respectively falling heights. Left: small penetration depth for small falling height; right: large penetration depth for large falling height.

A detailed analysis of the test results allowed to develop mathematical formulations quantifying the most important characteristics of the movement of the block during impact: the maximum penetration depth d_{\max} , the maximum force F_{\max} acting on the block during impact and (by means of F_{\max}) the maximum deceleration a_{\max} of the block, as well as the rotational velocity after impact ω_r . The basic ideas for the formulations proposed for d_{\max} and F_{\max} are inspired by the impact theory of Hertz and the formulations proposed by Montani-Stoffel for the maximum impulsive force induced by blocks falling on soil cushions covering rockfall protection galleries.

In case of d_{\max} and ω_r , the influence of different block forms is accounted for by means of varying factors. This emphasises the problem encountered by trying to express a very complex mechanism by means of a single, comprehensive formulation.

Further it is asserted that the acceleration plateau occurring for most of the present impact tests corresponds to the occurrence of a global base failure. Indeed, the acceleration a_{plateau} acting on the block during this phase corresponds rather well to the static bearing capacity of the ground material R_f (according to Lang & Huder) divided by the block mass. Except for impacts for which the rolling of the block on the ground surface preponderates (e.g. $H = 1\text{m}$, $\beta = 20^\circ$), global ground failure occurs for impacts exceeding a critical impact energy. For the present test conditions, this critical value is about 6 kJ.

Further, a new approach is proposed to calculate the coefficients of restitution R_n and R_t in function of the characteristics of block, ground material and kinematics. Based on the idea of the conservation of linear momentum during impact, the ratio of masses moving before and during impact: $m/(m+M)$ (m being the block and M the ground mass) is found to be a promising tool to define R_n and R_t . The ground mass M involved in the impact process is found to differ for the normal and the tangential coefficients of restitution:

- In case of normal loading and restitution, the ground volume involved in the impact process is related to the global base failure mechanism. Therefore, the ground mass M guiding the normal component of the coefficient of restitution R_n is proposed to depend on the product of maximum penetration depth d_{\max} , the section of an equivalent flat foundation A_d and a factor C_1 . As it was not possible to account exactly for all parameters concerning the block, as its shape and unit weight, the factor C_1 depends still on both parameters. This shows that the proposed formulation is not yet perfect.
- In case of tangential loading, the ground volume resisting to the block motion and moving during impact corresponds to the mass in front of the block, undergoing shear failure. M thus depends on the square of d_{\max} and on the radius r_d of an equivalent foundation.

By means of the formulations proposed to express ω_r and the coefficients R_n and R_t , the energetic coefficient of restitution R_{TE} can be evaluated. In the following, the formulations proposed to quantify the coefficients R_n , R_t and R_{TE} are recapitulated.

$$R_n = \frac{m}{m + C_1 \cdot \rho_{\text{ground}} \cdot (d_{\max} \cdot A_d)}$$

with $C_1 = a \cdot e^{-b \cdot \frac{\beta}{\varphi}}$, a and b being function of the block (form, unit weight)

$$R_t = \frac{m}{m + 43 \cdot \rho_{\text{ground}} \cdot (d_{\max}^2 \cdot r_d)}$$

$$R_{TE} = \frac{m \cdot \left[(R_t \cdot v_{t,i})^2 + (R_n \cdot v_{n,i})^2 \right] + I \cdot \omega_r^2}{m \cdot v_i^2 + I \cdot \omega_i^2}$$

The normal and tangential components of the coefficients of restitution R_n and R_t are defined based on ground failure mechanisms due to normal (R_n) and lateral

(R_t) loading of the ground material. Both failure mechanisms only occur if the penetration into the ground material is sufficient and if translation preponderates the rolling movement of the block (as it is the case for impacts on slopes ($\beta \neq 0^\circ$) and falling heights > 1 m). If the block penetrates only little into the ground material and rolls on the ground surface (as it is observed for impacts from $H = 1$ m on slopes), the proposed formulations are not adequate. In this case the formulations overestimate the rebound velocity. As the energetic coefficient of restitution R_{TE} depends on R_n and R_t , the same restriction is valid for R_{TE} : for small falling heights ($H = 1$ m) and slope inclinations $\geq 20^\circ$, the proposed formulation overestimates the energetic restitution of the blocks. However, for impacts with preponderating translational motion of the block, the proposed formulations are in general good agreement with the measured values of R_n , R_t and R_{TE} .

Furthermore, the proposed formulations are verified only for impact conditions similar to the half-scale impact tests, that is to say vertical impacts on a horizontal or inclined granular, cohesionless ground material (S0-4) at low energies ($H \leq 10$ m, $m \leq 1000$ kg) with spherical or spherical based blocks.

The problem encountered for R_n and R_t as well as for the formulations describing d_{max} and ω_r illustrate that it is extremely complicated to model a complex mechanism as the impact of a rock block on granular material by means of one or two comprehensive formulations of R_n and R_t . When the coefficients of restitution are defined for the mass centre of the block and by the ratio of rebounding and incident velocities (as it is the case for lumped mass trajectory models!), hence it is quite illusory to find a global, comprehensive formulation for the coefficients of restitution R_n and R_t . A better result could perhaps be obtained by using coefficients of restitution relative to the instantaneous contact point between block and ground.

5 Application and comparison with existing models

In this chapter the measured coefficients of restitution are compared to the values stated in literature for impacts on soft ground. Furthermore, the advantage of expressing the coefficients of restitution as function of the impact conditions, as proposed by the developed new formulations, is exemplified by means of an application to several tests performed on a half-scale. The results are compared to two other methods: the commonly used calculation of the rebound by means of “constant” coefficients of restitution only function of the slope material and the results yielded by the Colorado Rockfall Simulation Program CRSP.

The normal (R_n), tangential (R_t) and energetic (R_{TE}) coefficients of restitution measured during the half-scale testing campaign (impacts on slightly compacted sand) range between the following values:

- R_n : 0.003 - 0.257 ; mean over all tests: 0.04
- R_t : 0.07¹ - 1 ; mean over all tests: 0.48
- R_{TE} : 0.0003 - 0.336 ; mean over all tests: 0.03

The measured coefficients are found to meet quite well some of the values stated in literature for soft soil slopes (refer to Table 2.1). However, depending on the source of data, especially the values stated for R_n tend to be larger than the presently measured ones. As most values stated in literature are based on impact tests on soil slopes stiffer than the present sand, this tendency is plausible. Plotting R_n versus R_t (Figure 5.1) and comparing the resulting variability range with the ones presented by Fornaro & al. [1990] (Figure 2.8, data gathered from impact tests on detrital slopes) and Chau & al. [2002] (Figure 2.18, small-scale impact tests on soft soil slopes) reveals graphically this tendency.

¹ 0.07 represents the smallest value for non-normal impacts (free fall, $\beta \neq 0^\circ$). For normal impacts ($\beta = 0^\circ$), the tangential coefficient of restitution R_t is not defined (refer to p.85).

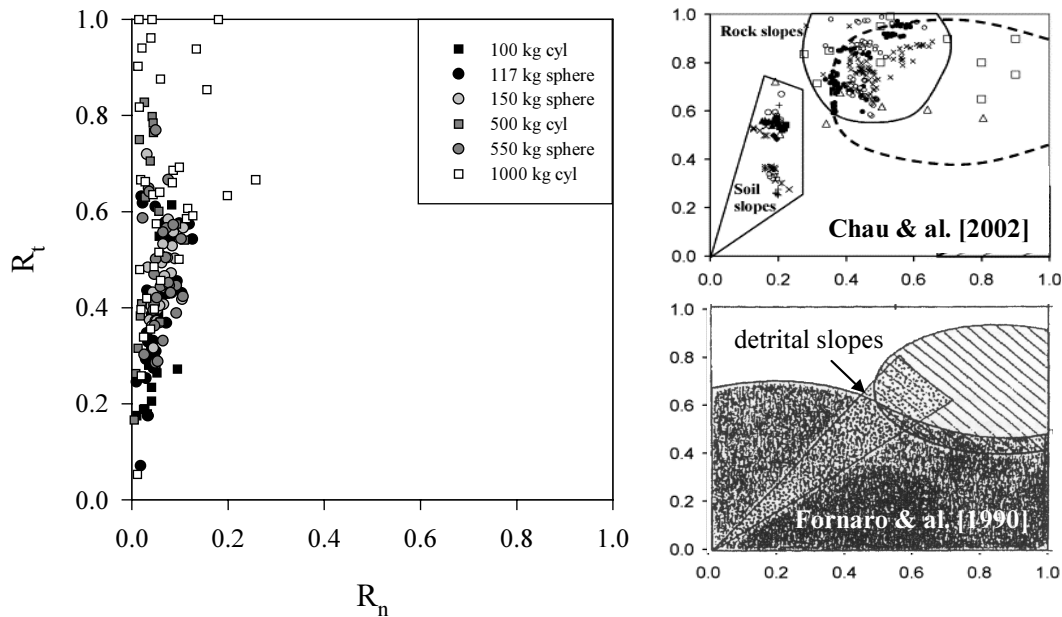


Figure 5.1: Variability ranges of the coefficients of restitution R_n and R_t (without values for normal impacts) according to the half-scale test results (left, impact tests on a sandy slope). The variability ranges stated by Chau & al. [2002] and Fornaro & al. [1990] are presented on the right hand side.

Unlike the “constant” coefficients of restitution conventionally used by most trajectory simulation programs, the new formulations take into account the influence of the impact conditions related to block, slope and kinematics. The following three examples illustrate how the influence of changing impact conditions is accounted for by the developed formulations. Table 5.1 sums up the impact conditions underlying the following three examples for spherical blocks impacting a sandy slope of S0-4. For each example, one impact characteristic is varied (highlighted cells) while all other characteristics stay constant.

block mass m [kg]	slope inclination β [°]	drop height H [m]	represented in Figure
550	20	1 - 10	Figure 5.2
550	0 - 30	5	Figure 5.3
100 - 1000	20	5	Figure 5.4

Table 5.1: Impact conditions underlying the following three examples. The highlighted cells show the variation range of the investigated values.

Figure 5.2 to Figure 5.4 illustrate the resulting dependence of the coefficients R_n and R_t and of the rebound velocity components and rotation ($v_{n,r}$, $v_{t,r}$, ω_r) on the variation of the drop height H , the slope inclination β and the block mass m , respectively. The use of conventional coefficients of restitution would yield constant values for R_n and R_t in all three figures.

It has to be mentioned that the influence of varying block masses on the coefficients of restitution as well as on the rebound velocities is only accurately taken into account by using the **non-homogeneous** formulation expressing d_{max} (Eq. 4-21 instead of 4-22). The use of the homogeneous formulation (Eq. 4-22) however leads to constant coefficients of restitution and thus rebound velocities $v_{n,r}$ and $v_{t,r}$, revealing the fact that the influence of the block mass and radius are not yet represented by the homogeneous formulation.

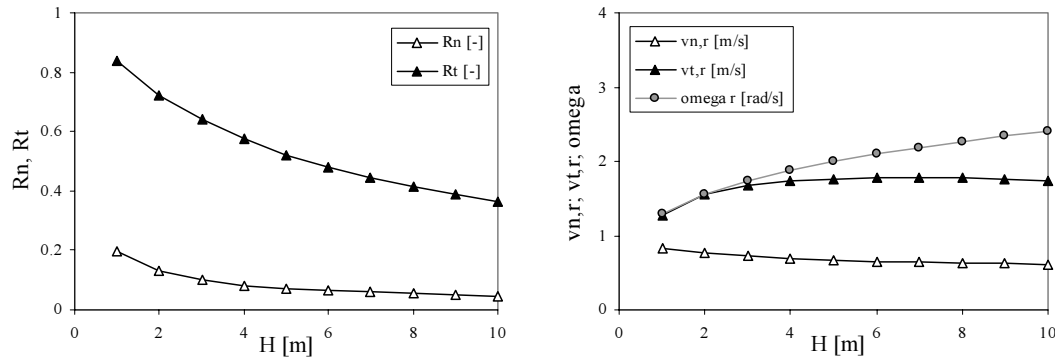


Figure 5.2: Variation of the coefficients of restitution R_n and R_t (left) and the translational and rotational rebound velocities (right) calculated by the developed formulations for various drop heights H .

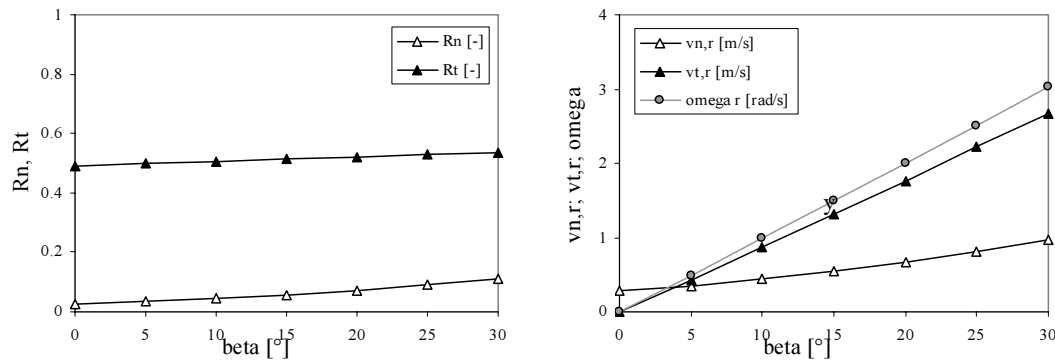


Figure 5.3: Variation of the coefficients of restitution R_n and R_t (left) and the translational and rotational rebound velocities (right) for various slope angles β .

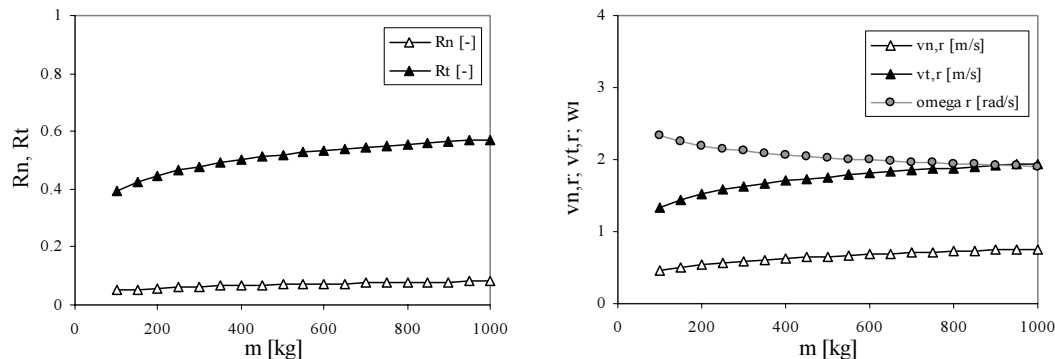


Figure 5.4: Variation of the coefficients of restitution R_n and R_t (left) and the translational and rotational rebound velocities (right) for various block masses m , calculated using the **non-homogeneous** formulation for d_{max} (Eq. 4-21).

In the following, the developed formulations are applied on the impact tests performed on a half-scale. The resulting coefficients of restitution and the normal, tangential and rotational rebound velocities are compared to the measured values. For the same impact conditions, the coefficients of restitution and rebound velocities are furthermore evaluated by means of the formulations used in the Colorado Rockfall Simulation Program CRSP [Pfeiffer & Bowen, 1989; refer to Chapter 2.3.5] and reported in the corresponding graph for comparison.

Before analysing the examples it has to be noted that the definition of the factors R_n and R_t used by the authors of the CRSP handbook does not correspond to the ratio of the rebound to the impact velocity components $v_{n,r}/v_{n,i}$ and $v_{t,r}/v_{t,i}$. These factors represent constants which are only function of the ground material and allow to calculate the rebound velocity by means of Eq. 2-18 and 2-19 and the scaling factors $f(F)$ and SF . For that reason, the CRSP factors will be named $R_{n,CRSP}$ and $R_{t,CRSP}$. For the following examples, $R_{n,CRSP}$ and $R_{t,CRSP}$ are chosen within the range of values proposed in the manual for soft soils ($R_{n,CRSP}$: 0.1 to 0.2; $R_{t,CRSP}$: 0.5 to 0.8) to equal $R_{n,CRSP} = 0.11$ and $R_{t,CRSP} = 0.8$. This couple of values is found to yield the *best possible fit* between the measured and the CRSP-calculated rebound velocities for the *entirety of impact tests* (without normal impacts) performed with concrete-filled blocks ($R^2 = 0.8996$). Based on the choice of $R_{n,CRSP} = 0.11$ and $R_{t,CRSP} = 0.8$, the coefficients of restitution R_n and R_t of CRSP presented graphically in the figures below are calculated by the ratios $v_{n,r}/v_{n,i}$ and $v_{t,r}/v_{t,i}$ respectively.

The investigated examples as well as the corresponding figures are listed in Table 5.2. The greyly highlighted cells indicate the varying impact condition (drop height, slope inclination and block mass), whereas all other values are kept constant. The blocks are dropped vertically from various heights and without initial rotation. The slope material consists of the sand S0-4, its characteristics can be found in Table 3.1. In all graphs, the measured values of the coefficients of restitution (R_n , R_t) and of the rebound velocities ($v_{n,r}$, $v_{t,r}$ and ω_r) are represented as triangles, whereas the black and grey lines represent the results yielded by the developed formulations and by the formulations used in CRSP, respectively.

block form	block mass m [kg]	slope inclination β [°]	drop height H [m]	represented in Figure
sphere	117	20	1 - 10	Figure 5.5
sphere	117	0 - 30	5	Figure 5.6
sphere	100 - 1000	20	5	Figure 5.7
cylinder	100 - 1000	20	5	Figure 5.8

Table 5.2: Impact conditions underlying the following three examples. The highlighted cells show the variation range of the investigated values.

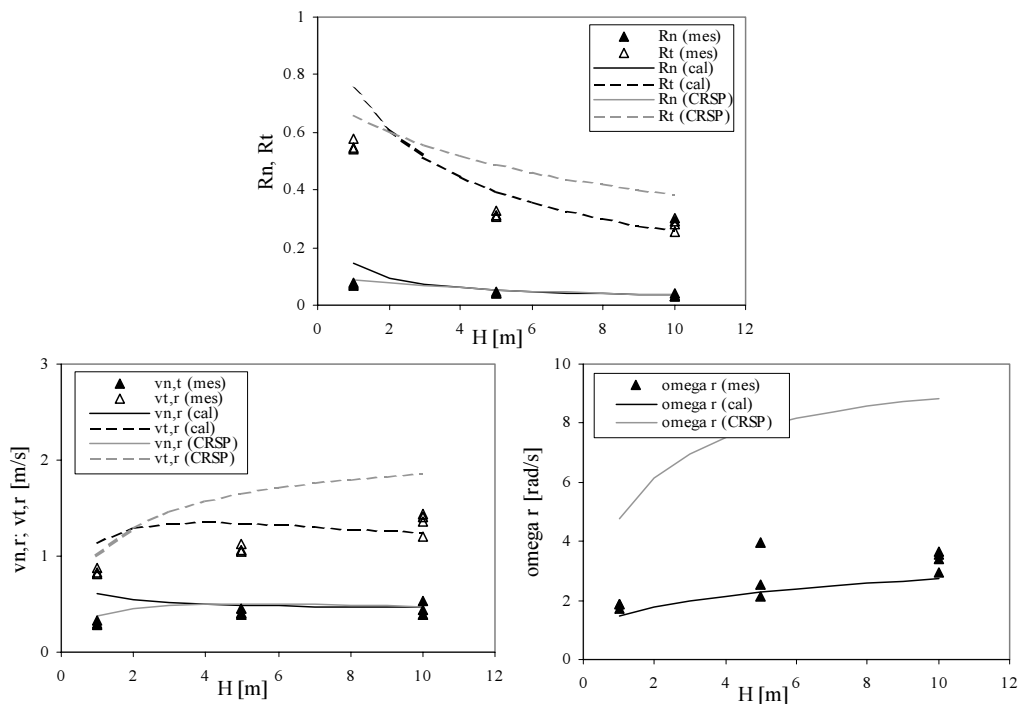


Figure 5.5: Comparison of measured and calculated coefficients of restitution (upper graph) and rebound velocities (lower graphs) for impact tests with the 117 kg sphere on a slope inclined at $\beta = 20^\circ$.

Figure 5.5 illustrates how the change of the drop height and thus of the impact velocity influences the coefficients of restitution (R_n , R_t) and the rebound velocity components ($v_{n,r}$, $v_{t,r}$ and ω_r) and how this change is taken into account by the developed formulations (black lines) and CRSP (grey lines). The analysis of Figure 5.5 reveals a very good correlation between the measured values of R_n and $v_{n,r}$ and the values calculated by means of the formulations proposed by CRSP (grey lines). The tangential component of the coefficient of restitution R_t and of the translational velocity $v_{t,r}$ do not meet as well the measured values, the tendencies however are rather well respected (relative to the measured data points, the curves seem to be vertically displaced). In case of the present as well as the following two examples, the chosen factors $R_{n,CRSP} = 0.11$ and $R_{t,CRSP} = 0.8$ are found to yield quite bad results (very high rotational velocity and generally too

high translational velocities). It has been found that the couple of $R_{n,CRSP} = 0.1$ and $R_{t,CRSP} = 0.6$ would yield a better fit for the first three examples with spherical blocks. However, as the slope material is the same for all impact tests, $R_{n,CRSP}$ and $R_{t,CRSP}$ should - according to their definition - not vary from one test to the other!

The formulations developed in this thesis overestimate the translational rebound velocities and the coefficients of restitution for small drop heights, whereas the correlation is better for drop heights larger than 5 m. As stated in the preceding chapter, this is due to the fact that for small drop heights the rolling mechanism prevails and, thus, the suggested formulations do not fully apply.

Considering the rotational velocity of the block after impact, the values calculated by means of the developed formulation expressing ω_r correspond very well to the measured values. The rotational velocity yielded by CRSP, however, exceeds by far the measurements (even for $R_{n,CRSP} = 0.1$ and $R_{t,CRSP} = 0.6$). This is probably due to the fact that CRSP assumes a pure rolling movement of the block at impact end ($v_{t,r} = \omega_r \cdot r$). In case of the present impact conditions (vertical drop) on sandy slopes inclined up to 30° , this assumption was however disproved.

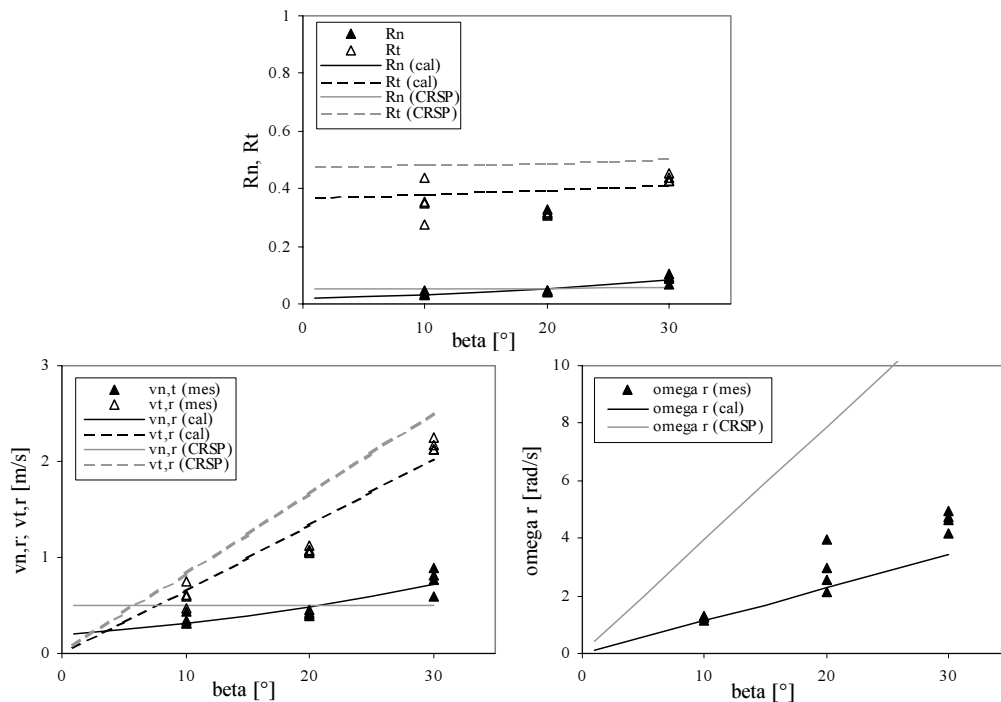


Figure 5.6: Comparison of measured and calculated data for impact tests with the 117 kg sphere dropped from 5 m on slopes with different inclinations.

The second example (Figure 5.6) illustrates how the influence of changing slope angles is taken into account by the investigated methods. The analysis of Figure 5.6 reveals that the developed formulations (black lines) reproduce very well the values and trends of the coefficients of restitution R_n and R_t as well as of the

rebound velocities $v_{n,r}$, $v_{t,r}$ and ω_r . As in the previous example, CRSP overestimates the tangential component of the coefficient of restitution and the rebound velocity. The tendencies of the data for changing slope angles are generally respected. The increase of rebound in normal direction with increasing slope angles, however, is not sufficiently taken into account by CRSP, as R_n and $v_{n,r}$ remain nearly constant. Further, CRSP models correctly an increase of rotational velocity with increasing slope angles; however, as for the first example, the evaluated rotational velocity is overestimated by far. As mentioned above, other couples of the factors $R_{n,CRSP}$ and $R_{t,CRSP}$ (e.g. 0.1 and 0.6) would yield a better fit

The two final examples investigate the rebound characteristics for increasing block masses (blocks with constant unit weight) in case of spherical (Figure 5.7) and cylindrical (Figure 5.8) blocks dropped from 5 m on a slope inclined at 20°. In both cases, the developed formulations represent well the measured data and the increasing tendency of the coefficients of restitution (R_n , R_t) and of the rebound velocities ($v_{n,r}$, $v_{t,r}$) as well as the decrease of ω_r . As shown by the grey lines, these tendencies are not well modelled by CRSP. On the contrary, the coefficients of restitution and the translational rebound velocities are constant for varying block masses. Yet it should be mentioned that CRSP is capable to reproduce a slight dependence of R_t and $v_{t,r}$ on the block mass in case of a non-zero initial rotation.

Concerning the rotational velocity of the block at impact end, CRSP still overestimates by far the rotation of the spherical block, whereas the results fit very well the measurements for the cylindrical block (as the cylinders have higher rotational velocities than e.g. the spheres, the results of CRSP fit better the measurements for cylindrical blocks). However, the fact that cylinders have higher rotational velocities than spheres is not respected by CRSP, evaluating higher rotational velocities for the spheres than for the cylinders.

In addition to the last two examples, Table 5.3 lists the mean measured values for $v_{n,r}$, $v_{t,r}$ and ω_r for two spherical blocks of different weights (117 kg and 550 kg) dropped from 5 m on a slope inclined at 20°. For comparison, the calculation results are listed for the developed formulations, CRSP and “constant” values of the coefficients of restitution R_n and R_t . The fields highlighted in grey indicate similar velocity values for both blocks, fact that does not correspond to reality. This indicates that, contrary to the newly developed method, neither the usual models with constant coefficients of restitution nor the model implemented in CRSP are able to account for a change of block mass.

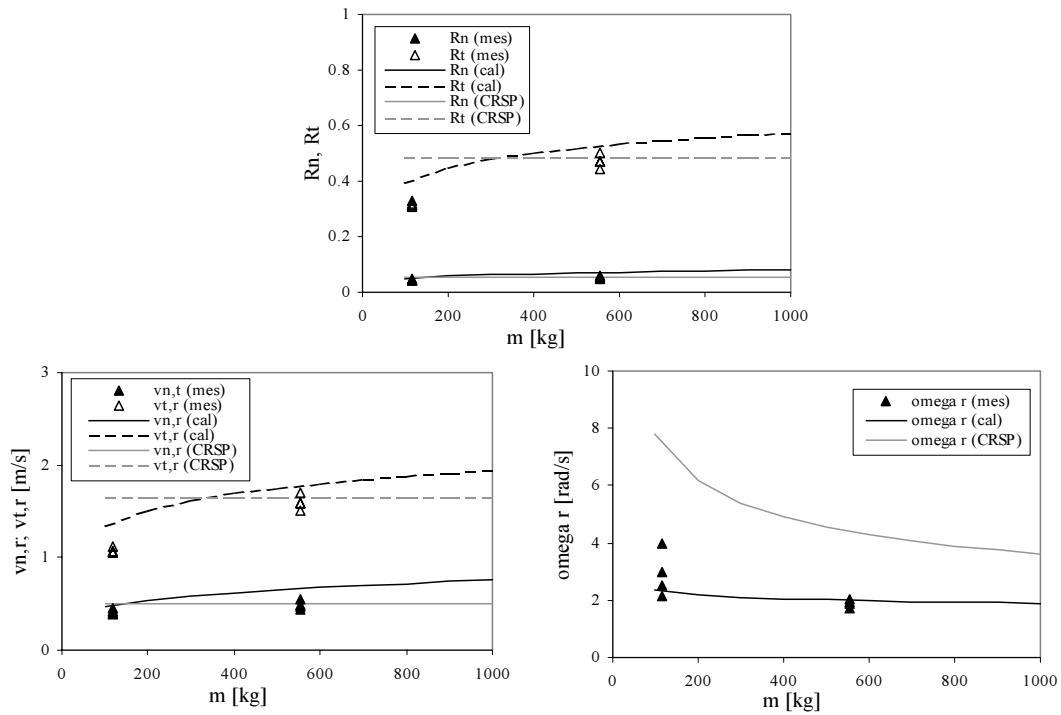


Figure 5.7: Comparison of measured and calculated data for impact tests of *spherical* blocks of various weights (117 kg and 550 kg) dropped from 5 m on a slope inclined at 20°.

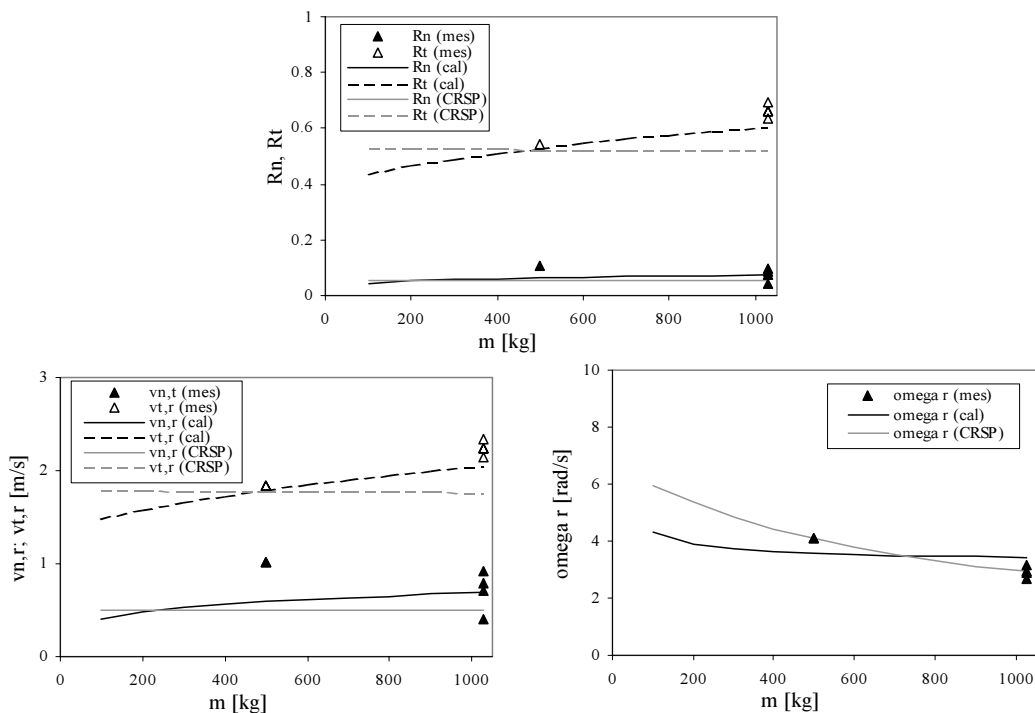


Figure 5.8: Comparison of measured and calculated data for impact tests of *cylindrical* blocks of various weights (500 kg and 1000 kg) dropped from 5 m on a slope inclined at 20°.

H = 5m $\beta = 20^\circ$	measured values (mean)	proposed formulations¹	CRSP: $R_{n,CRSP} = 0.11$ $R_{t,CRSP} = 0.8$	$R_n = 0.04$ $R_t = 0.35$ (fit for 117 kg)
117 kg				
$v_{n,r}$ [m/s]	0.4	0.5	0.5	0.4
$v_{t,r}$ [m/s]	1.1	1.3	1.7	1.1
ω_r [rad/s]	3.0	2.3	7.9	-
550 kg				
$v_{n,r}$ [m/s]	0.6	0.7	idem (0.5)	idem (0.4)
$v_{t,r}$ [m/s]	1.5	1.8	idem (1.7)	idem (1.1)
ω_r [rad/s]	2.8	2.0	4.5	-

Table 5.3: Comparison between measured and calculated values of the normal ($v_{n,r}$) and tangential ($v_{t,r}$) component of the translational rebound velocity as well as the rotational rebound velocity (ω_r).

Summing up the preceding observations, CRSP seems to reproduce very well (and admittedly better than the proposed formulations) the tendencies due to the influence of changing impact velocities on R_n , R_t , $v_{n,r}$ and $v_{t,r}$. The fact that the tangential components (R_t and $v_{t,r}$) are overestimated in the corresponding example (Figure 5.5) yet illustrates the problem that the factors $R_{n,CRSP} = 0.11$ and $R_{t,CRSP} = 0.8$, fitting best the entirety of the impact tests, are not adequate for all impact conditions (even if this should be the case, as the ground material does not change!). Further, the influence of the slope angle is not as well represented as by the proposed formulations. The influence of changing block masses, which is well represented by the proposed formulations, is not at all taken into account by CRSP.

These results are revealed as well by Figure 5.9, illustrating the correspondence between the measured values of R_n (left graph) and R_t (right graph) and their values computed by CRSP with $R_{n,CRSP} = 0.11$ and $R_{t,CRSP} = 0.8$. The corresponding comparison between measurement and computation with R_n (Figure 4.74) and R_t (Figure 4.80) calculated by means of the developed formulations show a much better fit, as illustrated in Figure 5.10. Finally, CRSP clearly overestimates the rebound rotation ω_r in all examples, whereas the proposed formulations fit very well the measurements.

¹ Due to the reasons discussed above, the non-homogeneous formulation expressing d_{max} is used (Eq. 4-21 instead of 4-22) for the calculation of the rebound velocities.

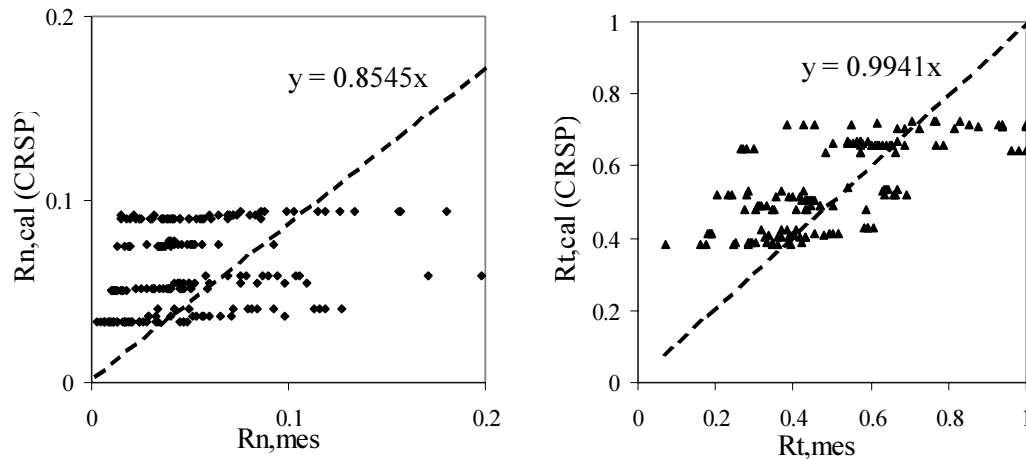


Figure 5.9: Correspondence between measured and calculated values of R_n and R_t using the program CRSP ($R_{n,CRSP} = 0.11$, $R_{t,CRSP} = 0.8$).

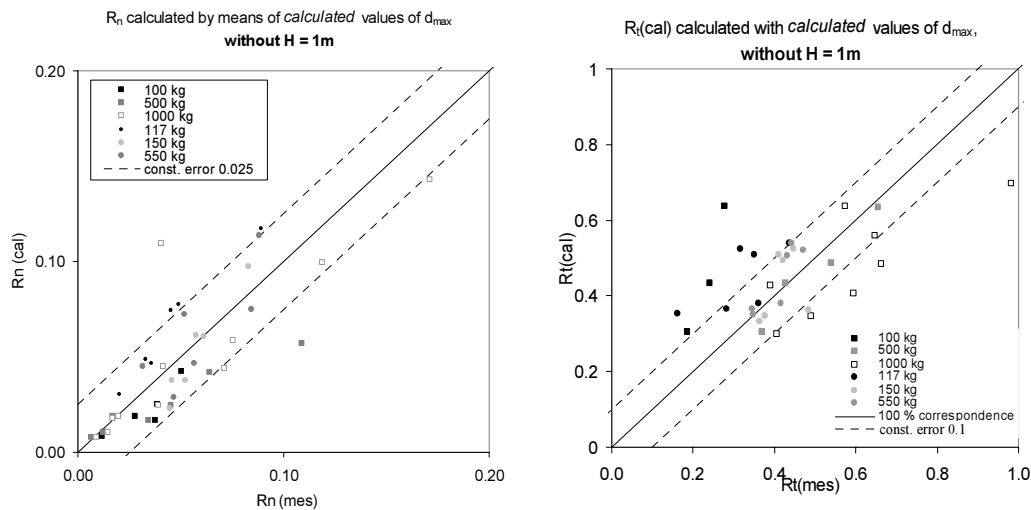


Figure 5.10: Correspondence between measured and calculated values of R_n (Figure 4.74) and R_t (Figure 4.80) using the developed formulations.

All examples illustrate the importance to account for the influence of the impact characteristics related to block, slope and kinematics in order to simulate adequately the highly complex mechanisms occurring during the impact of a rock block on a soft, granular slope. It could be shown that the developed formulations account well for all investigated parameters, even if the dependency of R_n and R_t and thus of $v_{n,r}$ and $v_{t,r}$ on the drop height could still be improved.

The impact tests performed on a half-scale in the framework of this thesis represent the particular conditions of a first impact of a rock block detached from a rock face (vertical drop on a sandy slope). Therefore, the proposed formulations should in future be verified and eventually adapted to other impact conditions, especially to impacts more tangent to the slope.

6 Conclusions and Prospects

Within the framework of this thesis, impact tests using different blocks on granular material have been performed on a small- and half-scale. The parameters supposed to govern the movement of the block during and after impact (its “rebound”) are investigated. The small-scale tests represent a preliminary study, which helped to calibrate the experimental set-up, to determine the most important parameters and to qualify their influence on the block movement after impact. Due to scale effects concerning the deformability of the ground material, the coefficients of restitution evaluated with the aid of the small-scale tests do not perfectly match similitude requirements. Consequently, a half-scale experimental campaign has been carried out to verify the qualitative conclusions and, above all, to quantify the influence of the various impact parameters as well as to develop a new and original mathematical formulation to express the coefficients of restitution.

On a **small-scale**, the following parameters have been varied at constant impact velocity (corresponding to 1 m of free fall):

- Block: weight (spheres of constant diameter but different weight)
- Ground: granular material (internal friction angle), degree of compaction
- Kinematics: slope inclination and impact direction (vertical or inclined)

The impact process has been filmed with the aid of a high-speed camera. By means of image analysing programs, a method has been developed to analyse the block movement before, during and after the shock and to gather information concerning the impact process itself (translational and rotational velocity and acceleration of the block, penetration into the ground material, duration of impact). A criterion has been defined for which the impact process is completed. By means of this criterion, the normal (R_n), tangential (R_t) and energetic (R_{TE}) coefficients of restitution have been evaluated, being the ratio of the normal or tangential velocities respectively the total energies before and after impact to the mass centre of the block. Finally, the influence of the varied parameters on the coefficients of restitution has been evaluated qualitatively. The following trends are emphasised as a consequence of the main results:

- Concerning the slope material characteristics, the motion of the block during and after impact is moderately influenced by the friction angle and significantly by the degree of compaction.
- The experiments also emphasise a clear dependency of the coefficients of restitution on parameters characterising the kinematics as the slope inclination, the impact angle or the impact direction: similar to observations made for impacts on rock slopes, the block rebounds less the

more normal the impact on the slope surface. The more tangent the impact is relative to the slope surface, the more distinct the rotation of the block at impact end.

- Concerning the block characteristics, testing series performed on spheres of identical diameter but of different weight show a certain decrease of the rebound and consequently of the coefficients of restitution for increasing block weights.
- Furthermore, it has been shown that small-scale impact tests are not appropriated for correct quantification of the test results, as the similitude requirements are extremely difficult to match regarding deformability of the ground material.

Based on the small-scale test results, the following parameters have been investigated on a **half-scale** for vertical impacts:

- Block: shape (spheres, cylinders of spherical base), weight (at constant unit weight), unit weight (at constant radius) and radius (at constant weight)
- Kinematics: slope inclination, impact velocity (by means of the dropping height)

The same interpretation methods have been used on a half-scale as for the small-scale tests. The qualitative interpretation of the half-scale tests confirmed a very clear dependency of the coefficients of restitution on parameters related to ground, block and kinematics. The following trends should be retained as a consequence of the main results:

- Concerning the kinematical characteristics of the impact, the clear dependency of the coefficients of restitution on the slope inclination is confirmed. Furthermore, the dropping height (corresponding to the impact velocity and thus the impact energy and impulsion) is found to have a very clear influence.
- Concerning the block characteristics, the block shape has been shown to have a certain influence, especially on steeper slopes (due to the block rotation). The block mass is also confirmed to have a certain influence, depending on the radius of the block. As has been shown (and will be reiterated below), different mechanisms occur during impact. It is therefore not surprising, that the trends observed for different block characteristics are not always very explicit.

The movement of the block during impact has been found to consist of three main mechanisms acting partly antagonistically:

- a normal translation (penetration), as a function of the bearing capacity of the ground material,

- a tangential translation (sliding), depending on the mass and shear resistance of the ground material in front of the block,
- rotation of the block, as a function of the slope inclination, the impact direction and the impact velocity (by means of the depth of the crater generated during impact).

It has been shown that these mechanisms are very much interdependent, as illustrated by the following four examples: for vertical impacts on horizontal ground, no rotation and lateral translation occur. For impacts of small incident velocity (corresponding to a free fall of about 1 to 2 m) on a stable slope, no distinct crater is formed (only little vertical translation) whereas the lateral translation and the rotation of the block are very clear. For an impact of high velocity on the same slope, the vertical translation preponderates (as the penetration is large), whereas the lateral translation (due to ground failure) and rotation are less clear. If the slope inclination is close to the internal friction angle of the ground material, the ground fails superficially at impact and causes a very distinct lateral movement of the block, whereas penetration and rotation are comparatively less important. These different mechanisms occurring during impact emphasise the complexity of the impact process and explain the difficulty encountered during the development of the formulations expressing the coefficients of restitution.

Based on the aforementioned observations, the maximum penetration depth (d_{\max}) of the block into the ground material, the vertical component of the maximum force $F_{y,\max}$ acting between block and ground material and thus the vertical component of the maximum acceleration $a_{y,\max}$ (as $F_{y,\max} = m \cdot a_{y,\max}$, m being the block mass) as well as the rotational velocity ω_r of the block at impact end, have been quantified. The formulations developed to express the stated terms are based on the characteristics found to govern the respective value. The following remarks sum up the results obtained, as well as some critical considerations:

- The formulation proposed for the maximum penetration depth d_{\max} is based on the propositions quoted in literature for impacts on elastic (theory of Hertz, Lang) and elasto-plastic (proposition of Azimi & Desvarreux) material and enhanced to include the influence of changing slope angles. It has been found that different block shapes require slightly different correction factors. A first proposition for the formulation of d_{\max} , matching the measured data very well is not homogeneous in terms of units. Thus, a second, homogeneous formulation has been proposed, for which the correlation with the measured data is slightly less pronounced, but still very satisfactory:

$$d_{\max} = 1.3 \cdot \left(\frac{mgH}{M_E \cdot r^{0.5}} \right)^{0.4} \cdot \begin{cases} \left(-0.029 \cdot \frac{\beta}{\varphi} + 0.3423 \right) & ; \text{ sphere} \\ \left(-0.1293 \cdot \frac{\beta}{\varphi} + 0.4175 \right) & ; \text{ cylinder} \end{cases}$$

- The formulation proposed for the maximum impulsive force acting on the block during impact, $F_{y,\max}$, has been developed based on the proposition of Montani-Stoffel [1998] for impacts on granular material resting on a concrete slab. Whereas the formulation proposed by Montani-Stoffel is valid only for blocks of a constant relation between mass and contact radius, the new formulation accounts also for changes in block density:

$$F_{y,\max}^{(E_{\text{pot}})} = 1.15 \cdot m^{0.2} \cdot r^{0.6} \cdot M_E^{0.4} \cdot (E_{\text{pot}})^{0.6}$$

However, it was not possible to find a homogeneous formulation of the factor accounting for the influence of the block density due to a lack of data. This point should clearly be re-examined in forthcoming studies. Furthermore, it has been shown that the slope angle has no significant effect on the vertical component of the maximum acceleration force. The correlation between measured and calculated values of $F_{y,\max}$ has been found to be very good.

- The formulation proposed to describe the rotational velocity ω_r has been developed based on the ratio of the dropping height H to the maximum penetration d_{\max} to account for the different mechanisms encountered during impact:

$$\omega_r = \left(\frac{H}{d_{\max}} \right)^{0.45} \cdot \frac{\beta}{\varphi} \cdot \begin{cases} 1.2 & ; \text{ cylindrical blocks} \\ 0.7 & ; \text{ spherical blocks} \end{cases}$$

The proposed formulation accounts also for the slope inclination and the slope stability (by means of the ratio β/φ) and matches the measured rotational velocities very well. However, here too, it was not possible to find a homogeneous formulation regarding units.

Furthermore, it has been stated that the rotation of the block increases at increasing slope angles up to a maximum value and decreases at further increases of β approaching the internal stability limit of the slope characterised by φ .

A further investigation of the impact mechanism revealed that the acceleration plateau observed for a large proportion of the impact tests corresponds probably to the occurrence of global base failure in the ground material. Consequently, the vertical component of the acceleration plateau $a_{y,plateau}$ can be calculated with the aid of the quotient of the maximum bearing capacity of the ground R_f (according to Lang & Huder [1990]) and the block mass m . Only for slope angles close to the limit equilibrium of the slope, R_f is found to underestimate slightly the real acting force meaning that the ground failure mechanism corresponds more to slope- than base failure. Furthermore, it has been shown that a critical impact energy (equal to 6 kJ under the test conditions) exists at which global ground failure occurs. However, as for certain impact conditions (small dropping heights, large slope angles) a significant part of impact energy has been found to be transmitted directly to block rotation, the vertical load applied on the ground material is stated to be insufficient to provoke global base failure even if the critical impact energy is reached. This result emphasises once more the complexity of the impact mechanisms.

Finally, using the knowledge acquired with the aid of the above-mentioned investigations, new formulations have been developed to express the normal and tangential components of the coefficients of restitution. Based on the idea of the conservation of linear momentum, the ratio of masses moving before and during impact ($m/(m+M)$, m being the block mass and M the ground mass) has been found to be a promising tool to define R_n and R_t . M has been found to be appropriately represented by the ground mass resisting the block movement in normal (global base failure) respectively tangential (shear failure of the mass in front of the block) direction. The formulations found to correlate best with the test results have been evaluated to be as follows:

- $R_n = \frac{m}{m + C_1 \cdot \rho_{ground} \cdot (d_{max} \cdot A_d)}$, where $C_1 = a \cdot e^{-b \frac{\beta}{\varphi}}$, a and b are factors

which are function of the block (form, unit weight) and A_d is the section of the block at level of the ground surface for the maximal penetration depth d_{max} . The fact that a differentiation has to be made for C_1 for blocks of different unit weights shows that the proposed formulation is not yet perfect. Further impact tests using blocks of different volume weight should help to improve the formula.

- $R_t = \frac{m}{m + 43 \cdot \rho_{ground} \cdot (d_{max}^2 \cdot r_d)}$, r_d being the radius of the block for the maximal penetration depth d_{max} .

- By means of the formulation proposed to express ω_r and the coefficients R_n and R_t , the energetic coefficient of restitution R_{TE} equals:

$$R_{TE} = \frac{m \cdot \left[\left(R_t \cdot v_{t,i} \right)^2 + \left(R_n \cdot v_{n,i} \right)^2 \right] + I \cdot \omega_r^2}{m \cdot v_i^2 + I \cdot \omega_i^2}.$$

As the normal and tangential components of the coefficients of restitution R_n and R_t have been defined based on ground failure mechanisms due to normal (R_n) and lateral (R_t) loading of the ground material, the proposed formulations apply only in case of sufficient penetration of the block into the ground material. In the case of small penetration depth and preponderating rolling movement of the block, the formulations have been found to overestimate the rebound velocity. As the energetic coefficient of restitution R_{TE} is a function of R_n and R_t , the same restrictions are valid for R_{TE} . However, for impacts with preponderating translational motion of the block (all dropping heights H on horizontal ground and $H > 1$ m for slopes, corresponding to most impacts *in situ*), the proposed formulations have been shown to produce good correlation with the measured values for R_n , R_t and R_{TE} .

By applying the developed formulations to several impact tests and by comparing the obtained rebound velocities and coefficients of restitution to the measured values (Chapter 5), it could be shown that the tendencies due to the influence of changing impact velocities on R_n , R_t , $v_{n,r}$, $v_{t,r}$ and ω_r are reproduced well by the proposed formulations in case of drop heights > 5 m. The influence of changing slope angles and block masses are reproduced very well. This represents an important progress compared to the existing methods. The comparison with calculation results provided by the program CRSP and by the most commonly used method of constant coefficients R_n and R_t has proved that the influences of changing slope angles and block masses are adequately reproduced only by the proposed formulations.

The fact that various distinctions of cases for different block shapes and impact conditions (affecting the rotation and direction of translation) had to be made concerning the validity of the formulations proposed for R_n , R_t and R_{TE} as well as for d_{max} and ω_r , illustrates the complexity of the occurring impact mechanisms. As it has been shown very clearly by this thesis, it is extremely difficult and even illusory to model all different mechanisms occurring during the impact of a rock block on granular material on one or two comprehensive formulations, such as R_n and R_t , expressing the rate of restituted velocity for the mass centre of the block. This simplification, actually adopted by most of the existing rockfall trajectory codes (!), is certainly convenient but incapable of reproducing the impact phenomenon, especially on granular material. It is possible that the impact

phenomenon could be better represented with the aid of formulations defining the coefficients of restitution not for the mass centre of the block, but for the instantaneous contact surface between block and ground material.

Therefore, research should be pursued to investigate whether real conditions can be matched more appropriately by means of coefficients of restitution defined at the contact surface between block and ground material to account for the block shape and rotation. The interaction between block and ground material should be investigated systematically based on kinematical equations. In this context it could be helpful to perform small-scale impact tests on granular material making it possible to observe the deformation pattern occurring in the ground material (as performed by Selig & McKee [1961] for impulsively loaded superficial foundations; refer to Chapter 4). Such tests could also help to verify the results of this thesis concerning the ground failure mechanisms, always bearing in mind the problems related to any form of down-scaling.

Only a small proportion of all imaginable impact conditions has been investigated within the scope of this thesis. It is thus important to keep in mind that some of the described results and proposed formulas may be influenced by the specificity of the half-scale testing program; that is to say: spherical or spherical based blocks, vertical impacts from a maximum height of 10 m without initial rotation, maximum block masses of 1000 kg and a sandy slope (friction angle of 33°). The kinematical impact conditions (vertical fall on a slope, no initial rotation, high energy loss during impact resulting in low coefficients of restitution) correspond to the first impact of a rock block detached from a steep rock face.

To improve the proposed formulations and verify their applicability to other impact conditions, further research should investigate definitively the influence of the following parameters:

- block: block shapes other than spheres and sphere-likes, configuration at impact,
- ground: materials with other characteristics: grain size distribution, internal friction angle, cohesion, water content (to verify the trends observed by Zinggler [1990] and by Chau & al. [1999a] for small-scale tests),
- kinematics: impacts with initial rotation and/or more tangent to the slope (corresponding to subsequent rebounds after the first impact), impacts with energies in excess of 100 kJ (“real-scale” *in situ* tests).

As regards the block shape, mention should be made that some impact tests using a cubic block have been performed within the scope of this thesis. It has been shown that the impact configuration for non-spherical blocks (as illustrated by

Figure 6.1) has a very important influence on the block movement during and after impact. The impact problem has been found to be three-dimensional (as for certain configurations the block topples to the side, leaving the image plan and rendering a 2-D analysis impossible), calling for a 3-D analysis of the phenomenon. The tests therefore could not be investigated more closely within the scope of this thesis, as only 2-D analysing methods (*one* camera, 2-D version of the motion analysing tool) were available. However, the few tests performed have already clearly shown the importance of further research in this direction.

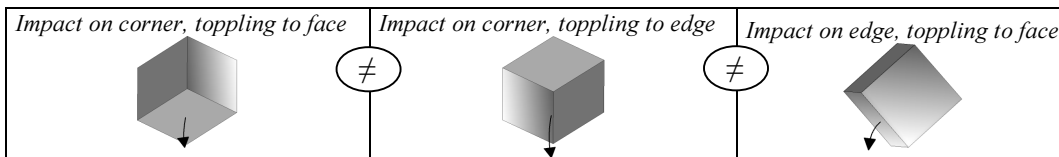


Figure 6.1: Example of different configurations of a cubic block at impact.

Pursuing rockfall research in the specified directions should lead to a better understanding of the rebound phenomenon. The subsequent implementation of the gained knowledge in rockfall codes should lead to a better prediction ability for rock block trajectories and to an improved delineation of areas at risk.

References

- Alfonsi, P.; Durville, J. L. (1996): Trajectographie des blocs. Rapport de stage d'initiation, présenté par M. Ladraa le 27 février 1996, Paris, F
- Azimi, C.; Desvarreux, P. (1977): Calcul de chutes de blocs et vérification sur modèle réduit. Rapport ADRGT
- Azimi, C.; Desvarreux, P. (1988): Les paravalanches: ouvrages de protection contre les avalanches et les chutes de pierres. Direction de la formation continue et de l'action internationale, Chambéry, 8-10 mars 1988, Paris, F
- Azimi, C.; Desvarreux, P.; Giraud, A.; Martin- Cocher, J. (1982): Méthode de calcul de la dynamique des chutes de blocs - Application à l'étude du versant de la montagne de La Pale (Vercors). Bulletin de liaison des laboratoires des ponts et chaussées 122(Nov./Dez.), pp. 93-102, Paris, F
- Azzoni, A. (1993): Methods for predicting rockfalls. MSc Dissertation, Imperial College of Science, Technology and Medicine, London, GB
- Azzoni, A.; Freitas, M. H. (1995): Experimentally Gained Parameters, Decisive for Rock Fall Analysis. *Rock Mechanics and Rock Engineering* 28(2), pp. 111-124, Wien, A
- Azzoni, A.; La Barbera, G.; Rossi, P. P.; Zaninetti, A. (1996): Fenomeni di caduta massi: sperimentazioni in sito e back analyses con il modello matematico CADMA. Giornata di Studio su " La protezione contro la caduta massi dai versanti rocciosi 24 ottobre 1996, pp. 15-27, Torino, I
- Azzoni, A.; La Barbera, G.; Zaninetti, A. (1995): Analysis and Prediction of Rockfalls Using a Mathematical Model. *Rock Mechanics and Mining Sciences* 32(7), pp. 709-724, London, GB
- Azzoni, A.; Rossi, P. P.; Drigo, E.; Giani, G. P.; Zaninetti, A. (1992): In situ observation of rockfall analysis parameters. *Proceedings of the sixth International Symposium of Landslides*; 10 - 14 Feb. 1992, Christchurch (Vol. I), pp. 307-314, Rotterdam, NL
- Barbieri, G.; Giani, G. P.; Uras, G.; Vernier, A. (1988): Modellizzazione della frana di crollo di Monte Oili in agro di Baunei (Nuoro). Presentato alla Riunione Plenaria delle Unità Operative del CNR a Roma il 19 e 20/12/1988.
- Benitez, M. A. H.; Bollo, M. F.; Rodriguez, M. P. H. (1977): Bodies Falling Down on Different Slopes - Dynamic Study. *Proceedings of the Ninth International Conference on Soil Mechanics and Foundation Engineering* Vol. 2, pp. 91-94, Tokyo
- Böll, A. (2001): Menace de chutes de pierres et protection contre les chutes de pierres en Suisse. Presentation à Walenstadt, 31.05.2001, CH
- Bozzolo, D.; Pamini, R. (1986): Simulation of Rock Falls down a Valley Side. *Acta Mechanica* 63, pp. 113-130, Wien, A
- Bozzolo, D.; Pamini, R.; Hutter, K. (1988): Rockfall analysis - A mathematical model and its test with field data. *Landslides - Proceedings of the fifth international symposium on landslides*, 10-15 July 1988 Vol. 1, pp. 555-560, Lausanne, CH
- Broili, L. (1974): Ein Felssturz im Grossversuch. *Rock Mechanics* (Suppl. 3), pp. 69-78
- Broili, L. (1977): Relations between scree slope morphometry and dynamics of accumulation processes. *Proceedings Meeting on Rockfall dynamics and protective works effectiveness*, pp. 11-23, Bergamo, I
- Bucher, K. (1997): Dynamische Berechnung von Steinschlageinwirkungen. *Publications de la Société Suisse de Mécanique des Sols et des Roches*, 7.11.1997, Montreux 135, pp. 39-47, Montreux, CH
- Budetta, P.; Santo, A. (1994): Morphostructural evolution and related kinematics of rockfalls in Campania (southern Italy): A case study. *Engineering Geology* 36, pp. 197-210

- Calvetti, F.; Genchi, R.; Nesta, L.; Nova, R. (1997): Numerical simulation of rock block impacts on rigid sheds. Proceedings of the Sixth Int. Symp. on Numerical Models in Geomechanics - NUMOG VI, Montreal, Canada, 2-4 July 1997, pp. 635-640
- Camponuovo, G. (1977): ISMES experience on the model of St. Martino. Proceedings Meeting on Rockfall dynamics and protective works effectiveness, 20-21 may 1976, pp. 25-38, Bergamo, I
- Cancelli, A.; Crosta, G. (1993): Rockfall Hazard in Italy: assessment, mitigation and control. Milano, I
- Chau, K. T.; Chan, L. C. P.; Wu, J. J.; Liu, J.; Wong, R. H. C.; Lee, C. F. (1998 b): Experimental studies on rockfall and debris flow. Proceedings of the One Day Seminar on Planning, Design and Implementation of Debris Flow and Rockfall Hazards Mitigation Measures, 27 October 1998, pp. 115-128, Hong Kong
- Chau, K. T.; Wong, R. H. C.; Lee, C. F. (1998 a): Rockfall Problems in Hong Kong and some new Experimental Results for Coefficients of Restitution. International Journal of Rock Mechanics and Mining Sciences: 3rd north American Rock Mechanics Symposium (NARMS '98) 35(4-5), pp. 662-663
- Chau, K. T.; Wong, R. H. C.; Liu, J.; Wu, J. J.; Lee, C. F. (1999 b): Shape effects on the coefficient of restitution during rockfall impacts. Proceedings of the 9th International Congress on Rock Mechanics, International Society for Rock Mechanics (ISRM), Paris 1999. Vol. 1, pp. 541-544
- Chau, K. T.; Wong, R. H. C.; Wu, J. J. (2002): Coefficient of restitution and rotational motions of rockfall impacts. International Journal of Rock Mechanics and Mining Sciences 39, pp. 69-77
- Chau, K. T.; Wu, J. J.; Wong, R. H.; Lee, C. F. (1999 a): The coefficient of restitution for boulders falling onto soil slopes with various values of dry density and water content. Proceedings of the Int. Symp. on Slope Stability Engineering: Geotechnical and Geoenvironmental Aspects, November 8-11, 1999, Matsuyama, Shikoku, Japan (Vol. 2), pp. 1355-1360
- Cheng, Y. M.; Zhang, Y. H. (2000): Rigid body rotation and block internal discretization in DDA analysis. International Journal for Numerical and Analytical Methods in Geomechanics Vol. 24(No. 6), pp. 567-578
- Crosta, G.; Agliardi, F. (2001): Frane di crollo e caduta massi: aspetti geomorfologici, modelli teorici e simulazione numerica.
- Cundall, P. (1971): A computer model for simulating progressive, large-scale movements in blocky rock systems. Symposium on Rock Fracture of the International Society of Rock Mechanics, pp. paper II-8-, Nancy, F
- De Col, R.; Cocco, S. (1996): Motivazioni tecniche ed economiche per la standardizzazione delle prove sulle opere paramassi nella Provincia Autonoma di Trento. Giornata di Studio su " La protezione contro la caduta massi dai versanti rocciosi 24 ottobre 1996, pp. 65-72, Torino, I
- Descoedres, F. (1990): L'éboulement des Crétaux: Aspects géotechniques et calcul dynamique des chutes de bloc. Publications de la Société Suisse de Mécanique des Sols et des Roches Session de printemps, 21.06.1990, N° 121, pp. 19-25, Sion, CH
- Descoedres, F. (1997): Aspects géomécaniques des instabilités de falaises rocheuses et des chutes de blocs. Publications de la Société Suisse de Mécanique des Sols et des Roches, 7.11.1997, Montreux, N° 135, pp. 3-11
- Descoedres, F.; Montani, S. (1996): Etude expérimentale de la chute de blocs impactant une dalle en béton armé recouverte par des matériaux amortissants. Département fédéral des transports, des communications et de l'énergie - Office fédéral des routes, Zürich, CH
- Descoedres, F.; Montani, S. (1996): Etude expérimentale de la chute de blocs impactant une dalle en béton armé recouverte par des matériaux amortissants. Mandats de recherche 98/92 et 92/95 effectués à la demande du groupe de travail Recherche en matière de ponts, Lausanne, CH

- Descoedres, F.; Zimmermann, Th. (1987): Three-dimensional dynamic calculation of rockfalls. International Society for Rock Mechanics: Proceedings of the Sixth International Congress on Rock Mechanics, Montreal / Canada (1987) Vol. 1, pp. 337-342
- Dudt, J. P.; Heidenreich, B. (2001): Treatment of the uncertainty in a three-dimensional numerical simulation model for rock falls. Proceedings of the International Conference on Landslides - Causes, Impacts and Countermeasures, 17-21 June 2001, Davos, Switzerland, pp. 507-514
- Dysli, M.; Bombeli, Ph. (2001): Contrôle du compactage des fouilles en tranchée par pénétromètre dynamique léger. Rapport final, Mandat de recherche 30/96
- El-Sabh, M. I.; Schenk, V.; Tsuchiya, Y. (1999): Natural Hazards. Journal of the International Society for the Prevention and Mitigation of Natural Hazards
- Erismann, T. H. (1986): Flowing, Rolling, Bouncing, Sliding: Synopsis of Basic Mechanisms. Acta Mechanica 64, pp. 101-110, Wien, A
- Erismann, T. H.; Abele, G. (2001): Dynamics of Rockslides and Rockfalls. Springer-Verlag
- Evans, S. G.; Hungr, O. (1993): The assessment of rockfall hazard at the base of talus slopes. Canadian Geotechnical Journal 30, pp. 620-636, Canada
- Falcetta, J. L. (1985 a): Etude cinématique et dynamique de chutes de blocs rocheux. Thèse d'ingénieur docteur.
- Falcetta, J. L. (1985 b): Un nouveau modèle de calcul de trajectoires de blocs rocheux. Revue Française de Géotechnique 30 (1er Trimestre 1985), pp. 11-17, Paris, F
- Fornaro, M.; Peila, D.; Nebbia, M. (1990): Block falls on rock slopes - application of a numerical simulation program to some real cases. Proceedings of the 6th International Congress IAEG, pp. 2173-2180, Rotterdam, NL
- Fossati, D.; Mazzocola, D.; Sciesa, E.; Ceriani, M. (2000): Procedure per la valutazione e la zonazione della pericolosità e del rischio da frana in regione Lombardia. Bollettino Ufficiale Regione Lombardia No. 51, Editione Speciale del 22 dicembre 2000, No. 318 bis, Milano, I
- Frischholz, R. (1997): Software zur automatischen Bewegungsanalyse. Biomechanik und Motorik. DSV Band 75, Hamburg, D
- Frischholz, R.; Spinnler, K. P. (1993): Class of algorithms for realtime subpixel registration. Europto Conference, Munich, June 1993, Munich, D
- Gerber, W. (1995): Auswertung von Feldversuchen. Unterlagen zum FAN-Kurs der Forstlichen Gruppe Naturgefahren zum Thema "Steinschlag", Vitznau, Oktober 1995 Kap. 9, Vitznau, CH
- Gerber, W.; Haller, B. (1997): Neue Schutzbauwerke gegen Steinschlag. Publications de la Société Suisse de Mécanique des Sols et des Roches, 7.11.1997, Montreux 135, pp. 25-29, Montreux, CH
- Giani, G. P. (1992): Rock Slope Stability Analysis. Balkema, Rotterdam
- Giani, G. P.; Alivernini, R.; Deangeli, C.; Ferrero, A. M. (1996): Aspetti progettuali generali del problema della caduta massi. Giornata di Studio sulla protezione contro la caduta massi dai versanti rocciosi 24 ottobre 1996, pp. 5-13, Torino, I
- Goldsmith, W. (1960): Impact. Edward Arnold LTD
- Gsteiger, P. (1990): Steinschlag Wald Relief - Empirische Grundlagen zur Steinschlagmodellierung, Bern, CH
- Guzzetti, F.; Crosta, G.; Detti, R.; Agliardi, F. (2002): STONE: a computer program for the three-dimensional simulation of rock-falls. Computers & Geosciences 28, pp. 1079-1093
- Habib, P. (1977): Note sur le rebondissement des blocs rocheux. Proceedings Meeting on Rockfall dynamics and protective works effectiveness, 20-21 mai 1976, pp. 123-125, Bergamo, I
- Harris, C. M. (1961): Shock and Vibration Handbook. Fourth edition, USA

- Hataf, N.; Aghaebrahimi, S. (1996): Stiffness and Damping Characteristics of Soils due to Dynamic Loading. Proceedings of the Asia-Pacific Conference on Shock & Impact Loads on Structures, Singapore, 23-24 January 1996, pp. 111-117
- Hayhurst, C. J.; Clegg, R. A.; Francis, N. J.; Birnbaum, N. K.; van den Berg, B. (1996): Numerical Simulation of Explosive and Impact Loading and Response Using AUTODYN-3D and AutoReaGas. Proceedings of the Asia-Pacific Conference on Shock & Impact Loads on Structures, Singapore, 23-24 January 1996, pp. 119-126
- Heidenreich, B.; Labiouse, V. (2003): Small-scale laboratory experiments of boulders bouncing on granular slopes. 10th Congress of the ISRM, "Technology Roadmap for Rock Mechanics" Symposium Series S33 (1), pp. 519-522, Johannesburg, South Africa
- Heidenreich, B.; Labiouse, V. (2004): Small-scale experimental study of rockfall impacts on granular slopes. *Rivista Italiana di Geotecnica* 2/2004, pp. 80-91.
- Heierli, W.; Merk, A.; Temperli, A. (1985): Schutz gegen Steinschlag / Protection contre chutes de pierres; 2. Auflage. Département fédéral des transports, des communications et de l'énergie - Office fédéral des routes, Forschungsarbeit 21/83
- Heim, A. (1882): Über Bergstürze. *Neujahresblatt* 84, pp. 1-31, Zürich, CH
- Hertz, H. (1882): Über die Berührung fester elastischer Körper. *Journal für die reine und angewandte Mathematik*, N° 92, pp. 156-171
- Hoek, E. (1987): Rockfall: a computer program for prediction rockfall trajectories. Vancouver, CA
- Hungr, O.; Evans, S. G. (1988): Engineering evaluation of fragmental rockfall hazards. *Landslides - Proceedings of the fifth international symposium on landslides, 10-15 July 1988, Vol. 1*, pp. 685-690, Lausanne, CH
- Hutchings, I. M.; Macmillan, N. H.; Rickerby, D. G. (1981): Further studies of the oblique impact of a hard sphere against a ductile solid. *Int. J. Mech. Sci.* 23(11), pp. 639-646, Great Britain
- Ishikawa, N. (1996): Some recent Impact Problems on Civil Engineering in Japan. Proceedings of the Asia-Pacific Conference on Shock & Impact Loads on Structures, Singapore, 23-24 January 1996, pp. 143-152, Singapore
- Japan Road Association (JRA) (1983): Rockfall Handbook. Tokyo, Japan
- Japanese highway public corporation (1973): Research report on rock falling tests.
- Jones, C. L.; Higgins, J. D.; Andrew, R. D. (2000): Colorado Rockfall Simulation Program Version 4.0. Colorado Geological Survey, Colorado, USA
- Jones, N. (1989): Structural impact.
- Kamijo, A.; Onda, S.; Masuya, H.; Tanaka, Y. (2000): Fundamental test on restitution coefficient and frictional coefficient of rock fall. Proceedings of the 5th Symposium on Impact Problems in Civil Engineering, Japan Society of Civil Engineers, June 8-9, 2000, pp. 83-86
- Kawahara, S.; Muro, T. (1999): Effect of soil slope gradient on motion of rockfall. Proceedings of the International Symposium on Slope Stability Engineering, November 8-11, 1999, Matsuyama, Shikoku, Japan. Vol. 2, pp. 1343-1348
- Ko Ko, C.; Flentje, P.; Chowdhury, R. (1999): Landslide risk assessment - Development of a hazard-consequence approach. *Slope Stability Engineering*, pp. 1309-1315, Rotterdam, NL
- Kobayashi, Y.; Harp, E. L.; Kagawa, T. (1990): Simulation of Rockfalls triggered by earthquakes. *Rock Mechanics and Rock Engineering* 23, pp. 1-20, Wien, A
- Krummenacher, B.; Keusen, H.-R. (1997): Steinschlag-Sturzbahnen - Modell und Realität. *Publications de la Société Suisse de Mécanique des Sols et des Roches*, 7.11.1997, Montreux 135, pp. 17-23, Montreux, CH
- Labiouse, V. (1994): Facteurs de dimensionnement des galeries de protection contre les chutes de blocs, rapport interne, Ecole polytechnique Fédérale de Lausanne, CH
- Labiouse, V.; Descoeudres, F. (1999): Possibilities and Difficulties in predicting Rockfall Trajectories. Proceedings of the Joint Japan-Swiss Scientific Seminar on Impact Load by

- Rock Falls and Design of Protection Structures; Kanazawa, Japan, 4-7 October 1999, pp. 29-36
- Labiouse, V.; Descoedres, F.; Montani, S. (1996): Experimental Study of Rock Sheds Impacted by Rock Blocks. *Science and Technology - Structural Engineering International* 3/96, pp. 171-176
- Labiouse, V.; Descoedres, F.; Montani, S.; Schmidhalter, C.-A. (1994): Etude expérimentale de la chute de blocs rocheux sur une dalle en béton armé recouverte par des matériaux amortissants. *Revue Française de Géotechnique* 69, pp. 41-62, Paris, F
- Labiouse, V.; Heidenreich, B.; Desvarreux, P.; Viktorovitch, M.; Guillemin, P. (2001): Chapitre IV: Etudes trajectographiques. Programme Interreg II C - "Falaises", pp. 155-211, Aosta, I
- Labous, L.; Rosato, A. D.; Dave, R. N. (1997): Measurements of collisional properties of spheres using high-speed video analysis. *Physical Review E* 56(5), pp. 5717-5725
- Lalanne, C. (1999): Chocs Mécaniques (Tome 2). *Vibrations et chocs mécaniques*, Paris, F
- Lang, H.-J.; Huder, J. (1990): *Bodenmechanik und Grundbau*. Springer-Lehrbuch, 4. Auflage
- Lee, K.; Elliott, G. M. (1998): Rockfall: Application of Computer Simulation to Design of Preventive Measures. *Proceedings of the One Day Seminar on Planning, Design and Implementation of Debris Flow and Rockfall Hazards Mitigation Measures*, 27 October 1998, pp. 47-65, Hong Kong
- Lee, K.; et al. (1998): Record of discussion. *Proceedings of the One Day Seminar on Planning, Design and Implementation of Debris Flow and Rockfall Hazards Mitigation Measures*, 27 October 1998, pp. 177-183, Hong Kong
- Lewis, A. D.; Rogers, R. J. (1988): Experimental and numerical study of forces during oblique impact. *Journal of sound and vibration* 125(3), pp. 403-412
- Lied, K. (1977): Rockfall problems in Norway. 90, pp. 51-53, Bergamo, I
- Lun, C. K. K.; Savage, S. B. (1986): The Effects of an Impact Velocity Dependent Coefficient of Restitution on Stresses Developed by Sheared Granular Materials. *Acta Mechanica* 63, pp. 15-44, Wien, A
- Masuya, H. (1993): The state of the art concerning the impact problem by rock falls in Japan. Internal report, LMR, Ecole Polytechnique Fédérale de Lausanne, CH
- Masuya, H. (1996): Study on Load Resistance Factor Design to Protection Structures in Mountain Roads. *Proceedings of the Asia-Pacific Conference on Shock & Impact Loads on Structures*, Singapore, 23-24 January 1996, pp. 285-292
- Masuya, H.; Nakata, Y.; Kajikawa, Y. (1996): Application of Combination Method of Distinct Element and Finite Element to Analysis of Impact on Structures. *Proceedings of the Asia-Pacific Conference on Shock & Impact Loads on Structures*, Singapore, 23-24 January 1996, pp. 279-283
- Mitha, S.; Tran, M. Q.; Werner, B. T.; Haff, P. K. (1986): The Grain-Bed Impact Process in Aeolian Saltation. *Acta Mechanica* 63, pp. 267-278, Wien, A
- Montani Stoffel, S. (1998): Sollicitation dynamique de la couverture des galeries de protection lors de chutes de blocs. Ph. D. thesis n° 1899, Ecole Polytechnique Fédérale de Lausanne, CH
- Montani Stoffel, S.; Labiouse, V. (1999): Sollicitation dynamique de la couverture des galeries de protection lors de chutes de blocs, Lausanne, CH
- Montani Stoffel, S.; Labiouse, V.; Descoedres, F. (1997): Essais d'impact de blocs sur un modèle de toit de galerie de protection. *Publications de la Société Suisse de Mécanique des Sols et des Roches*, 7.11.1997, Montreux N° 135, pp. 31-37
- Montani, S.; Descoedres, F.; Bucher, K. (1997): Numerical analysis of rock blocks impacting a rock shed covered by a soil. *Proceedings of the Sixth International Symposium on Numerical Models in Geomechanics NUMOG VI*, Montreal, Canada, 2-4 July 1997. pp. 641-646

- Montani, S.; Descoedres, F.; Egger, P. (1996): Impact de blocs rocheux sur des galeries de protection. Giornata di Studio su " La protezione contra la caduta massi dai versanti rocciosi 24 ottobre 1996, pp. 55-63, Torino, I
- Murata, S.; Shibuya, H. (1997): Measurement of impact loads on the rockfall prevention walls and speed of falling rocks using a middle size slope model. 2nd Asia-Pacific Conference on Shock & Impact Loads on Structures, Melbourne, Australia, November 25-27, 1997, pp. 383-393
- Newton, I. (1686): *Philosophiae naturalis principia mathematica*. London, GB
- Nishi, H.; Matsuoka, K. G.; Sato, M.; Sato, T.; Kaneko, M.; Nishimura, A. (1996): Impact test of PC Rock-Shed with Sand Cushion. Proceedings of the Asia-Pacific Conference on Shock & Impact Loads on Structures, Singapore, 23-24 January 1996, pp. 347-354
- OFEFP (Schäfer, W.); FNP (Ammann, W.); CEAC (Baumann, R.) (2001): Directive sur l'homologation de filets de protection contre les chutes de pierres. Switzerland
- Pamini et al. (1985): Modello matematico per lo studio della caduta dei massi.
- Paronuzzi, P. (1987 a): Rockfall: un programma basic per la simulazione cinematica dei crolli litoidi. Boll. Assoc. Min. Subalpina 24(1-2), pp. 185-196
- Paronuzzi, P. (1987 b): Modelli di calcolo per analisi della propagazione di blocchi rocciosi in frana. Rivista Italiana Geotecnica 21(4), pp. 145-165
- Paronuzzi, P. (1989): Probabilistic approach for design optimization of rockfall protective barriers. Q. J. Eng. Geol. 22, pp. 175-183, London, GB
- Peila, D. (1996): Uso di prove in vera grandezza per il dimensionamento di barriere paramassi. Giornata di Studio sulla La protezione contro la caduta massi dai versanti rocciosi 24 ottobre 1996, pp. 45-54, Torino, I
- Peila, D.; Pelizza, S.; Sassudelli, F. (1996): Risultati di un campo prove su barriere paramassi deformabili. Giornata di Studio sulla protezione contro la caduta massi dai versanti rocciosi 24 ottobre 1996, pp. 37-44, Torino, I
- Pfeiffer, T.; Bowen, T. (1989): Computer Simulation of Rockfalls. Bulletin of the Association of Engineering Geologists 26(1), pp. 135-146
- Pfeiffer, T.; Higgins, J. D. (1990): Rockfall Hazard Analysis using the Colorado Rockfall Simulation Program. Transportation Research Record 1288, pp. 117-126, Washington, USA
- Piteau, D. R. (1977): Computer Rockfall Model. 90, pp. 127-127, Bergamo, I
- Piteau, D. R.; Clayton, R. (1977): Discussion of paper Computerized design of rock slopes using interactive graphics for the input and output of geometrical data. By P. Cundall. 16th Symposium on Rock Mechanics, Minneapolis, pp. 62-63, Minneapolis, USA
- Press, W. H.; Teukolsky, S. A.; Vetterling, W. T.; Flannery, B. P. (1992): Numerical Recipes in C - Chapter 14: Savitzky-Golay Smoothing Filters. pp. 650-655
- Reynaud, S. (1999): Analyse de la dynamique de propagation d'éboulements rocheux. Etude présentée pour l'obtention du DEA: Mécanique des Milieux Géophysiques et Environnement - Promotion 1998-99, Grenoble, F
- Richards, L. R. (1988): Rockfall Protection: a review of current analytical and design methods. Pendii naturali e fronti di scavo, Atti del secondo circolo di conferenze di Meccanica ed Ingegneria delle Rocce (MIR), Politecnico di Torino, pp. (11-1)-(11-13), Torino, I
- Rickerby, D. G.; Macmillan, N. H. (1980): On the oblique impact of a rigid sphere against a rigid-plastic solid. Int. J. Mech. Sci. 22, pp. 491-494, Great Britain
- Ritchie, A. M. (1963): Evaluation of rockfall and its control. Highway research record 17, pp. 13-28, Washington, USA
- Rochet, L. (1987): Application des modèles numériques de propagation à l'étude des éboulements rocheux. Bulletin de liaison des laboratoires des ponts et chaussées 150-151 (juil.-août / sept.-oct. 1987), pp. 84-95, Paris, F

- Rochet, L. (1987): Development of numerical models for the analysis of propagation of rock-falls. Proceedings of the 6th International Congress on Rock Mechanics Vol. 1, pp. 479-484, Montreal, CA
- Rochet, L. (1987): Développement des modèles numériques dans l'analyse de la propagation des éboulements rocheux. Proceedings of the International Congress on Rock Mechanics, ISRM (1), pp. 479-484, Montreal
- Rochet, L. (1987): Développement des modèles numériques dans l'analyse de la propagation des éboulements rocheux.
- Rouiller, J.-D.; Jaboyedoff, M.; Marro, Ch.; Philipposian, F. (1997): MATTERROCK: Méthodologie d'étude d'instabilités de falaise et d'appréciation du danger. Société Suisse de Mécanique des Sols et des Roches, 7.11.1997, Montreux, N° 135, pp. 13-16
- Salençon, J.; Matar, M. (1982): Capacité portante des fondations superficielles circulaires. Journal de Mécanique théorique et appliquée 1(2), pp. 237-267
- Sato, M.; Kishi, N.; Iwabuchi, T.; Tanimoto, T.; Shimada, T. (1996): Shock Absorbing Performance of Sand Cushion. Proceedings of the Asia-Pacific Conference on Shock & Impact Loads on Structures, Singapore, 23-24 January 1996, pp. 393-400, Singapore
- Savitzky, A.; Golay, M. J. E. (1964): Smoothing and Differentiation of Data by Simplified Least Square Procedures. Analytical Chemistry 36, N° 8, pp. 1627-1639
- Selig, E. T.; McKee, K. E. (1961): Static and dynamic behavior of small footings. Journal of the soil mechanics and foundations division, Proceedings of the American Society of Civil Engineers SM6, pp. 29-47, USA
- Spang, R. M. (1998): Rockfall Barriers - Design and Practice in Europe. Proceedings of the One Day Seminar on Planning, Design and Implementation of Debris Flow and Rockfall Hazards Mitigation Measures, 27 October 1998, pp. 91-98, Hong Kong
- Spang, R. M.; Rautenstrauch, R. W. (1988): Empirical and mathematical approaches to rockfall protection and their practical applications. Landslides - Proceedings of the fifth international symposium on Landslides, Lausanne, 10 - 15 July 1988 (2), pp. 1237-1243
- Spang, R. M.; Sönsner, Th. (1995): Optimized Rockfall Protection by "Rockfall". Proceedings of the 8th International Congress in Rock Mechanics, Tokyo, Japan
- Statham, I. (1979): A simple dynamic model of rockfall: some theoretical principles and model and field experiments. ISMES: Int. Colloquium on Physical and Geomechanical Models, pp. 237-258, Bergamo, I
- Stevens, W. D. (1998): Rocfall: A tool for probabilistic analysis, design of remedial measures and prediction of rockfalls. Internet, Toronto, CA
- Stronge, W. J. (1990): Rigid body collision with friction. Proceedings: Mathematical and Physical Sciences (Royal Soc. London) A431(1881), pp. 169-181
- Sundararajan, G. (1990): The energy absorbed during the oblique impact of a hard ball against ductile target materials. Int. J. Impact Engineering 9(3), pp. 343-358, Great Britain
- Szabo, I. (1966): Einführung in die Technische Mechanik, Berlin, D
- Teraoka, M.; Iguchi, H.; Ichikawa, T.; Nishigaki, Y.; Sakurai, S. (2000): Analysis of motion for rock falling on a natural slope by using digital video image. Proceedings of the 5th Symposium on Impact Problems in Civil Engineering, Japan Society of Civil Engineers, June 8-9, 2000, pp. 87-90, Japan
- Timoshenko, S. P.; Goodier, J. N. (1970): Theory of elasticity. Third edition, USA
- Ujihira, M.; Takagai, N.; Iwasa, T. (1993): An experimental study on the characteristics of the impact load of falling rock. Int. J. of Surface Mining and Reclamation 7, pp. 81-89, Rotterdam, NL
- Urciuoli, G. (1988): Sperimentazione sulla caduta di blocchi lungo un pendio nella formazione calcareo-dolomitica della Penisola Sorrentina. Convengo sul tema: Cartografia e

- monitoraggio dei movimenti franosi, Bologna, 10-11 novembre 1998 pubbl. n° 164, pp. 35-54
- Urciuoli, G. (1996): Analisi cinematica di crolli per la progettazione di barriere paramassi. Giornata di Studio su " La protezione contro la caduta massi dai versanti rocciosi 24 ottobre 1996, pp. 29-36, Torino, I
- Ushiro, T.; Matsumoto, Y.; Akesaka, N.; Yagi, N. (1999): Study of accidents caused by rockfall in Kochi Prefecture. *Slope Stability Engineering*, pp. 1349-1354
- Ushiro, T.; Shinohara, S.; Tanida, K.; Yagi, N. (2000): A study on the motion of rockfalls on slopes. *Proceedings of the 5th Symposium on Impact Problems in Civil Engineering*, Japan Society of Civil Engineers, June 8-9, 2000, pp. 91-96, Japan
- Wallace, W. L. (1961): Displacement of long footings by dynamic loads. *Journal of the soil mechanics and foundations division*, *Proceedings of the American Society of Civil Engineers SM5*, pp. 45-68, USA
- Wang, W. L. (1971): Low velocity projectile penetration. *Journal of the soil mechanics and foundations division*, *Proceedings of the American Society of Civil Engineers SM12*, pp. 1635-1655, USA
- Wong, R. H.; Ho, K. W.; Chau, K. T. (1999): Experimental study for rockfall simulation. *Proceedings of Construction challenges into the next century*, Hong Kong, pp. 92-97, Hong Kong
- Wong, R. H.; Ho, K. W.; Chau, K. T. (2000): Shape and mechanical properties of slope material effects on the coefficient of restitution on rockfall study. *Proceedings of the 4th North American Rock Mechanics Symposium NARMS 2000*, Seattle, Washington, USA, 31 July - 3 August 2000: *Pacific Rocks 2000 - "Rock around the Rim"*, pp. 507-514
- Wu, S. S. (1985): Rockfall evaluation by computer simulation. *Transportation Research Record* 1031, pp. 1-5, Washington, USA
- Yoshida, H. (1998): Movement of boulders on slope and its simulation. Japan
- Yoshida, H. (1998): Recent studies on rockfall control in Japan. Japan
- Yoshida, H.; Masuya, H.; Ihara, T. (1988): Experimental study of impulsive design load for rock sheds. *IABSE Proceedings P-127/88 (3)*, pp. 61-74
- Zimmermann, Th.; Rebola, B.; Davalle, E.; Descoedres, F. (1989): A three-dimensional numerical simulation model for rockfalls. *IREM Internal Report 89/1*, January 1989, Lausanne, CH
- Zinggler, A. (1990): Steinschlagsimulation in Gebirgswäldern - Modellierung der relevanten Teilprozesse. Bern, CH

Appendix

Appendix I: Coefficients of restitution R_t , R_n , R_{TE} evaluated for small-scale tests

METAL SPHERE						CONCRETE SPHERE						LIGHT SPHERE								
ground	R_t	R_n	R_{TE}	beta	theta	ground	R_t	R_n	R_{TE}	beta	theta	ground	R_t	R_n	R_{TE}	beta	theta			
SF I	s1e11	0.400	0.006	0.009	0	78	SF II	s1e11	0.421	0.007	0.010	0	78	SF I	s1e11	0.531	0.017	0.018	0	78
	s1e12	0.408	0.005	0.009				s1e12	0.350	0.008	0.008				s1e12	0.571	0.123	0.033		
	s1e13	0.501	0.008	0.010				s1e13	0.226	0.009	0.002				s1e13	0.574	0.013	0.022		
	MEAN	0.456	0.006	0.009				MEAN	0.332	0.008	0.007				MEAN	0.559	0.015	0.024		
	s1e21	0.418	0.037	0.022	0	68		s1e21	0.440	0.012	0.044	0	68		s1e21	0.567	0.028	0.060	0	68
	s1e22	0.394	0.026	0.025				s1e22	0.379	0.015	0.026				s1e22	0.604	0.028	0.053		
	s1e23	0.367	0.038	0.020				s1e23	0.477	0.004	0.039				s1e23	0.510	0.032	0.043		
	MEAN	0.393	0.033	0.023				MEAN	0.432	0.013	0.037				MEAN	0.561	0.029	0.052		
	s1e31	0.393	0.043	0.068	0	58		s1e31	0.316	0.030	0.032	0	58		s1e31	0.565	0.055	0.115	0	58
	s1e32	0.342	0.042	0.057				s1e32	0.324	0.032	0.038				s1e32	0.509	0.064	0.110		
	s1e33	0.406	0.045	0.065				s1e33	0.366	0.033	0.044				s1e33	0.640	0.057	0.136		
	MEAN	0.380	0.043	0.063				MEAN	0.342	0.032	0.038				MEAN	0.571	0.058	0.120		
SF I	s2e11				0	90	SF II	s2e11	3.063	0.002	0.000	0	90	SF I	s2e11	1.367	0.006	0.007	0	90
	s2e12							s2e12	16.450	0.003	0.000				s2e12	13.618	0.007	0.000		
	s2e13							s2e13	1.235	0.003	0.000				s2e13	0.103	0.003	0.000		
	MEAN							MEAN	6.916	0.003	0.000				MEAN	5.029	0.005	0.003		
	s2e21	0.433	0.013	0.008	12	78		s2e21	0.412	0.020	0.012	12	78		s2e21	0.667	0.032	0.024	12	78
	s2e22	0.378	0.016	0.007				s2e22	0.332	0.018	0.010				s2e22	0.687	0.031	0.028		
	s2e23	0.426	0.017	0.010				s2e23	0.424	0.020	0.012				s2e23	0.677	0.031	0.026		
	MEAN	0.412	0.015	0.008				MEAN	0.390	0.019	0.011				MEAN	0.677	0.031	0.026		
	s2e31	0.398	0.026	0.025	22	68		s2e31	0.384	0.034	0.028	22	68		s2e31	0.536	0.020	0.029	22	68
	s2e32	0.305	0.009	0.020				s2e32	0.457	0.029	0.035				s2e32	0.536	0.020	0.029		
	s2e33	0.375	0.024	0.018				s2e33	0.466	0.032	0.030				s2e33	0.620	0.046	0.086		
	MEAN	0.359	0.025	0.021				MEAN	0.436	0.032	0.031				MEAN	0.578	0.033	0.058		
	s2e41	0.375	0.051	0.043	32	58		s2e41	0.583	0.090	0.171	32	58		s2e41	0.715	0.069	0.171	32	58
	s2e42	0.379	0.038	0.059				s2e42	0.618	0.056	0.164				s2e42	0.651	0.073	0.186		
	s2e43	0.357	0.035	0.041				s2e43	0.590	0.054	0.142				s2e43	0.648	0.081	0.174		
	MEAN	0.370	0.041	0.048				MEAN	0.597	0.067	0.159				MEAN	0.671	0.074	0.177		
							SF I+G	s3e11	1.303	0.080	0.006	0	90	SF II	s3e11	0.186	0.014	0.000	0	90
								s3e12	0.017	0.003	0.003				s3e12	0.596	0.004	0.002		
								s3e13	2.905	0.079	0.006				s3e13	2.332	0.006	0.002		
								MEAN	1.408	0.071	0.005				MEAN	1.838	0.008	0.001		
								s3e21	0.360	0.099	0.019	12	78		s3e21	0.549	0.025	0.016	12	78
								s3e22	0.382	0.103	0.020				s3e22	0.661	0.031	0.021		
								s3e23	0.446	0.099	0.025				s3e23	0.540	0.030	0.014		
								MEAN	0.463	0.100	0.021				MEAN	0.583	0.029	0.017		
								s3e31	0.328	0.148	0.046	22	68		s3e31	0.514	0.055	0.054	22	68
								s3e32	0.314	0.150	0.043				s3e32	0.480	0.059	0.045		
								s3e33	0.341	0.151	0.043				s3e33	0.485	0.053	0.041		
								MEAN	0.328	0.150	0.044				MEAN	0.493	0.056	0.046		
								s3e41	0.395	0.197	0.093	32	58		s3e41	0.607	0.048	0.128	32	58
								s3e42	0.461	0.176	0.108				s3e42	0.600	0.047	0.126		
								s3e43	0.466	0.187	0.101				s3e43	0.547	0.057	0.125		
								MEAN	0.428	0.187	0.101				MEAN	0.585	0.051	0.126		
							SF I+G	s4e11	0.528	0.100	0.020	0	78	SF II	s4e11	0.300	0.030	0.013	0	78
								s4e12	0.434	0.118	0.015				s4e12	0.387	0.006	0.010		
								s4e13	0.508	0.092	0.024				s4e13	0.383	0.014	0.011		
								MEAN	0.490	0.103	0.020				MEAN	0.357	0.017	0.011		
								s4e21	0.483	0.136	0.041	0	68		s4e21	0.480	0.039	0.037	0	68
								s4e22	0.402	0.122	0.035				s4e22	0.514	0.020	0.044		
								s4e23	0.473	0.115	0.039				s4e23	0.527	0.030	0.029		
								MEAN	0.452	0.124	0.038				MEAN	0.507	0.030	0.037		
								s4e31	0.405	0.161	0.062	0	58		s4e31	0.594	0.075	0.106	0	58
								s4e32	0.411	0.163	0.068				s4e32	0.545	0.070	0.114		
								s4e33	0.429	0.153	0.066				s4e33	0.479	0.055	0.092		
								MEAN	0.415	0.159	0.065				MEAN	0.539	0.067	0.104		
							SF I	s5e11	0.428	0.010	0.008	0	78	SF I+G	s5e11	0.816	0.059	0.005	0	90
								s5e12	0.598	0.012	0.020				s5e12	1.113	0.066	0.005		
								s5e13	0.511	0.015	0.023				s5e13	0.889	0.077	0.006		
								MEAN	0.512	0.012	0.017				MEAN	0.673	0.067	0.005		
								s5e21	0.559	0.023	0.050	0	68		s5e21	0.587	0.079	0.025	12	78
								s5e22	0.518	0.031	0.037				s5e22	0.575	0.085	0.025		
								s5e23	0.443	0.025	0.032				s5e23	0.553	0.089	0.029		
								MEAN	0.507	0.026	0.040				MEAN	0.572	0.085	0.026		
								s5e31	0.518	0.049	0.109	0	58		s5e31	0.404	0.122	0.057	22	68
								s5e32	0.421	0.048	0.088				s5e32	0.476	0.113	0.044		
								s5e33	0.456	0.046	0.077				s5e33	0.593	0.108	0.066		
								MEAN	0.465	0.048	0.091				MEAN	0.491	0.114	0.055		
								s5e41/4							s5e41/4	0.482	0.171	0.122	32	58
								s5e45							s5e45	0.516	0.178	0.150		
								s5e46							s5e46	0.448	0.110	0.162		</

Appendix III
Coefficients of restitution R_t , R_n , R_{TE} evaluated by half-scale tests

100 kg CYLINDER				500 kg CYLINDER				1000 kg CYLINDER				1.1 kg SPHERE				150 kg SPHERE				150 kg SPHERE (Inclined)							
R_t	R_n	RTE	MEAN	R_t	R_n	RTE	MEAN	R_t	R_n	RTE	MEAN	R_t	R_n	RTE	MEAN	R_t	R_n	RTE	MEAN	R_t	R_n	RTE	MEAN				
C6H1	0.106	0.054	0.085	D1eH1	0.61	0.041	0.092	M1eH1	0.369	0.024	0.000	01eH1	0.61	0.041	0.092	02eH1	0.61	0.041	0.092	03eH1	0.61	0.041	0.092	04eH1	0.61	0.041	0.092
C6H2	0.52	0.054	0.085	D1eH2	0.61	0.041	0.092	M1eH2	0.369	0.024	0.000	01eH2	0.61	0.041	0.092	02eH2	0.61	0.041	0.092	03eH2	0.61	0.041	0.092	04eH2	0.61	0.041	0.092
C6H3	6.57	0.054	0.085	D1eH3	0.61	0.041	0.092	M1eH3	0.369	0.024	0.000	01eH3	0.61	0.041	0.092	02eH3	0.61	0.041	0.092	03eH3	0.61	0.041	0.092	04eH3	0.61	0.041	0.092
MEAN	5.74	0.045	0.084	MEAN	0.61	0.041	0.092	MEAN	0.369	0.024	0.000	MEAN	0.61	0.041	0.092	MEAN	0.61	0.041	0.092	MEAN	0.61	0.041	0.092	MEAN	0.61	0.041	0.092
C6C1	4.50	0.054	0.085	D1eC1	1.139	0.035	0.062	M1eC1	0.238	0.020	0.000	01eC1	1.139	0.035	0.062	02eC1	1.139	0.035	0.062	03eC1	1.139	0.035	0.062	04eC1	1.139	0.035	0.062
C6C2	1.920	0.037	0.091	D1eC2	5.83	0.034	0.061	M1eC2	1.904	0.043	0.000	01eC2	5.83	0.034	0.061	02eC2	5.83	0.034	0.061	03eC2	5.83	0.034	0.061	04eC2	5.83	0.034	0.061
C6C3	7.953	0.040	0.093	D1eC3	5.107	0.036	0.061	M1eC3	0.983	0.043	0.000	01eC3	5.107	0.036	0.061	02eC3	5.107	0.036	0.061	03eC3	5.107	0.036	0.061	04eC3	5.107	0.036	0.061
MEAN	4.808	0.039	0.091	MEAN	5.464	0.035	0.061	MEAN	0.72	0.047	0.000	MEAN	5.464	0.035	0.061	MEAN	5.464	0.035	0.061	MEAN	5.464	0.035	0.061	MEAN	5.464	0.035	0.061
C6S1	0.175	0.010	0.000	D1eS1	2.430	0.010	0.000	M1eS1	0.053	0.000	0.000	01eS1	2.430	0.010	0.000	02eS1	2.430	0.010	0.000	03eS1	2.430	0.010	0.000	04eS1	2.430	0.010	0.000
C6S2	1.208	0.012	0.000	D1eS2	0.750	0.016	0.000	M1eS2	1.021	0.047	0.000	01eS2	0.750	0.016	0.000	02eS2	0.750	0.016	0.000	03eS2	0.750	0.016	0.000	04eS2	0.750	0.016	0.000
C6S3	4.93685	0.016	0.001	D1eS3	29.090	0.010	0.000	M1eS3	16.146	0.045	0.000	01eS3	4.93685	0.016	0.001	02eS3	4.93685	0.016	0.001	03eS3	4.93685	0.016	0.001	04eS3	4.93685	0.016	0.001
MEAN	14.923	0.013	0.000	MEAN	10.57	0.012	0.000	MEAN	5.740	0.045	0.000	MEAN	14.923	0.013	0.000	MEAN	14.923	0.013	0.000	MEAN	14.923	0.013	0.000	MEAN	14.923	0.013	0.000
C6A1	7.662	0.011	0.001	D1eA1	0.323	0.005	0.000	M1eA1	0.020	0.006	0.000	01eA1	7.662	0.011	0.001	02eA1	7.662	0.011	0.001	03eA1	7.662	0.011	0.001	04eA1	7.662	0.011	0.001
C6A2	3.423	0.013	0.000	D1eA2	0.166	0.005	0.000	M1eA2	2.526	0.047	0.001	01eA2	3.423	0.013	0.000	02eA2	3.423	0.013	0.000	03eA2	3.423	0.013	0.000	04eA2	3.423	0.013	0.000
C6A3	5.000	0.010	0.000	D1eA3	4.694	0.007	0.000	M1eA3	25.406	0.063	0.000	01eA3	5.000	0.010	0.000	02eA3	5.000	0.010	0.000	03eA3	5.000	0.010	0.000	04eA3	5.000	0.010	0.000
MEAN	5.862	0.012	0.000	MEAN	1.641	0.007	0.000	MEAN	11.651	0.069	0.000	MEAN	5.862	0.012	0.000	MEAN	5.862	0.012	0.000	MEAN	5.862	0.012	0.000	MEAN	5.862	0.012	0.000
C5A1	0.53	0.057	0.04	D2eH1	0.6	0.038	0.024	M2eH1	0.656	0.066	0.026	02eH1	0.53	0.057	0.04	02eH1	0.53	0.057	0.04	03eH1	0.53	0.057	0.04	04eH1	0.53	0.057	0.04
C5A2	0.18	0.056	0.039	D2eH2	0.528	0.036	0.024	M2eH2	0.317	0.045	0.029	02eH2	0.18	0.056	0.039	02eH2	0.18	0.056	0.039	03eH2	0.18	0.056	0.039	04eH2	0.18	0.056	0.039
C5A3	0.384	0.056	0.009	D2eH3	0.528	0.036	0.024	M2eH3	0.317	0.045	0.029	02eH3	0.384	0.056	0.009	02eH3	0.384	0.056	0.009	03eH3	0.384	0.056	0.009	04eH3	0.384	0.056	0.009
MEAN	0.454	0.061	0.012	MEAN	0.746	0.036	0.026	MEAN	0.723	0.040	0.021	MEAN	0.454	0.061	0.012	MEAN	0.454	0.061	0.012	MEAN	0.454	0.061	0.012	MEAN	0.454	0.061	0.012
C5B1	0.72	0.051	0.011	D2eB1	0.78	0.044	0.029	M2eB1	0.485	0.046	0.009	02eB1	0.72	0.051	0.011	02eB1	0.72	0.051	0.011	03eB1	0.72	0.051	0.011	04eB1	0.72	0.051	0.011
C5B2	0.297	0.049	0.007	D2eB2	0.574	0.022	0.023	M2eB2	0.662	0.028	0.016	02eB2	0.297	0.049	0.007	02eB2	0.297	0.049	0.007	03eB2	0.297	0.049	0.007	04eB2	0.297	0.049	0.007
C5B3	0.728	0.050	0.007	D2eB3	0.62	0.022	0.023	M2eB3	0.62	0.028	0.016	02eB3	0.728	0.050	0.007	02eB3	0.728	0.050	0.007	03eB3	0.728	0.050	0.007	04eB3	0.728	0.050	0.007
MEAN	0.728	0.050	0.007	MEAN	0.653	0.024	0.024	MEAN	0.574	0.042	0.014	MEAN	0.728	0.050	0.007	MEAN	0.728	0.050	0.007	MEAN	0.728	0.050	0.007	MEAN	0.728	0.050	0.007
C5C1	0.305	0.041	0.002	D2eC1	0.370	0.039	0.014	M2eC1	0.419	0.031	0.007	02eC1	0.305	0.041	0.002	02eC1	0.305	0.041	0.002	03eC1	0.305	0.041	0.002	04eC1	0.305	0.041	0.002
C5C2	0.280	0.035	0.004	D2eC2	0.630	0.028	0.014	M2eC2	0.355	0.039	0.007	02eC2	0.280	0.035	0.004	02eC2	0.280	0.035	0.004	03eC2	0.280	0.035	0.004	04eC2	0.280	0.035	0.004
C5C3	0.234	0.041	0.005	D2eC3	0.332	0.030	0.006	M2eC3	0.397	0.047	0.009	02eC3	0.234	0.041	0.005	02eC3	0.234	0.041	0.005	03eC3	0.234	0.041	0.005	04eC3	0.234	0.041	0.005
MEAN	0.240	0.039	0.004	MEAN	0.428	0.046	0.009	MEAN	0.391	0.039	0.008	MEAN	0.240	0.039	0.004	MEAN	0.240	0.039	0.004	MEAN	0.240	0.039	0.004	MEAN	0.240	0.039	0.004
C5A41	0.189	0.026	0.003	D2eA1	0.383	0.017	0.006	M2eA1	0.479	0.016	0.007	02eA1	0.189	0.026	0.003	02eA1	0.189	0.026	0.003	03eA1	0.189	0.026	0.003	04eA1	0.189	0.026	0.003
C5A42	0.224	0.024	0.002	D2eA2	0.315	0.013	0.005	M2eA2	0.396	0.019	0.008	02eA2	0.224	0.024	0.002	02eA2	0.224	0.024	0.002	03eA2	0.224	0.024	0.002	04eA2	0.224	0.024	0.002
C5A43	0.179	0.023	0.003	D2eA3	0.408	0.021	0.006	M2eA3	0.338	0.024	0.005	02eA3	0.179	0.023	0.003	02eA3	0.179	0.023	0.003	03eA3	0.179	0.023	0.003	04eA3	0.179	0.023	0.003
MEAN	0.185	0.028	0.003	MEAN	0.349	0.017	0.005	MEAN	0.405	0.020	0.007	MEAN	0.185	0.028	0.003	MEAN	0.185	0.028	0.003	MEAN	0.185	0.028	0.003	MEAN	0.185	0.028	0.003
C5B41	0.641	0.083	0.061	D2eB4				M2eB4	0.676	0.060	0.045	02eB4	0.641	0.083	0.061	02eB4	0.641	0.083	0.061	03eB4	0.641	0.083	0.061	04eB4	0.641	0.083	0.061
C5B42				D2eB5				M2eB5	1.000	0.085	0.123	02eB5				02eB5				03eB5				03eB5			
C5B43				D2eB6				M2eB6	0.941	0.021	0.119	02eB6				02eB6				03eB6				03eB6			
MEAN				MEAN				MEAN	0.939	0.032	0.119	MEAN				MEAN				MEAN				MEAN			
C5C41				D2eC4				M2eC4	1.000	0.042	0.105	02eC4				02eC4				03eC4				03eC4			
C5C42				D2eC5				M2eC5	1.000	0.042	0.122	02eC5				02eC5				03eC5				03eC5			
C5C43				D2eC6				M2eC6	1.000	0.042	0.112	02eC6				02eC6				03eC6				03eC6			
MEAN				MEAN				MEAN	0.981	0.041	0.118	MEAN				MEAN				MEAN				MEAN			
C5C44				D2eC7				M2eC7	0.692	0.098	0.072	02eC7				02eC7				03eC7				03eC7			
C5C45				D2eC8				M2eC8	0.635	0.044	0.053	02eC8				02eC8				03eC8							

Appendix III

Half-scale test results: maximal acceleration $a_{y,max}$, acceleration plateau $a_{y,plateau}$ and maximal penetration depth d_{max}

bars [°]	H [m]	maximal acceleration $a_{y,max}$ [m/s ²]			acceleration plateau $a_{y,plateau}$ [m/s ²]			maximal penetration depth d_{max} [m]											
		100 kg CYL	500 kg CYL	1000 kg CYL	100 kg CYL	500 kg CYL	1000 kg CYL	100 kg CYL	500 kg CYL	1000 kg CYL									
0	1	170	144	127	0	21	10	0.06	0.10	0.12									
0	1	172	151	142	0	16	19	0.07	0.07	0.11									
0	1	172	156	138	0	16	19	0.05	0.11	0.11									
0	2	206	211	239	0	24	29	0.06	0.13	0.16									
0	2	234	207	223	0	28	33	0.06	0.11	0.15									
0	2	278	220	217	0	30	33	0.06	0.11	0.20									
0	5	456	347	406	0	35	36	0.08	0.19	0.21									
0	5	440	346	388	87	36	41	0.09	0.19	0.23									
0	5	473	343	375	23	41	42	0.10	0.19	0.21									
0	10	691	641	598	22	53	57	0.11	0.20	0.28									
0	10	596	606	627	22	47	44	0.21	0.24	0.26									
0	10	686	599	576	22	48	50	0.16	0.27	0.28									
10	1	192	152	122	32	19	13	0.06	0.09	0.10	0.04	0.08	0.03						
10	1	176	124	132	41	22	13	0.05	0.10	0.14	0.07	0.08	0.06						
10	1	158	133	140	35	30	19	0.07	0.08	0.14	0.10	0.10	0.07						
10	2	314	217	219	35	41	19	0.06	0.13	0.14									
10	2	249	250	179	33	29	23	0.08	0.10	0.12									
10	2	248	210	227	19	59	17	0.07	0.12	0.16									
10	5	482	459	478	42	44	10	0.11	0.12	0.21	0.13	0.13	0.05						
10	5	427	406	401	43	48	18	0.11	0.16	0.18	0.10	0.18	0.08						
10	5	372	384	388	48	38	19	0.14	0.16	0.21	0.14	0.19	0.06						
10	10	632	627	628	55	26	34	0.18	0.13	0.27	0.14	0.19	0.09						
10	10	701	632	610	70	50	32	0.12	0.19	0.22	0.21	0.22	0.11						
10	10	622	683	617	47	56	30	0.14	0.23	0.23	0.19	0.20	0.12						
20	1	147	158	184	14	15	0	0.06	0.04	0.13	0.04	0.10	0.03						
20	1	126	143	144	13	0	6	0.11	0.06	0.10	0.06	0.10	0.04						
20	1	142	135	119	7	7	0	0.10	0.07	0.11	0.07	0.11	0.03						
20	2	251	251		10	10				0.11									
20	2	254	254		10	10				0.10									
20	2	249	249		7	7				0.10									
20	5	437	345	342	38	15	15	0.15	0.15	0.15	0.09	0.15	0.13						
20	5	389	350	322	22	52	27	0.18	0.18	0.16	0.16	0.16	0.09						
20	5	391	378	450	19	0	30	0.15	0.15	0.15	0.15	0.19	0.06						
20	10	618	577	564	19	24	25	0.20	0.19	0.20	0.19	0.20	0.09						
20	10	649	508	611	30	30	20	0.22	0.18	0.21	0.18	0.21	0.13						
20	10	568	490	555	32	22	24	0.28	0.28	0.28	0.13	0.26	0.07						
30	1	99	173	121	11	11	6	0.09	0.06	0.06	0.06	0.13	0.06						
30	1	120	153	144	8	8	11	0.10	0.04	0.13	0.04	0.13	0.04						
30	1	111	170	120	7	24	15	0.11	0.05	0.14	0.05	0.14	0.04						
30	2																		
30	2																		
30	2																		
30	5	308	356	317	17	5	5	0.16	0.11	0.14	0.11	0.14	0.08						
30	5	407	370	296	16	65	16	0.16	0.10	0.21	0.10	0.21	0.08						
30	5	402	371	303	19	31	20	0.14	0.10	0.20	0.10	0.20	0.13						
30	10	556	541	566	17	14	18	0.28	0.16	0.21	0.16	0.21	0.16						
30	10	688	543	508	14	53	18	0.28	0.17	0.23	0.17	0.23	0.15						
30	10	612	512	380	20	38	20	0.30	0.12	0.17	0.12	0.17	0.14						

Curriculum Vitae

Nom Barbara Heidenreich
Adresse Av. de Riant Mont 16
1004 Lausanne, Suisse
e-mail barbara_heidenreich@gmx.de

**Dates personnelles**

née le 14.05.1973 à Munich nationalité: allemande

Formation scolaire

09/1979 à 06/1992 Ecole élémentaire et Lycée à Munich : baccalauréat (Abitur)

Etudes de Génie Civil à l'Université Technique de Darmstadt

10/1992 à 10/1999 Etudes au Département Génie Civil à l'Université Technique de Darmstadt (TUD), spécialités approfondies: géotechnique, constructions hydrauliques et constructions en béton, terminé avec diplôme

10/1995 à 08/1996 études au Département Génie Civil de l'Ecole Polytechnique Fédérale de Lausanne (Suisse), subventionnée par le programme ERASMUS

08/1999 à 10/1999 Travail de diplôme à l'Institut de Géotechnique de la TUD

Doctorat

Depuis 05/2000 assistant-doctorant au Laboratoire Mécanique de Roches LMR à l'Ecole Polytechnique Fédérale de Lausanne EPFL (Suisse) : thèse dans le domaine des dangers naturels liés aux chutes de blocs rocheux

05/2000 – 10/2001 travail de comparaison des logiciels de trajectographie dans le cadre du programme Interreg IIC, le LMR étant partenaire dans ce programme